Functional Fluorescence Imaging of Receptor Tyrosine Kinase Activity in Cells

Andrew Robert Reynolds

This thesis is submitted in fulfilment
of the requirements for the degree of

Doctor of Philosophy

University College
University of London

February 2002

Cell Biophysics Laboratory
Cancer Research UK London Research Institute
Lincoln's Inn Fields Laboratories*
44 Lincoln's Inn Fields
London
WC2A 3PX

* Formerly the Imperial Cancer Research Fund

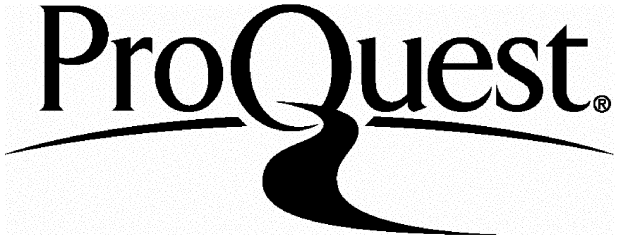

This thesis is dedicated to the memory of my father

Gerald James Reynolds (1939-1991)

Half the joy of working with nature
is the originality of the result

Ernest and Julio Gallo

Abstract

Receptor tyrosine kinases (RTKs) are key players in the regulation of cell behaviour. These receptors share a common mode of action, i.e. ligand binding is coupled to downstream signalling pathways that co-ordinate diverse cellular activities. The ErbB family of RTKs consists of four receptors: ErbB1, ErbB2, ErbB3 and ErbB4. They are involved in mitogenic signalling and tissue development. Ligand binding initiates receptor dimerisation and receptor autophosphorylation at tyrosine residues, providing docking sites for the recruitment of downstream signalling molecules. Interactions between ErbB receptors, involving every possible combination of receptor hetero- and homodimer, have been proposed to mediate transphosphorylation between receptors. This receptor cross-talk may act to diversify the nature of the downstream signalling response. Receptor phosphorylation is additionally modulated by the action of protein tyrosine phosphatases (PTPs). PTPs have 10-1000 times greater catalytic activity than RTKs which entails that PTP activity must be switched off in order for RTKs to become stably phosphorylated in response to ligand. This thesis describes the application of functional fluorescence imaging methods to study the activation mechanisms of ErbB receptors in intact cells.

Previous work from our laboratory has demonstrated the use of fluorescence lifetime imaging microscopy (FLIM) to measure fluorescence resonance energy transfer (FRET) between GFP-tagged ErbB1 and Cy3 labelled anti-phosphotyrosine antibodies, thereby allowing ErbB1 phosphorylation to be imaged in single cells. In this thesis, global analysis of FLIM data allows ErbB1 phosphorylation levels to be quantified in single cells. The approach is used to show that the delivery of a highly localised threshold dose of EGF results in equivalent levels of ErbB receptor phosphorylation to a saturating dose of soluble EGF. In contrast, a locally delivered subthreshold stimulus only activates receptors locally. Evidence is presented which suggests that the extent of receptor phosphorylation induced by ligand stimulus is regulated by hydrogen peroxide mediated PTP inhibition.

Acknowledgements

Foremost, I thank my PhD supervisor, Philippe Bastiaens, for his guidance, inspiration and patience throughout the last 4 years. A special thanks is also due for the considerable amount of time he invested in helping me prepare the final draft of this thesis. Finally, I should thank him for giving me the opportunity to look at biochemistry in a new 'fluorescent' light!

I owe considerable gratitude to Fred Wouters for teaching me many things and for providing entertainment on numerous occasions. A special thanks is also due to Peter Verveer for performing the global analysis and for continued support and good humour. Cheers to Tony Squire for building such a robust FLIM instrument and the ICRF electronics department for assistance with maintenance of the hardware. Thanks also to Banafshe Larijani and Tony Ng for keeping me company during the final 18 months of my PhD period. I also thank Mark Marsh and Peter Parker for their support and useful discussions. A big thanks also to Kairbaan Hodivala-Dilke (Kebs) for giving me some more time to finalise my thesis.

Many thanks to scientists and friends at the ICRF, EMBL and throughout the world who have discussed things with me or provided help in any way. In particular I should like to acknowledge the following people: Gertrude Bunt, Richard Evans, Martin Lowe, Bjorn Lillemeier, Rob Moore, Laurence Pelletier, Rainer Pepperkok, Liz Roper, Sandra Schmidt, Dave Shima, Jyoti Srivastava, Jim Shorter and Christian Tischer. Cheers to the members of the various ICRF research services and admininistration departments for making life easier and thanks to all those in Heidelberg who made me welcome during my visits.

Last, but by no means least, I must thank numerous friends for making me laugh and for just being there when I needed you. In particular: Marc & Jayne, Austin, Kieron & Cheryl, Chesham & Brinny, Matt & Sophia, Chris & Veronika, Ben, Brett, Julian, Steve and Rose. Cheers!

And finally...a very, very big heart-felt thanks to Ceri Edwards, my grandparents and my mother, Joan Reynolds. You have all supported me so much and I cannot begin to thank you enough.

Andy.

Collaborative work

I should like to acknowledge my supervisor, Philippe Bastiaens (P.B), and colleagues Peter Verveer (P.V) and Fred Wouters (F.W), for their practical contribution to the work presented in this thesis. The global analysis of all FLIM data was performed by P.V. All other experimental procedures, including microscopy, were performed by myself, with the exception that the experiment presented in Fig 3.3 was performed jointly by myself and P.B; the experiment presented in Fig 3.4 was performed jointly by myself and F.W; the experiment presented in Fig 3.5 was exclusively the work of F.W; the program used to calculate the diffusion coefficient of ErbB1-GFP (Chapter 4.4) was written by P.B.

Publications arising from this thesis

Verveer, P. J[‡]., F. S. Wouters[‡], **A. R. Reynolds**[‡] and P. I. H. Bastiaens (2000). Quantitative imaging of lateral ErbB1 receptor signal propagation in the plasma membrane. **Science** 290(5496): 1567-70.

Reynolds, A. R[‡]., C. Tischer[‡], P. J. Verveer, I. Yudushkin, O. Rocks, & P. I. H. Bastiaens. ErbB1 activation coupled to inhibition of protein tyrosine phosphatases causes lateral signal propagation. *Manuscript submitted.*

[‡] These authors contributed equally.

Table of Contents

List of Tables

List of Figures

List of Abbreviations

AKAP, A-kinase anchoring protein

AOM, see **SW-AOM**

APS, ammonium persulphate

ATP, adenosine 5'-triphosphate

BSA, bovine serum albumin

°C, degrees centigrade

cAMP, 3':5'-cyclic adenosine monophosphate

CCD, charge-coupled device

CFP, cyan fluorescent protein

cm, centimetre

CW, continuous wave

DC, direct current

DMEM, Dulbecco's modified Eagle's medium

DMF, N,N-dimethylformamide

DMSO, dimethyl sulphoxide

DNA, deoxyribonucleic acid

DTT, dithiothreitol

EDAC, 1-ethyl-3-(3-dimethylaminopropyl) carbodiimide hydrochloride

EDTA, ethylene diamine *N, N, N',N'*-tetraacetic acid

e.g. for example

EGF, epidermal growth factor

EGTA, ethylene glycol-bis(β-aminoethyl ether)-*N, N, N',N'*-tetraacetic acid

ER, endoplasmic reticulum

Fab, fragment 'antibody binding'

FCS, foetal calf serum

FGF, fibroblast growth factor

FGFR, fibroblast growth factor receptor

FLIM, fluorescence lifetime imaging microscopy

GAP, GTPase activating protein

GEF, GTPase exchange factor

Fig, figure

FRAP, fluorescence recovery after photobleaching

FRET, fluorescence resonance energy transfer

GDP, guanosine 5'-diphosphate

GFP, green fluorescent protein

GPCR, G-protein coupled receptor

GPI, glycosylphosphatidyl inositol

GPIB, general purpose interface bus

GTP, guanosine 5'-triphosphate

HEPES, N-(2-hydroxyethyl)piperazine-N'-(2- ethanesulphonic acid)

hGH, human growth hormone

hGHR, human growth hormone receptor

hPa, millibars

Hz, Hertz

ICRF, Imperial Cancer Research Fund

i.e. that is to say

kDa, kiloDaltons

M, molar

MAPK, mitogen activated protein kinase

MAPKK, mitogen activated protein kinase kinase

MAPKKK, mitogen activated protein kinase kinase kinase

MCP, micro-channel plate

MES, 2-N-(Morpholino)ethanesulphonic acid

mg, milligram

MHz, MegaHertz

min(s), minute(s)

ml, millilitre

mm, millimeter

mM, millimolar

mol, mole

ms, millisecond

mW, milliWatt

NA, numerical aperture

NADP, nicotinamide adenine dinucleotide phosphate

NADPH, nicotinamide adenine dinucleotide phosphate (reduced)

ng, nanogram

NHS, N-hydroxysuccinimde

nm, nanometer

nM, nanomolar

NRG, neuregulin

ns, nanosecond

PAGE, polyacrylamide gel electrophoresis

PAO, phenyl arsine oxide

PBS, phosphate buffered saline

PC, personal computer

PDGF, platelet-derived growth factor

PDGFR, platelet-derived growth factor receptor

PFA, paraformaldehyde

PH, pleckstrin homology

PI3 kinase, phosphatidyl inositol 3-kinase

PKC, protein kinase C

PLC, phospholipase C

PTB, phosphotyrosine binding

PtdIns, phosphatidyl inositol

PtdIns 3P, phosphatidyl inositol 3-phosphate

PtdIns (3,4) P_2, phosphatidyl inositol 3,4-bisphosphate

PtdIns (4,5) P_2, phosphatidyl inositol 4,5-bisphosphate

PtdIns (3,4,5) P_3, phosphatidyl inositol 3,4,5-trisphosphate

PTK, protein tyrosine kinase

PTP, protein tyrosine phosphatase

RF, radio frequency

RGB, red, green and blue channel

ROI, region of interest

ROS, reactive oxygen species

RPM, revolutions per minute

RPTP, receptor protein tyrosine phosphatase

RTK, receptor tyrosine kinase

SDS, sodium dodecyl sulphate

sec(s), second(s)

SH, Src homology

SW-AOM, standing wave acousto-optic modulator

TEMED, *N,N,N',N'*-tetramethylenediamine

TGF, transforming growth factor

TIFF, tagged image file format

Tris, (Tris[hydroxymethyl]aminomethane)

UV, ultra-violet

v/v, volume per volume

W, Watt

w/v, weight per volume (in grams per 100 ml)

YFP, yellow fluorescent protein

µg, microgram

µl, microlitre

µM, micrometre

µM, micromolar

Chapter 1

General Introduction

General Introduction

1.1 Functional imaging of biochemical activity in cells

The cell can be viewed as a biochemical machine, whose behaviour is dependent on the transfer of information between biological macromolecules. Mechanisms which mediate transfer of the biochemical information include: 1. the direct association of macromolecules with other macromolecules (e.g. protein-protein, protein-lipid and protein-DNA interactions) or small ligands (e.g. steroid hormones, GTP, ATP), 2. the covalent modification (e.g. phosphorylation, acetylation and methylation), cleavage or conformational change of proteins, and 3. changes in the intracellular concentration of proteins, lipids, small metabolites (e.g. cAMP, reactive oxygen species) and ions (e.g. calcium). Existing biochemical techniques have begun to show how specific macromolecules use these processes to co-ordinate a variety of cellular activities, e.g. cell movement and shape, cell cycle progression, control of protein localisation, apoptosis and cell differentiation. However, few biochemical approaches can fully account for the subcellular compartmentalisation of biochemical reactions, the cellular concentration of participating intermediates or all the possible interconnections with other components. Only by studying chemical reactions in the context of their natural environment, the living cell, can these factors be completely integrated in the analysis of subcellular biochemistry.

The most promising non-invasive method to study molecular organisation and activity within the context of the intact cell is the application of fluorescence microscopy. Immunofluorescence analysis of cells is widely used to demonstrate the spatial organisation of molecules within cells. The recent discovery of green fluorescent protein (GFP), a genetically encoded fluorescent protein, has increased the ease via which the dynamics of fluorescently labeled proteins can be studied *in situ.* In addition, fluorescent probes which are sensitive to changes in intracellular ion concentrations have proved extremely powerful tools to study biologically functional calcium fluxes within living cells (Berridge *et al.*, 2000; Bootman *et al.*, 2001).

An obvious progression of this technology is to use fluorescent probes to study other biological activities within intact cells e.g. phosphorylation, macromolecular association or conformational change. The spectroscopic properties of fluorescent probes are sensitive to the local (nanometer scale) environment and, serendipitously, the pertinent chemical reactions that biological macromolecules undergo also involve changes in the local environment of the macromolecule which occur within a similar distance range. Therefore, by labelling macromolecules of interest with suitable fluorescent probes, the spectroscopic properties of the conjugated fluorophores can be exploited to investigate the activity of macromolecules in cells. In this thesis, the use of a GFP-tagged receptor tyrosine kinase (RTK) has been employed to study the activation mechanisms which regulate RTK signalling within the context of the living cell.

1.2. Molecular basis of receptor tyrosine kinase signalling

1.2.1 Extracellular signal-coupled receptors

The role of signalling receptors is to recognise and bind ligands such as cytokines, growth factors, hormones or neurotransmitters and transduce these messages into cellular responses by engaging the appropriate intracellular machinery. Some ligands are membrane permeant and the receptor is localised to the intracellular space e.g. nuclear receptors. Binding of ligand to these receptors causes them to enter a state where they are competent to exert effects on gene expression by directly interacting with DNA (Mangelsdorf *et al.*, 1995). However, many ligands are not membrane permeant and are only present in the extracellular milieu as immobilised or soluble factors. The receptors for these ligands are localised to the plasma membrane, where they bind ligand on the outside of the cell and transduce the signal to proteins on the inside. Four broad functional classes of transmembrane receptor are recognised: ligand-gated ion channels, G-protein coupled receptors (GPCRs), receptor serine/threonine kinases and receptor tyrosine kinases (RTKs; Hunter, 2000). Downstream signalling cascades engaged by these receptors exert effects on cell behaviour by regulating cycle progression, apoptosis, gene expression, protein and lipid synthesis and the activity of cytoskeletal components

(Schlessinger, 2000). Since the focus of this thesis is signalling via RTKs the nature of the signalling events elicited by this class of receptor will be focused upon primarily.

1.2.2 Receptor tyrosine kinases

The classical RTK (e.g. epidermal growth factor receptor, EGF receptor, or platelet derived growth factor receptor, PDGFR) consists of an extracellular domain with ligand binding activity that is linked to an intracellular protein tyrosine kinase domain via a single transmembrane region (Fig. 1.1 A). The tyrosine kinase domain catalyses transfer of the γ phosphate of ATP to the hydroxyl group of tyrosine residues on target proteins. The intracellular domain also contains tyrosine residues which are phosphorylation targets themselves. Ligand binding to the extracellular domain facilitates tyrosine phosphorylation of the intracellular domain. It is generally considered that the clustering of receptors into dimers or higher oligomeric forms, upon ligand binding, allows phosphorylation of other receptors *in trans* (Fig. 1.1 B). Downstream signalling is dependent on the phosphorylation of the receptor at tyrosines in the intracellular domain, which provide docking sites for effector proteins (Fig. 1.1 C; Fig. 1.2; Schlessinger, 2000).

Apart from the classical RTK, variations on ligand-activated receptor-coupled tyrosine kinase activity are known. Tyrosine kinase activity can be provided by a non-receptor protein tyrosine kinase (PTK) which is associated, albeit non-covalently, with the receptor chain (e.g. epo and interferon receptors associate with Jak family PTKs; Ihle & Kerr, 1995) or receptor chain phosphorylation can be mediated by non-receptor chain-associated PTKs (e.g. T- and B-cell and Fc receptors are phosphorylated by Src-family kinases; Thomas & Brugge, 1997). Another variation is displayed by members of the insulin receptor-like family of RTKs, which possess intrinsic tyrosine kinase activity, but relatively few tyrosine autophosphorylation sites that mediate protein docking. Instead, the receptor phosphorylates a separate membrane tethered 'docking protein,' e.g. insulin receptor substrate-1 (IRS-1), to which extensive recruitment of signalling molecules occurs (Myers *et al.*, 1993).

1.2.3 Modular domain structure of signalling molecules

Downstream signalling from RTKs is mediated by proteins which possess a modular domain structure. These domains can be categorised into three broad functional groups: 1. domains that mediate docking interactions with other molecules, 2. domains which possess defined enzymatic activity, such as kinase, phosphatase, phospholipase or GTPase activity, and 3. domains which regulate the activity of GTPases, i.e. GTPase exchange factors (GEFs) or GTPase activating proteins (GAPs). Individual domains may also be involved in intramolecular interactions that mediate conformation-dependent activity regulation mechanisms.

Domains which mediate the docking of proteins with other molecules are critically important for achieving signalling specificity. Docking domains can be conveniently grouped into families on the basis of structural homology and shared ability to recognise a core protein motif or lipid species (see Table 1.1). However, the binding specificity of individual domains belonging to different proteins is not generic (see comments, Table 1.1). Significantly, SH2 and PTB domains from different proteins preferentially recognise phosphotyrosine in different sequence contexts, which allows different RTKs to recruit specific combinations of signalling molecules (Pawson & Scott, 1997; Schlessinger, 2000).

1.2.4 Adaptor proteins

The majority of SH2, SH3 and PTB domain-containing proteins also possess domains with intrinsic enzymatic activity. For example, phospholipase Cγ (PLCγ) contains an SH2 domain and can therefore bind directly to phosphorylated receptor chains. However, there also exists a class of molecules known as 'adaptors' which consist only of the above mentioned binding domains (see Tables 1.1, 1.2). Adaptors serve to link two or more separate signalling molecules together or act as regulatory subunits for separate catalytic subunits. Adaptor proteins associate with different, yet overlapping, sets of proteins with enzymatic, GEF or GAP activity. The p85 subunit of phosphatidyl inositol 3-kinase (PI3 kinase) is a specialised adaptor subunit which associates only with the p110 catalytic subunit of PI3 kinase. Adaptors play a role in diversifying the

complement and activity of effectors that are activated downstream of RTKs (Pawson & Scott, 1997; Cattaneo & Pelicci, 1998; Cantrell, 2001)

1.2.5 The functional role of docking with the activated receptor

The direct, or adaptor-mediated, binding of enzymes to activated RTKs via phosphotyrosine docking appears to perform at least two functions. Firstly, binding can stimulate the catalytic activity of the enzyme via allosteric mechanisms. For example, binding to appropriate phosphotyrosine motifs has been shown to stimulate the catalytic activity of PI 3 kinase 2 - 3 fold, ZAP-70 / Syk PTKs 5 - 10 fold and SHP-2 phosphatase 35 - 50 fold (Shoelson, 1997). In the case of SHP-2, and the Src PTK, receptor association appears to activate the enzymatic activity of the PTK by inducing an intramolecular conformational change in the protein which releases autoinhibition of the catalytic domain (Weiss & Schlessinger, 1998). Secondly, immobilisation near the membrane brings effectors into close proximity with plasma membrane-restricted substrates or cognate signalling partners. For example, the substrates of many phospholipid modifying enzymes are concentrated at the plasma membrane. Therefore, membrane recruitment of these enzymes increases the access to their substrates.

Proteins which dock directly or indirectly with the RTK can become phosphorylation substrates of the receptor or other membrane-proximal kinases. Phosphorylation of docked proteins has at least two roles. Firstly, tyrosine phosphorylation provides new docking sites for phosphotyrosine binding proteins. Secondly, phosphorylation can regulate the activity of the docked protein, potentiating its function as a downstream effector.

1.2.6 Activation of small GTPases

The coupling of RTKs to downstream enzymes via the use of adaptors is best characterised for the activation of the small GTPase, Ras. The adaptor protein, Grb2, is constitutively associated with Sos1 (a Ras GEF) in the cytoplasm and is recruited to the phosphorylated RTK through direct binding of its SH2 domain to receptor chain phosphotyrosines or other tyrosine phosphorylated sites on proteins already associated with the receptor e.g. Shc or SHP-1. The reason for these different, apparently redundant

recruitment mechansims to the RTK is unclear. However, many phosphotyrosine docking proteins appear to be able to dock both directly with receptors or with receptor-associated enzymes or adaptors. The process of bringing Grb2-Sos1 to the RTK allows the Sos1 Ras-GEF to physically interact with plasma membrane anchored Ras-GDP, causing it to enter the active GTP-bound state by promoting exchange of GDP for GTP (Downward, 1996). Ras-GTP is competent to activate downstream signalling via a number of pathways by physical association with Ras effectors (Vojtek & Der, 1998; Olson & Marais, 2000).

Ras constitutes one member of a large family of small GTPases that are activated downstream of RTKs. Downstream effectors of small GTPases include phospholipid modifying enzymes, GEFs, GAPs and cytoskeleton-associated proteins, allowing GTPases to activate a diverse array of downstream signalling pathways (Bar-Sagi & Hall, 2000). Most notably, GTPases are activators of mitogen activated protein (MAP) kinase or extracellular signal-related kinase (ERK) cascades, which mediate a broad range of cytoplasmic and nuclear phosphorylation events involved in cell proliferation and differentiation (Marshall 1995; Marais & Marshall, 1996; Schaeffer & Weber, 1999).

1.2.7 Activation of the Class I PI3 kinase

Activation of Class I PI3 kinase by RTK signalling can occur via direct recruitment to receptor phosphotyrosines or indirectly through a mechanism involving Ras (Rodriguez-Viciana *et al.*, 1994). Active Class I PI3 kinase phosphorylates PtdIns $(4,5)P_2$ at the 3' position to generate PtdIns $(3,4,5)P_3$. This lipid species is rare in resting cells, but stimulation of PI3 kinase activity results in a substantial increase in the plasma membrane PtdIns $(3,4,5)P_3$ content. PtdIns $(3,4,5)P_3$ is bound by a large complement of proteins which possess the appropriate phosphoinositide binding domain (Table 1.2), including enzymes, GEFs, GAPs, adaptors, and structural proteins, resulting in translocation of these proteins from the cytosol to the membrane (Vanhaesebrook & Waterfield, 1999; Cantrell 2000; Fig.1.2). PtdIns $(3,4,5)P_3$-binding appears to potentiate the ability of these proteins to elicit further downstream signalling due to a change in localisation, conformation or activity of the protein. Signalling which results from PtdIns $(3,4,5)P_3$ synthesis is involved in a diverse array of cellular behaviours including motility, cell survival and metabolic regulation (Fig. 1.2; Rickert *et al.*, 2000; Xu *et al.*, 2001).

Class I PI3 kinase constitutes one member of a large family of PI3 kinases involved in signalling (Vanhaesbrook & Waterfield, 1999).

1.2.8 Activation of the phospholipase Cγ - protein kinase C pathway

Activation of phospholipase Cγ by RTK signalling occurs via direct recruitment to receptor phosphotyrosines and maximal activity of the enzyme requires tyrosine phosphorylation of the enzyme at Y738. Active PLCγ hydrolyses PtdIns $(4,5)P_2$ to generate soluble Ins $(1,4,5)P_3$ and diacylglycerol (DAG). Ins $(1,4,5)P_3$ induces the release of calcium from intracellular stores which, in concert with DAG, leads to the plasma membrane translocation and activation of the serine/threonine kinase PKC (Noh *et al.*, 1995; Parekh *et al.*, 2000).

1.2.9 Signalling connections with non-receptor PTKs

A reciprocal relationship of phosphorylation exists between non-receptor PTKs which are immobilised at the membrane (e.g. Src) or cytoplasmic RTKs which dock with the receptor (e.g. Abl, Zap-70) because they can both undergo phosphorylation by the receptor and can phosphorylate the receptor chain themselves, processes which clearly regulate signalling in both directions (Thomas & Brugge, 1997; Blume-Jensen & Hunter, 2001).

1.2.10 Direct signalling to transcription factors

Finally, tyrosine phosphorylation can directly regulate the activity of transcription factors (TFs). Receptor chain docked STAT (Signal Transducers and Activators of Transcription) TFs undergo tyrosine phosphorylation, which initiates the dissociation of the STAT from the receptor and dimerisation of the STAT proteins, a step that is required for nuclear translocation of the STAT dimer. Nuclear localised STATs are then able to exert effects on transcription by binding to specific promotor regions within DNA that possess the appropriate consensus STAT binding sequence (Ihle & Kerr, 1995; Bromberg, 2001).

1.2.11 Regulation of tyrosine phosphorylation cascades by phosphatases

Phosphate groups incorporated into proteins at serine, threonine and tyrosine residues and into the inositol head group of lipids are removed by the action of phosphatases. Since the subject of this thesis is the regulation of RTK phosphorylation, the biology of protein tyrosine phosphatases (PTPs) will be focused upon primarily (see also section 1.5.6). PTPs are a structurally diverse family which, like other signalling molecules, possess domains outside the catalytic region that mediate additional functions such as regulation of phosphatase activity and subcellular targeting. The family is defined by a conserved catalytic motif: H-C-X-X-G-X-X-R-[S/T]-G. The enzymes can be broadly classified into two sub-categories: receptor PTPs (RPTPs), which possess a transmembrane segment and non transmembrane PTPs, which may be cytosolic or targeted to specific membrane domains by post-translational modifications (Fischer *et al.*, 1991; Neel & Tonks, 1997).

The catalytic mechanism of dephosphorylation by most PTPs is critically dependent on the presence of a cysteine and aspartate residue within the active site. During catalysis the phosphorous atom of the substrate undergoes nucleophilic attack by the cysteine, resulting in the formation of a cysteinyl-phosphate intermediate. The aspartate residue is required to facilitate the cleavage of the P-O bond between the phosphorous and the phenolic oxygen of the tyrosine side chain, which results in dephosphorylation of the tyrosine and the release of the substrate from the PTP active site (Denu *et al.*, 1996).

Phosphatases are not merely enzymes which act to switch off events initiated by phosphorylation, but play an equal role with kinases in regulating the phospho content of proteins and the fidelity of signalling. Studies on both tyrosine and serine/threonine phosphorylation regulated signalling events have shown that appropriately regulated signal transduction requires not only stimulation of protein kinase activity, but also correct positive and/or negative regulation of phosphatase activity (Hunter 1995; Bae *et al.*, 1997; Lee *et al.*, 1998; Zhang *et al.*, 2000; Tamir *et al.*, 2000; Penninger *et al.*, 2001). At least three mechanisms have emerged via which the activity of phosphatases can be regulated: 1. direct phosphorylation of the PTP which, dependent on the context, can inhibit or induce the activity of the enzyme (Weiss & Schlessinger, 1998; Petrone & Sap, 2000), 2. ligand-induced homo-oligomerisation is inhibitory in the case of RPTPs (Weiss

& Schlessinger, 1998), and 3. oxidation of the active site cysteine in the PTP by reactive oxygen species (ROS) is inhibitory (Finkel, 2000; Rhee *et al.*, 2000).

By mapping the substrates of PTPs it has emerged that a single RTK can be dephosphorylated by multiple PTPs and a single PTP can regulate the signalling of several RTKs (Ostman & Bohmer, 2001). This apparent redundancy may be explained by two emerging concepts of phosphatase regulation. Within the context of the intact cell, access of phosphatases to substrate is controlled by temporal and spatial regulation of phosphatase and substrate contact (Flint *et al.*, 1997; Inagaki *et al.*, 1994; Fischer, 1999) and phosphatases can perform different roles, dependent on the nature of the substrate e.g. positive or negative regulation of downstream signalling (Hunter, 1995; Zhang *et al.*, 2000; Penninger *et al.*, 2001).

1.2.12 Summary and perspective

Intracellular signalling is mediated by proteins with defined biochemical activities. Each component of the intracellular signalling machinery interacts with multiple upstream and downstream effectors in order to co-ordinate the response to extracellular signals. In the next section, the organisation of this signalling network is discussed.

1.3 The architecture of the subcellular signalling network

1.3.1 The intracellular signalling network as an information processing device

In general, the molecular basis of signalling has been determined by analysing the composition of discrete pathways, where individual molecular species act consecutively in a defined order (e.g. Ras-Raf-MAPKK-MAPK). In reality, extensive cross-talk between signalling pathways occurs. Therefore, signalling molecules should be viewed as individual components of a complex signalling network. Furthermore, extracellular signal-coupled receptors utilise a dramatically overlapping set of downstream effectors. For example, the activation of Ras, PLCγ and PI3 kinase and raised intracellular levels of calcium and cAMP are common downstream signalling events elicited by many extracellular signals. This combination of complexity, and apparent redundancy, has

made it difficult to understand how specific combinations of input signals give rise to specific outcomes.

A significant step in improving our understanding is the realisation that a signalling network will possess emergent properties that are not immediately obvious from the study of individual pathways (Jordan *et al.*, 2000). In this area, computer modelling of biochemical networks is emerging as a powerful tool (Bhalla & Iyengar, 1999). Furthermore, cDNA microarray technology now provides the opportunity to assess the full gene expression profile that results from various input signal combinations. This is an insight which is not possible by studying the behaviour of isolated signalling pathways (Fambrough *et al.*, 1999; Sweeney *et al.*, 2001).

Another important concept is that the spatial and temporal organisation of the signalling network components and their activity is critical in determining signalling outcomes, both in terms of the amplitude and the qualities of the response. In order to fully appreciate this, it is necessary to study the spatio-temporal dynamics of signalling in intact, and preferably living, cells and tissues. Fluorescence microscopy provides a convenient, non-invasive method with which to approach these issues (Bastiaens & Pepperkok, 2000). The discovery of a genetically encoded green fluorescent protein (GFP), and spectral variants thereof, has significantly improved the potential to perform these types of experiment (Pollok & Heim, 1999; Bastiaens & Pepperkok, 2000).

1.3.2 Emergent properties of signalling networks

The purpose of interconnectivity between signalling pathways can be better understood by defining the interconnecting mediators as either 'junctions' or 'nodes' (Jordan *et al.*, 2000). Junctions receive and integrate inputs from multiple pathways. For example, multiple pathways elicit the production of cAMP or calcium, thus the intracellular levels of these mediators at any given time could serve as an indicator of the balance of signals from many pathways. Nodes split the signal they receive by mediating the activation of multiple downstream pathways that regulate distinct cellular functions, but are all required for eliciting the appropriate responses to a particular extracellular signal. For example, activated EGF receptors signal to multiple downstream effectors including the PLCγ-PKC and Ras-Raf-MAPK pathways and by activating Src, which are all involved in the mitogenic response.

A major function of the signalling network is to place a value on signals it receives and integrate them so that the level of biological response produced can be controlled (Jordan *et al.*, 2000). In order to elicit this control, individual enzymes must possess activation thresholds, or multiple activation requirements, that allow the quantity of input to be gauged. In other words, a certain magnitude of a single signal e.g. high concentrations of an activating ligand, or qualitatively different activation signals, e.g. phosphorylation by multiple kinases, must be obtained in order to activate the enzyme. Positive and negative feedback loops also operate in signalling networks, which modulate the amplitude of the response in a fashion which is non-linear. For example, positive feedback is used to amplify calcium signals (Clapham, 1995).

The ability to integrate signals over time and produce differential responses is also an important feature of the network (Jordan *et al.*, 2000). For example, it has been proposed that in some cell types transient stimulation of the Ras-Raf-MAPK pathway induces proliferation of cells, whilst sustained stimulation induces differentiation (Marshall, 1995).

1.3.3 Immobilisation and anchoring of signalling proteins

Groups of signalling molecules involved in a specific signalling cascade are often physically associated with specialised scaffold / anchoring proteins. Scaffold association creates a 'hard wired' signalling module and can direct the intracellular location of the module. For example, the 3 kinases which constitute a single MAPK cascade are immobilised together on a single scaffold molecule. In this scenario, activation of the MAPKKK results in downstream signalling only through the physically associated MAPKK and MAPK, ensuring that maximal signalling specificity is achieved (Whitmarsh & Davis, 1998; Garrington & Johnson, 1999). Scaffold proteins of the AKAP, PDZ and β-arrestin family act to cluster signalling modules made up of kinases and phosphatases either in close proximity to appropriate receptors which activate the module, or in close proximity to downstream effectors of the module, such as cytoskeletal components. In this way, scaffolds ensure efficient signalling at the correct intracellular location and spatial insulation from inappropriate signals (Pawson & Scott, 1997; Edwards & Scott, 2000; Harris & Lim, 2001; Miller & Lefkowitz, 2001)

1.3.4 Translocation of signalling proteins between compartments

The subcellular location of kinases, phosphatases and GTPases is regulated either by targetting motifs within the molecules themselves or by association with anchoring proteins. Potential cognate partners in a signalling cascade can therefore be maintained in separate cellular compartments to reduce the chance that they will interact at the inappropriate time. However, the translocation of signalling mediators to a compartment where cognate mediators and substrates are also located, upon receipt of the appropriate signal, provides a potent ON/OFF switch for many signalling pathways. The translocation of cytosolic signalling molecules to the plasma membrane, by association with phosphorylated RTKs, is one example of this.

Under physiological conditions, where various extracellular cues are being interpreted all at once, the membrane may represent a location where these signals are integrated, subject to the dynamic concentration changes of individual mediators. Recently, live cell imaging of GFP-tagged PH (pleckstrin homology) domain proteins has shown that the turnover of PtdIns(3,4,5)P_3 by the action phosphatases at the membrane is extremely fast and that PH domain proteins can rapidly respond to changes in these concentrations (Venkateswarlu *et al.*, 1998; Haugh *et al.*, 2000). Furthermore, studies on the mobility of GFP-tagged proteins have shown that many are not statically associated with binding partners, but are highly mobile and can move around the cell without assistance from the cytoskeleton (Gillham *et al.*, 1999; Sakai *et al.*, 1997; Lillemeier *et al.*, 2000; Phair & Misteli, 2000). Therefore, many signalling proteins appear to diffuse at random, exhibiting high off-rates for binding. This would allow them to respond rapidly to changes in the cellular signalling context (Tureul & Meyer, 2000).

It is also worthwhile to mention that many transcription factors and kinases shuttle between the cytoplasm and the nucleus (Karin & Hunter, 1995). These factors may only exert regulation of gene expression whilst in the nucleus, therefore this also represents a mechanism whereby signalling outcomes are regulated by control of subcellular localisation.

1.3.5 Compartmentalisation in membrane subdomains

Due to differing physical properties, various lipids, such as cholesterol, glycosphingolipids, gangliosides and saturated phospholipids segregate from unsaturated phospholipids to form discrete subdomains in the lateral plane of cellular membranes. These are commonly referred to as lipid rafts and have been estimated to be in the range of 50 - 500 nm in diameter. The physiological relevance of rafts is controversial, because the isolation of rafts and associated components is dependent on detergent extraction methods which may be prone to artifacts. However, it has been proposed that the translocation of signalling molecules between subdomains of the plasma membrane may be an important mechanism that controls interactions between signalling proteins (Ikonen & Simons, 1997; Jacobson & Dietrich, 1999; Simons & Toomre, 2000).

Certain proteins appear to preferentially associate with rafts, including: GPI-anchored proteins and doubly–acylated proteins, such as Src (Ikonen & Simons, 1997). A number of reports have suggested that raft association is correlated with the activation state of a particular protein. For example, according to Prior and co-workers, H-Ras is sequestered within rafts in its GDP-bound state, but it dissociates from rafts upon GTP-loading, which is a requisite event for the activation of Raf (Prior *et al.*, 2000). Furthermore, the complex spatio-temporal reorganisation of membrane-associated proteins that is coupled to immune-receptor activation is thought to be controlled by lipid raft dynamics (Wilson *et al.*, 2000; Dustin & Chan, 2000; Dykstra *et al.*, 2001).

1.3.6 Gradients, waves and oscillations

Biochemical information can also be transmitted via the asymmetrical distribution of signalling mediators or by oscillations in the concentration of a particular mediator. For example, by using a GFP-tagged PH domain in living cells it has been shown that the exposure of cells to a gradient of the chemotactic ligand PDGF results in polarised PtdIns $(3,4,5)P_3$ production, with more at the leading edge and less at the trailing edge (Servant *et al.*, 2000). The polarised gradient would appear to establish the polarity of the signalling response that is required for cell migration (Rickert *et al.*, 2000).

The nature of intracellular calcium release in excitable and non-excitable cells has been studied using fluorescent dyes. Within the cell the release of calcium can be

controlled spatially to generate local or widespread intracellular calcium release. Low magnitude stimulus of cells may induce only sufficient calcium release from the ER / extracellular space to produce a spatially localised 'puff' of calcium, due to buffering of the calcium by various intracellular calcium binding proteins. Alternatively, a stimulus of sufficient magnitude may initiate the spread of a 'calcium wave' which travels through the entire cell by means of a positive feedback loop between calcium and calcium-sensitive calcium channels (Clapham, 1995). Calcium release can also be controlled temporally in cells, such that the intracellular concentration oscillates between high and low at a defined frequency. The frequency of the calcium release is critical to the nature of the response produced and is implicated in controlling many different processes in many different cell types (Berridge *et al.*, 2000).

1.3.7 Summary and perspective

Many important concepts have emerged already from the study of the spatial and temporal dynamics of signalling mediators. Microscopy analysis of fixed and live cell preparations, in which the concentration and localisation of signalling intermediates is monitored on the basis of fluorescence intensity, is playing a significant role in the analysis. Conventional microscopy techniques cannot, however, adequately reveal the nanometer scale organisation of molecular events or how the activity of all enzymes and metabolites are organised temporally and spatially within the living cell. To solve this problem, novel imaging methods, based on the measurement of excited state reactions of fluorophores within cells, are being developed.

1.4 Measuring excited-state reactions within biological samples

1.4.1 Steady state and time-resolved fluorescence measurements

Conventional confocal and epifluorescence microscopes measure steady state fluorescence. In steady state measurements the fluorescence emission is averaged by exciting the probe, and measuring the emission, over a relatively long time period (typically milliseconds to seconds). The fluorescence intensity measured is dependent on the concentration, quantum yield and fluorescence decay kinetics of the probe. In

contrast, time-resolved fluorescence detection directly measures the concentration-independent fluorescence decay kinetics of the probe. The decay kinetics of the probe are very sensitive to the local environment of the fluorophore and may be altered by parameters such as the charge and hydrophobicity of adjacent molecular species, proximity of other fluorophores and rotational freedom of the fluorophore. For this reason, time-resolved fluorescence measurements are useful to study the environment and activity of biological macromolecules. In order to understand the use of time-resolved measurements it is necessary to discuss the photophysics of fluorophores.

1.4.2 Definition of the excited-state lifetime (fluorescence lifetime)

The processes that occur upon excitation of a fluorophore can be described by reference to a Jablonski diagram (Fig. 1.3 A). Upon absorbtion of a photon of the appropriate energy ($h\nu$) an electron undergoes a transition from a ground-state electronic and vibrational level, denoted S_0, to an excited-state electronic and vibrational energy level, either S_1 or S_2 (k_{ex}). This process occurs in the order of 10^{-15} seconds. Generally, the molecule reverts rapidly (10^{-12} seconds) to the S_1 state via the release of heat, a process known as internal conversion (k_{ic}). A subsequent transition from the S_1 state to the S_0 state, through loss of energy by release of a photon (k_f), produces fluorescence emission. A measure for the average time that the molecule remains in the excited-state is known as the excited-state or fluorescence lifetime (τ).

Besides loss of energy from the S_1 excited state via emission of a photon (radiative decay) there also exist a number of routes via which energy may be lost from the excited-state without emission of a photon (non-radiative decay). The most significant non-radiative processes which may depopulate the excited-state include:

1. Intersystem crossing (the transition of an electron from the singlet excited-state S_1, to the triplet-state, T_1; k_{isc}).
2. Collisional quenching (loss of excited-state energy to the triplet-state due to spin-orbit coupling by short range interaction between the fluorophore and a heavy molecule or atom; k_q).

3. Photobleaching (conversion of the fluorophore into a new non-fluorescent chemical species due to a chemical reaction which occurs whilst the molecule is in the excited state; k_{bl})
4. Internal conversion (the transition of an electron from the singlet excited state S_1 to the ground state, via vibrational transition, with concomitant release of heat; k_{ic}).
5. Resonance energy transfer, also known as fluorescence resonance energy transfer (k_{fret}; see section 1.4.3).

The lifetime of the excited state is therefore dependent on the rate at which the excited state is depopulated by fluorescence emission (radiative decay) and dark processes (non-radiative decay).

The loss of energy from the excited-state via emission is best described by first-order reaction kinetics, resulting in an exponential fluorescence decay function (Fig. 1.3 B) of the form:

$$I(t) = I_0 \, exp\,(-t / \tau) \qquad [1]$$

where, $I(t)$ is the fluorescence intensity as a function of time, I_0 is the fluorescence intensity at time zero, t is time and τ is the fluoresence lifetime. From this equation it is easy to derive that the fluorescence lifetime is defined as the time taken for $1/e$ (~63%) of the excited molecules to decay to the ground state after a brief pulse of excitation light (delta-pulse excitation; Fig. 1.3 B). It is important to clarify that the fluorescence lifetime, τ, is the reciprocal of the sum of both radiative and non-radiative processes.

Radiative decay and non-radiative decay processes compete to depopulate the excited state. An increase in the rate of a non-radiative decay process will therefore reduce the potential for fluorescence emission and as a consequence shorten the fluorescence lifetime (Fig. 1.3 B). Although the rate of various non-radiative decay processes cannot be individually measured, the fluorescence lifetime can be measured using microscopy techniques. Therefore, by measuring the lifetime of a fluorescent probe within a biological specimen, information can be gained about the local environment of the probe, because the local environment will change the rate of non-radiative decay (Lakowicz, 1999).

Under optimal conditions fluorescence resonance energy transfer (FRET), which is a non- radiative decay process, can lead to large changes in the rate of radiative decay. These changes can be monitored with relative ease in biological samples by measuring the fluorescence lifefime, or steady–state fluorescence intensities, of the probes involved (Squire & Bastiaens, 1999). The use of FRET to measure protein interactions in cells will be discussed in detail in the following text.

1.4.3 The nature and physical properties of fluorescence resonance energy transfer

1.4.3.1 Dipole-dipole coupling

FRET is a photophysical process by which energy is transferred non-radiatively from an excited molecular chromophore (the donor) to another chromophore (the acceptor) by means of intermolecular dipole-dipole coupling (Forster, 1946; 1951). When the donor is excited, an electron moves from the ground-state orbital to a higher energy excited-state orbital (Fig. 1.3 A), producing a change in the charge distribution across the molecule. The transition from the excited state back to the ground state creates a transition dipole within the donor molecule. The transition dipole of the donor generates an electric field that can induce the formation of a similar dipole within the acceptor i.e. the transition of electrons from the ground-state to the excited-state S_1 in the acceptor. As a result, the acceptor may emit fluorescence photons by relaxation to the ground state via radiative S_1 to S_0 transition, a consequence of FRET that is known as sensitised emission. This dipole coupling therefore mediates the transfer of excited-state energy from the donor to the acceptor. The electric field is generated due to the oscillations of excited-state electrons in the donor, which transfer energy by resonance with electrons in the acceptor, hence the name fluorescence 'resonance energy' transfer (Clegg, 1996).

1.4.3.2 Distance dependency of FRET

The efficiency of energy transfer between donor and acceptor, E, is inversely dependent on the sixth power of the distance between the two participating fluorophores, and is given:

$$E = R_0^6 / (R_0^6 + r^6) \qquad [2]$$

where r (nm) is the distance between the two fluorophores and R_0 (nm) is the distance at which energy transfer is 50% efficient. This sixth power of the distance-dependence of the FRET efficiency produces a steep curve when plotted (Fig. 1.4 A) and illustrates why FRET is useful to measure the activity of biological macromolecules. Firstly, the distance over which FRET can be detected is ideally suited to measuring the interactions of proteins. In conventional optical systems FRET can be detected when the FRET efficiency is 5% or higher. Within these detection limits, equation [2] shows that FRET is detectable between two fluorophores that lie within a distance of up to 1.6 x R_0 (see also Fig. 1.4 A). Typical values of R_0 are between 2 and 7 nm and so FRET is measurable across distances up to 11 nm, which is in a similar range to protein diameters (Fig. 1.4 B). Secondly, the steep distance relationship makes FRET useful to quantify processes which are based on transitions between discrete states, as is often the situation with proteins (e.g. bound and unbound to ligand, phosphorylated versus nonphosphorylated, etc), as long as a suitable assay can be designed to exploit the relationship (Fig. 1.5).

The value of R_0 itself is dependent on various parameters associated with the fluorophore pair and their environment and is given:

$$R_0 = [\kappa^2 \times J(\lambda) \times n^{-4} \times Q]^{1/6} \times 9.7 \times 10^2 \qquad [3]$$

where κ^2 is the relative orientation of the transition dipoles of the fluorophores; $J(\lambda)$ (cm^6 mol^{-1}) is the overlap integral, a measure of the spectral overlap between the donor emission (em) and acceptor absorbtion (abs) spectra (Fig. 1.4 C); n, is the refractive index of the intervening medium; Q, is the quantum yield of the donor.

1.4.3.3 Selection of donor-acceptor pairs

Energy is absorbed by a fluorophore as quanta (photons of defined energy) resulting in the quantised transition of electrons from the ground state to the excited state energy levels. The absorbtion spectrum of a fluorophore is an explicit representation of this, as it represents the distribution of photon energies that can be absorbed. The emission spectrum likewise represents the energy distribution of photons emitted by quantised transitions back to the ground state and is typically shifted to higher wavelengths (Stoke's shift). The emission spectrum of the donor must overlap significantly with the absorbtion spectrum of the acceptor (Fig. 1.4 C), in order for the resonance condition to be fulfilled so that FRET can occur. The overlap integral, $J(\lambda)$, is a measure of the extent of overlap between the spectra and is also a measure of the resonance energies in common between donor and acceptor. When the other parameters of equation [3] are known, the theoretical value of R_0 for different fluorophore combinations can be calculated based on the overlap integral of the pair (Table 1.3). Therefore, ideal donor-acceptor pairs for FRET experiments are those which possess a high overlap integral. Inspection of equation [3] also shows that the ideal donor is one which has a high quantum yield, so selection of a donor with a high quantum yield and selection of an acceptor which results in a large overlap integral between donor and acceptor provides the basis for selection of donor-acceptor pairs with a large enough R_0 for measuring FRET between proteins.

Finally, in experiments where FRET is measured by detecting sensitised emission of the acceptor, an important consideration for selecting donor and acceptor pairs is that it should be possible to selectively excite the donor without significant excitation of the acceptor. Excitation of the acceptor at the donor wavelength will clearly give a false positive result due to the contribution of acceptor emission caused by direct excitation. However, minimal excitation of the acceptor can be corrected for (see also section 1.4.5.1).

1.4.4 FRET microscopy and the fluorescent labelling of macromolecules *in situ*

Cuvette-based FRET measurements can be made on living cells in suspension or with *in vitro* reconstituted preparations. However, if FRET measurements are made with

a fluorescence microscope equipped with a digital camera, spatially-resolved measurements can be made within histological sections and within live or fixed tissue culture cells (Squire & Bastiaens, 1999). A range of microscopy protocols are available to measure FRET in cells and tissues (see sections 1.4.5, 1.4.6). All methods are reliant on the ability to fluorescently label macromolecules *in situ*. The choice of labelling procedure will be dependent on the biological system under study and the microscopy technique via which FRET is measured. In experiments where two separate macromolecules are to be labelled it may be desirable to use different labelling methods for each partner.

Direct conjugation of proteins with fluorophores can be achieved via chemical modification of the purified molecules *in vitro*, followed by introduction back into the cell via microinjection, electroporation or other appropriate procedures which allow transfer across the plasma membrane (Bastiaens & Jovin, 1996; Stephens & Pepperkok, 2001). However, plasmid-driven expression of a protein which has been tagged by genetic fusion to an intrinsically fluorescent protein variant (e.g. cyan fluorescent protein, CFP; green fluorescent protein, GFP; or yellow fluorescent protein, YFP) has many advantages over the chemical modification method, including the fact that it allows transmembrane proteins to be labelled and the precise site of modification is always known (Chamberlain & Hahn, 2000; Bastiaens & Pepperkok, 2000). A number of novel site-specific methods for protein labelling are also available, which are based on genetic modification of the protein either by site-specific modification of specific amino acids (Cornish *et al.*, 1994; Kraynov *et al.*, 2000) or via introduction of a fluorophore-binding sequence (Griffin *et al.*, 1998). Indirect fluorescent labelling can be achieved with fluorophore-conjugated antibodies or monovalent antibody Fab fragments, which can be microinjected into living cells or used to stain fixed samples (e.g. Bastiaens *et al.*, 1996; Wouters & Bastiaens, 1999; Ng *et al.*, 1999). The applicability of antibodies is limited by issues relating to the position and function of the epitope within the target molecule and its accessibility in the preparation. In any approach requiring direct chemical modification of the protein, the stoichiometry of dye-protein labelling must also be carefully controlled in order to maximise the chance that FRET can be measured (see section 1.4.5.3). Furthermore, attention must always be paid to the effects that fluorophore-conjugation has on the biological activity of the protein in question, regardless of the means via which labelling is achieved.

1.4.5 Steady-state fluorescence intensity-based FRET microscopy measurements

In the event that FRET occurs between a donor and acceptor fluorophore pair, donor fluorescence intensity is quenched due to depopulation of the donor excited state. For the acceptor the converse is true: population of the excited state by FRET results in emission of the acceptor without prior absorbtion of photons, a process known as sensitised emission. Measurements of the steady state fluorescence intensity of the donor emission alone, acceptor emission alone or the donor/acceptor emission can therefore be used to determine FRET efficiencies at each pixel of an image recorded in the microscope.

1.4.5.1 Donor-acceptor fluorescence intensity measurements

In the ratiometric method the donor is selectively excited, and the emission of both the donor and the acceptor are measured separately. The acceptor / donor emission intensity ratio is calculated and is used to monitor a change in the FRET efficiency. This method is only reliable in systems where the donor and acceptor stoichiometry remains constant throughout the experiment, e.g. measurements upon conformation sensors where the donor and acceptor fluorophores are physically connected through a single polypeptide (Fig. 1.5; e.g. Miyawaki *et al.*, 1997; Nagai *et al.*, 2000; Ting *et al.*, 2001). Otherwise, it cannot be excluded that measured differences in the intensities of the donor and acceptor may reflect local changes in probe concentration due to protein redistribution. FRET can also be measured by exciting the donor and monitoring sensitised emission of the acceptor alone (e.g. Sorkin *et al.*, 2000). However, sensitised emission detection methods must always be corrected for fluorescence emission that might occur due to direct excitation of the acceptor at the donor excitation wavelength and bleed through of the donor fluorescence into the acceptor emission filter set.

1.4.5.2 Acceptor photobleaching

FRET efficiencies can be determined by comparing the donor emission intensity, in the presence and absence of the acceptor, at every pixel of the image. If the acceptor can be irreversibly photobleached by continuous illumination it will no longer be capable

of acting as an acceptor. This phenomenon provides the basis of the measurement: the intensity of the donor is measured before and after complete photodestruction of the acceptor. It is important that the wavelength used to bleach the acceptor excites the acceptor only, without concomitant excitation and bleaching of the donor. This is usually easy to achieve, because absorbtion spectra are generally steeper at the 'red edge.'

In the acceptor photobleaching method, pixel-by-pixel FRET efficiencies, E_i, are determined by image arithmetic based on the following equation:

$$E_i = 1 - (I_i / I_{i0}) \qquad [4]$$

where I_i = fluorescence intensity of the donor and I_{i0} = fluorescence intensity of the donor after complete photodestruction of the acceptor (Bastiaens *et al.*, 1996; Bastiaens & Jovin, 1996; Bastiaens & Jovin, 1998; Wouters & Bastiaens, 1999).

Unfortunately, this type of measurement is limited to fixed samples because of the possibility of protein movement or free radical-mediated damage within the sample during bleaching of the acceptor. However, it has some advantages over other techniques. Firstly, it is simple to implement; only a fluorescence microscope equipped with a digital camera and some rudimentary imaging software is required. Secondly, there is no need for measurements to be corrected for excitation of the acceptor at the donor excitation wavelength. Thirdly, measurements which make use of the donor fluorescence signal alone (donor-based measurements) are advantageous because the acceptor fluorophore can be present in excess. In order to understand the relevance of this final statement some discussion of the requirements for donor-acceptor labelling stoichiometries, for different FRET microscopy methods, is required.

1.4.5.3 Stoichiometry considerations for FRET experiments

There are two general stoichiometry considerations for the donor- and acceptor-labelled molecules. Firstly, the ratio of donor labelled molecules to acceptor labelled molecules present and secondly, the number of conjugated fluorescent labels per individual molecular species. These labelling considerations are an important factor to

optimise in any FRET experiment and are largely dependent on the means via which FRET is measured.

In donor-based measurements it is preferable that the acceptor-labelled species is present in excess of the donor and/or is conjugated with more fluorescent species than the donor-labelled species. In acceptor-based measurements the opposite is true: the donor should ideally be present in excess of the acceptor. In both cases, an excess of labelling on one partner increases the chance of optimal orientation between the transition dipoles when donor and acceptor molecules come within 1.6 x R_0. Optimal orientation of transition dipoles is independent of how close the donor and acceptor lie, but the chance of optimal orientation increases when more fluorescent species are present in close proximity.

In FRET-based assays of biochemical activity in cells, the amount of molecules present in complexes where FRET could be achieved can be low. Of course, in donor-based measurements it is advantageous to have the acceptor in excess because it minimises the likelihood of fluorescence contribution from donors which are not undergoing FRET to an acceptor. Likewise, when implementing sensitised emission measurements it is advantageous to have the donor-labelled species in excess, because it minimises the chance that fluorescence will be collected from acceptors which are not coupled to a donor by FRET. Unfortunately, the presence of excess donor molecules has a significant caveat: it may lead to bleed through of donor fluorescence in the acceptor emission channel, leading to false positive results in measurements of the sensitised emission. Finally, in ratiometric measurements a 1:1 stoichiometry of donor:acceptor species and labelling is preferred, in order for measured differences in the intensity of both fluororescent species to significantly alter the ratio of the intensities.

In summary, donor-based FRET measurements are particularly powerful because FRET is measured independently of acceptor emission intensity. This means that an excess of acceptor labelling can be used and no account needs to be made for excitation of the acceptor at the donor excitation wavelength or bleed through of the donor into the acceptor channel.

1.4.5.4 Donor photobleaching kinetics

This technique utilises steady-state measurements of the donor intensity, but is an indirect measure of the donor fluorescence lifetime. The method exploits the fact that the photobleaching time of a fluorophore (τ_{bl}) is inversely proportional to its fluorescence lifetime (τ)when the fluorophore is excited with low intensity excitation light (Bastiaens & Jovin, 1996). This is due to the fact that photobleaching only occurs in the excited-state (see section 1.4.2). Therefore, if a molecule photobleaches quickly then the excited-state lifetime (τ) must also be relatively long. The method is implemented by bleaching the donor and periodically recording the donor fluorescence intensity, in the presence and absence of the acceptor. From this data the photobleaching time constant of the donor in the presence ($\tau_{bl,i}$), and abscence ($\tau_{bl,r}$), of the acceptor can be determined. The pixel-by-pixel FRET efficiency, E_i, can then be calculated:

$$E_i = 1 - (\tau_{bl,i} / \tau_{bl,r}) \qquad [5]$$

1.4.6 Time-resolved fluorescence-based FRET microscopy measurements

The major caveat of intensity-based FRET measurements is that the intensity of the donor and acceptor fluorescence at each pixel of an image is dependent on the concentration of each fluorescent species. Reliable measurements of FRET efficiencies can be made using intensity-based methods in fixed cells where a reference measurement can be made by photodestroying one of the fluorophores in the FRET complex (section 1.4.5.3, 1.4.5.4; Bastiaens & Jovin, 1998) or by making control measurements in identical samples where one of the fluorophores in the complex is omitted (e.g. Majoul *et al.*, 2001). As a means to measure FRET in cells, time-resolved measurements of fluorescence decay kinetics offer distinct advantages. Unlike the steady-state fluorescence intensity, the fluorescence lifetime of the probe is independent of the probe's concentration or the optical path length, two parameters which are difficult to control in cells. In addition, time-resolved measurements usually contain more information than steady-state measurements. By implementing the appropriate analysis methods, time-resolved measurements can reveal the existence of different populations of fluorescent

species which are each associated with discrete decay kinetics (discrete fluorescent lifetimes) and the relative abundance of each species. This is useful because if each species, and its associated lifetime component, can be attributed to a different biochemical state (e.g. bound and unbound to substrate), then the amount of molecules present in each state can be determined as molar fractions.

1.4.6.1 Time-domain fluorescence lifetime measurements

In time-domain lifetime measurements the sample is excited with a brief pulse of light. The duration of the pulse is significantly shorter than the fluorescence lifetime of the fluorophore and is therefore typically in the order of tens to hundreds of picoseconds. The pulse excitation produces a population of fluorophores which are in the excited-state and these will relax to the ground-state producing a fluorescence decay profile (equation [1]; Fig. 1.6 A). In a time-domain FLIM instrument the exponential decay in intensity is directly measured after delivery of the pulse, either by counting the number of photons in time bins using gated detection or by time-correlated single photon counting (TCSPC). The fluorescence lifetime of the fluorophore at each pixel can then be determined by fitting the decay curves to the appropriate decay models (Lakowicz, 1999).

1.4.6.2 Frequency-domain fluorescence lifetime measurements

The time-resolved fluorescence measurements presented in this thesis are acquired using frequency-domain FLIM. In a frequency-domain FLIM instrument the intensity of the excitation light is sinusoidally modulated. When a fluorophore is excited in this manner the emitted fluorescent light oscillates at the same modulation frequency. However, because fluorescence takes a finite time (characterised by the fluorescence lifetime) the emission is, on average, delayed. This results in a waveform that is phase-shifted with respect to the excitation light (Fig. 1.6 B).

By determining the phase-shift ($\Delta\phi$) between the excitation and emission sinus waves, at every pixel, the apparent fluorescence lifetime can be calculated:

$$\tau_\phi = \tan \Delta\phi / \omega \qquad [6]$$

where τ_ϕ is the lifetime according to the measured phase shift (phase lifetime), ω is the circular modulation frequency ($2\pi f$, where f is the excitation frequency in Hz) and $\Delta\phi$ is the phase shift which occurs between the excitation and emission sinus waves (Fig. 1.6 B). Another property of the emission wave is that it is reduced in amplitude with respect to the excitation wave, a phenomenon known as demodulation. The fluorescence lifetime can also be calculated from the depth of the demodulation:

$$\tau_m = 1 / \omega (1/ m^2 - 1)^{1/2} \qquad [7]$$

where, τ_m is the lifetime according to the measured demodulation (modulation lifetime) and m is the demodulation, which is a measure of the amplitude of the emission wave relative to the excitation wave:

$$m = (B / A) / (b / a) \qquad [8]$$

where A, B, b and a refer to the amplitudes and offsets of the excitation and emission sinus waves (see Fig. 1.6 B).

In a frequency-domain FLIM instrument the emitted fluorescence waveform can be sampled by heterodyne or homodyne detection. The instrument used for the measurements presented in this thesis uses the homodyne detection method, in which the high-frequency fluorescence emission from a biological sample is converted into a static phase-dependent signal (see Figs 1.7, 1.8) which contains information on the modulation and phase of the emitted fluorescence. With the aid of a zero-lifetime reference signal, which is acquired in a similar fashion to the fluorescence of the biological sample, the phase dependent data can then be used to extract the phase shift ($\Delta\phi$) and demodulation (m) values at each pixel by the use of a Fourier transform. From this data the average

phase and modulation lifetimes (τ_ϕ and τ_m) at each pixel of an image are calculated. The procedure is summarised in Fig. 1.9. More complete details of the instrument and FLIM data acquistion are given in Chapter 2.4, whilst the mathematical methods used to extract the values of $\Delta\phi$ and m are described in depth elsewhere (Squire & Bastiaens, 1999; Harpur & Bastiaens, 2000; Verveer *et al.*, 2001).

1.4.7 Applications of FRET microscopy measurements in cells

An increasing number of articles report the application of FRET-based assays to measure biochemical activity in cells, by utilising one of the measurement methods described above, or combinations thereof (reviewed in Wouters *et al.*, 2001). Some applications of FRET-based assays are summarised here.

1.4.7.1 Detecting the functional interactions of proteins

The direct association of physically distinct proteins can be detected by measuring FRET between separate donor- and acceptor-labelled proteins. In most of these experiments the physical interaction of the proteins has been previously demonstrated by immunoprecipitation, or via the use of covalent cross-linking reagents, and so the application of FRET to measure the interaction provides new information regarding the nature of the interaction under physiological circumstances or demonstrates a spatio-temporal aspect in cells. Protein-protein interactions which have been demonstrated using FRET microscopy include the interactions of: Bcl-2 with Bax (Mahajan *et al.*, 1998), PKCα with β1 integrin (Ng *et al.*, 1999b) and Grb2 with the EGF receptor (Sorkin *et al.*, 2000). Clustering of molecules into homo-oligomers can also be demonstrated with FRET microscopy (Fig. 1.5 B). For example, the detection of FRET between fluorescently labelled GPI–anchored proteins suggests that they form discrete subdomains in the plasma membrane, providing some of the most convincing proof, thus far presented, for the existence of lipid rafts in living cells (Varma & Mayor, 1998; Jacobson & Dietrich, 1999).

Monitoring the loss of FRET upon physical separation of donor- and acceptor-labelled components has allowed the oligomeric status of proteins to be studied within intact cells. For example, this approach has been used to confirm that the A-subunit of

cholera toxin separates from the B-subunit in an endosomal/ Golgi compartment after endocytosis (Bastiaens *et al.*, 1996) and that dissociation of the PKC βI regulatory and catalytic domains, after phorbol ester treatment, allows the catalytic subunit to selectively enter the nucleus (Bastiaens & Jovin, 1996).

1.4.7.2 Biochemical 'activity sensors'

Biochemical 'activity sensors' are designed so that a change in FRET efficiency gives some measure of the activity of a specific protein or the concentration of a specific metabolite or ion. Most sensors so far reported consist of donor and acceptor fluorophores that are conjugated to either end of a protein domain or subunit which changes its conformation upon ligand binding and results in a change in FRET efficiency (Fig. 1.5 C). The donor and acceptor fluorophores are generally spectral variants of the GFP protein and thus these sensors are genetically encoded, which offers numerous advantages, including the fact that the construct can be targeted to a specific organelle. Sensors based on this principle have been designed to detect calcium (Miyawaki *et al.*, 1997), cAMP (Nagai *et al.*, 2000), nitric oxide (Pearce *et al.*, 2000) and tyrosine phosphorylation (Ting *et al.*, 2001) in living cells.

The activation state of a given protein determines whether or not it can associate with a binding partner and this provides the basis for another type of sensor. For example, GTPases cycle between a GTP- and GDP-bound state which dictates whether or not they can associate with binding partners. By labelling the GTPase with a donor fluorophore and its GTPase-state conditional binding partner with an acceptor fluorophore, FRET between donor and acceptor can be used to gauge the activity of the GTPase cascade (Fig. 1.5 A, D). This approach has been applied to study the activity of the small GTPases Rac (Kraynov *et al.*, 2000) and Ras (Mochizuki *et al.*, 2001) and heterodimeric G-proteins (Janetopoulos *et al.*, 2001) in living cells.

Finally, the activity of proteolytic enzymes can be studied by fusing donor and acceptor fluorophores to either end of a sequence which encodes the protease sensitive sequence. Proteolytic activity is detected by monitoring the loss of FRET when the sequence undergoes cleavage (Fig. 1.5 E). Sensors based on this principle have been applied to study the activity of the caspase family of enzymes in cells (Mahajan *et al.*, 1999; Harpur *et al.*, 2001).

1.4.7.3 Detecting post-translational modifications

Here, the term post-translational modification is applied to any stable or reversible covalent modification to an amino acid side chain which occurs after synthesis of the protein. This includes, but is not limited to: acylation, glycosylation, phosphorylation, acetylation, methylation and nucleotide binding. A protein is labelled with a donor fluorophore and the post-translational modification of that protein is detected by an acceptor-labelled antibody which specifically binds to the post-translational modification. FRET is detected only when the acceptor-labelled antibody is bound to the donor-conjugated protein (Fig. 1.5 F). Under circumstances where the covalent modification is reversible and modulates the activity of the protein, this assay can also be regarded as an activity sensor. The approach has been applied to monitor the phosphorylation status of PKCα and the EGF receptor in cells (Ng *et al.*, 1999a; Wouters & Bastiaens, 2000).

1.4.8 Summary and perspective

A number of strategies can be employed to utilise FRET as an assay of biochemical activity in cells. As a result, new insights are being made into biochemical pathways. Much of the work presented in this thesis utilises a FRET-based assay to monitor the phosphorylation status of the EGF receptor (ErbB1) in cells. In the final section of this general introduction the biology of the ErbB receptor family is discussed.

1.5 The ErbB family of RTKs

1.5.1 Introduction to the ErbB family

The ErbB family of RTKs consists of four receptors: the EGF receptor (ErbB1), HER-2 or neu (ErbB2), HER-3 (ErbB3) and HER-4 (ErbB4). Each ErbB receptor consists of a 600-630 residue extracellular region, which is divided into two cysteine-rich domains, a single transmembrane domain of approximately 22 amino acids and a C-terminal intracellular domain of approximately 600 amino acids. The intracellular portion of all the receptors contains a membrane proximal kinase domain which is catalytically

active in all receptors, except ErbB3, which has severely impaired kinase activity. The intracellular domains of all receptors contain multiple threonine, serine and tyrosine phosphorylation sites, the exception being ErbB3 which contains no threonine sites. Sequence variability between the receptors in the regions flanking the tyrosine autophosphorylation sites allows each receptor to recruit different, yet overlapping, sets of downstream effectors (Fig. 1.1 D)

The ErbB receptors are expressed in a number of epithelial, mesenchymal and neuronal tissues. They have a prominent role in the proliferation and differentiation of cells and the development of tissues. ErbB receptor signalling is subject to regulation at several levels: 1. the concentration of activating ligands and the receptor family members expressed in a tissue can vary spatially within the tissue and temporally as a function of different developmental stages (Burden & Yarden, 1997), 2. interactions between ErbB receptors, involving every possible combination of receptor hetero- and homo-dimer have been demonstrated; these associations appear to regulate the nature of the downstream signalling elicited (Alroy & Yarden, 1997; Olayioye *et al.*, 2000), 3. receptor phosphorylation is modulated by events that are independent of ligand binding e.g. the action of other signalling factors, such as kinases, phosphatases, integrins and GPCRs (Carpenter, 1999; Luttrell *et al.*, 1999; Ostman & Bohmer, 2001), and 4. intracellular trafficking and degredation of the receptors influences the signalling potential (Carpenter, 2000; Waterman & Yarden, 2001).

Abnormal signalling by RTKs has been implicated in a variety of disease states (Robertson *et al.*, 2000). In particular, deregulated signalling by the ErbB family, generally caused by receptor overexpression or mutations in the receptor sequence, is implicated in the development of neoplasias in many tissues (Gullick, 1986; Hynes & Stern, 1994; Salomon, 1995; Olayioye *et al.*, 2000). Therefore, further elucidation of the mechanisms which regulate RTK signalling may provide important insights for the design of new drugs designed to combat these diseases.

1.5.2 ErbB family ligands

A growing number of ligands have been shown to bind and activate ErbB receptors. The most well-characterised ligands are synthesised as plasma membrane-associated pro-peptides which can activate ErbB receptors in this membrane-anchored

form or after cleavage from the membrane anchor as soluble factors in solution, or presented in association with the extracellular matrix (Massague & Pandiella, 1993; Taipale & Keski-Oja, 1997). The ligands can be conveniently classified into three groups according to which receptors they bind (Riese & Stern, 1998). EGF, transforming growth factor-α (TGF-α) and amphiregulin, can be termed 'EGF agonists' because they bind directly only to ErbB1. A second class of ligand, which bind only ErbB3 and / or ErbB4 have been termed the neuregulins (NRG's). NRG1 (also known as: neu differentiation factor, heregulin, acetylcholine receptor-inducing activity and glial growth factor) and NRG 2 bind both ErbB3 and ErbB4, whereas NRG3 and NRG 4 bind ErbB4, but not ErbB3. Betacellulin, epiregulin and heparin binding-EGF (HB-EGF) comprise a third class of 'bispecific' ligands which can bind directly to both ErbB1 and ErbB4. As yet, no ligand has been isolated which directly binds and activates ErbB2.

1.5.3 Early evidence for the activation of ErbB1 receptor by ligand-induced dimerisation

The EGF receptor (ErbB1), a 1186 residue glycoprotein with an apparent molecular mass of 170 kDa, was the first member of the ErbB family to be isolated and cloned (Cohen *et al.*, 1982; Ullrich *et al.*, 1984). EGF binding to the extracellular domain of the intact receptor was found to result in tyrosine phosphorylation of the receptor at distinct sites in the intracellular domain (autophosphorylation) and an increase in the phosphorylation level of other cellular proteins (Hunter & Cooper, 1981; Cohen *et al.*, 1982; Downward *et al.*, 1984; Hunter & Cooper, 1985). It was concluded that the receptor is an allosteric enzyme; ligand binding to the extracellular domain is transduced into a change in the kinase activity of the intracellular domain. Early microscopy studies on EGF-treated cells suggested that activation of ErbB1 by EGF binding was associated with the local aggregation of ligand-receptor complexes in the plasma membrane (Schechter *et al.*, 1979; Zidovetki, 1981, van Belzen *et al.*, 1988). *In vitro* studies performed with purified ErbB1 also suggested that EGF caused receptors to aggregate into dimers or higher order oligomers and that aggregation was necessary and sufficient for autophosphorylation, supporting a mechanism of activation that is dependent on inter-receptor interactions (Yarden & Schlessinger, 1987a, 1987b). Furthermore, the immunoprecipitation of stable ErbB1 receptor dimers from cells can be achieved in the

presence of EGF and covalent cross-linking reagents (Cochet *et al.*, 1988; Kashles *et al.*, 1991; Sorokin *et al.*, 1994). Further studies suggested that the kinetics of dimer formation (induced either by addition of EGF, cross-linking antibodies or chemical cross-linking agents) and the kinetics of receptor autophosphorylation were comparable (Spaargaren *et al.*, 1991; Canals, 1992; Mohammadi *et al.*, 1993) and that chemically cross-linked ErbB1 dimers bound EGF with higher affinity, and exhibited increased kinase activity, than ErbB1 monomers (Zhou *et al.*, 1993; Sorokin *et al.*, 1994). Critically, it was also shown that receptor phosphorylation can occur due to intermolecular cross-phosphorylation between receptors (Honegger, 1990a).

On the basis of these studies and concurrent studies on other receptor families (mainly human growth hormone receptor, hGHR, and PDGFR) the following model for the activation of RTKs was proposed: ligand binding to the RTK extracellular domain induces dimerisation of receptors, which brings the cytoplasmic tyrosine kinase domains into close proximity. Inter-receptor interactions activate the intrinsic kinase activity of the receptor, which allows the receptors to phosphorylate each other *in trans* at tyrosine residues within the intracellular domain (Ullrich & Schlessinger, 1990; Heldin 1995). To date, the exact mechanism via which the kinase activity of the EGF receptor kinase domain is invoked is unknown. Unlike other PTKs, the phosphorylation of a tyrosine in the activation loop of the kinase domain does not induce the kinase activity of ErbB1 (Hubbard & Till, 2000).

1.5.4 Signalling between receptors by heterodimerisation

ErbB2 was first identified as an 185 kDa proto-oncogene that has structural homology to ErbB1 and can transform fibroblasts (Schechter *et al.*, 1984; Drebin *et al.*, 1984). The receptor possesses a high level of kinase activity, yet no ligand which directly binds an ErbB2 homodimer has ever been identified. Cellular transformation by ErbB2 can be caused by an oncogenic mutation in the transmembrane region or receptor overexpression, both of which induce receptor aggregation and receptor phosphorylation (Hynes & Stern, 1994). The first evidence for heterodimer formation between ErbB family members was the finding that in the presence of ErbB1, ErbB2 can become phosphorlyated in an EGF-dependent manner (King *et al.*, 1988; Stern & Kamps, 1998) and that in the presence of covalent cross linking agents ErbB2 can be isolated in

complexes with ErbB1, in an EGF-dependent manner (Goldman *et al.*, 1990, Wada *et al.*, 1990). It appears that under normal physiological conditions ErbB2 activation requires heterodimerisation with another ligand-activated ErbB family member (Sliwkowski *et al.*, 1994; Kurunagaran *et al.*, 1996; Zhang *et al.*, 1996), involving a mechanism which does not appear to require the kinase activity of the ligand-activated partner, be it ErbB3 (Sliwkowski *et al.*, 1994) or ErbB1 (Spivak-Kroizman *et al.*, 1992; Deb *et al.*, 2001).

ErbB3 and ErbB4 were both identified by degenerate PCR approaches based on their homology to other ErbB family members (Plowman *et al.*, 1990; Plowman *et al.*, 1993). ErbB3 and ErbB4 hetero- and homo-dimers can act as functional receptors for the NRG ligands (Carraway *et al.*, 1994; Carraway & Cantley, 1994), however ErbB3 has impaired kinase activity (Guy *et al.*, 1994). Phosphorylation of ErbB3 in response to EGF or NRG requires the coexpression of ErbB1 or ErbB2/ErbB3/ErbB4, respectively. The intrinsically kinase-dead ErbB3 therefore appears to become activated by phosphorylation *in trans* due to hetero-dimerisation with a kinase-active ErbB receptor (Prigent & Gullick, 1994; Soltoff *et al.*, 1994; Kim *et al.*, 1994; Sliwkowski *et al.*, 1994; Carraway & Cantley, 1994).

Ligand-induced formation of every possible combination of ErbB family hetero-dimer has been demonstrated by experiments using radioactive ligand affinity labelling and/or co-immunoprecipitation in the presence of covalent cross-linking agents (Carraway & Cantley, 1994; Tzahar *et al.*, 1996). A hierarchy of preferential interactions exists: ErbB receptors appear to form more stable interactions with ErbB2 and the most stable heterodimeric species appears to be ErbB2-ErbB3 (Tzahar *et al.*, 1996; Karunagaran *et al.*, 1996; Graus-Porta *et al.*, 1997). In correlation with this, co-overexpression of ErbB2 and ErbB3 elicits a more potent mitogenic signal, and is associated with a higher potential for neoplastic transformation, than overexpression of either family member alone (Alimandi *et al.*, 1995; Karunagaran *et al.*, 1996). Numerous studies have shown qualitative and quantitative differences in downstream signalling events within cells expressing different combinations of ErbB receptors (Kokai *et al.*, 1989; Pinkas-Kramarski *et al.*, 1996; Zhang *et al.*, 1996; Olayioye *et al.*, 1998) and after stimulation with different ligands (Beerli & Hynes, 1996; Sweeney *et al.*, 2001), observations which have lead to the conclusion that combinatorial receptor interactions in the lateral plane of the membrane act as a signalling network to diversify the signalling

response (Lemmon & Schlessinger, 1994; Iris & Alroy, 1997; Riese & Stern, 1998; Olayioye *et al.*, 2000; Gullick, 2001).

1.5.5 The mechanism of RTK dimerisation

Ligand-induced dimerisation is the paradigm for the mechanism via which tyrosine-kinase linked receptors become activated in cells. Despite this fact, crystallographic data, and other evidence, show that the structure of cognate ligands and the mechansims via which they bind their receptors are suprisingly diverse. Some ligands are bivalent monomers which induce the formation of a receptor dimer by cross-linking receptors in a 1:2 ligand:receptor stoichiometry (e.g. human growth hormone, hGH; Wells, 1996) or 2:2 ligand:receptor stoichiometry (e.g. vascular endothelial growth factor, VEGF; Hubbard & Till, 2000). In the case of hGH, the ligand is thought to bind to a single receptor first and then dimerisation proceeds due to contacts formed by the ligand with a second receptor and the dimer is further stabilised by receptor-receptor contacts (Wells, 1996). Other ligands exist as dimers (e.g. PDGF; Fretto *et al.*, 1993) or trimers (e.g. TGF-β; Massague & Pandiella, 1993) and their multivalency dictates the number of receptors cross-linked. Finally, some ligands exist as monomers in solution and only become dimers when complexed with heparin, which is required for potent receptor dimerisation (e.g. fibroblast growth factor, FGF; Spivak-Kroizman, 1994; Plotnikov *et al.*, 1999, 2000). Structural analysis of ErbB ligands has prompted suggestions that they are bivalent monomers which could cross-link receptors in a mechanism similar to hGH (Tzahar *et al.*, 1997), but also that EGF forms dimers that could cross-link receptors in a mechanism similar to PDGF (Lu *et al.*, 2001).

Despite efforts by many groups, no crystal structure of the ErbB1 ligand binding domain complexed with ligand has been produced. The precise nature of the ligand-receptor, receptor-receptor interactions and the stoichiometry of the ligand-receptor interaction is therefore unclear. The most favourable model for ligand-receptor stoichiometry is based on detailed *in vitro* binding studies with the ErbB1 extracellular domain. A two-step mechanism has been proposed in which EGF binds to one receptor initially, forming a complex with a 1:1 ligand:receptor stoichiometry (Weber *et al.*, 1984). Two 1:1 complexes then associate to form a 2:2 complex (Lemmon *et al.*, 1997; Domagala *et al.*, 2000). Dimerisation is therefore predicted to be dependent on a bivalent

ligand which binds one receptor with high affinity and a second receptor with low affinity (Gullick, 1994; Tzahar *et al.*, 1997; Lemmon *et al.*, 1997). However, a recent FRET study in living cells suggested an alternative two-step model, in which ErbB1 monomers become cross-linked by a single EGF molecule (2:1 receptor-ligand stoichiometry) onto which a second EGF molecule is then recruited (Sako *et al.*, 2000). It has also been proposed that receptors exist already as pre-formed dimers and that ligand-binding induces a conformation change of the pre-formed dimers, which allows receptors to become phosphorylated (Gadella & Jovin, 1995; Bell *et al.*, 2000; Moriki *et al.*, 2001)

Several models have emerged concerning the role of the ligand in the formation of heterodimers. Studies on the structure and properties of native ErbB ligands, or chimeras consisting of domains from different ligands, prompted the proposal that ErbB ligands also mediate heterodimer formation by a bivalent interaction with two receptors (Fig. 1.10 A; Tzahar *et al.*, 1997). Other studies have shown that whilst purified ErbB extracellular domains can be induced to undergo ligand-induced homodimerisation, heteroassociation of isolated extracellular domains cannot be recapitulated *in vitro,* suggesting that bivalency of EGF ligands is insufficient to stabilise heteroassociation of receptors and that intracellular interactions may be involved (Ferguson *et al.*, 2000). Another model states that ligand binding induces the formation of a stable receptor homodimer, which recruits and activates two heterologous receptors in a heterotetrameric configuration (Fig. 1.10 B; Huang *et al.*, 1998; Schlessinger, 2000). Others have proposed that ligand binding induces the formation of a transient dimer (primary dimer) which dissociates, allowing the activated monomeric species to transiently dimerise with other monomeric ErbB species (secondary dimer), leading to the phosphorylation of the new receptor partner in the secondary dimer (Fig. 1.10 C; Gamett *et al.*, 1997).

1.5.6 Regulation of ErbB receptor phosphorylation state by PTP activity

Treatment of cells with PTP inhibiting compounds results in ligand-independent phosphorylation of ErbB receptors and downstream substrates (Jallal *et al.*, 1992; Knebel *et al.*, 1996). In fact, extensive ligand-independent tyrosine phosphorylation of cellular proteins after PTP inhibitor treatment is a well-known phenomenon (Heffetz *et al.*, 1990; Garcia-Morales *et al.*, 1990). The specific activity of PTPs for phosphotyrosine substrates is 10-1000 times higher than the specific activity of tyrosine kinases for their substrates

as determined *in vitro* (Fischer *et al.*, 1991). Furthermore, ligand-activated RTKs in intact cells undergo rapid dephosphorylation after kinase activity is inhibited pharmacologically (Bohmer *et al.*, 1995; Sorby & Ostman, 1996). These observations have established at least three important concepts: 1. in intact cells RTKs are kinase active, even in the absence of ligand, but are maintained in a state of low net phosphorylation by the superior catalytic activity of PTPs, 2. ligand binding to RTKs must act to reverse the equilibrium, such that kinase activity exceeds PTP activity, and 3. the phosphorylation level of a given protein is dependent on a balance between kinase activity and PTP activity.

It is clear then that PTP activity must be suppressed in order to allow maximal tyrosine phosphorylation of receptors and downstream substrates. The question of how ligand binding to RTKs induces PTP inhibition is beginning to be addressed. The stimulation of cells with a variety of biologically active ligands induces the formation of reactive oxygen species (ROS), such as the superoxide anion ($O.^-$) or nitric oxide (NO). ROS appear to constitute a novel form of diffusable second messenger which modulate the activity of proteins by oxidation of specific amino acid residues and have been implicated in the regulation of a variety of intracellular signalling pathways. ROS are proposed to inhibit PTPs by oxidising the thiol group of the active site cysteine residue to a non-reactive sulfenic acid group (Lander, 1997; Finkel, 2000; Rhee *et al.*, 2000). Furthermore, evidence has been presented which suggests that ROS-dependent inhibition of PTP activity is required for maximal receptor phosphorylation, and effective downstream signalling, after ligand stimulus of the EGF receptor (Bae *et al.*, 1997; Lee *et al.*, 1998), PDGF receptor (Sundaresan, 1995; Bae *et al.*, 2000) and insulin receptor (Mahadev *et al.*, 2001). Therefore, ROS appear to be good candidates for regulating the balance between RTK and PTP activity.

The identification of specific PTPs which negatively regulate signalling by specific RTKs has been performed by assessing phosphorylation of the receptor chain, and downstream signalling potency, within cells in which the expression of the PTP has been ablated by gene knock-out, suppressed by antisense techniques or via novel approaches such as the use of substrate trapping mutants (Ostman & Bohmer, 2001). These approaches have lead to the identification of five PTPs which can dephosphorylate ErbB1, i.e. LAR (Kulas *et al.*, 1996), PTP-1B (Flint *et al.*, 1997), SHP-1 (Keilhack *et al.*, 1998), RPTP-σ (Suarez Pestana *et al.*, 1999) and T-cell PTP (Tiganis *et al.*, 1999). To

date, there has been only one report identifying a PTP which dephosphorylates ErbB2 (prostatic acid phosphatase; Meng & Lin, 1998), but no reports identifying PTPs for ErbB3 or ErbB4 have been published.

1.5.7 ErbB agonist-independent phosphorylation of ErbB1

A variety of other proteins and stimuli have been shown to induce stable ErbB1 phosphorylation, demonstrating that binding of an agonist to the receptor is not the only means via which receptor phosphorylation is achieved. For example, treatment of cells with arsenite, sulfhydryl reagents, UV irradiation, gamma irradiation, oxidants, heat shock and hyperosmotic or membrane depolarising conditions all induce ErbB1 phosphorylation. In most cases the mechanisms are not clear, whilst some of these effects may be attributed to PTP inhibition (Carpenter, 1999).

Phosphorylation of ErbB1 can occur via Src, which phosphorylates ErbB1 at all the known autophosphorylation sites and at an additional four novel sites that are: Y845, Y891, Y920 and Y1101 (Fig. 1.1; Olayioye *et al.*, 2000) and evidence has been presented which supports a role for Src in the transactivation of ErbB1 downstream of the activation of other receptors (Thomas & Brugge, 1997). There may be a number of PTKs present in the cell which can phosphorylate ErbB family members. There have also been some reports identifying a role for integrin activation in inducing or potentiating ErbB1 phosphorylation, but the mechanisms involved are unclear (Carpenter, 1999).

Stimulation of cells with a variety of ligands which bind to GPCRs can induce ErbB1 tyrosine phosphorylation and subsequent activation of the MAPK and other downstream pathways (Luttrell *et al.*, 1999). It had been thought that this occurred via an exclusively intracellular signalling pathway, but it is becoming increasingly clear that the metalloproteinase-mediated cleavage of surface-bound EGF agonists is involved (Gschwind *et al.*, 2001). Stimulation of RTKs from outside the ErbB family may also result in ErbB phosphorylation, i.e. PDGFR stimulation (Countaway *et al.*, 1989; Saito *et al.*, 2001).

The ErbB1 intracellular domain also contains sites which can be phosphorylated by serine / threonine kinases, such as PKC or protein kinase D (PKD). Threonine phosphorylation has been shown to mediate a number of effects on the receptor including decreased ligand-binding affinity (Downward *et al.*, 1985), attenuation of capability to

elicit downstream signalling (Bagowski *et al.*, 1999) and inhibition of receptor degradation following internalisation (Lund *et al.*, 1990; Bao *et al.*, 2000)

1.5.8 Endosomal trafficking of ErbB1

Ligand binding to ErbB1 receptors is shortly followed by internalisation of ligand-receptor complexes within small clathrin-coated vesicles, a process that requires the kinase activity of the receptor and phosphorylation of the intracellular domain (Honegger, 1990b; Sorkin *et al.*, 1992). The internalised receptors proceed to accumulate in large multivesicular bodies, which then fuse with the lysosomes, with little or no receptor recycling back to the cell surface occuring (Miller *et al.*, 1986; Futter *et al.*, 1996). In contrast, the steady state distribution of ErbB2, ErbB3 and ErbB4 after ligand stimulus is predominantly on the cell surface, suggesting that they are internalisation impaired or undergo increased recycling back to the plasma membrane after ligand stimulation. (Baulida *et al.*, 1996; Waterman *et al.*, 1998). Furthermore, the stable heterodimerisation of ErbB1 with ErbB2 allows ErbB1 to recycle back to the plasma membrane, thereby delaying its delivery to the lysosome (Lenferink *et al.*, 1998).

The assembly of the endocytic machinery and the fate of ErbB1 during endocytosis is at least partially co-ordinated through the receptor itself, by tyrosine phosphorylation events and through the association of phosphotyrosine binding proteins with the receptor (Carpenter, 2000; Waterman & Yarden, 2001). For example, the formation of the clathrin coat requires the activity of the Eps15 and Eps15R proteins, which must become tyrosine phosphorylated by the receptor in order for endocytosis to proceed (Carpenter, 2000). Likewise, it has been demonstrated that the activation of Src tyrosine kinase activity by ErbB1 is necessary for receptor endocytosis, which is probably because Src phosphorylates clathrin heavy chains, thereby initiating the clathrin coat formation (Wilde *et al.*, 1999). Once the receptor has been endocytosed, other proteins associated with the receptor mediate roles in the regulation of receptor trafficking and down-regulation. For example, Cbl associates with Y1045 of the activated EGF receptor via its SH2 domain and becomes phosphorylated by the receptor at Y371. This allows Cbl to mediate ubiquitination of the receptor, which must target it for degradation by the proteasome (Carpenter, 2000).

The internalisation of ErbB1 receptors is generally considered to mediate downregulation of ErbB1 signalling capacity by clearing receptors from the surface and by degradation. However, accumulating evidence suggests that endosome-localised receptors continue to mediate downstream signalling and some reports have suggested that endocytosis is actually required to achieve full activation of the MAPK pathway (Carpenter, 2000). The mechanisms which regulate receptor trafficking, and the role of receptor internalisation in determining the quality and quantity of ErbB signalling are both, as yet, incompletely understood processes.

1.6 Aims of this thesis

The signalling network of the cell is regulated by stimuli which are received through receptors, such as the ErbB family of RTKs. Tyrosine phosphorylation of these receptors correlates with the ability to elicit downstream signalling and can therefore be regarded as an indicator of receptor activation. The tyrosine phosphorylation status of the ErbB receptors is subject to modulation by extensive cross talk with other receptors, both within the ErbB family and outside of it, including other RTKs and GPCRs. Receptor activity is also modulated by direct phosphorylation by PTKs and serine / threonine kinases and by receptor trafficking and cell adhesion. It is also clear that phosphorylation state is critically dependent on a balance between tyrosine kinase activity and protein tyrosine phosphatase activity. Deregulated ErbB signalling is implicated in a number of disease states including cancers. Therefore, an improved understanding of the means via which ErbB receptor signalling is modulated may be useful for rational drug design. Now that many of the fundamental players involved in receptor function are identified, the way is clear for the application of novel biophysical methods to gain new insight into mechanisms of receptor activation.

In this area, the application of FRET measurements may prove to be a powerful tool, allowing biochemical activity to be viewed within intact cells. This has at least two advantages: 1. biochemical reactions can be resolved temporally and spatially in living cells providing information on signalling dynamics, and 2. the cellular context of the reaction under consideration is preserved. This laboratory has designed FRET-based assays to assess ErbB signalling in cells. The ongoing aim is to use these and other

functional fluorescence assays to further elucidate the mechanisms of RTK activation in cells, using the ErbB family as a model system.

Extensive evidence has been provided for the role of receptor dimerisation in mediating receptor crosstalk. Direct ligand binding to an individual receptor subtype can lead to phosphorylation of other members of the ErbB family, which is currently thought to be mediated by transphosphorylation in stable receptor dimers. Dimerisation therefore appears to mediate diversification of signals in the plane of the membrane, by allowing the phosphorylation of ligand-unoccupied receptors. Given this fact, it was considered feasible that the delivery of growth factor locally to cells, rather than homogeneously, should potentiate spread of phosphorylation in the lateral plane of the membrane via transphosphorylation, thus mediating signal amplification. Here, in order to test this prediction, cells are stimulated with EGF that is covalently attached to 0.8 μm diameter latex beads and the spatial extent of receptor phosphorylation is followed using a FRET-based phosphorylation assay. Evidence is provided to suggest that receptor phosphorylation is amplified in the plane of the membrane via a mechanism that requires protein tyrosine phosphatase (PTP) inhibition by reactive oxygen species (ROS) production.

Table 1.1 Modular protein domains involved in protein-protein interactions

Domain	Protein motif recognised	Comments
SH2	pY-X-X-hy	Specificity of recognition by SH2 domains is mediated by hydrophobic amino acids that lie 3-5 residues C-terminal to the pY.
PTB	N-P-X-pY	Specificity of recognition by PTB domains is mediated by hydrophobic amino acids that lie 5-8 residues N-terminal to the pY.
14-3-3	R-S-X-pS-X-P	Phosphoserine motif recognition.
SH3	P-X-X-P-X	Tyrosine phosphorylation of a serine residue within an SH3 recognition motif may result in uncoupling of SH3 binding.
WW	P-P-X-Y or P-P-L-P	Recognises proline-rich sequences.
PDZ	e.g. -E-S/T-D-V-COOH	PDZ binding motif must lie adjacent to the C-terminus of the protein. Specificity of recognition is conferred by amino acids that lie 2-4 residues N-terminal to the protein's C-terminus.

Single letter amino acid code is used. Abbreviations: COOH, free C-terminal carboxylate group; hy, hydrophobic residue; PDZ, post-synaptic density 95 kDa protein, *D. melanogaster* discs large protein and zonula occludens 1 protein; pS, phosphoserine; PTB, phosphotyrosine binding; pY, phosphotyrosine; SH2, Src homology 2; SH3, Src homology 3; X, any amino acid. Protein sequences are presented in the N-to-C terminal orientation. Adapted from Pawson & Scott, 1997.

Table 1.2 Modular protein domains involved in protein-lipid interactions

Domain	PtdIns species recognised	Comments
PH	Group I - PtdIns (3, 4, 5) P_3 Group II- PtdIns (4, 5) P_2 Group III- PtdIns (3, 4) P_2, PtdIns (3, 4, 5) P_3 Group IV- Low affinity for PtdIns	At least four different types of PH domain identified on basis of differing PtdIns binding preferences.
FYVE	PtdIns 3P	Highly selective for PtdIns 3P binding.
ENTH	PtdIns (4, 5) P_2	Highly selective for PtdIns (4, 5) P_2 binding.
PX	PtdIns 3P, PtdIns (3, 4) P_2, PtdIns (3, 4, 5) P_3	Broad specificity for 3-OH phosphorylated lipids.

Abbreviations: ENTH, epsin N-terminal homologue; FYVE, (Fab1p, YOTB, Vac1p and EEA1) homology; PH, pleckstrin homology; PtdIns, phosphatidylinositol; PX, Phox homology. Adapted from Xu *et al.*, 2001.

Table 1.3 **Theoretical R_0 values for GFP spectral variants and Cy dyes as donor-acceptor fluorophore pairs**

		Acceptor					
		ECFP	**EGFP**	**EYFP**	**Cy3**	**Cy3.5**	**Cy5**
Donor	**ECFP**	n.d	4.65	4.87	n.d.	n.d.	n.d.
	EGFP		4.61	5.47	6.0	5.7	n.d.
	EYFP			5.05	n.d.	n.d	n.d.
	Cy3				4.4	5.1	5.3
	Cy3.5					4.6	6.4

Abbreviations: ECFP, enhanced cyan fluorescent protein; EGFP, enhanced green fluorescent protein; EYFP, enhanced yellow fluorescent protein; n.d., not determined. Adapted from Harpur & Bastiaens, 2001.

Figure 1.1 Receptor tyrosine kinase structure and function

A. The classical receptor tyrosine kinase consists of an extracellular ligand binding domain (dark blue), a short α-helical transmembrane sequence (yellow) and an intracellular domain which contains a tyrosine kinase domain, phosphorylation sites and other regulatory sequences (red). **B.** Binding of ligand (purple) initiates clustering of receptors and phosphorylation of intracellular tyrosine residues by the receptors' kinase domains. **C.** Phosphorylated tyrosines (Y-P) provide docking sites for the binding of downstream signalling effectors (cyan blue), which mediate downstream signalling. **D.** Schematic showing the intracellular phosphotyrosine binding sites for signalling effectors; sites present within all four members of the ErbB RTK family are shown. Note that autophosphorylation sites within ErbB1 and ErbB2 have been identified by phosphopeptide mapping, but phosphopeptide analysis of ErbB3 and ErbB4 have not been reported and phosphotyrosine site designations are based mostly on phosphopeptide-binding competition studies. Grey-shaded residues in ErbB1 indicate sites phosphorylated uniquely by the Src PTK. Panel **D** is adapted from Olayioye *et al.*, 2000, and the appropriate references for information depicted in the figure are also contained in this article.

Fig. 1.1

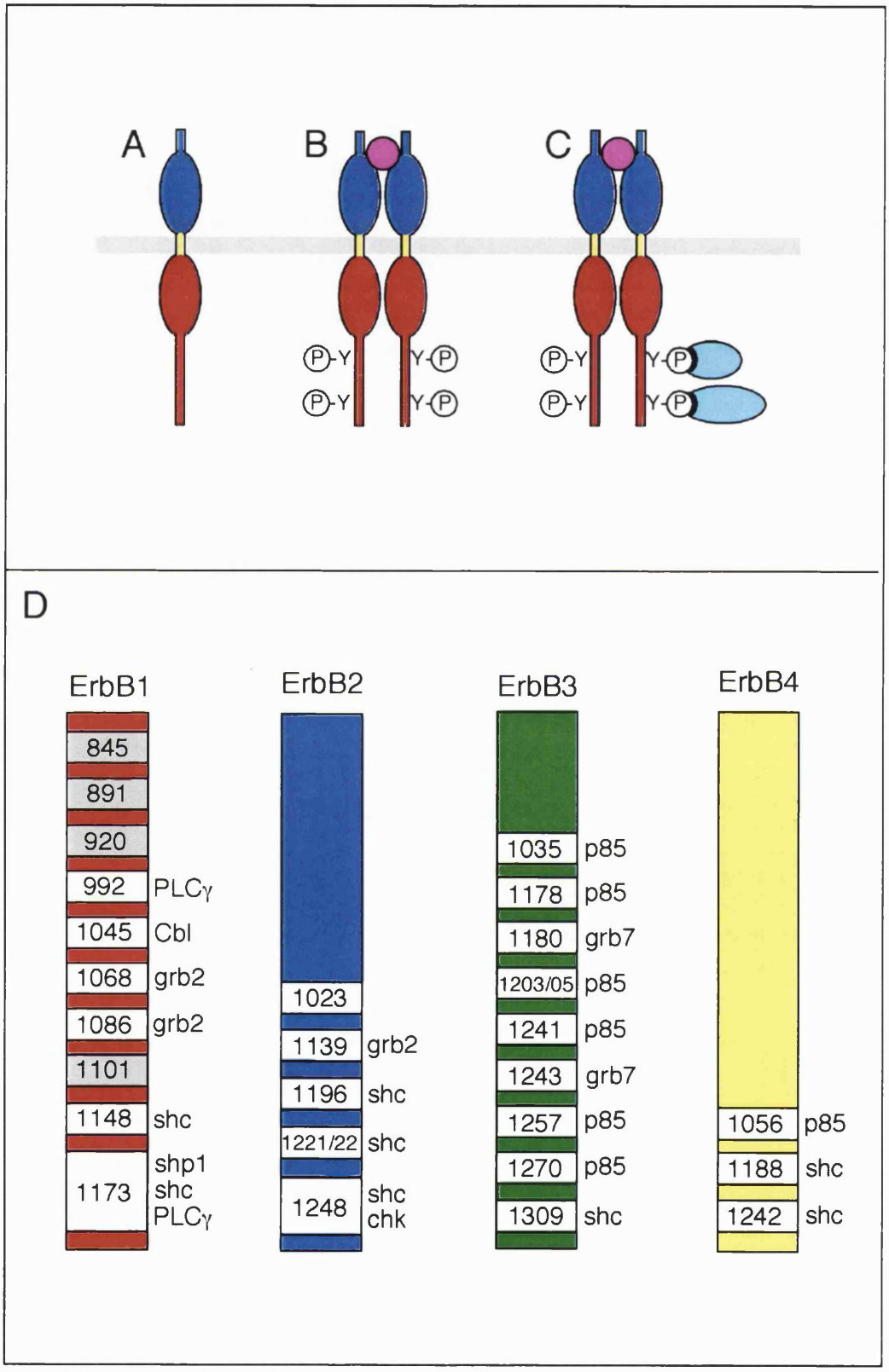
A
B
C
P-Y
Y-P
D
ErbB1
845
891
920
992 PLCγ
1045 Cbl
1068 grb2
1086 grb2
1101
1148 shc
1173 shp1 shc PLCγ
ErbB2
1023
1139 grb2
1196 shc
1221/22 shc
1248 shc chk
ErbB3
1035 p85
1178 p85
1180 grb7
1203/05 p85
1241 p85
1243 grb7
1257 p85
1270 p85
1309 shc
ErbB4
1056 p85
1188 shc
1242 shc

Figure 1.2 Examples of downstream signalling pathways that emanate from receptor tyrosine kinases
The phosphorylated RTK (yellow) activates downstream signalling proteins (cyan blue) by recruitment to receptor phosphotyrosine residues (Y-P) and / or by direct phosphorylation (red curly arrows). Examples of signalling connections between downstream proteins and substrates are indicated by black arrows. See main text for further details.

Fig. 1.2

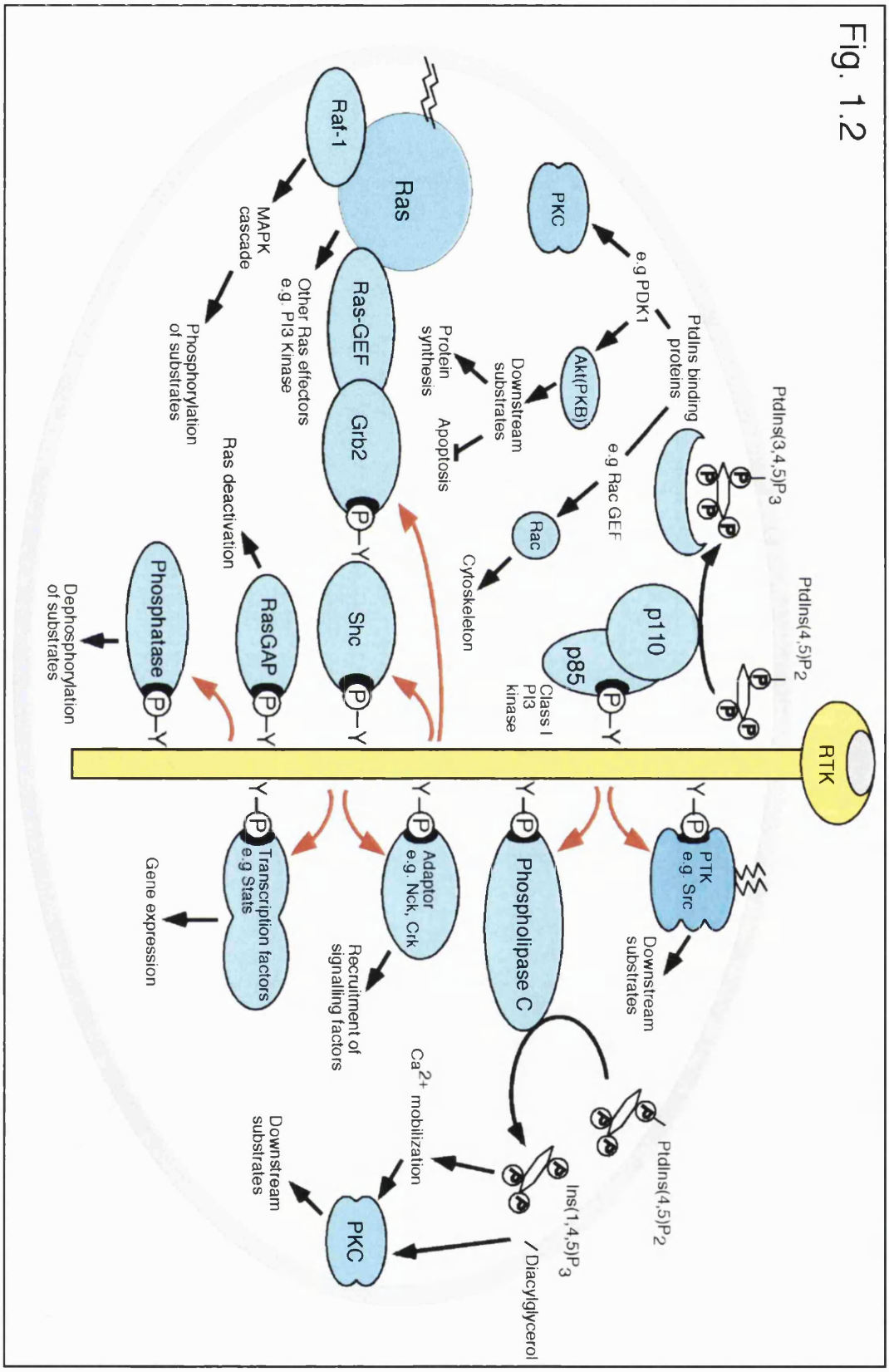
PtdIns(3,4,5)P3
PtdIns(4,5)P2
RTK
PKC
e.g PDK1
PtdIns binding proteins
Akt(PKB)
e.g Rac GEF
p110
p85
Class I PI3 kinase
Protein synthesis
Downstream substrates
Apoptosis
Rac
Cytoskeleton
Raf-1
Ras
MAPK cascade
Ras-GEF
Other Ras effectors e.g. PI3 Kinase
Grb2
Phosphorylation of substrates
Ras deactivation
RasGAP
Shc
Phosphatase
Dephosphorylation of substrates
PTK e.g. Src
Downstream substrates
Phospholipase C
PtdIns(4,5)P2
Ins(1,4,5)P3 / Diacylglycerol
Ca2+ mobilization
Downstream substrates
PKC
Adaptor e.g. Nck, Crk
Recruitment of signalling factors
Transcription factors e.g Stats
Gene expression

Figure1.3 Physical basis of excited state-reactions

A. Jablonski diagram of FRET donor and acceptor chromophores. Illustrates transitions between electronic and vibrational energy levels that can occur in a fluorophore and excited state reactions which may depopulate the excited state, including fluorescence resonance energy transfer. See main text for details. **B.** Graph depicting exponential fluorescence decays of fluorophores. The decays for two fluorophores are shown: one with a long (τ_1, solid curve), and one with a shorter fluorescence lifetime (τ_2, dashed curve). The fluorescence lifetime (τ) is defined as the time taken for the fluorescence intensity to fall from its initial value (F_0) to 1/e of its initial value (~37%F_0).

Fig. 1.3

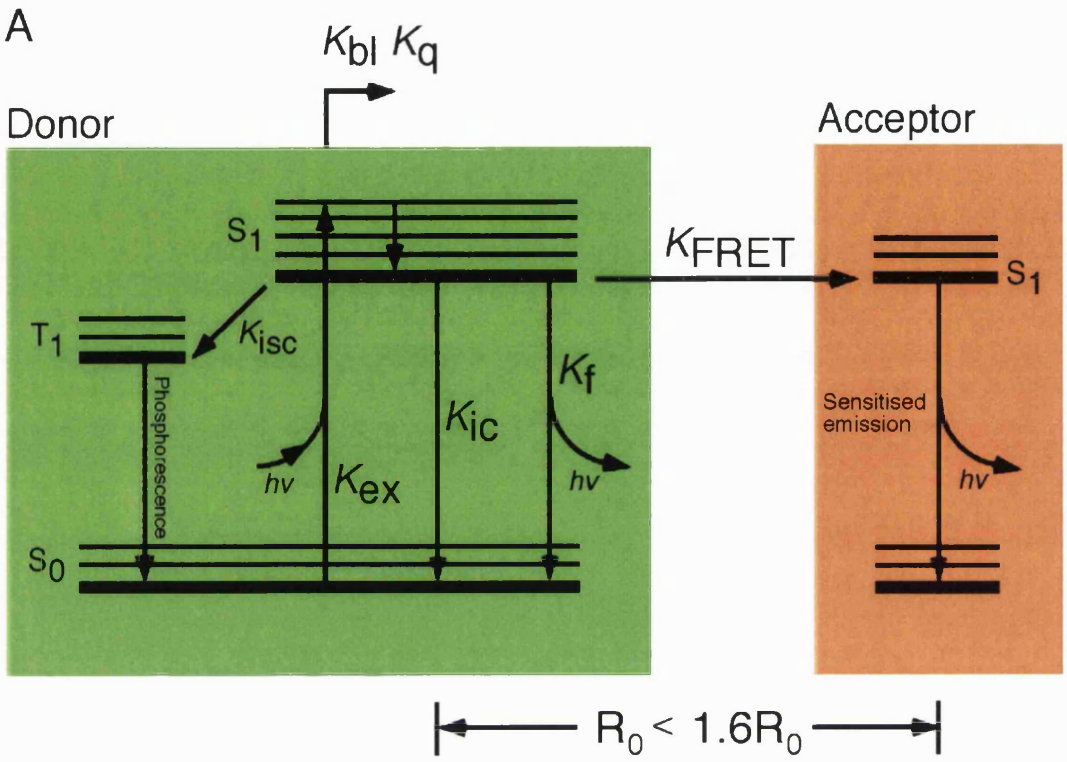
A
K_{bl} K_q
Donor
Acceptor
S_1
K_{FRET}
S_1
T_1
K_{isc}
K_f
K_{ic}
Sensitised emission
Phosphorescence
hv
K_{ex}
hv
hv
S_0
$R_0 < 1.6R_0$

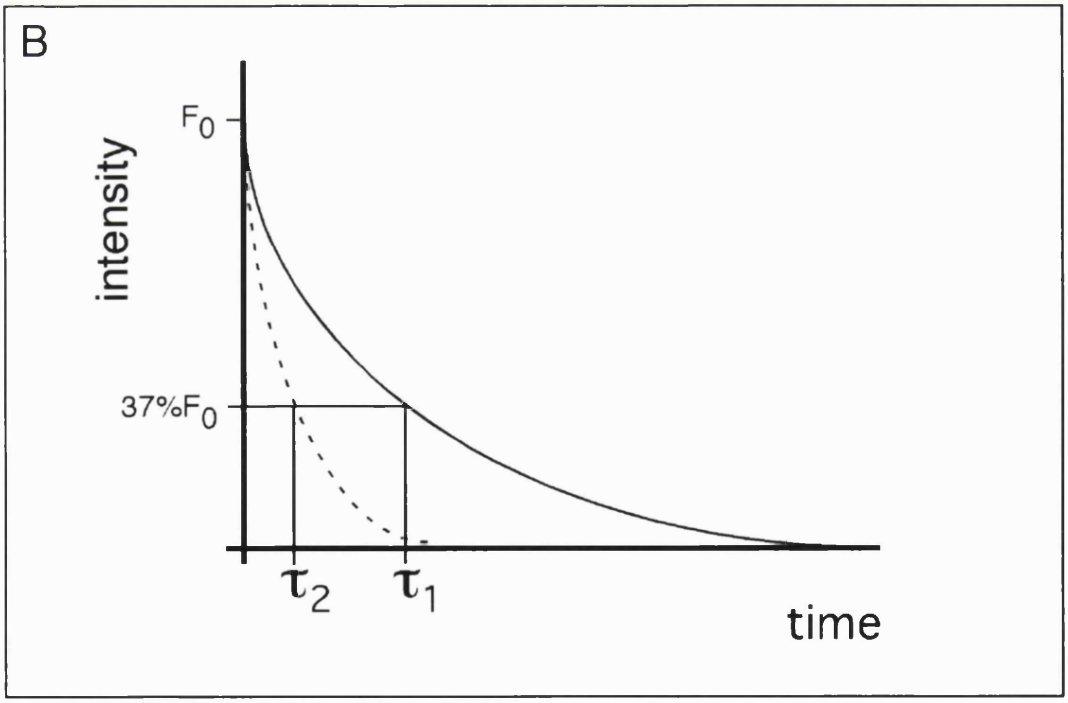
B
F_0
intensity
37%F_0
τ_2
τ_1
time

Figure 1.4 Parameters related to the use of FRET as a spectroscopic probe of biochemical reactions

A. Distance relationship of FRET efficiency. Fluorophore seperation distance is given in units of R_0. **B.** Graph to demonstrate the relationship between protein molecular weight and protein radius (for a spherical protein). Calculation is based on the assumption that the protein is a perfect sphere, with a specific volume per unit mass of 0.74 cm^3/gm and so protein radius (r) in nm can be calculated by substituting the molecular weight into the equation:

$$r = (6.76 \times 10^{-2}) \times (\sqrt[3]{MW})$$

where MW is the molecular weight of the protein in Daltons. **C.** Alignment of CFP emission spectrum (solid line) and YFP absorbtion spectrum (dashed line) to demonstrate spectral overlap of a typical donor-acceptor FRET pair (grey shading). Spectra are from enhanced CFP and enhanced YFP spectral variants, commercially available in plasmid vectors from Clontech.

Fig. 1.4

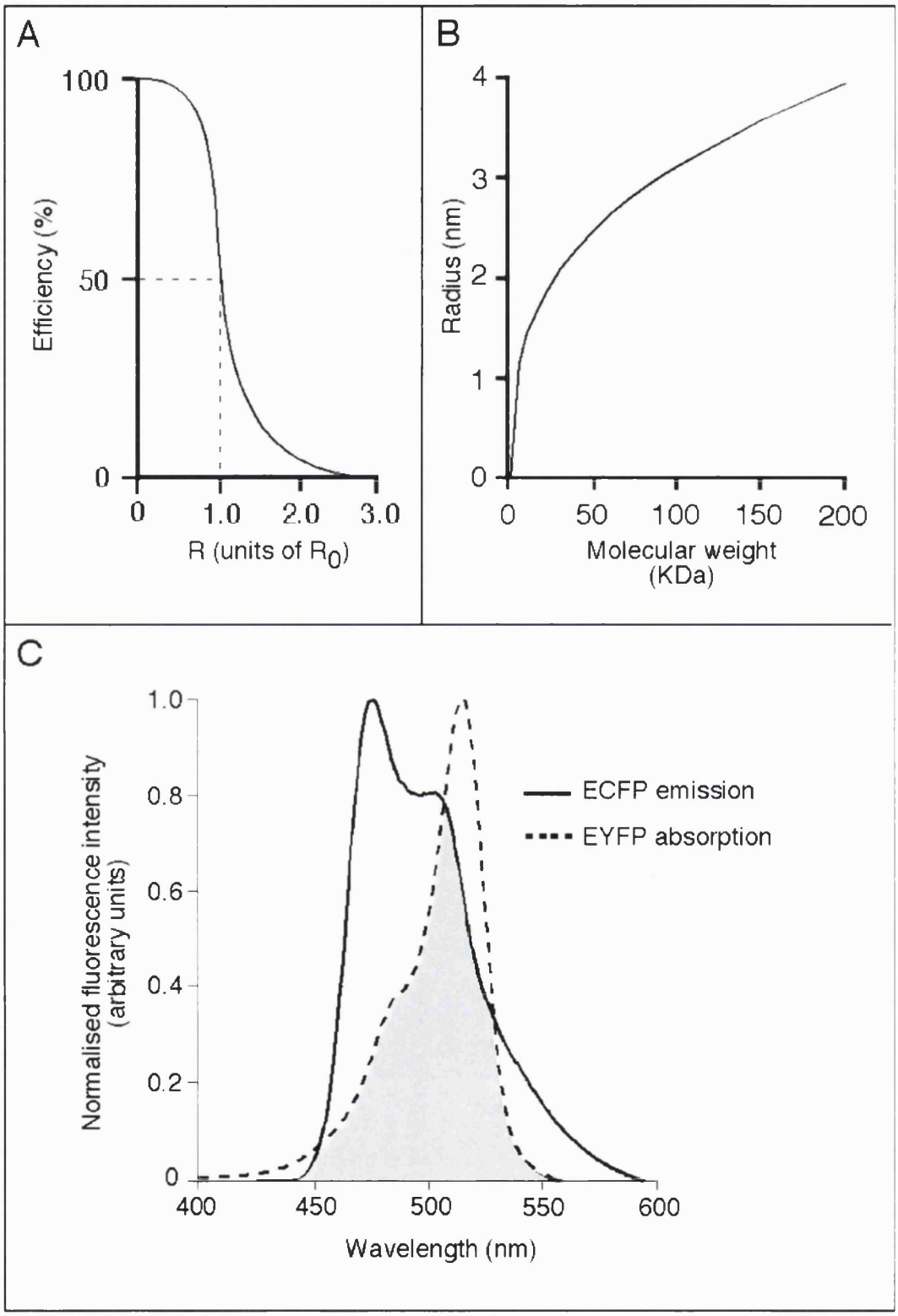
A
100
50
0
Efficiency (%)
0
1.0
2.0
3.0
R (units of R_0)
B
4
3
2
1
0
Radius (nm)
0
50
100
150
200
Molecular weight
(KDa)
C
1.0
0.8
0.6
0.4
0.2
0
Normalised fluorescence intensity
(arbitrary units)
ECFP emission
EYFP absorption
400
450
500
550
600
Wavelength (nm)

Figure 1.5 Generic designs for FRET-based biochemical activity assays

Schemes for various generic FRET-based assays that utilise the fusion of protein moieties to donor and acceptor fluorophores. Donor fluorophores (D, green icons) acceptor fluorophores (A, orange icons), protein molecules / peptide sequences (black lines, grey icons and blue icons), small ligand or ion (blue sphere), proteolytic enzyme (scissors icon) and donor-acceptor FRET (curly arrow). In each example, the sensor is presented as an equilibrium reaction with the biochemically 'inactive' sensor conformation on the left and the 'active' conformation on the right. The exception is that the cleavage reaction is a unidirectional reaction. **A.** Method for detecting protein-protein interactions where one protein species is labelled with a donor fluorophore and the other with an acceptor fluorophore. Equally valid is the use of fluorophore-conjugated antibodies instead. **B.** Method for detecting protein homo-oligomerisation, where the same protein species is labelled with a donor or acceptor fluorophore and both types of conjugated protein are present in the same cell. **C.** Method for detecting changes in the concentration of a small ligand or ion. A protein moiety, that changes conformation upon ligand-binding, is fused between donor and acceptor fluorophores. Ligand binding will change the proximity of the attached donor and acceptor fluorophores. **D.** Method for detecting binding activity of a protein. Proteins are fused to donor and acceptor fluorophores in the configuration: donor - protein X - protein Y – acceptor. Changes in the affinity of protein X for protein Y will change the proximity of the attached donor and acceptor fluorophores. **E.** Method for detecting proteolytic activity. Donor and acceptor are fused through a short linker sequence which contains the recognition sequence for a proteolytic enzyme. Cleavage results in separation of the donor and acceptor fluorophores. **F.** Method for detecting covalent protein modifications. Protein is labelled with donor fluorophore and covalent modification is detected with acceptor-conjugated antibody, which brings the acceptor into range of the donor.

Fig. 1.5

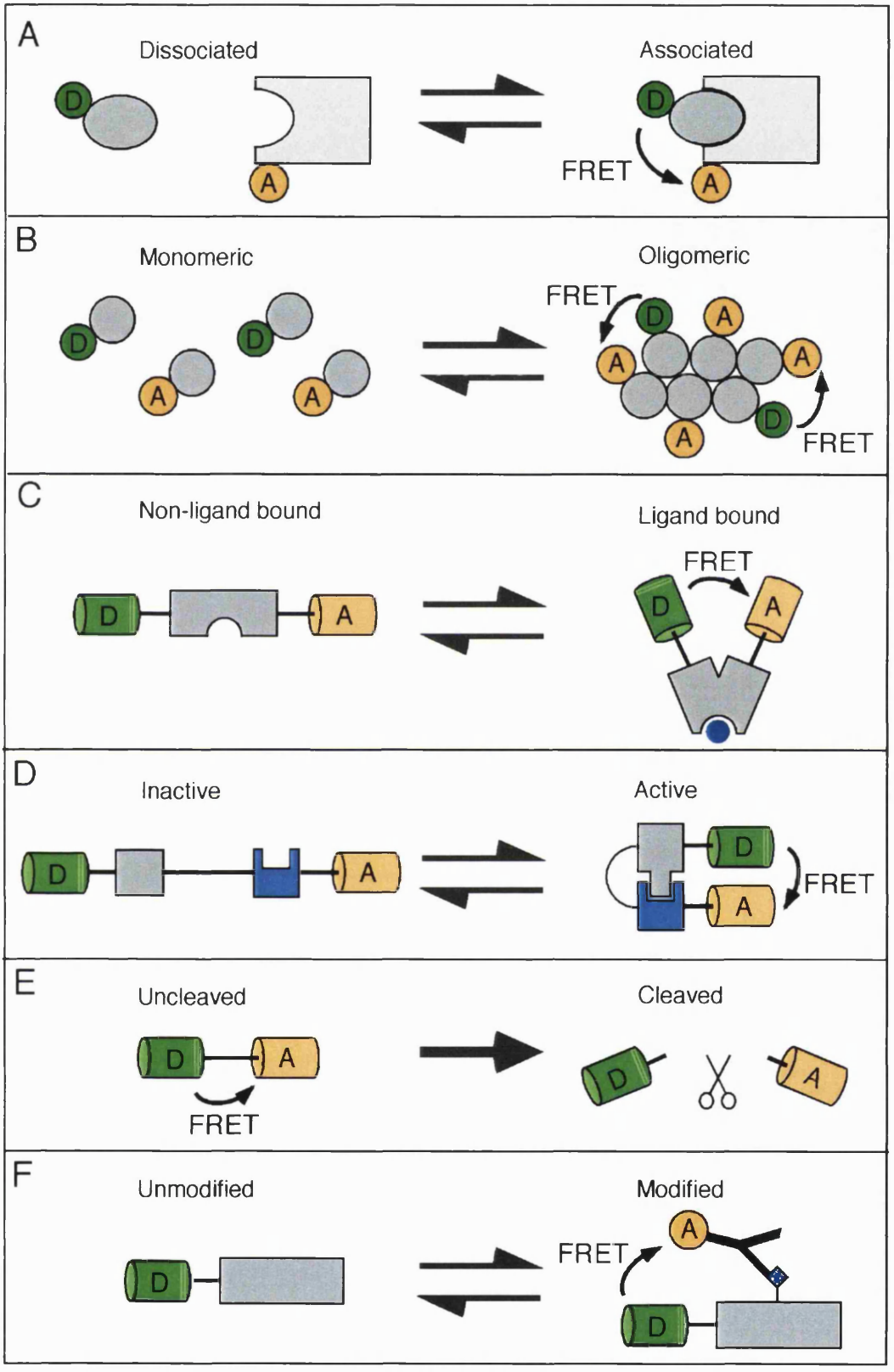
A
Dissociated
Associated
D
A
FRET
B
Monomeric
Oligomeric
FRET
FRET
C
Non-ligand bound
Ligand bound
FRET
D
Inactive
Active
FRET
E
Uncleaved
Cleaved
FRET
F
Unmodified
Modified
FRET

Figure 1.6 Principles behind time-domain and frequency-domain FLIM measurements

Fluorescence lifetimes are generally determined by utilising one of two methodologies: time-domain FLIM measurements or frequency-domain FLIM measurements (Lacowicz, 1999). For each method the means of excitation is illustrated on the left and a typical fluorescence emission profile is shown on the right, where $I(t)$ is intensity as a function of time and t is time. **A.** In time-domain FLIM measurements the sample is excited with a pulse of light and the fluorescence decay is sampled by using gated detection. In the case of an exponential decay the average fluorescence lifetime is determined by measuring the time taken for the fluorescence to fall to $1/e$ of its initial value ($37\%F_0$; see also Fig 1.3 B). **B.** In frequency-domain FLIM measurements the sample is excited with a sinusoidally modulated light source. The fluorescence emission is also sinusoidal, but is phase-shifted and reduced in amplitude (demodulated) with respect to the excitation sinus wave. Two determinations of the average fluorescence lifetime of the sample can be calculated by measuring the phase shift and the depth of the demodulation at a single excitation frequency. The phase shift ($\Delta\phi$) is related to the lifetime by equation [6] (see main text). The demodulation (m) can be calculated by substituting the geometric parameters A, B, b and a into equation [8] (see main text). The demodulation is related to the lifetime by equation [7] (see main text).

Fig. 1.6

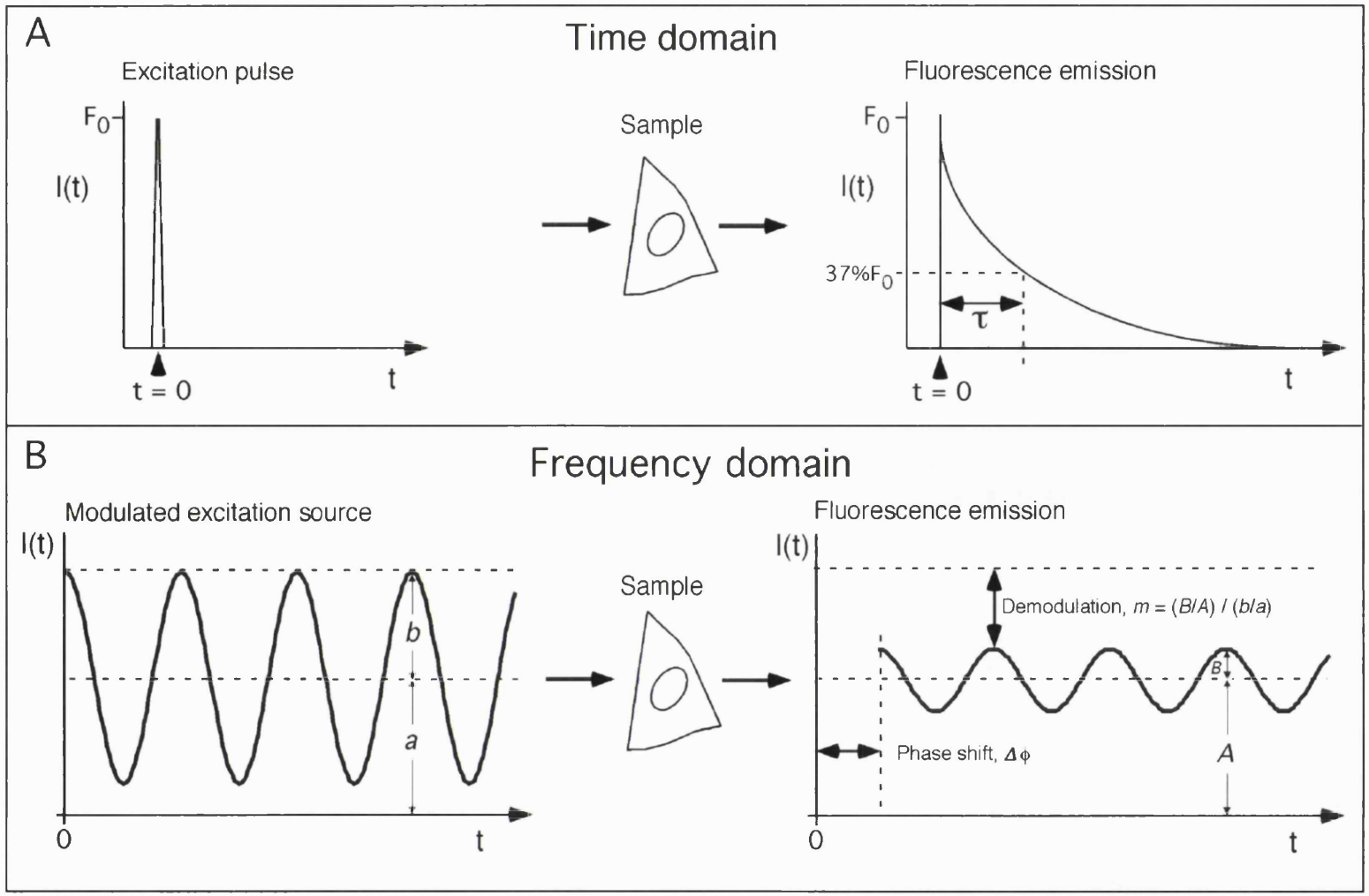
A
Time domain
Excitation pulse
F0
I(t)
t = 0
t
Sample
Fluorescence emission
F0
I(t)
37%F0
τ
t = 0
t
B
Frequency domain
Modulated excitation source
I(t)
b
a
0
t
Sample
Fluorescence emission
I(t)
Demodulation, m = (B/A) / (b/a)
B
Phase shift, Δφ
A
0
t

Figure 1.7 Homodyne detection using an image intensifier in a light microscope
A. In frequency domain FLIM, the light which excites the sample is sinusoidally modulated using a standing wave acousto-optic modulator (SW-AOM). The incident light from the sample (fluorescence emission) is collected by a specialised detector which contains two components: a photocathode surface, which acts as a signal mixing device, and a microchannel plate (MCP), which acts as an image intensifier. The photocathode surface amplifies the incident light signal using an input voltage as a reference signal. The output from the photcathode is therefore proportional to the incident light intensity multiplied by the amplitude of the reference signal. In homodyne detection the voltage across the photocathode (the reference signal) is modulated at the same frequency as the light used to excite the sample, using phase locked frequency generators, allowing mixing of the signals. The resulting output from the photocathode is then further amplified through the capillaries of the MCP. The output from the MCP then strikes a phosphor screen which, because it has a slow response time, filters out high frequency oscillations. This leaves only a signal which is dependent on the phase difference between the emitted fluorescence of the sample and the reference signal, and is proportional to the amplitudes of both signals. This signal is then captured as an image on a charge-coupled device (CCD) camera. **B.** The waveforms of the fluorescence emission, $F(t)$, and the modulated MCP gain, $G(t)$, can be described by functions incorporating terms for the AC (a_F, a_G), DC (d_F, d_G), frequency (ω), time (t) and phase (ϕ_F, ϕ_G) components of the sinus waves. Mixing of these signals at the detector (see also **A**) results in an output which contains, 1. a high frequency component (tens to hundreds of MHz) consisting of DC, ω and t terms, and 2. a low frequency component that is independent of ω and t and contains only DC terms and the phase difference ($\Delta\phi$) between $F(t)$ and $G(t)$. Low pass filtering of this signal (by the phosphor screen, see also **A**) removes the high frequency component, transmitting only the low frequency component to the CCD camera, where it is recorded as a single intensity value (homodyne component) at each pixel of a single image. By phase-stepping the modulated gain of the MCP, and taking an image at every phase-step, the phase-dependent intensity (homodyne component) of the fluorescence emission can be measured at each pixel (see also Fig 1.8). The phase shift and demodulation at every pixel can be extracted from the phase-dependent intensities by Fourier transform.

Fig. 1.7

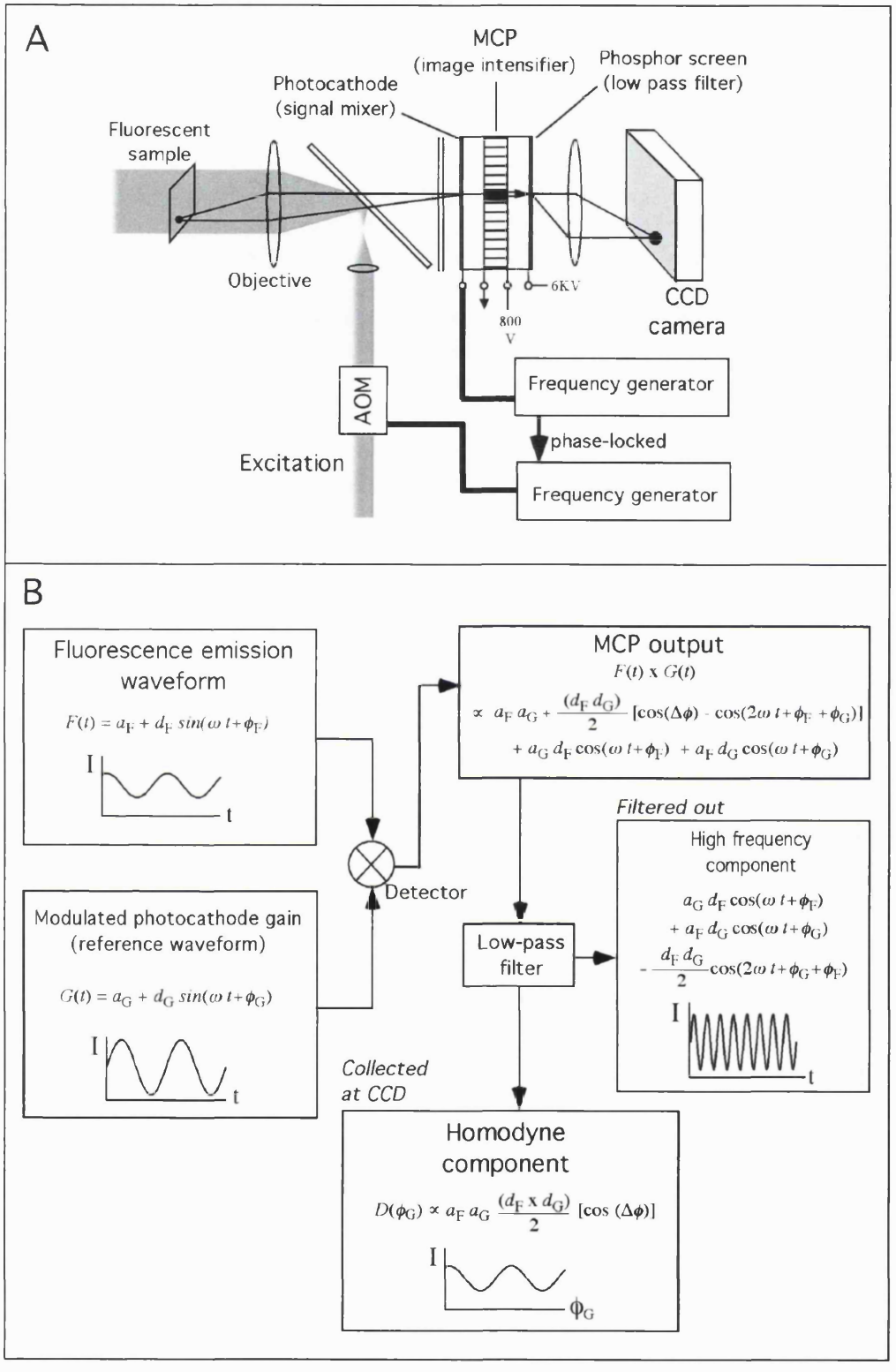
A
MCP
(image intensifier)
Phosphor screen
(low pass filter)
Photocathode
(signal mixer)
Fluorescent
sample
Objective
6KV
800
V
CCD
camera
AOM
Frequency generator
phase-locked
Excitation
Frequency generator
B
Fluorescence emission
waveform
$F(t) = a_F + d_F\, sin(\omega t+\phi_F)$
I
t
MCP output
$F(t)$ x $G(t)$
$\propto a_F a_G + \frac{(d_F d_G)}{2}[\cos(\Delta\phi) - \cos(2\omega t+\phi_F+\phi_G)]$
$+ a_G d_F \cos(\omega t+\phi_F) + a_F d_G \cos(\omega t+\phi_G)$
Filtered out
High frequency
component
$a_G d_F \cos(\omega t+\phi_F)$
$+ a_F d_G \cos(\omega t+\phi_G)$
$-\frac{d_F d_G}{2}\cos(2\omega t+\phi_G+\phi_F)$
Detector
Low-pass
filter
Modulated photocathode gain
(reference waveform)
$G(t) = a_G + d_G\, sin(\omega t+\phi_G)$
Collected
at CCD
Homodyne
component
$D(\phi_G) \propto a_F a_G \frac{(d_F \text{ x } d_G)}{2}[\cos(\Delta\phi)]$
ϕ_G

Figure 1.8 Basic principle of phase-dependent homodyne detection

A. Each graph can be assumed to represent 1 pixel within a single phase-dependent image of a FLIM series. The sinusoidally modulated detector gain is phase-shifted, with respect to the excitation sinus wave, by a fixed angle for each image in a FLIM data series (left hand column). For illustrative purposes, only four phase steps, with a fixed angle of 90° per step, are shown. The mixing of the signal with the fluorescence emission wave (middle-left column) at the MCP, combined with low pass filtering at the phosphor screen (middle-right column), produces a single intensity value at each pixel (right hand column). By phase-stepping the detector gain a phase-dependent intensity series at each pixel is generated across the image series, which is plotted in **B.** Note that the intensities recorded at each phase step (y-axis, right hand column, **A**) produce a sinusoid when plotted against the corresponding phase step (x-axis, **B**). For clarity, each phase-dependent signal shown in **A** is indicated as a box superimposed onto the waveform in **B.** The same data is recorded at every pixel of each image in the FLIM series. The phase shift and demodulation at every pixel can then be extracted from the phase-dependent intensities by Fourier transform.

Fig. 1.8

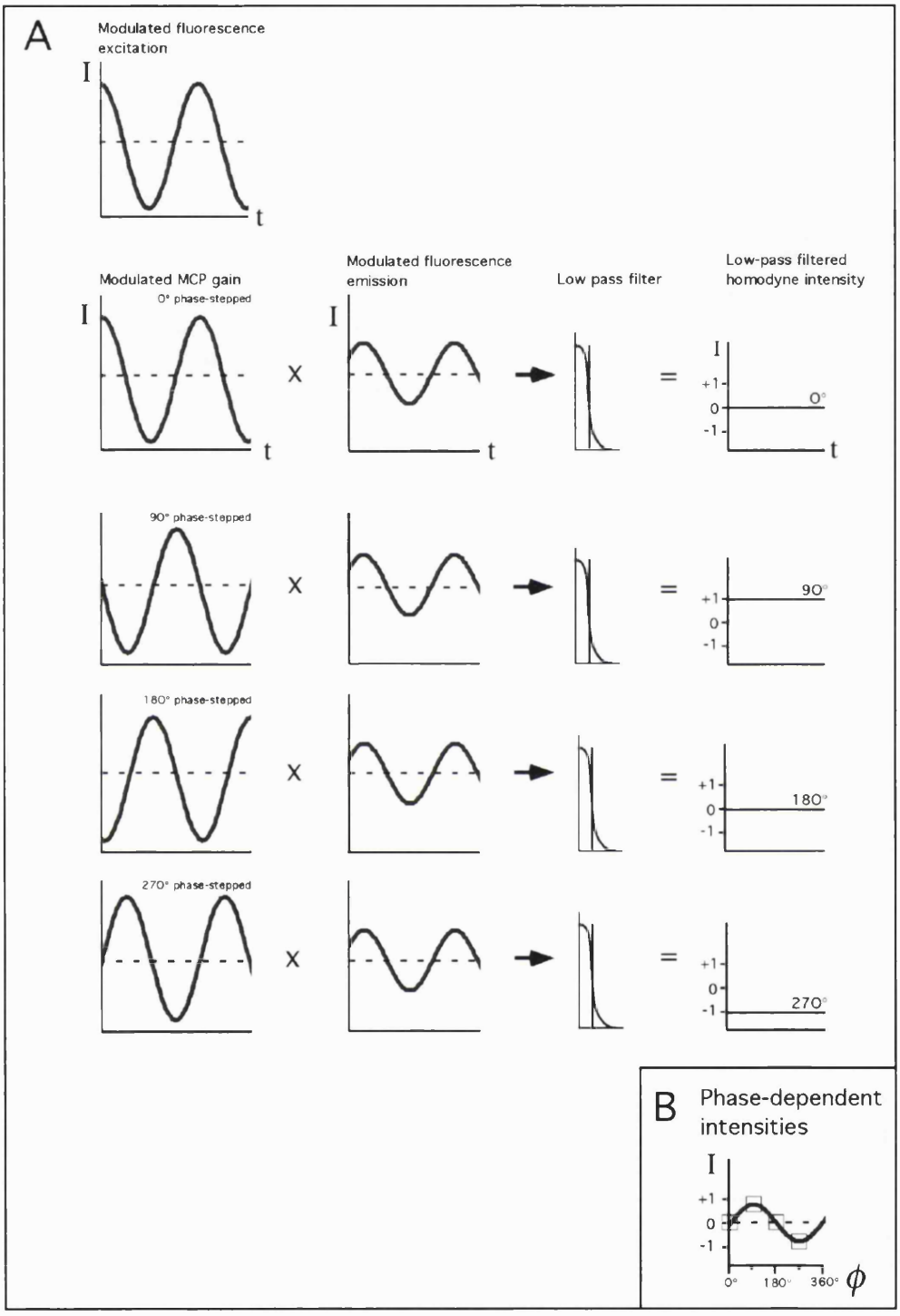
A
Modulated fluorescence excitation
I
t
Modulated MCP gain
0° phase-stepped
Modulated fluorescence emission
Low pass filter
Low-pass filtered homodyne intensity
90° phase-stepped
180° phase-stepped
270° phase-stepped
+1
0
-1
B
Phase-dependent intensities
0°
180°
360°
ϕ

Figure 1.9 Overview: calculating fluorescence lifetimes using frequency-domain FLIM measurements

A scheme is presented to illustrate the procedure for acquiring frequency-domain FLIM data and the image processing required to extract images showing the average phase lifetime (τ_ϕ) and modulation lifetime (τ_m) at each pixel. **A.** A phase-dependent FLIM data series is recorded from the biological sample and an equivalent phase-dependent FLIM data series is recorded from a scattering source (zero lifetime reference). **B.** A standard Fourier transform may be used to calculate the Fourier coefficients from the FLIM data acquired from the biological sample and from the averaged scatter data. **C.** The Fourier coefficients are then used to calculate the phase shift values ($\Delta\phi$) and demodulation values (m) at each pixel. **D.** Equations [6] and [7] (see main text) are then used to calculate images presenting the τ_ϕ and τ_m values at each pixel. For a more complete description of the calculations involved see Squire & Bastiaens, 1999; Harpur & Bastiaens, 2001; Verveer *et al* ., 2001.

Fig. 1.9

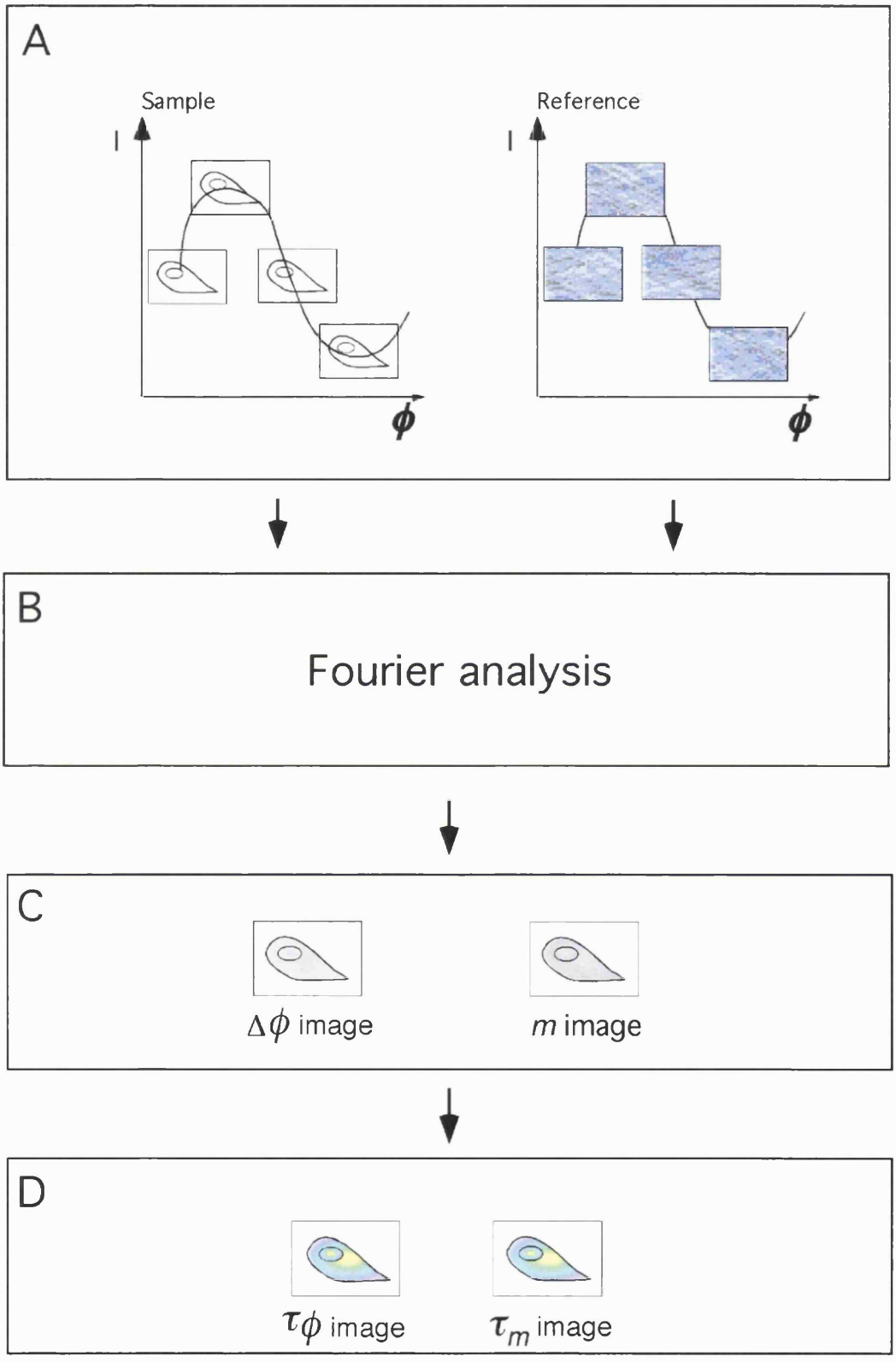
A
Sample
I
ϕ
Reference
I
ϕ
B
Fourier analysis
C
Δϕ image
m image
D
τϕ image
τm image

Figure 1.10 Proposed alternative models for the formation of ErbB receptor heterodimers

A. In this model it is assumed that ErbB ligands are intrinsically bivalent and can bind one receptor with high affinity and another member of the ErbB receptor family with low affinity, thus mediating the formation of a heterodimer in which transphosphorylation occurs (red curly arrow). **B**. In this model, ligand binding triggers the formation of a preliminary, stable dimer in which transphosphorylation occurs. Ligand-unoccupied members of the ErbB receptor family may then be recruited in a heterotetrameric configuration which facilitates transphosphorylation of the ligand-unoccupied receptors. **C**. Ligand binding triggers the formation of a preliminary, transient dimer in which transphosphorylation occurs. The receptors may then dissociate and form transient dimers with ligand-unoccupied members of the ErbB family, which facilitates transphosphorylation of the ligand-unoccupied partners in the heterodimers. Note that in **B** and **C** the ligand is shown to be a monomer that binds to one receptor only, but nothing is inferred about the valency of the ligand in these models. It is therefore not excluded that the ligands present in these models make contacts with both receptors in a dimer.

Fig. 1.10

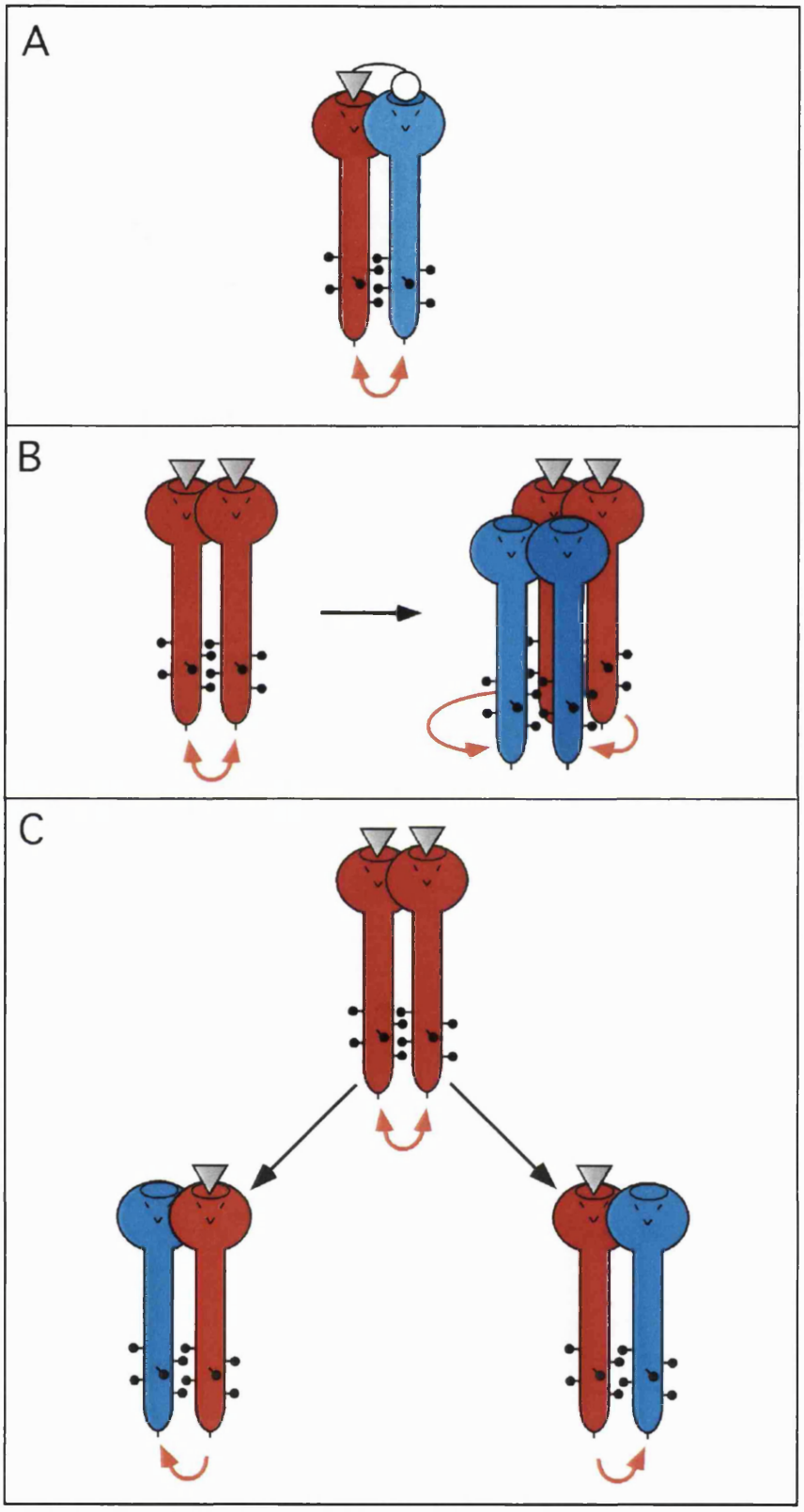

Chapter 2

Materials & Methods

Materials and Methods

2.1 Materials

2.1.1 Chemicals and media

Unless an alternative source is indicated in parenthesis when first mentioned, all chemicals and reagents described herein were purchased from Sigma, with the exception that acetic acid, dimethyl sulphoxide (DMSO), ethanol, glycerol, hydrogen peroxide solution, methanol and sodium dodecyl sulphate (SDS) were purchased from Merck. Distilled water, Luria-Bertani broth, phosphate buffered saline (PBS), tissue culture media and trypsin/versene solution were prepared by the Imperial Cancer Research Fund (ICRF) Research Services Department.

2.1.2 Antibodies

Antibodies used in this study were from the following sources: monoclonal anti-phosphotyrosine clone PY72, monoclonal anti-ErbB1 clone F4 (ICRF Research Monoclonal Antibody Department), rabbit polyclonal anti-mouse epidermal growth factor (Sigma), rabbit polyclonal anti-human erythrocyte catalase (Calbiochem), Cy5-labelled goat anti-rabbit IgG and Cy5-labelled donkey anti-mouse IgG secondary antibodies (Jackson Immunoresearch Laboratories). Cy3-labelled goat anti-rabbit IgG secondary antibodies were generated by labelling purified IgG (Sigma) with Cy3 as described (see section 2.2.3).

2.1.3 Plasmid DNA

Plasmid DNA was amplified in *E.coli* using standard molecular biology techniques (Sambrook *et al.*, 1989) and purified using a commercially available kit (Midi Prep kit, Qiagen). Plasmid DNA constructs used in the work for this thesis are listed in Table 2.1.

Table 2.1 Plasmid DNA constructs

Construct	Backbone vector	Source
ErbB1-GFP	pEGFP-C3 (Clontech)	Dr. F. Wouters Cell Biophysics Laboratory
ErbB3-GFP	pEGFP-C3 (Clontech)	Dr. F. Wouters Cell Biophysics Laboratory
ErbB1	pCDNA3 (Invitrogen)	Dr. C. Dickson, Viral Carcinogenesis Laboratory, ICRF
Human fibroblast catalase	PZeoSV2 (Invitrogen)	Dr. J. Mendelez, Albany Medical College, New York

2.1.4 Formulation of commonly used reagents

4% paraformaldehyde. 8 grams of paraformaldehyde (PFA) powder was dissolved in 150 ml of distilled water (supplemented with 1 ml of concentrated sodium hydroxide solution) with stirring at 50°C. After the solution had cleared, 20 ml of 10X PBS was added and the pH of the solution was brought to 7.4 with hydrochloric acid. Finally, the solution was brought to a volume of 200 ml with distilled water and filtered through a vacuum-driven 0.22 μm filter flask (Nalgene). The 4% PFA solution was stored at 4°C for a few weeks or for months at -20°C. Just prior to use the PFA solution was filtered once more through a Millex-GP 0.22 μm syringe driven filter unit (Millipore).

Mowiol mounting solution. 2.4 g of Mowiol 4-88 (Calbiochem) was mixed with 6 ml glycerol and 6 ml distilled water. The mixture was vortexed and then shaken for 2 hours. 12 ml of 200 mM Tris pH 8.5 was added and the mixture was incubated at 50°C with stirring until the Mowiol had dissolved (typically 24-48 hours). The solution was then filtered through a Millex-GP 0.45 μm syringe driven filter unit (Millipore) and stored in aliquots at -20°C. When aliquots were defrosted they were kept for a few weeks at 4°C for practical use. The solution was allowed to warm to room temperature before use.

2.2 Methods I : Protein chemistry

2.2.1 Biorad protein assay

18 protein concentration standards in the range 2.4–24 μg/ml were made by diluting a 200 μg/ml bovine serum albumin solution in distilled water. 150 μl of each protein standard solution was pipetted in duplicate into the wells of a 96-well plate. Solution A was generated by mixing 1.6 ml of protein assay reagent (Biorad) with 4.4 ml of distilled water. 50 μl of solution A was added to each well of the 96-well plate containing the protein standards or containing 150 μl of the protein sample, which was diluted in duplicate at various concentrations within a similar range to the protein standards. The absorbtion of each well was measured at 595 nm in a 96-well plate reader (Biorad) and protein concentrations were calculated using the plate reader software (Biorad).

2.2.2 Generation and purification of antibody Fab fragments

Purified monoclonal PY72 antibody was obtained in sterile filtered PBS from the ICRF Research Monoclonal Antibody Department. The antibody was concentrated to a protein concentration of 15–20 mg/ml and the buffer exchanged for 20 mM Na-phosphate, 10 mM EDTA, pH 7.0. This was performed using a disposable YM100 Centricon centrifugation concentrating device (100 kDa molecular weight cut-off; Amicon). The digestion reaction consisted of 250 μl of the concentrated antibody preparation (~ 4–5 mg), 500 μl of digestion buffer (20 mM Na-phosphate, 10 mM EDTA, 20 mM cysteine / HCl , pH 7.0) and 500 μl of a 50% slurry (in digestion buffer) of papain immobilised to agarose beads. Digestion was performed for 6 hours at 37°C with vigorous shaking (400 RPM on a rotating platform).

The Fab fragments were separated from Fc fragments and non-digested antibodies using a protein A-sepharose column (Econo-Pac 2 ml column, BioRad). The column was equilibrated with 20 bed volumes (40 ml) of 20 mM Na-phosphate buffer pH 7.0, before applying the digestion reaction (1250 μl) to the upper bed of the column. After the digested material had moved into the column matrix a further 2 ml of equilibration buffer

was added. The flow-through, which contains purified Fab fragments, was collected in 25 x ~200 µl fractions. To identify which fractions contained the purified Fab fragments, the absorbance was measured at 280 nm in a UV-visible spectrophotometer (Agilent technologies) and the peak fractions were pooled. The pooled fractions were then concentrated to a volume below 0.5 ml and buffer exchanged into PBS using a YM10 Centricon centrifugation concentrating device (10 kDa molecular weight cut-off; Amicon). Fab fragments were fluorescently labeled as described in section 2.2.3.

2.2.3 Labelling antibodies with Cy dyes

The monofunctional Cy dyes used here are indocyanine fluorophores that are derivatised with a single N-succinimidyl ester group to facilitate covalent coupling to primary amino groups and were obtained from Amerhsam Pharmacia Biotech. The ester group may be hydrolysed by water which destroys the reactivity of the dye with amino groups. To prevent the dye from reacting with condensed water, a single aliquot of lyophilised Cy dye was removed from 4°C storage just prior to labelling and allowed to warm to room temperature before opening. The solid was dissolved in 20 µl of dry N,N-dimethylformamide (DMF). The precise concentration of dye present in solution was determined by diluting the dye solution 1:10000-1:40000 in distilled water and measuring the absorbance in a 1 cm light-path cuvette. The concentration of the dye (M) was then calculated from the following formula:

$$[\text{dye}] = (A / \varepsilon_c) \times \text{dilution factor}$$

where A is the absorbance of the dilute dye solution at 554 nm (Cy3) or 650 nm (Cy5) and ε_c is the extinction coefficient (mol^{-1} cm^{-1}) of the dye (Cy3 = 150,000; Cy5 = 250,000; source: Amerhsam Pharmacia Biotech).

Prior to labelling, antibodies were concentrated to 10–20 µM and the buffer was exchanged for 100 mM bicine pH 8–9 by the use of a Centricon. Alternatively, if the protein was present already at the desired concentration, buffering of the PBS solution was achieved by adding 1/10 of the final volume 1 M bicine pH 8-9.

To initiate the protein labelling reaction, a 30-fold molar excess of dye solution was added to 100 µg of antibody. High concentrations of DMF in the reaction can denature proteins and therefore dye was added in a volume of DMF that did not exceed 10% of the total volume of the labelling reaction. The dye solution was added slowly whilst mixing the reaction with the pipette tip to ensure even mixing of dye and protein solution. The reaction was incubated at room temperature for 30 minutes.

During the labelling reaction a desalting column, with a molecular weight cut-off of 6 kDa (10-DG column, Biorad), was equilibrated with at least 3 bed volumes (10 ml) of elution buffer (PBS) using gravity-assisted flow only. Immediately following elapse of the labelling incubation time the protein sample was loaded drop-wise onto the upper bed of the column. A further 300 µl of PBS was added drop-wise onto the bed to ensure that the labelled material had moved from the bed into the matrix. At this point 5 ml of PBS was added to the top of the column. The labelled protein fraction was visible to the eye, as it separated from free label during elution, and was collected from the column on the basis of this.

The dye-protein labelling ratio of the eluted material was then calculated using one of the following equations:

$A_{554} \times M / [(A_{280} - 0.05 \times A_{554}) \times 150]$ for Cy3

$A_{650} \times M / [(A_{280} - 0.05 \times A_{650}) \times 250]$ for Cy5

Where A_x is the absorbtion at wavelength x and M is the molecular mass of the protein in kDa.

2.2.4 Assay of antibody phosphotyrosine binding activity

A binding reaction was formulated, consisting of 100 µl of Cy3-labelled PY72 Fab fragments (~ 1 nmol), 100 mg of O-phospho-L-tyrosine-agarose beads (~ 5 µmol O-phospho-L-tyrosine) and 800 µl of PBS. The reaction was incubated for 45 minutes on a rotating wheel, before pelleting the beads (10 minutes at 14,000 RPM in a bench top centrifuge cooled to 4°C) and carefully removing the supernatant. The absorbance of the

supernatant at 554 nm was compared before and after incubation with the beads in order to calculate what percentage of the antibody was bound to the beads.

2.2.5 Protein analysis by SDS-PAGE electrophoresis

SDS-PAGE electrophoresis was performed using a mini-gel electrophoresis system (Biorad). The resolving gel solution consisted of 12% w/v acrylamide, 0.32% w/v bisacrylamide, 0.1% w/v SDS, 375 mM Tris pH 8.8. Gel polymerisation was initiated by adding 20 µl of *N,N,N',N'*-tetramethylenediamine (TEMED) and 100 µl of a 10% w/v ammonium persulphate (APS) solution, followed by brief, gentle mixing. The gel was then immediately cast by pipetting ~ 3 ml of the solution between glass plates. The stacking gel consisted of 3% w/v acrylamide, 0.08% w/v bisacrylamide, 0.1% w/v SDS, 125 mM Tris pH 6.8. Stacking gel polymerisation was initiated by adding 20 µl of TEMED and 50 µl of 10% w/v APS solution. ~ 1 ml of the stacking gel solution was then immediately pipetted between the glass plates on top of the polymerised resolving gel and a plastic comb inserted. After stacking gel polymerisation, the comb was removed and the wells washed with distilled water. Just prior to sample loading the gel was transferred to the electrophoresis tank, which was filled with SDS-PAGE running buffer (200 mM glycine, 0.1% w/v SDS, 40 mM Tris pH 8.3).

Protein samples were diluted in 1 x Laemmli sample loading buffer (10% v/v glycerol, 2% w/v SDS, 100 mM DTT, 0.1% w/v bromophenol blue, 50 mM Tris pH 6.8). The samples were then boiled in a heating block for 10 minutes, briefly spun down and then loaded into the wells of the gel. Electrophoresis was performed for 1 hour at 100 Volts.

Following electrophoresis the resolving gel was separated from the stacking gel and transferred to Coomasssie staining solution (0.1% w/v Coomassie brilliant blue R-250, 50% v/v methanol, 10% v/v acetic acid). The gel was gently agitated on a rotary shaker at room temperature for 1 hour, before transferring to de-stain solution (50% v/v methanol, 10% v/v acetic acid). Gels were de-stained for ~ 3 hours with at least four changes of the de-stain solution. The wet gel was illuminated using a light box and images were captured using a digital camera and the relevant software (Kodak).

2.2.6 Covalent coupling of EGF to latex beads

Epidermal growth factor purified from mouse submaxillary gland and lyophilised from 15 mM acetic acid (Calbiochem) was resuspended at 100 μg/ml in a 50 mM acetic acid solution. The solution was buffered by adding 75 μl of 500 mM bicine pH 9 per 200 μl of the EGF solution, which was found by titration to produce a final pH of approximately 8.3.

0.8 μm diameter latex beads, that were surface modified with carboxylate groups, were purchased as a 10% slurry from the supplier (Cat No. CLB-9, Sigma). Just prior to coupling, the required volume of beads was washed twice and resuspended in 100 mM 2-N-(Morpholino)ethanesulphonic acid (MES) pH 6.1 (100 μl of buffer per 1 μl dry volume of beads). During all steps bead washing was achieved by pelleting the beads for 2 minutes at 14,000 RPM in a bench top centrifuge cooled to 4°C and by resuspending with repeated pipetting.

1-ethyl-3-(3-dimethylaminopropyl) carbodiimide hydrochloride (EDAC; Pierce) and N-hydroxysuccinimde (NHS; Calbiochem) were dissolved separately in DMF just prior to initiation of the coupling reaction at a concentration of 100 mM and 350 mM respectively. The carboxylate moieties on the beads were derivatised to NHS ester groups by reacting the equivalent of 2 μl dry volume of beads in the presence of 2 mM EDAC, 5 mM NHS and 100 mM MES pH 6.1, in a total aqueous volume of 500 μl. After briefly vortexing the reaction it was left on a turning wheel at room temperature for 20 minutes. The reaction was stopped by quenching excess EDAC via the addition of β-mercaptoethanol to a final concentration of 20 mM. The NHS ester groups have a $t_{1/2}$ of 40 minutes in aqueous solution, due to hydrolysis. It is important to note therefore, that no longer than 10 minutes elapsed between termination of the derivatisation reaction with β-mercaptoethanol and addition of the EGF solution.

The beads were washed twice in 1 ml of 100 mM MES pH 6.1, followed by resuspension of the pelleted beads in 138 μl of EGF solution (10 μM EGF, 65 mM acetic acid, 150 mM bicine pH 8.3) per 1 μl dry volume of beads. In reactions where lower densities of EGF coupling were required Tris was also included in the reaction at a concentration of 10 μM. The beads were left to react with EGF for 2 hours at room temperature on a spinning wheel followed by 16 hours at 4°C with gentle agitation. The coupling reaction was terminated by the addition of 1 M hydroxylamine at a final

concentration of 10 mM and left for a further 15 minutes at 4°C. Free EGF was removed from the coupling reaction by washing 5 times in 1 ml of ice cold PBS, per 1 µl dry volume of beads. The supernatant from the coupling reaction and the wash steps was retained, stored at 4°C and checked for biological activity later. Finally, the beads were resuspended in 100-200 µl 60:40 glycerol-PBS solution, per 1 µl of dry volume of beads, and stored at –20°C.

2.2.7 Staining of beads with anti-EGF antibodies

Glass coverslips were coated with poly-L-lysine by incubation in the presence of 0.01% w/v poly-L-lysine for 60 minutes at 37°C, followed by washing in PBS. Each coverslip was incubated with 30 µl of EGF coupled beads diluted in PBS (~1 x 10^6 beads) for 3 hours at 4°C, followed by fixation with 4% paraformaldehyde (PFA), in order to immobilise the beads. Bead-coated coverslips were incubated for 60 minutes with rabbit polyclonal anti-mouse EGF antibodies, diluted 1:10,000 in 1% BSA/PBS. After careful washing with PBS, the coverslips were incubated for a further 30 minutes with Cy3-conjugated goat anti-rabbit secondary antibodies diluted 1:250 in 1% BSA/PBS. After further washing in PBS, coverslips were mounted on glass slides in Mowiol mounting solution.

2.2.8 Labelling EGF-coated beads with Cy dyes

Cy3 and Cy5 dyes were reconstituted in 20 µl of DMF. 5-10 µl of bead slurry was diluted with 90 µl of PBS and then 10 µl of 1 mM bicine pH 8 was added. Cy dyes were non-covalently absorbed to the surface of beads by mixing 1 µl of Cy dye slowly into the solution (see section 2.2.3), followed by incubation on ice for 30 minutes. Beads were washed extensively in PBS before applying to cells.

2.3 Methods II : Experimental procedures with cultured MCF-7 cells

2.3.1 Tissue culture

MCF-7 cells were obtained as subconfluent monolayers from the ICRF Cell Production Department, but were originally obtained from the European Collection of Animal Cell Cultures. ErbB1-GFP expressing cells were obtained from Christian Tischer (European Molecular Biology Laboratory, Heidelberg, Germany) and were recovered from frozen stocks according to standard protocols (Sambrook *et al.*, 1989). Cells were cultured in Dulbecco's modified Eagle's medium (DMEM) supplemented with 10% foetal calf serum (FCS; Autogen Bioclear) and 10 μg/ml insulin and split twice a week by digestion with trypsin/versene solution. Media for culturing stable cells was additionally supplemented with 100 μg/ml G418 (Gibco BRL).

2.3.2 Transfection of MCF-7 cells with plasmid DNA

24-48 hours before transfection, MCF-7 cells were plated onto 13 mm diameter glass coverslips (Chance Glass Ltd) or 30 mm diameter glass-bottomed petri dishes (MatTek Corporation). Cells were 40-60% confluent on the day of transfection. Just prior to transfection glass coverslips were transferred to six well plates, at a density of 3 coverslips per 30 mm diameter well. The volumes of DNA, fugene and media described below are per 30 mm diameter dish or 30 mm diameter well. All cells were bathed in normal culture medium containing FCS and insulin (as described in section 2.3.1) during transfection.

3 μl of 0.3 mg/ml plasmid DNA was transferred to an Eppendorf tube (tube A). 3 μl of Fugene was added to 97 μl of serum-free DMEM in a second Eppendorf tube (tube B). After gentle mixing, tube B was allowed to stand for 15 minutes at room temperature before adding the contents to tube A. After gentle mixing, the fugene-DNA cocktail was allowed to stand for a further 10 minutes before pipetting 100 μl directly into the 2 ml of media bathing cells in a 30 mm diameter dish / well.

Cells were returned to the incubator for a further 16-24 hours to transfect. 5-6 hours before stimulation the transfecting medium was removed and replaced with starvation medium (DMEM without FCS or insulin).

2.3.3 Capillary microinjection of adherent MCF-7 cells

DNA and protein samples were prepared for microinjection by brief centrifugation through a Millex-GV 0.22 μm syringe filter (Millipore). Microinjection needles were generated from borosilicate glass capillaries (1.2 mm outer diameter / 0.94 mm inner diameter; Clark Electronic Instruments) with the use of a Flaming-Brown micropipette puller (Model P-97, Sutter Instrument Company).

Cells were microinjected using a semi-automated capillary microinjection system (Eppendorf). The micromanipulator arm was mounted onto the 37°C heated stage of a Zeiss inverted light microscope. Just prior to microinjection of plasmid DNA, MCF-7 cells were transferred to injection medium. Injection medium was DMEM containing a low bicarbonate concentration and supplemented with 25 mM N-(2-hydroxyethyl)piperazine-N'-(2-ethanesulphonic acid) (HEPES) pH 7.4. Typically, 100-300 cells were microinjected over a period of 10-30 minutes with an injection pressure of 150-300 hPa, back pressure of 50 hPa and injection time of 0.1- 0.3 secs/cell. After microinjection was completed the media was exchanged for normal DMEM plus FCS/insulin and cells were transferred back to the CO_2 incubator.

2.3.4 Live cell imaging of ErbB1-GFP expressing cells

MCF-7 cells grown on glass-bottomed petri dishes were transfected and starved as described (see section 2.3.2). Immediately prior to the experiment the media bathing the cells was exchanged for 2 ml of live cell imaging medium (phenol red, riboflavin and antibiotic free, low bicarbonate DMEM medium supplemented with 25 mM HEPES pH 7.4, pre-warmed to 37°C). The cells were then transferred to the stage of the FLIM instrument, the ambient temperature of which was maintained at 37°C during the course of the entire experiment. Groups of cells visually confirmed to be expressing ErbB1-GFP were microinjected in the cytoplasm with Cy3-labelled Fab fragments of PY72 (0.3 mg/ml concentration in PBS) using a semi-automated microinjection system (Eppendorf).

Injected cells were checked for incorporation of Cy3-labelled material in the Cy3 fluorescence channel. A FLIM series of the ErbB1-GFP fluorescence was then taken (see section 2.4). To achieve a homogeneous stimulation of live cells, 2 µl of soluble EGF (100 µg/ml) was applied to the medium bathing the cells to give a final dose of 100 ng/ml and the optical table was shaken briefly. For focal stimulation of live cells, Cy5-labelled EGF-coated beads were diluted in live cell imaging media at a concentration of 2×10^5 beads/µl. Excess media was drained from the dish, followed by application of 100-200 µl of bead solution to the central well of the dish. FLIM series of ErbB1-GFP fluorescence were recorded at suitable intervals after stimulation. At the end of the experiment an image of the antibody was acquired in the Cy3 channel and the position of EGF-coated beads recorded by acquiring an image in the Cy5 channel (see section 2.4).

2.3.5 Preparation of fixed samples of ErbB1-GFP expressing cells

For experiments on fixed specimens MCF-7 cells grown on glass coverslips, or sometimes glass-bottomed petri dishes, were transfected and starved as described (see section 2.3.2). For stimulation with soluble EGF, excess media was drained from cells and they were overlaid with DMEM containing soluble EGF (100 ng/ml). For focal stimulation times up to 1 minute, cells were drained and overlaid with 25 µl (4×10^5 beads/µl) suspension. For longer stimulation times, 25 µl (2×10^5 beads/µl) of suspension was added to coverslips. At these dilutions approximately 1-5 beads per cell had landed by the time of fixation (as confirmed by microscopic observation).

Pharmacological agents were purchased in a lyophilised form and reconstituted to make a concentrated stock solution that was diluted into culture media just prior to the experiment. Bisindoylmaleimide I (Alexis Biochemicals) was reconstituted in DMSO (10 mM stock solution), LY294002 (Calbiochem) was reconstituted in ethanol (10 mM stock solution), phenyl arsine oxide (PAO; ICN Biomedicals Inc.) was reconstituted in water (1 mM stock solution) and PP2 (Calbiochem) was reconstituted in water (10 mM stock solution). Hydrogen peroxide was purchased as a ~30% solution in water and diluted into culture medium.

Immediately following the application of media containing growth factors, drugs or hydrogen peroxide, cells were returned to the incubator (37°C, 7.5% CO_2). After the prescribed stimulation period, the media was removed and cells were fixed rapidly with

4% PFA at room temperature for 20 minutes. Free aldehyde groups were quenched by washing once with 100 mM Tris pH 7.4, 50 mM NaCl followed by incubating in the same solution for a further 5 minutes. Cells were permeabilised with 0.1% triton in PBS for 10 minutes, briefly washed in PBS and then incubated with 15 μg/ml Cy3-PY72 in 1% BSA / PBS for 60 minutes. For fixed cell experiments, whole PY72 IgG labelled with 5 Cy3 dye residues per antibody molecule was used. Antibody incubations were performed at room temperature in a sealed chamber to prevent evaporation of the antibody solution. After termination of antibody incubation cells were washed 3 times with PBS. Cells on glass-bottomed petri dishes were then transferred to the microscope stage and immediately imaged. Cells on glass coverslips were mounted on glass slides in ~7 μl of Mowiol mounting solution. After Mowiol polymerisation, slides were either imaged immediately or stored at 4°C for less then a week before imaging.

2.3.6 Immunofluorescence

In experiments where the samples were stained with primary antibodies in parallel with Cy3-PY72, the primary antibody was diluted into the same solution as the Cy3-PY72 and incubated with the cells for 1 hour. Dilutions were as follows: monoclonal anti-ErbB1 clone F4 (1 μg/ml), rabbit polyclonal anti-mouse EGF (1:5000) and rabbit polyclonal anti-human erythrocyte catalase (1:5000). After 3 washes with PBS the cells were incubated with Cy5-labelled donkey anti-mouse secondary antibodies (1:250) for detection of monoclonal antibody F4, or Cy5-labelled goat anti-rabbit secondary antibodies (1:250) for detection of rabbit antisera. Incubation with secondary antibodies lasted for 20 minutes and was followed by further washing in PBS before mounting in Mowiol mounting solution.

2.3.7. Confocal microscopy and fluorescence recovery after photobleaching

Cells were grown on glass-bottomed petri dishes, transfected and starved as described (see section 2.3.2) and transferred to live cell imaging medium (see section 2.3.4) just prior to the experiment. Images were acquired with a Zeiss LSM 510 confocal microscope. A large part of the microscope was enclosed within a perspex thermostatic chamber which was heated to 37°C during live cell experiments. Incorporating most of

the microscope in this chamber eliminates temperature gradients between the microscope components (such as objectives) and the sample during image acquisition at 37°C. A 100 mW, 488 nm argon laser was used to excite GFP and images acquired through an 505-530 nm band pass emission filter. A 5 mW, 543 nm HeNe laser was used to excite Cy3 and images acquired through a 590 nm long pass emission filter. A 5 mW, 633 nm HeNe laser was used to excite Cy5 and images acquired through a 650 nm long pass emission filter.

FRAP experiments were performed using the bleaching time-lapse facility within the LSM 510 software. A 2.5 or 5 μm diameter circular region of interest (ROI) was bleached to background levels by rapid scanning with the 488 nm laser at 100% transmission for no longer than 15 seconds. Pre- and post-bleach images in both the GFP and Cy3 channels were acquired simultaneously using the 488 nm and 543 nm laser lines set at low transmission levels (typically 1-5%), with 1x averaging to minimise bleaching of the fluorescence.

2.3.8. Streptolysin-O permeabilisation

The streptolysin-O permeabilisation conditions were based on those previously published (Buday & Downward, 1993) and streptolysin-O (12 units/ml in PBS) was obtained from Wellcome. MCF-7 cells grown on glass coverslips were transfected with GFP (driven by the pEGFP-C3 vector, Clontech), or ErbB1-GFP, and serum starved as described (section 2.3.2). Each coverslip was washed once with 37°C PBS and then transferred to 1 ml of 37°C permeabilisation buffer: 150 mM KCl, 37.5 mM NaCl, 6.25 mM $MgCl_2$, 0.8 mM ethylene glycol-bis(β-aminoethyl ether)-*N, N, N',N'*-tetraacetic acid (EGTA), 1mM $CaCl_2$, 1.25 mM ATP, 3 mM DTT, 12.5 mM piperazine-N, N'- bis(2-ethanesulphonic acid) (PIPES) pH 7.4 which was supplemented with or without 2 units/ml streptolysin-O (ATP, DTT and streptolysin-O were added just prior to the experiment). After 10, 30 or 60 minutes of permeabilisation at 37°C, GFP expressing cells were fixed and mounted on glass coverslips. Observation of the cells showed that maximal loss of GFP fluorescence occurred by 30 minutes. Therefore, after 30 minutes of permeabilisation, ErbB1-GFP expressing cells were stimulated with EGF or EGF-beads as described (see section 2.3.5) except that stimulation was performed in permeabilisation

buffer with or without streptolysin-O. Coverslips were then fixed and processed for FLIM measurements as described (see section 2.3.5).

2.4 Methods III : Fluorescence lifetime imaging microscopy set-up

2.4.1. Configuration of the frequency-domain fluorescence lifetime imaging microscope

A schematic of the single frequency FLIM set-up used in the presented work is shown in Fig. 2.1. The instrument was based around an inverted microscope (Zeiss Axiovert 135 TV) which, along with the other optical components of the set-up, was mounted on a 2 x 1 metre optical table (Technical Manufacturing Corporation). The table was supported on pneumatic pistons providing vibrational isolation of the entire instrument. A large part of the microscope was enclosed within a perspex thermostatic chamber which was heated to 37°C during live cell experiments. Incorporating most of the microscope in this chamber eliminated temperature gradients between the microscope components (such as objectives) and the sample during image acquisition at 37°C. Measurements on fixed samples were performed at the ambient temperature of the microscope room (15°C).

The light source for FLIM measurements was a tunable argon laser (Innova Spectrum 70C, Coherent). The output of the laser source was sinusoidally modulated at 80 MHz by a standing wave acousto-optic modulator (SW-AOM; Intra-Action Corporation). An iris diaphragm (Comar) placed ~1.5 metres from the SW-AOM was employed to selectively isolate the central (zero-order) modulated beam from the higher-order diffracted beams that the SW-AOM generates. In order to minimise thermal phase drift in the SW-AOM it was coupled to a thermostatic water bath/circulator and the microscopy room was temperature stabilised at 15°C. This kept the SW-AOM to within ± 0.1°C of a set temperature, which is essential for phase coherence between the fluorescent signal and the modulated gain of the detector. The modulated central light beam was then directed into a 1.5 metre step index silica fibre (1 mm core, numerical aperture 0.37; Technical Video Ltd) using a 2.5 cm diameter, 12 cm focal length lens

(Newport Corporation). The coherence of the laser light was disrupted by vibrating the fibre at frequencies of approximately 100 Hz, resulting in a randomly moving speckled illumination of the specimen, which was integrated during detection. Koehler illumination at the sample plane was achieved by incorporating an achromatic lens (3.8 cm diameter, 7.6 cm focal length; Newport Corporation) just prior to the epi-illumination port of the microscope to collect and collimate the laser light. This focal length is sufficient for the fibre core to appear as a point source, thus giving a collimated beam resulting in flat illumination in the sample plane. A 100 W mercury arc lamp (Zeiss HBO 100 W/2) was attached to the second epi-illumination port of the microscope to provide an alternate illumination source. A rotating mirror facilitated rapid switching between the laser and the lamp. The laser illumination was used for donor fluorescence lifetime imaging whereas the lamp was employed for imaging, or bleaching, the acceptor.

A TV port situated directly below the sample and objective was used for coupling to the detector, thus providing the shortest route for fluorescence emission with minimal losses. Light from the sample was imaged onto the photocathode of a high frequency-modulated image intensifier (Hamamatsu C5825). This device employs proximity-focussing of photoelectrons ejected from the photocathode onto the face of a micro-channel plate (MCP). The electron image at the output of the MCP strikes a phosphor screen to generate an intensified light image. For homodyne detection, the effective gain of the image intensifier was modulated at a frequency equal to that of the SW-AOM (80 MHz) by the application of a biased sinusoidal voltage to the photocathode. The amplified, phase-locked outputs from two high-frequency synthesisers (IFR 2023, Marconi) was used to provide highly stable sinusoidal voltage sources for modulating both the excitation light (at the SW-AOM) and the gain of the image intensifier unit. The output driving the SW-AOM was further amplified via the use of a signal amplifier (ENI 403LA). A telescopic lens, with a magnification of 0.5, was used to project the amplified image, at the phosphor screen of the MCP, onto the chip of a scientific grade cooled charge-coupled device (CCD) camera (Quantix, Photometrics). The magnification of 0.5 matched the full surface area of the CCD chip with that of the phosphor on the MCP. The 12 bit CCD camera housed a Kodak KAF1400 chip with a 1317 X 1035 array of 6.8 μm square pixels. Two-by-two binning was applied during image acquisition on the CCD in order to accommodate the lower resolution (12l line-pairs/mm) of the MCP. A phase-dependent signal at each pixel of the image was achieved by sequential phase-stepping

the gain source and recording a series of images throughout an entire cycle (0-360 degrees).

16 phase-dependent images of approximately 300 x 300 pixels were acquired in a FLIM sequence. With a maximal readout rate of 5 x 10^6 pixel/sec, each phase-dependent image was read in approximately 20 ms. Photobleaching was minimised by illuminating the sample only during image acquisition. This was achieved with an external high speed shutter (Uniblitz VS25 shutter and D122 shutter driver, Vincent Associates) located between the filter block and the epi-illumination port of the microscope. Synchronous triggering of the shutter was controlled with a BNC output on the CCD, indicating shutter status. The phase setting of the frequency synthesiser modulating the image intensifier gain was precisely stepped via commands sent over a GPIB interface housed in a G3 Macintosh computer. The incorporation of extensions into IPLab Spectrum (Signal Analytics Corporation) for phase-stepping control, and downloading images from the CCD, provided the software interface for the collection of FLIM data.

2.4.2. Calibration of the FLIM instrument

The electrical components of the FLIM instrument were switched on ensuring that those with the highest current drainage were switched on first. The components of the instrument were then calibrated for FLIM measurements.

Laser set up. The 488 nm excitation wavelength of the argon laser was selected by adjusting the wavelength selector prism. The output power was optimised by fine-tuning the position of the high reflector mirror using the control knob at the back of the laser.

SW-AOM calibration. The frequency synthesiser driving the SW-AOM was set to a resonance frequency of 40.112 MHz, which gives rise to an oscillation in the laser light beam at twice the driving frequency (80.224 MHz). The diffraction in the AOM, and thereby the modulation depth, was optimised by adjusting the angle of incidence and monitoring the intensity of the undiffracted zero order beam with a power meter (Nova Display and 2A-SH, Ophir). This is possible because the optimal angle of diffraction (corresponding to maximal diffraction) gives rise to a minimum in the output power of the zero order beam.

MCP and CCD settings. The master frequency synthesiser driving the MCP was set to 80.224 MHz, a value exactly double that driving the AOM. The bias of the photocathode voltage was set to –2 Volts and the gain was set at 1.5 - 2. Typically the Hamamatsu C5825 CCD camera gain was set at 1 - 2.

Acquiring a zero lifetime reference image and calibrating the phase of the master frequency synthesiser. The phase of the master frequency synthesiser must be at a maximum in order to acquire calibrated phase-dependent FLIM data. However, the phase of the master frequency synthesiser is not generally at a maximum when the instrument is first switched on. In order to calibrate the phase a reference measurement must be taken. For reference measurements the intensity of the 488 nm laser line was reduced to a minimum by using a variable density filter wheel (Laser Components) and the incident light was projected into the microscope objective via a half-silvered mirror in the microscope filter block. A Zeiss FLUAR 100X/1.4 NA oil objective was used to focus on the specimen. To obtain a zero lifetime reference image, a cycle of 16 phase-dependent images, each separated by 22.5 degrees, was recorded from a strong scattering surface (a small piece of aluminum foil placed on the imaging surface of a glass slide or glass-bottomed petri dish). From this sequence the phase setting at which maximum intensity is reached in the image series was calculated. This allowed the phase to be set to zero degrees on the master frequency synthesiser. The procedure was repeated at least every 30 minutes during the acquisition of FLIM data in order to ensure the phase of the master frequency generator remained at a maximum throughout the measurements (and therefore in phase coherence with the modulated detector gain).

2.4.3 Acquiring FLIM data and accompanying images

GFP fluorescence was acquired using the 488 nm laser line. The incident laser light was projected onto the sample via a dichroic mirror (Q495 long pass) in the filter block and the emission light collected through an HQ510/20 band pass filter in the base of the filter block. A Zeiss FLUAR 100X/1.4 NA oil objective was used to focus on the GFP fluorescence within the specimen. A FLIM series consisted of two contiguous series of 8 phase-dependent images (45 degree phase-stepped) one forward cycle (8 images) and one reverse cycle (8 images). The reverse cycle was employed in subsequent image analysis to correct for photobleaching that occurs during image acquisition. The FLIM

series also included an additional image in the absence of sample illumination (background image). The exposure time employed for acquisition of a FLIM series was optimised for each sample to ensure maximal intensities at each pixel of the acquired image and was typically 200-400 ms. The exposure time was then kept constant for every phase-dependent image in a single FLIM series.

Images of the Cy3 or Cy5 fluorescence present in the same image field were generally acquired immediately after FLIM series acquisition, except where stated otherwise. Illumination of the sample was achieved using the mercury arc lamp. Cy3 fluorescence was acquired through a filter set in the microscope filter block (excitation, HQ545/30 band pass filter; dichroic mirror, Q565 long pass; emission, HQ610/75 band pass filter; from Chroma). Cy5 fluorescence was acquired through a filter set in the filter block (excitation: HQ620/60 band pass filter, dichroic mirror: Q660 long pass, emission: HQ700/75 band pass filter; Chroma).

2.5 Methods IV : Image processing

2.5.1 Calculation of ErbB1-GFP diffusion coefficient

Each frame from an individual FRAP time lapse sequence (as recorded on the confocal microscope) was saved as a 12-bit TIFF file. The data was analysed by importing the raw data into a program which was written in the software package Mathematica (Wolfram research). The program was designed to calculate the diffusion coefficient, D, from an individual FRAP time lapse sequence. Firstly, the fluorescence intensity in the bleached ROI was corrected for any bleaching of the sample that occurred during image acquisition. This was achieved by calculating the average intensity of the fluorescence in a region outside the bleached ROI, and dividing the signal from the bleached ROI by this value, for every image in the time-lapse sequence. D was then calculated by fitting the normalised data to the following function:

$$f(t) = exp\,(-2\tau_D / t)\,[I_0(\,2\tau_D / t\,) + I_1(\,2\tau_D / t\,)]$$

where, I_0 and I_1 are modified Bessel functions and $\tau_D = w^2 / 4D$, where w = is the radius of the bleached ROI (Soumpasis, 1983). The value of D was then estimated by solving the equation: $\tau_D = w^2 / 4D$ for D (i.e. $D = w^2 / 4\tau_D$). The process was repeated for 10 time lapse sequences allowing the mean value of D, and the standard deviation over the 10 measurements, to be calculated.

2.5.2 Analysis of FLIM data

FLIM data series were saved as IPlab image files consisting of a stack of 17 images (16 phase-dependent images and 1 background image). Image processing was performed using a PC running the Linux operating system, and proceeded via a series of sequential steps. *1. Correction for backgound.* The average intensity of the background image was subtracted from all phase images in the FLIM series. This background-corrected series was used for all further image processing. 2. *Calculate DC image.* An

image representing the mean average fluorescence intensity at each pixel across the series ('direct current' image or DC image) was calculated by summing all the images across the series. *2. Intensity thresholding*. Using the DC image, an image 'mask' was generated where pixels of interest = 1 and unwanted pixels = 0. Unwanted pixels included any pixels below a certain threshold intensity value (as defined by the operator) and any pixels where the fluorescence signal was saturated. Note that the mask is a separate image from the data. *3. Correction for photobleaching*. Each of the pairs of equivalent phase images of the forward and reverse cycles were summed to first order correct for photobleaching of the donor. *4. Application of the analysis to determine fluorescence lifetimes*. Each background- and photobleaching-corrected FLIM data series was analysed using only pixels where the corresponding pixels in the mask = 1. Two types of analysis were performed on the data to resolve the lifetimes. Firstly, each FLIM data series was analysed individually using a standard Fourier transform to calculate frequency-weighted lifetime estimates according to the phase shift and the demodulation at each pixel of the image, producing two separate images showing the phase lifetime and modulation lifetime at each pixel, respectively (see Squire & Bastiaens, 1999; Harpur & Bastiaens, 2000; Verveer *et al.*, 2001). Secondly, the pixels from many FLIM data sets were linked in a global analysis which assumed the presence of two populations of receptors associated with one of two spatially invariant lifetimes. The details of the algorithm employed are described elsewhere (Verveer *et al.*, 2000a). The global analysis generated the following outputs: 1. the spatially invariant lifetimes of each ErbB1-GFP species: ErbB1-GFP in the presence of FRET (τ_2) and ErbB1-GFP in the absence of FRET (τ_1), and 2. a fractional population map, for each FLIM data series, showing the molar fraction of ErbB1-GFP molecules with lifetime τ_2 at each pixel (α map). Application of an appropriate pseudocolor table to the population maps allowed the level of phosphorylation at every pixel of the images to be examined. For statistical purposes, the α map raw data was used to calculate the percentage of ErbB1-GFP molecules with lifetime τ_2 in each image i.e. the percentage of phosphorylated ErbB1-GFP molecules present was calculated for each FLIM series.

Fig. 2.1

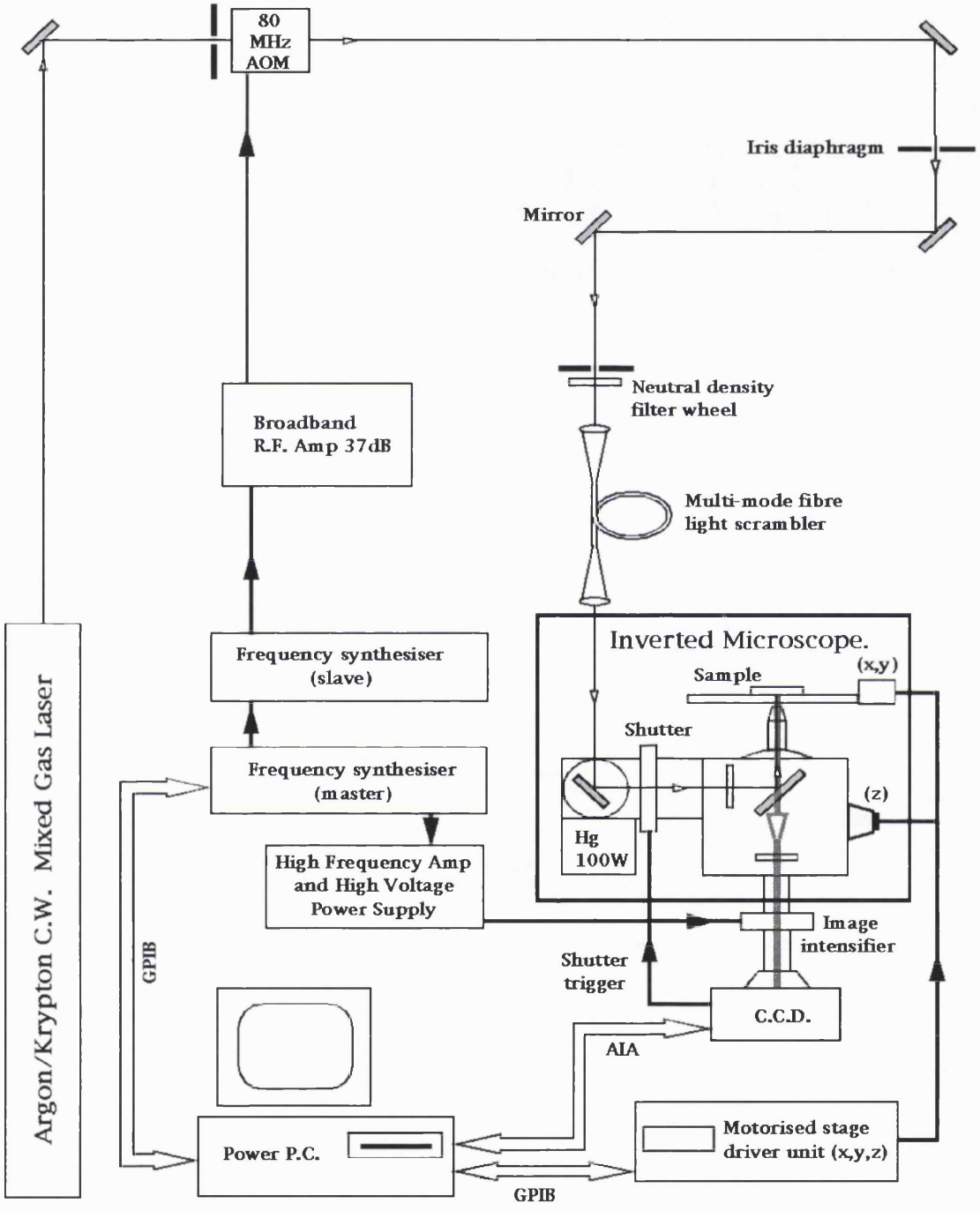

Figure 2.1 Frequency-domain FLIM set-up

See main text for details.

Chapter 3

Quantitative Imaging of ErbB1 Lateral Signal Propagation

Quantitative imaging of ErbB1 lateral signal propagation

3.1 Introduction

Phosphorylated proteins can be detected in cells by performing immunofluorescence using anti-phosphoamino acid antibodies and acquiring images of the fluorescence signal. The intensity of the fluorescence signal detected at each pixel of an image can be used to infer the level of phosphorylation present. However, the measured intensity is also dependent on the concentration of the protein and yields no information about the relative populations of phosphorylated versus non-phosphorylated protein present. However, FRET-based assays, in conjunction with appropriate image analysis techniques, can be used to obtain a quantitative measure of phosphorylation levels in cells.

A chimeric construct consisting of GFP fused to the intracellular C-terminus of ErbB1, via a short linker sequence, has been constructed and provides the basis for such an assay (Fig 3.1 A; Wouters & Bastiaens, 1999). In response to EGF, such a chimera can become phosphorylated, internalised and activate downstream signalling pathways in a manner that is indistinguishable from the wild type receptor (Carter *et al.*, 1998). Phosphorylation of the ErbB1-GFP can be measured by incubating cells with anti-phosphotyrosine antibodies that are conjugated to the fluorescent dye, Cy3, which is a good FRET acceptor for GFP (see Table 1.3). Binding of the antibody to the receptor brings the conjugated Cy3 into an appropriate distance range of the GFP for FRET to occur (Fig 3.1 A). By monitoring the fluorescence lifetime of the donor this assay specifically measures the amount of GFP-tagged protein present in the phosphorylated state, because only antibodies binding directly to the GFP-tagged protein are reported on due to their close proximity to the GFP. Antibodies that are bound to other tyrosine phosphorylated proteins are not detected because they are not close enough to the GFP to participate in FRET. This means that generic, non-specific antiphosphotyrosine antibodies can be used. The principle is general and therefore generic antibodies which recognise any post-translational modifications, such as methylation or acetylation, can be used to detect specific protein reactions in cells (Fig 1.5 F).

This method has been used to report on the spatial and temporal nature of GFP-PKCα activation in cells, due to threonine phosphorylation in response to phorbol ester treatment (Ng *et al.*, 1999), and ErbB1-GFP tyrosine phosphorylation in cells in response to EGF (Wouters & Bastiaens, 1999). In the latter report, MCF-7 cells expressing ErbB1-GFP were serum starved and fixed immediately after stimulation with EGF for different time periods. Following permeabilisation they were incubated with a generic anti-phosphotyrosine monoclonal antibody (clone PY72) that had been directly labelled with Cy3. It was shown that at 5-10 minutes after EGF stimulation FRET could be observed between the ErbB1-GFP and Cy3-PY72 over the entire plasma membrane. The presence of FRET at early time points correlated with the ligand-induced phosphorylation of the receptor. The magnitude of the apparent FRET efficiency was reduced at 30 minutes, by which time extensive receptor internalisation was observed. The reduction in FRET efficiency at 30 minutes was interpreted as being due to shielding of phosphorylated epitopes i.e. due to the association of phosphotyrosine-binding proteins with internalised ErbB1. In this report, frequency-domain FLIM measurements were analysed using a conventional analysis that computes an average fluorescence lifetime from the phase shift and demodulation of the fluorescence wave at each pixel (only a frequency weighted average lifetime estimate is associated with each pixel; Fig 1.3 B). The FRET efficiency at each pixel was calculated from fluorescence lifetime images, or steady-state fluorescence intensity images, acquired before and after photodestruction of the Cy3 acceptor (see section 1.4.5.2). The calculation of apparent FRET efficiencies yields a measure of the amounts of phosphorylated receptor present at each resolvable volume element (pixel) in a manner that is independent of receptor concentration. However, an exact measure of the molar fractions (populations) of phosphorylated versus nonphosphorylated ErbB1-GFP present would be of greater biological interest.

In the work presented here this problem is solved by globally analysing the FLIM data. In a global analysis the results of multiple experiments are analysed simultaneously under the assumption that some of the parameters are interrelated, or identical, across all experiments. For example, global analysis can be used to determine the relative concentrations of two different fluorophores present in a mixture in a series of cuvettes, each cuvette containing an unknown concentration of each fluorophore. The frequency-domain fluorescence lifetime data, recorded from the cuvettes, is analysed assuming that only two species of fluorophore are present; each associated with a discrete fluorescence

lifetime. The global analysis yields the discrete fluorescence lifetimes of the two species and the fractional contribution of each to the measured fluorescence (i.e. the relative concentration of each species as a fraction; Beecham *et al.*, 1992).

The successful application of global analysis to frequency-domain FLIM data has recently been published by our laboratory (Verveer *et al.*, 2000). In this report, global analysis of FLIM data, acquired at a single excitation frequency and modulation frequency, was used to resolve the spatial distribution of two discrete fluorescent proteins targeted to different cellular compartments (Golgi apparatus or cytoplasm). The global analysis successfully reported on the different spatial localisation of each protein on the basis of the assumption that each was associated with a discrete fluorescence lifetime and that these fluorescence lifetimes were independent of spatial localisation within the cell and did not vary between experiments.

In this thesis, global analysis of frequency-domain FLIM data, acquired at a single excitation frequency and modulation frequency, has been used to determine the relative populations of phosphorylated versus nonphosphorylated ErbB1-GFP present in a cell, by making the following assumptions: 1. two receptor species, bound and unbound to antibody, exist at each resolvable volume element (pixel) and each species is associated with a unique fluorescence lifetime corresponding to the presence (τ_2) or absence (τ_1) of FRET, and 2. these fluorescence lifetimes are independent of spatial localisation within the cell and do not vary between experiments and can therefore be linked in a global analysis (Fig. 3.1 A).

The global analysis of the FLIM data therefore yields:

1. the spatially invariant lifetimes of each ErbB1-GFP species (τ_1, τ_2). From these data it is possible to calculate the FRET efficiency (E_c) between donor and acceptor in the complex, which is given by the equation: $E_c = 1 - (\tau_2 / \tau_1)$.

2. a fractional population map showing the relative levels of each species, bound and unbound to antibody, at every pixel (α map). The α map therefore shows the fraction of phosphorylated ErbB1 receptors present at each resolvable volume element (pixel).

The ability to accurately quantify the levels of phosphorylated ErbB1-GFP present at each resolvable volume element (pixel) facilitates a spatial analysis of phosphorylation levels within a single cell. It also allows the average amount of phosphorylated receptor present in the entire cell to be quantified and compared directly with other cells. Here, MCF-7 cells expressing ErbB1-GFP are stimulated with a saturating dose of soluble EGF or a highly localised stimulus with EGF-coated beads. It is demonstrated that both forms of stimulus produce an equivalent level and spatial extent of receptor phosphorylation. This shows that receptor phosphorylation can be propagated across the plasma membrane after a focal stimulus.

3.2 Quantitative imaging of ErbB1 receptor phosphorylation in living cells after a soluble or focal EGF stimulus

Fluorescently labelled antibodies can be introduced into the cytoplasm of cells by microinjection. It was reasoned that it should be possible to measure the tyrosine phosphorylation of ErbB1-GFP in living cells (that had been previously microinjected with Cy3-labelled anti-phosphotyrosine antibodies) by measuring the drop in fluorescence lifetime of the GFP caused by FRET to the bound antibody. A similar approach has been applied to measure the phosphorylation of GFP-PKCα in living cells by using microinjected acceptor fluorophore-labelled anti-phosphothreonine (T250) antibodies (Ng *et al* ., 1999). In the case of ErbB1, fluorescently labelled monovalent Fab fragments are preferable to the use of bivalent immunoglobulins to avoid the possibility that the antibodies could cause cross-linking of phosphorylated receptors.

3.2.1 Generation and characterisation of reagents

The procedures used to generate and isolate Fab fragments of PY72 are described in depth in section 2.2.2. In brief, PY72 IgG was digested by incubation with papain beads followed by separation of Fab fragments from Fc fragments / uncleaved IgG by loading the supernatant from the beads onto a protein A column. The size and purity of the eluted Fab fragments was confirmed by loading them onto an SDS PAGE gel under reducing conditions (Fig. 3.2A). Undigested PY72 yielded two bands with apparent molecular weights of ~50 and ~30 kDa, corresponding to IgG heavy and light chains

respectively. However, the Fab fraction from the protein A column ran as a single band with a molecular weight of ~30 kDa representing the cleaved light and heavy chains which comprise the Fab. The Fab fragments were then labelled with Cy3 and the absorbance of the labelled sample was measured at 280 and 554 nm in order to determine the dye molecule per protein molecule labelling ratio (see Fig. 3.2B and section 2.2.3). The labelling ratio was found to be 2 dye molecules per Fab molecule. Cy3-PY72 Fab fragments were used within 72 hours of preparation and the phosphotyrosine binding capacity of the material was checked prior to each experimental session by measuring binding to phosphotyrosine beads (see section 2.2.4). Approximately 30-40% of the material was found to be active according to this binding assay.

In order to facilitate the localised presentation of growth factors to cells EGF was covalently coupled to 0.8 μm diameter latex beads (see section 2.2.6). The carboxylate groups, present on the surface of commercially available latex beads, were derivatised to succinimidyl ester groups. Succinimidyl ester groups are reactive with primary amines in a reaction which liberates NHS, resulting in the formation of a stable peptide bond between the carboxylate group and the primary amine (Grabarek & Gergey, 1990). EGF contains no lysine residues and therefore the only primary amino group available for coupling via this method is the N-terminal amino group. The succinimidyl ester group-derivatised beads were therefore reacted with EGF resulting in the covalent coupling of the EGF to the beads via the N-terminus of EGF. It has previously been reported that derivatisation of, or immobilisation to a solid substratum via, the N-terminus of EGF does not abrogate the biological activity of this growth factor (Zidovetki, 1981; Kuhl & Griffith-Cima, 1996). Following completion of the coupling reaction excess EGF was removed by extensive washing in PBS. Covalent coupling of EGF to the beads was confirmed by immobilising beads on poly-L-lysine coated coverslips and staining with anti-EGF antibodies (section 2.2.7).

3.2.2 Imaging ErbB1 tyrosine phosphorylation in living cells

ErbB1-GFP expressing MCF-7 cells were microinjected with Cy3-PY72 Fab fragments and imaged after stimulation with a saturating dose of EGF (Fig. 3.3 A). To deliver a highly localised EGF stimulus, cells were also stimulated with EGF-coated beads (Fig. 3.3 B). The EGF-coated beads were stained with Cy5 prior to an experiment

to facilitate the localisation of beads that landed on cells (see section 2.2.8). The spatial distribution of phosphorylated receptors was monitored by acquiring FLIM data using a 488 nm laser line to excite the GFP and the appropriate emission filter to collect the fluorescence emission (see section 2.4). FLIM data were recorded prior to, and at suitable time points after, stimulus. The FLIM data was analysed using a global analysis as described above. The emergence of a homogeneous distribution of phosphorylated receptors could be visualised over the entire plasma membrane of cells as early as 5 minutes after stimulation via both methods (middle right panel, Fig. 3.3 A and B). Levels of phosphorylated receptor then increased over time reaching maximal levels 15 minutes post-stimulation.

The location of coated beads that landed on cells can be seen in the top left panel, Fig. 3.3B. Despite the focal nature of this stimulation, receptor phosphorylation was never observed to be confined to the membrane area below the bead, but always appeared as an extended pattern. As a negative control, one of the ErbB1-GFP expressing cells in the centre of the field was not microinjected with Cy3-PY72 Fab fragments (marked by a yellow asterisk, Fig. 3.3B). Throughout the experiment the populations of phosphorylated receptor present in this cell remained higher than surrounding cells. This indicates that the reduction in fluorescence lifetime of the ErbB1-GFP chimera was dependent on the binding of Cy3-PY72 antibodies to the phosphorylated receptor.

The experiment demonstrates the successful use of an ErbB1-GFP chimera, and microinjected Cy3-labelled anti-phosphotyrosine antibody Fab fragments, to monitor ErbB1-GFP phosphorylation in living cells. The spatial extent of receptor phosphorylation appeared to be similar whether a heterogeneous or focal stimulation was applied.

3.3 Quantitative imaging of ErbB1 receptor phosphorylation in fixed cells

Monitoring phosphorylation levels by microinjection of Fab fragments has two pitfalls: 1. antibody binding kinetics are rate-limiting, and 2. binding of antibodies to the receptor may stearically inhibit receptor interactions resulting in attenuated receptor transphosphorylation. These pitfalls prevent accurate determination of the spatial extent of receptor phosphorylation at early time points. Therefore, in order to more accurately determine the extent of phosphorylation, experiments were performed on

paraformaldehyde fixed cells (see section 2.3.5). Firstly, the precise spatial distribution of receptor phosphorylation at early time points after bead stimulation was analysed. Liquid handling during fixation, antibody incubation and washing of cells on coverslips is liable to remove cell-bound beads. However, by avoiding excessive turbulence during liquid handling, cell-bound beads could be retained in their original position on cells due to the strong interaction between EGF and the ErbB1 receptor. This enabled the spatial distribution of receptor phosphorylation to be correlated with EGF-bead position in fixed samples (Fig. 3.4). At stimulation times shorter than 1 minute after bead application, cells could be found where receptor phosphorylation was present in spatially confined 'patches' or polarised across one side of a cell. Under these conditions, bead position could be correlated with the polarised phosphorylation (10s and 30s, Fig. 3.4 A). In contrast, after 1 minute of bead stimulation all cells exhibited a distributed phosphorylation pattern around the entire rim of the cell that was no longer polarised (60s, Fig. 3.4 A). Elevated phosphorylation levels in a rim around the edge of cells were also observed with soluble EGF stimulus.

The apparent presence of higher phosphorylation levels around the rim of cells can be explained as follows. In general, most transfected cells contain two spatially distinct populations of ErbB1-GFP receptors: a major portion of the receptors are localised to the plasma membrane, but some are present in membranes of the secretory pathway or in endosomes. The FLIM images are acquired in a wide field microscope and consequentially the fluorescence measured at each pixel is contributed by GFP both on the surface of the cells and intracellular GFP. Intracellularly-retained ErbB1-GFP is inaccessible to ligand and remains nonphosphorylated, therefore where the cells are thickest (in the centre of the cell) there is a greater contribution of fluorescence from internal, nonphosphorylated receptors. This gives rise to lower apparent levels of phosphorylated receptors measured in the centre of the cells. In contrast, cells are thinner at the edge, so there is less contribution from intracellular ErbB1-GFP. Therefore, around the edge of cells, the signal from surface phosphorylated receptors predominates and phosphorylated receptor populations appear higher at the edge than in the centre.

The data from fixed cells confirmed that, after focal stimulus of ErbB1 receptors, phosphorylation is propagated to ligand-unoccupied receptors across the entire plasma membrane. However, the presence of free EGF or PTP inhibiting compounds in the bead preparation, or leakage of non-covalently absorbed EGF from the beads, might also

produce the observed widespread phosphorylation pattern. Some observations were made which rule out these possibilities. In Fig 3.4 B two cells imaged at 60 seconds after bead stimulus are shown. The bottom cell exhibiting raised phosphorylation levels is in contact with a bead whereas the top cell that is not directly contacted, but lies proximal to several beads, is quiescent. This demonstrates that contact of an EGF-coated bead with a cell is required to induce ErbB1-GFP phosphorylation and that possible leaching of non-covalently bound EGF from the beads did not occur. As a further precaution in several experiments beads were also washed again prior to use, but this had no significant effect on the results indicating that the preparation was free from contaminants.

In order to quantitatively compare the levels of phosphorylated receptor generated after both homogeneous and focal stimulation, large sets of cells were processed and imaged after stimulation for different times (5 seconds - 30 minutes). The average percentage of phosphorylated receptors was quantified at different time points after both soluble and focal stimulation (Fig. 3.5 C). Examples of cells used to calculate each data point are presented in Fig. 3.5 A and B. Both types of stimuli induced phosphorylated receptor levels exceeding those in non-stimulated cells as early as 5 seconds after stimulation and this phosphorylated population increased over time reaching a maximum at 1 minute after stimulation. Cells treated with soluble EGF exhibited a homogeneous pattern of phosphorylated receptor at the pre-1 minute time points (Fig. 3.5 A) whereas focal stimulation often resulted in the appearance of polarised receptor phosphorylation, as observed previously (Fig. 3.5 B). In accordance with this, the average phosphorylated receptor levels observed in cells at early time points after focal stimulus are lower than those detected after a soluble stimulus (Fig. 3.5 C).

The levels of phosphorylated receptors detected after 1 minute with both forms of stimulus were equivalent (EGF = 52 ± 3%; EGF-beads = 47 ± 7%). Additionally, the population images of these cells showed that, regardless of the means of stimulus, a similar pattern of phosphorylation was apparent after 1 minute: cells showed a homogeneous distribution of phosphorylated receptors in pixels around the entire periphery of the cell. In these pixels, the populations of phosphorylated receptors approached 100%. The populations of phosphorylated receptors fell after 1 minute (Fig. 3.5 C), in keeping with previously published data. This is due to the shielding of epitopes by phosphotyrosine binding proteins that associate with the receptor after internalisation (Wouters & Bastiaens, 1999).

3.4 A morphological study of cells provides independent evidence of receptor phosphorylation across the entire plasma membrane after bead stimulus

ErbB1 expressing cells stimulated with EGF typically show extensive plasma membrane ruffling within minutes of stimulation and elevated internalisation of ErbB1 leading to the accumulation of the receptor in many large endocytic vesicles. Confocal sections of serum starved, ErbB1-GFP expressing MCF-7 cells showed that the receptor is mostly concentrated at the plasma membrane of quiescent cells (Fig. 3.6 A). Receptors can be seen within relatively small membrane ruffles on the upper and lower surfaces of cells and also within small, internal vesicular structures. Cells stimulated with EGF-beads accumulated large membrane ruffles across the entire surface of the membrane and large cytoplasmic vesicles of endocytosed receptor (Fig. 3.6 B). Note that ruffling and internalisation in bead stimulated cells is not limited to the area of contact with beads. This provides additional evidence that a focal stimulus can elicit activation of receptors across the entire plasma membrane.

3.5 Discussion

FRET between ErbB1-GFP and a Cy3-labelled anti-phosphotyrosine antibody can be used to detect receptor phosphorylation in cells using FLIM (Wouters & Bastiaens, 1999). Here, a global analysis of the FLIM data was employed (Verveer *et al.*, 2000a), based on the assumption that each ErbB1-GFP molecule should be associated with one of two spatially-invariant lifetimes corresponding to the presence (phosphorylated receptor) or absence (nonphosphorylated receptor) of FRET. This has allowed the percentage of phosphorylated receptors present in single cells to be quantified.

Focal stimulus of cells with beads covalently-coupled to EGF results in rapid and extensive propagation of ErbB1 receptor phosphorylation across the surface of the entire cell (Fig. 3.3, 3.4 and 3.5). The level and spatial distribution of phosphorylation obtained after one minute of stimulus is equivalent whether growth factor is applied as a saturating soluble EGF dose or using EGF-beads (Fig. 3.5). EGF-beads can initiate the same changes in cell morphology and ErbB1 localisation as soluble EGF (Fig. 3.6). The spread of phosphorylation is not due to leaching of EGF from the bead because direct contact between beads and a cell is required for activation of ErbB1 receptors (Fig. 3.4 B).

Instead, a bead-position correlated, polarised distribution of phosphorylation captured at pre-1 minute time points suggests that the phosphorylation signal spreads from the point source of ligand (Fig. 3.4 A). A lag in the levels of phosphorylated receptor detected after bead stimulus, as compared to soluble stimulus, supports the presence of an intermediate phase of signal spreading that occurs prior to the peak levels detected at 1 minute (Fig. 3.5 C). It is concluded that a focal stimulus with EGF results in lateral propagation of ErbB1 receptor phosphorylation in the plane of the plasma membrane.

There are several conceivable interpretations as to the mechanism via which the spreading of phosphorylation might occur. It is convenient to split these hypothetical models into two broad categories: models that are dependent on long-range diffusion of protein tyrosine kinases and those that are based on a wavefront propagation of phosphorylation.

A. Diffusion-based models

(1). A cytosolic or membrane-associated protein tyrosine kinase (PTK), other than ErbB1, is activated by bead-bound ErbB1 receptors and can then diffuse across the cell phosphorylating ligand–unoccupied ErbB1 receptors (Fig. 3.7 A). This could be tested by measuring lateral propagation of phosphorylation under conditions which inhibit downstream signalling to PTKs.

(2). Rapid diffusion of ErbB1 receptors through the area under the bead leads to phosphorylation of the receptors as they pass through (Fig 3.7 B). This could occur via one of two mechanisms. For example, passing receptors could be transphosphorylated by a stable pool of active, bead-bound receptors. Alternatively, receptors could become phosphorylated as a consequence of transiently binding EGF presented on the beads. In the latter case, a rapid exchange of bead-bound receptors with the free receptor pool would be necessary to elicit such an effect. In both cases, after activation at the bead, ErbB1 must diffuse away from the bead and into the periphery of the cell to account for the widespread distribution of phosphorylated receptors observed after bead stimulus. The relevance of this model can be tested by characterising the diffusion of ErbB1-GFP in living cells.

B. Wavefront propagation models

(1). ErbB1 receptors bound to the EGF-beads are able to transphosphorylate adjacent ligand-unoccupied ErbB1 molecules, thereby activating the kinase activity of these receptors. The signal is then propagated outside the bead contact area via consecutive transphosphorylation events between adjacent ligand-unoccupied receptors (Fig. 3.7 C). The phosphorylation signal therefore proceeds via a 'domino effect' that spreads in a wavefront across the plasma membrane.

(2). A localised increase in ErbB1 kinase activity underneath the bead inhibits the activity of protein tyrosine phosphatases (PTPs). In this model, ErbB1 tyrosine kinase activity drives PTP inhibition, which in turn permits ligand-unoccupied receptors outside the bead contact point to become phosphorylated. Activation of these receptors invokes more PTP inhibition, which in turn leads to phosphorylation of more receptors i.e. a positive feedback mechanism is invoked. This is expected to also spread the phosphorylation signal in the form of a wavefront (Fig. 3.7 D). Significantly, this allows ligand-unoccupied ErbB1 receptors outside the bead contact point to become phosphorylated without any requirement to be directly phosphorylated by bead-coupled receptors. This is in contrast to wavefront propagation model 1.

In wavefront propagation model 1, spreading of the phosphorylation signal is dependent on an enhanced ErbB1 tyrosine kinase activity that is induced by tyrosine phosphorylation of the receptors, whilst in model 2, ErbB1 tyrosine kinase activity is independent of the tyrosine phosphorylation status of the receptor, but sustained PTP inhibition is required. In order for either model 1 or 2 to be true, it must be the case that transphosphorylation can occur in transient, ligand-independent receptor dimers. In order for model 2 to be correct, pharmacological agents that inhibit PTPs must be able to induce ligand-independent phosphorylation of ErbB1 to a similar extent as EGF-beads.

In the next Chapter the mechanisms underlying the observed signal spreading are further investigated. Experiments are performed to test predicted features of the above models in order to decipher between them.

Figure 3.1 Global analysis of FLIM data from an ErbB1-GFP phosphorylation assay

A. Tyrosine phosphorylation of GFP-tagged ErbB1 can be detected by measuring the fluorescence lifetime of the donor GFP when a Cy3-labelled antiphosphotyrosine antibody (Cy3-PY72) is bound. For the purpose of global analysis it is assumed that in all experiments: 1. all nonphosphorylated ErbB1-GFP molecules within the cell possess a unique, spatially invariant fluorescence lifetime, τ_1, and 2. all receptors bound to antibody are associated with a unique, spatially invariant fluorescence lifetime, τ_2. **B.** At every resolvable volume element of a cell (pixel) there will exist phosphorylated and nonphosphorylated ErbB1-GFP receptors (white box). In the given example, it is assumed that nonphosphorylated receptors are all associated with a lifetime of 2.2 ns (τ_1) and all phosphorylated receptors with a shorter lifetime of 0.8 ns (τ_2) due to FRET to the acceptor on the bound antibody. In the volume element (pixel) shown, 40% of the receptors have a lifetime of 0.8 ns and 60% have a lifetime of 2.2 ns. Conventional analysis of frequency-domain FLIM data returns two measures of the fluorescence lifetime at each pixel (see Fig. 1.9). These estimates, calculated from the phase shift and demodulation values at each pixel, are frequency-weighted averages of the fluorescence lifetime which are dependent on the lifetimes of each individual species and the relative abundance of each species. For the given example, a conventional analysis of FLIM data acquired at a single modulation frequency of 80 MHz would yield a phase lifetime estimate of 1.62 ns for the pixel. In contrast, a global analysis of the FLIM data would yield the lifetimes of each individual species (i.e. 2.2 and 0.8 ns) and the fraction of each species present (i.e. 0.4 and 0.6) in the pixel. **C.** The global analysis of ErbB1-GFP FLIM data makes use of the assumptions described in **A** and fits the data from each pixel to a two lifetime component model. This yields the true lifetime of each species (τ_1 and τ_2 ; blue box), and the relative populations of each species as a molar fraction, on a pixel-by-pixel basis (α map; yellow box). Colour bar indicates populations of the τ_2 species (phosphorylated receptors) as a decimal fraction at each pixel.

Fig. 3.1

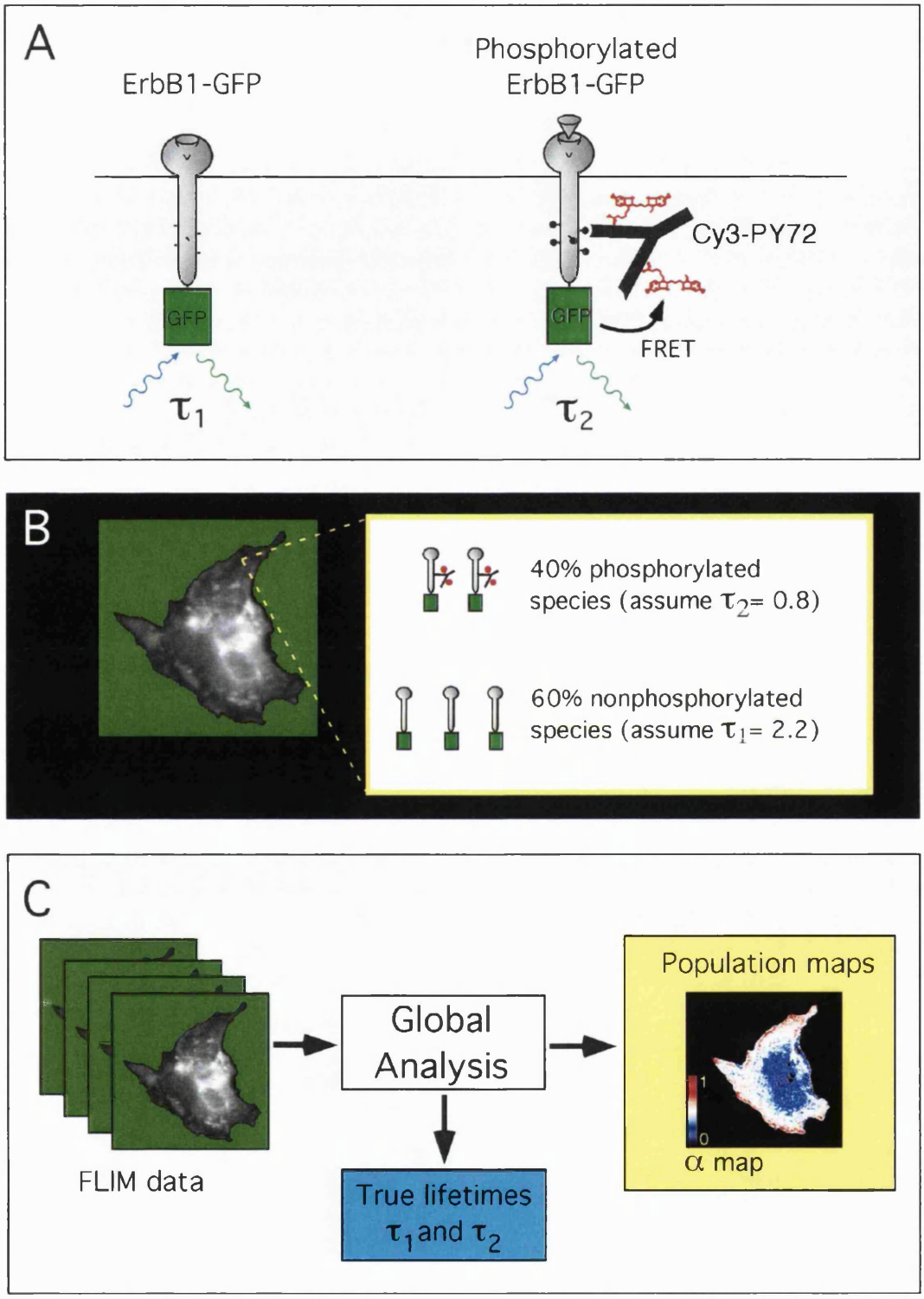
A
ErbB1-GFP
Phosphorylated
ErbB1-GFP
Cy3-PY72
GFP
GFP
FRET
τ1
τ2
B
40% phosphorylated
species (assume τ2= 0.8)
60% nonphosphorylated
species (assume τ1= 2.2)
C
FLIM data
Global
Analysis
True lifetimes
τ1 and τ2
Population maps
1
0
α map

Figure 3.2 Characterisation of Cy3-PY72 Fab fragments

A. Coomassie-stained SDS page gel. Lanes 1,2; 1 and 2 μg of PY72 whole IgG prior to Fab fragment generation. Lane 3; molecular weight markers (Biorad). Lanes 4, 5; 1 and 2 μg of PY72 Fab fragments. **B.** Absorbance spectra of Cy3-PY72 Fab fragments. The spectra was recorded from a 50 μl cuvette sample using a UV-visible spectrophotometer (Agilent Technologies).

Fig. 3.2

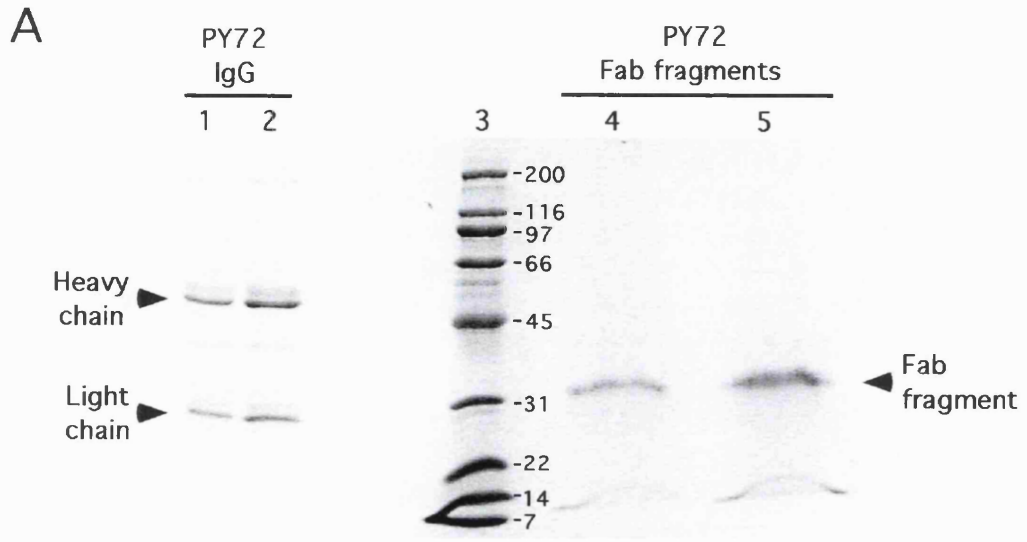
A
PY72
IgG
1 2
PY72
Fab fragments
3 4 5
-200
-116
-97
-66
-45
-31
-22
-14
-7
Heavy chain
Light chain
Fab fragment

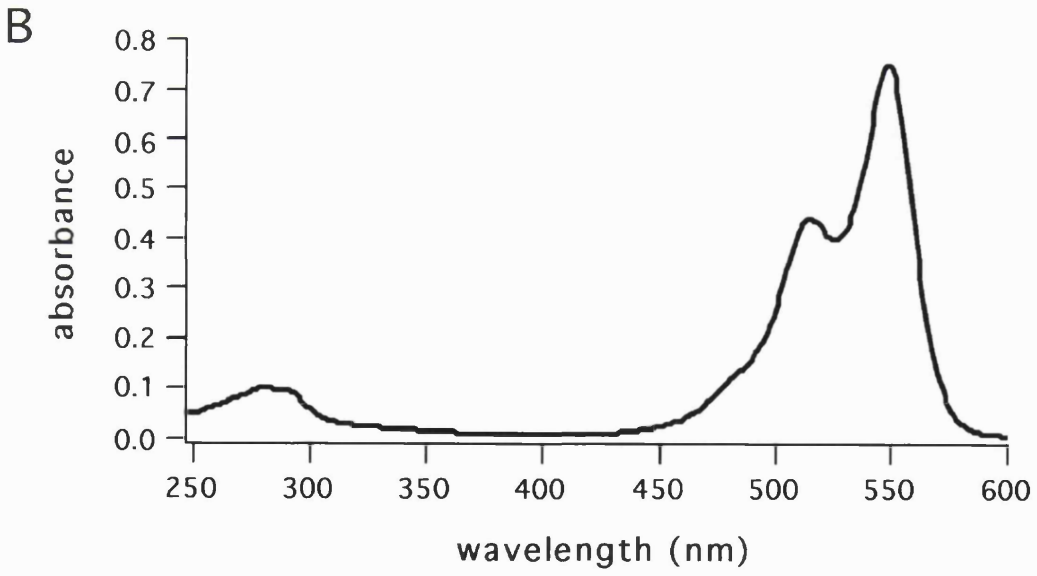
B
absorbance
0.8
0.7
0.6
0.5
0.4
0.3
0.2
0.1
0.0
250 300 350 400 450 500 550 600
wavelength (nm)

Figure. 3.3 Quantitative imaging of ErbB1 receptor phosphorylation in living cells

MCF-7 cells grown on glass-bottomed petri dishes were transfected with ErbB1-GFP and serum starved for 5 hours (see section 2.3.2). The cells were transferred to the stage of the FLIM instrument within a 37°C temperature-controlled environment and microinjected in the cytoplasm with Cy3-PY72 Fab fragments. The lifetime of ErbB1-GFP was recorded by acquiring a FLIM series of microinjected, ErbB1-GFP expressing cells before, and at suitable time points after, a stimulus with either soluble EGF **(A)** or EGF-coated beads **(B)**. Top left panels in **A** and **B**, ErbB1-GFP fluorescence intensity images; top right panels, Cy3-PY72 Fab fluorescence intensity images; lower panels, populations of phosphorylated ErbB1-GFP (α_2 population maps) at different time points. An image of bead position was recorded after completion of the experiment (red dots, top left panel, **B**). The populations data was generated by a single global analysis of 12 FLIM data series and yielded fluorescence lifetimes of $\tau_1 = 2.2$ ns and $\tau_2 = 0.56$ ns ($E_c = 75\%$).

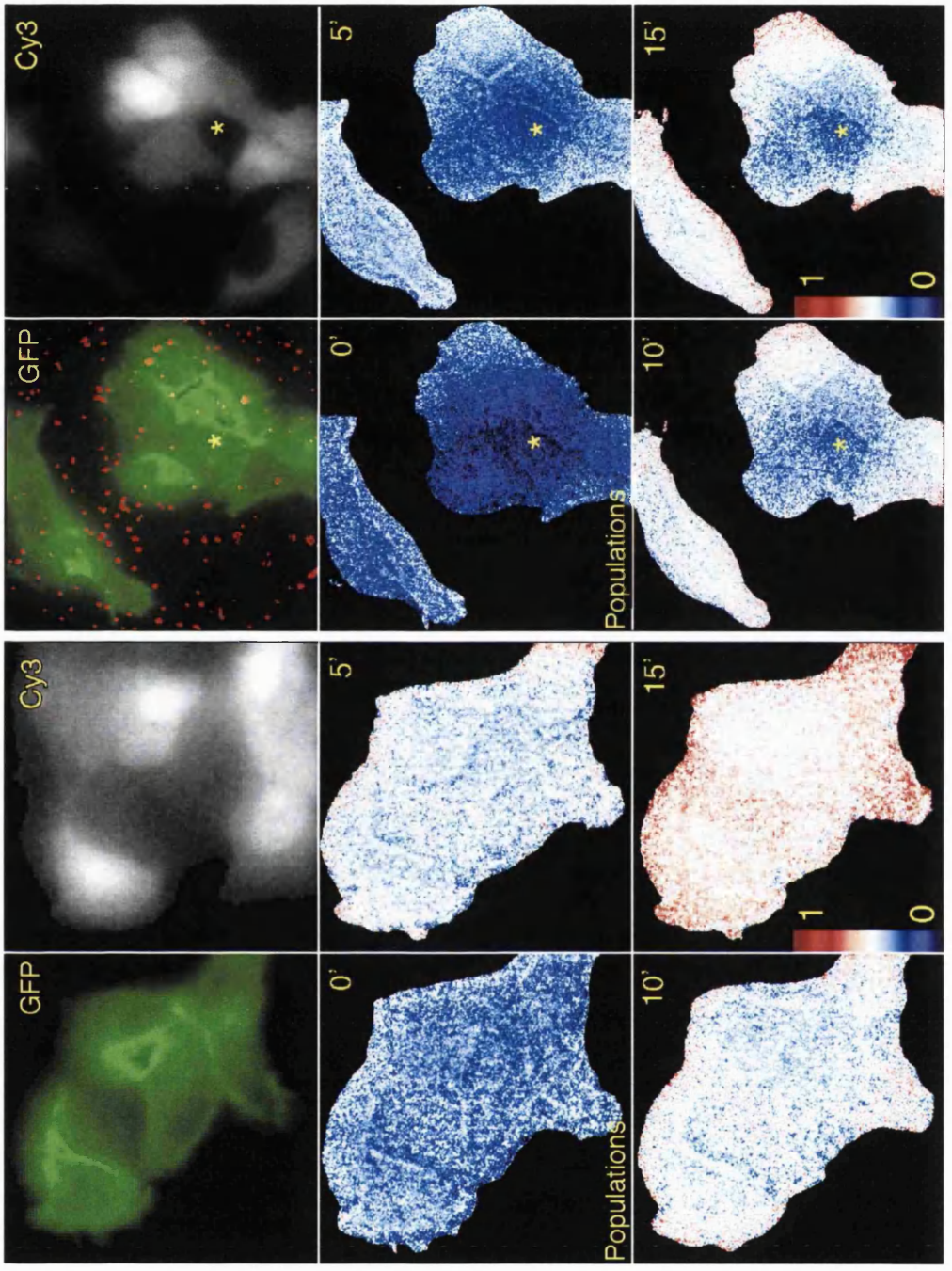
A. Soluble EGF stimulus
B. EGF-bead stimulus
GFP
Cy3
0'
5'
10'
15'
Populations
1
0

Fig. 3.3

Figure. 3.4 Correlation of bead position with phosphorylation of receptors

Serum starved, ErbB1-GFP expressing MCF-7 cells grown on glass-bottomed petri dishes were rapidly fixed after stimulation with Cy5-labelled EGF-coated beads for 10, 30 or 60 seconds. They were then permeabilised and incubated for 1 hour with Cy3-labelled PY72 antibody (see section 2.3.5). **A.** Top row, ErbB1-GFP fluorescence (green) with Cy5-labelled beads (red); middle row, Cy3-PY72 staining; bottom row, populations of phosphorylated receptors. **B.** Left panel, ErbB1-GFP fluorescence (green) with Cy5-labelled beads (red); middle panel, Cy3-PY72 staining; right panel, populations of phosphorylated receptors. Populations data was generated from a single global analysis of 55 FLIM data series, yielding fluorescence lifetimes of $\tau_1 = 2.4$ ns and $\tau_2 = 0.94$ ns ($E_c = 61\%$).

Fig. 3.4

A

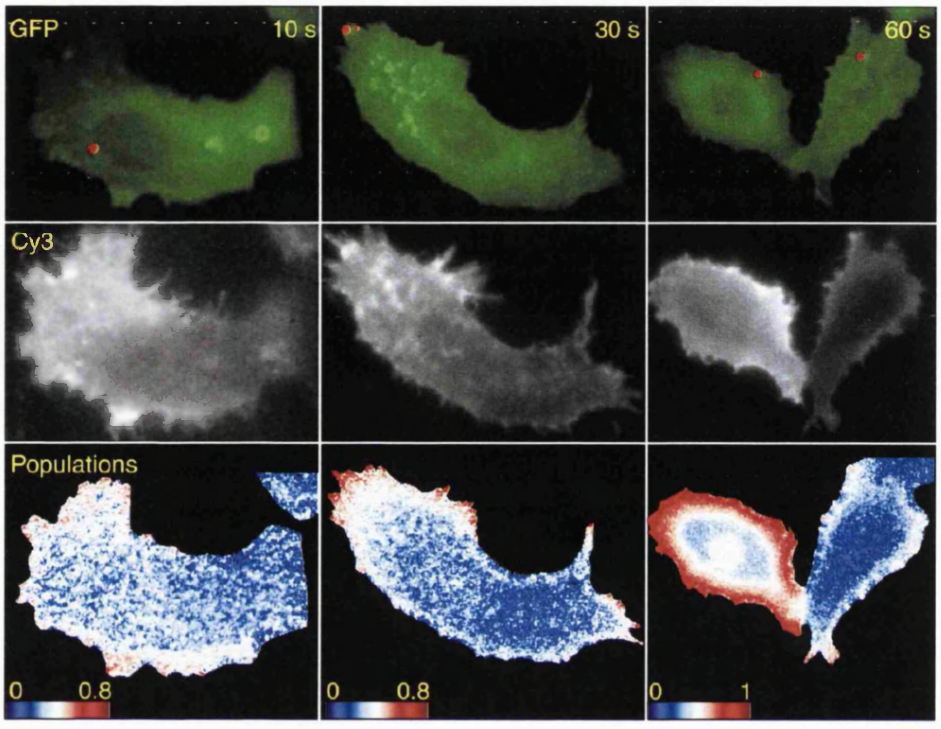
GFP
10 s
30 s
60 s
Cy3
Populations
0
0.8
0
0.8
0
1

B

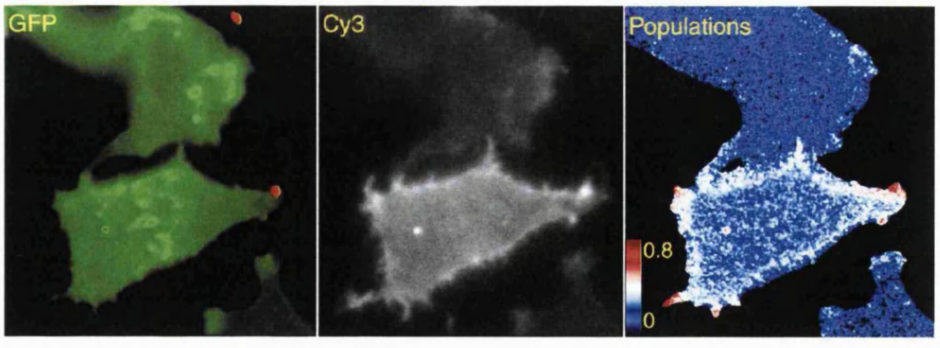
GFP
Cy3
Populations
0.8
0

Figure 3.5 Time course of ErbB1-GFP phosphorylation

Serum starved, ErbB1-GFP expressing MCF-7 cells grown on coverslips were rapidly fixed after stimulation with 100 ng/ml soluble EGF (**A**) or EGF-beads (**B**) for different times. Cells were then permeabilised and stained with Cy3-PY72. A single representative cell is shown for each time point. Top panels, ErbB1-GFP fluorescence intensity; middle panels, Cy3-PY72 fluorescence intensity ; lower panels, populations of phosphorylated receptor. In **A**, a single global analysis (97 FLIM data sets, ~10 cells per time point) returned fluorescence lifetimes of $\tau_1 = 2.23$ ns and $\tau_2 = 0.84$ ns ($E_c = 62\%$). In **B**, a single global analysis (81 FLIM data sets, ~10 cells per time point) yielded fluorescence lifetimes of $\tau_1 = 2.23$ ns and $\tau_2 = 0.83$ ns ($E_c = 63\%$). **C.** The mean average population of phosphorylated receptors detected at each time point is plotted for stimulation with soluble EGF and EGF-beads (see overleaf).

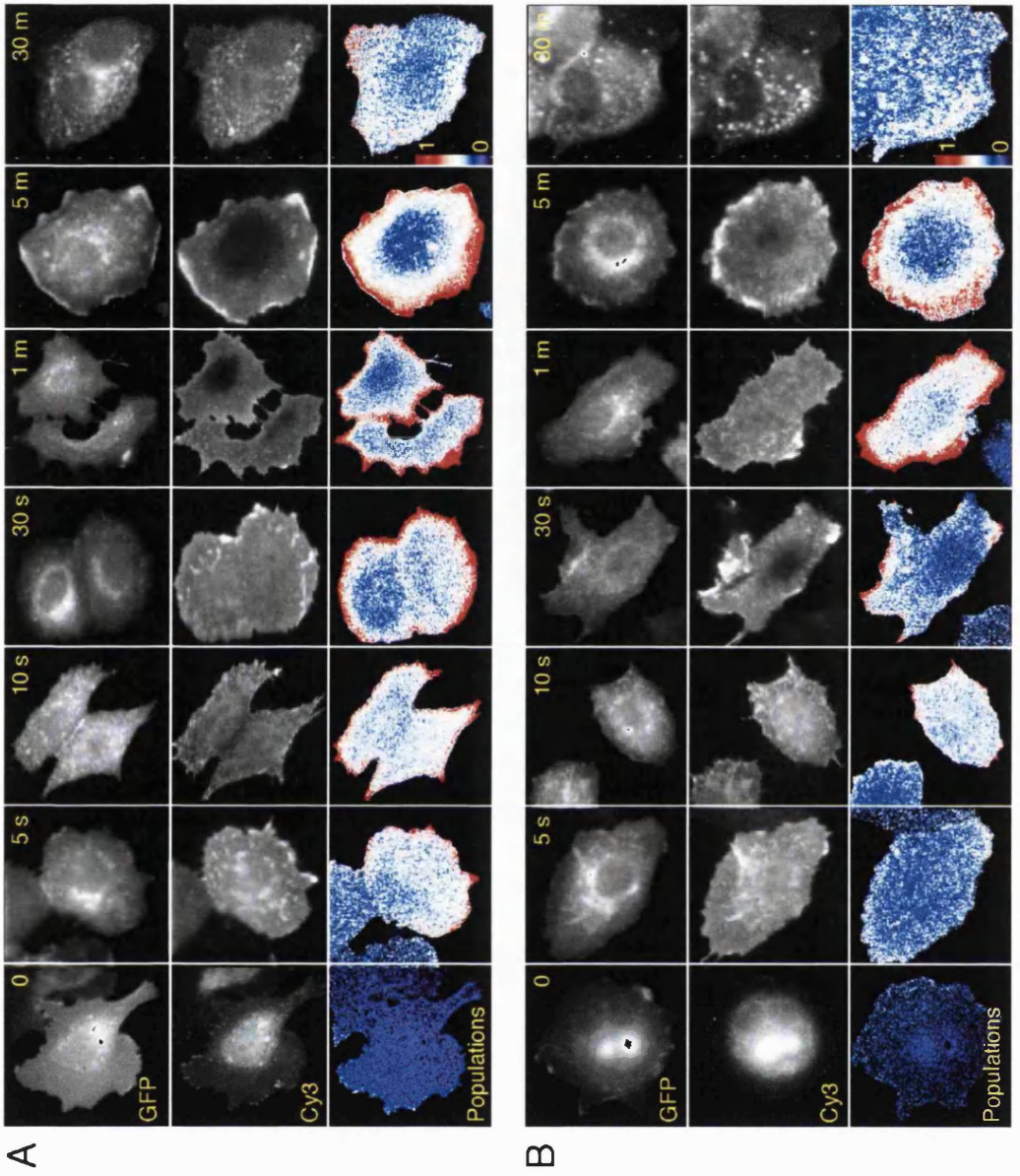

Fig. 3.5

Fig. 3.5 C

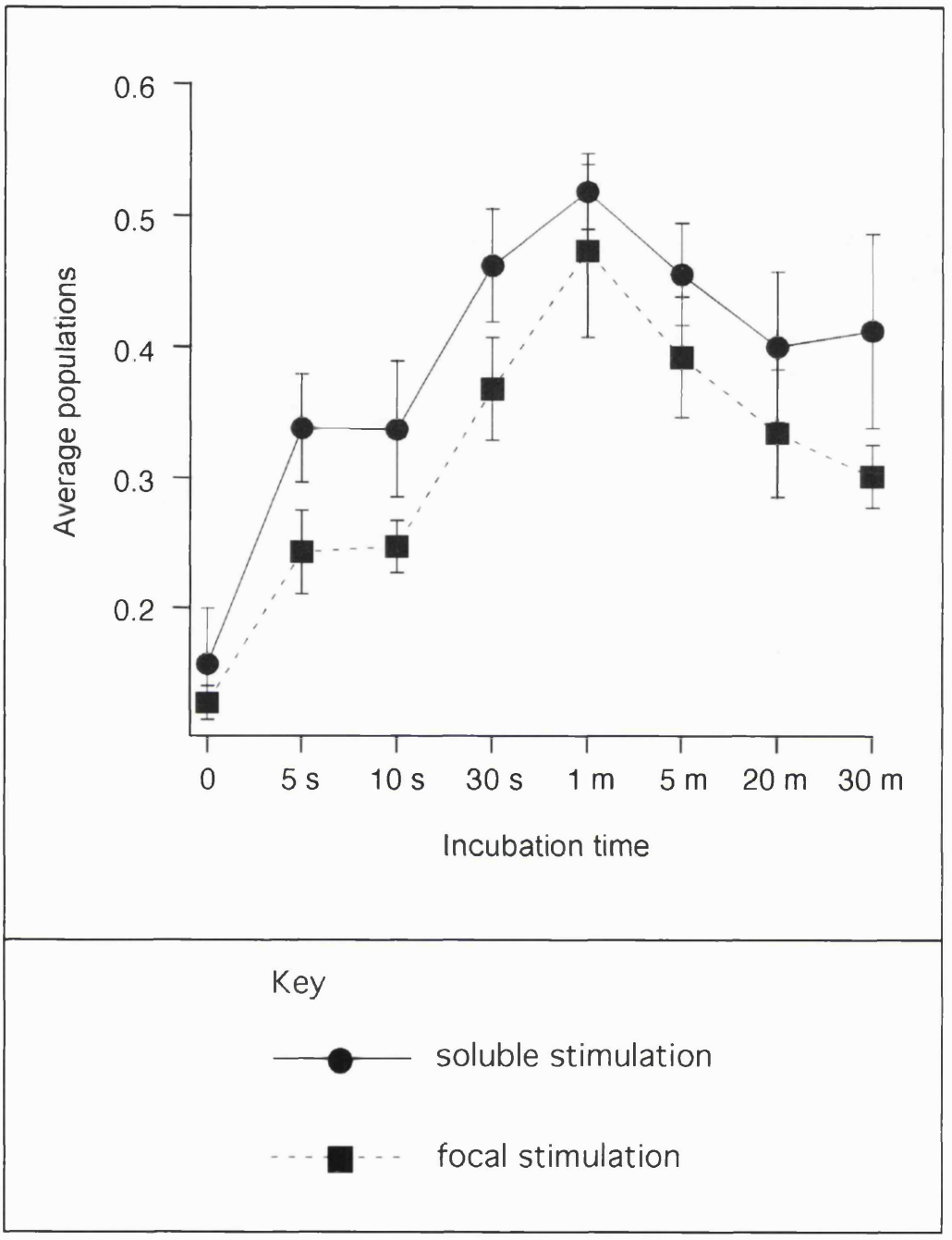
0.6
0.5
0.4
0.3
0.2
Average populations
0
5 s
10 s
30 s
1 m
5 m
20 m
30 m
Incubation time
Key
soluble stimulation
focal stimulation

Figure 3.6 Confocal sectioning of ErbB1-GFP expressing MCF-7 cells before and after stimulus

Serum starved, ErbB1-GFP expressing cells grown on glass-bottomed petri dishes were imaged at 37°C on the confocal microscope (see section 2.3.7). Confocal sections were recorded at 0.5 μm intervals in the z-axis. Representative sections from a single cell are shown in panel **A**. The cells were then stimulated with EGF-beads and returned to the incubator (37°C, 10% CO_2) for 30 minutes prior to acquisition of a second set of confocal images (panel **B**). Green fluorescence is ErbB1-GFP, red fluorescent structures are Cy5-labelled EGF-coated beads and arrowheads indicate the location of endsomes containing internalised ErbB1-GFP.

Fig. 3.6

A. Pre-stimulus

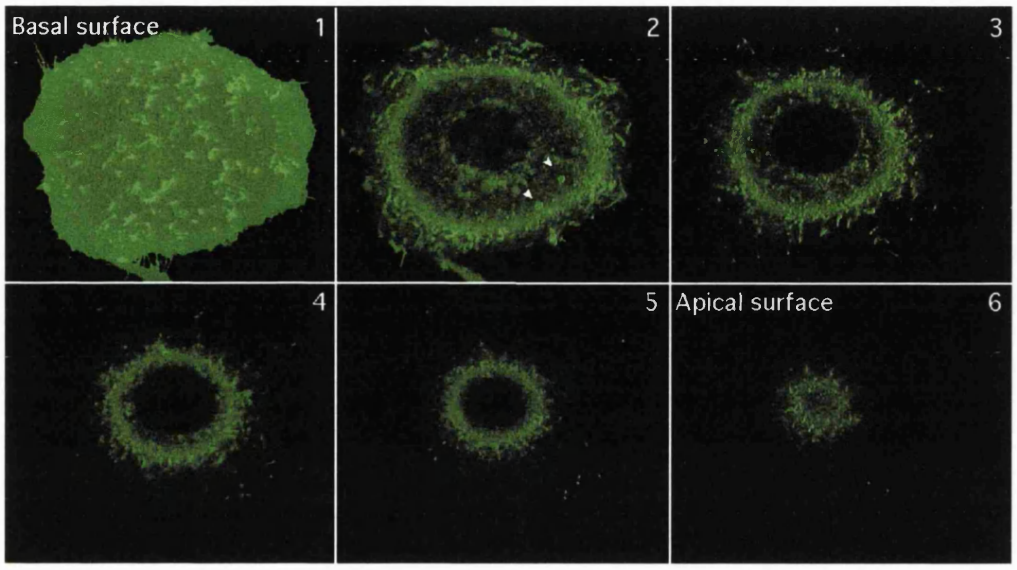

B. 30 mins post-stimulus

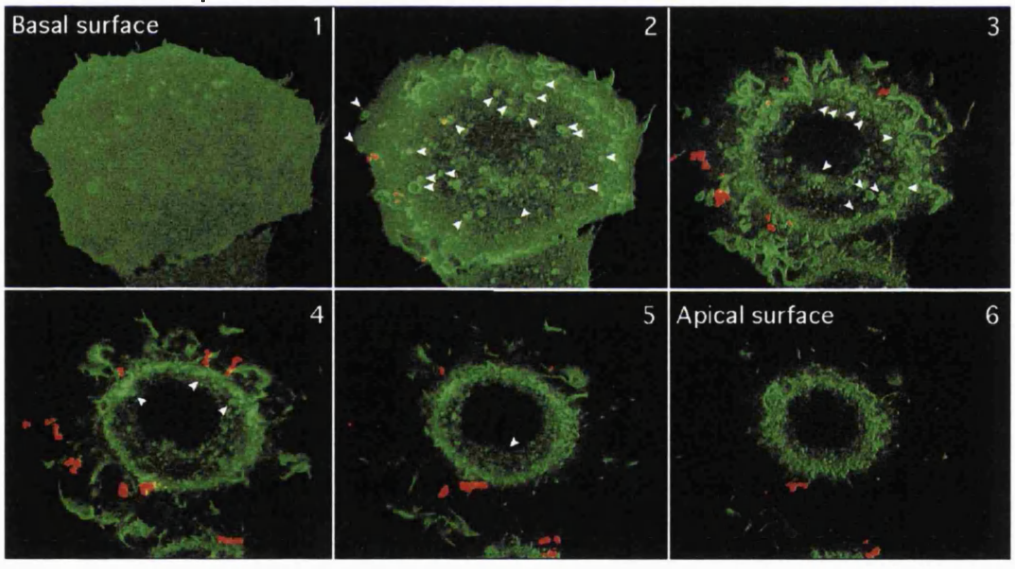

Figure 3.7 Possible mechanisms for the observed spreading of ErbB1 phosphorylation

A. Contact of beads with the cell initiates a localised, ligand-dependent clustering of ErbB1 receptors (1). The phosphorylated receptors activate a cytosolic or plasma membrane-associated PTK via direct phosphorylation (2). This independent kinase is able to diffuse out of the bead contact area and phosphorylate peripheral ligand-unoccupied ErbB1 molecules (3). **B.** ErbB1 receptors diffuse at random in the plasma membrane (1). These receptors become transphosphorylated by ligand-bound ErbB1 receptors under the bead (2a), or as a consequence of transiently binding EGF presented by the bead (2b). Upon dissociation from the bead the phosphorylated receptors diffuse into the area peripheral to the bead contact point (3). **C.** Contact of beads with the cell initiates a localised, ligand-dependent clustering of ErbB1 receptors (1). Ligand-bound phosphorylated receptors can phosphorylate adjacent ligand-unoccupied receptors, thereby increasing their intrinsic kinase activity (2). These phosphorylated, ligand-unoccupied receptors go on to phosphorylate other ligand-unoccupied receptors in the periphery, increasing their intrinsic kinase activity (3). Phosphorylation then spreads by consecutive transphosphorylation events between ligand-unoccupied receptors (4). **D.** Collisions between ErbB1 receptors in the plasma membrane allows transphosphorylation to occur in the absence of ligand, but high PTP activity maintains a low net population of phosphorylated receptors (1). Phosphorylated ErbB1 receptors, activated by EGF-beads, give rise to PTP inhibition via a mechanism that is initiated by concentration of receptors. Ligand-unoccupied receptors close to the bead also become phosphorylated, because the silencing activity of PTPs is removed, thereby allowing receptor collisions to result in stable transphosphorylation (2). Ligand-unoccupied phosphorylated receptors induce further PTP inhibition thereby leading to phosphorylation of more ligand-unoccupied receptors (3).

Fig. 3.7

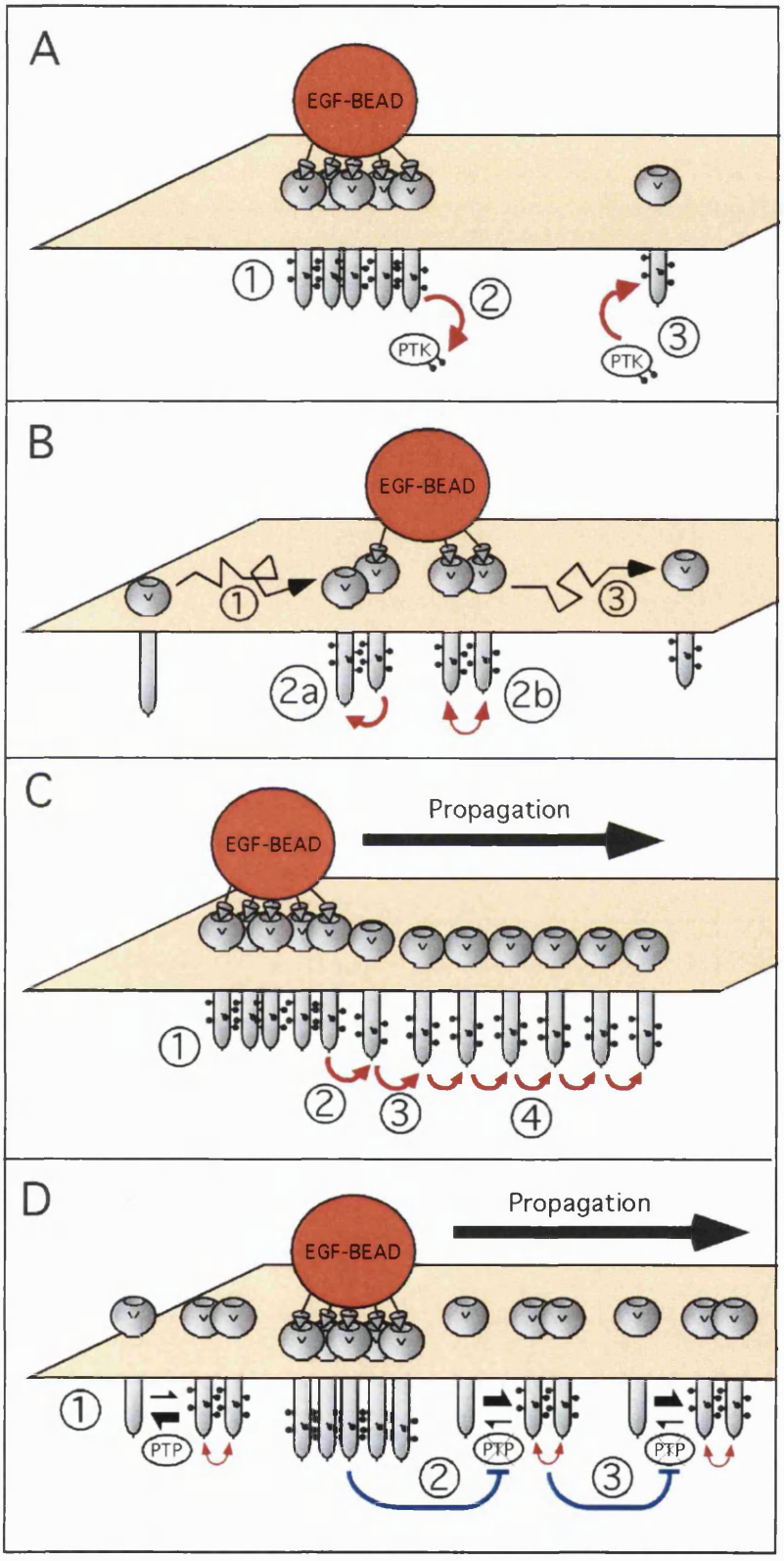
A
EGF-BEAD
①
②
PTK
③
PTK
B
EGF-BEAD
①
③
2a
2b
C
EGF-BEAD
Propagation
①
②
③
④
D
EGF-BEAD
Propagation
①
PTP
②
PTP
③
PTP

Chapter 4

An Investigation into the Mechanisms which Mediate Lateral Propagation of ErbB1 Receptor Phosphorylation

An investigation into the mechanisms which mediate lateral propagation of ErbB1 receptor phosphorylation

4.1 Introduction

In the previous chapter quantitative imaging of ErbB1 phosphorylation was employed to study the lateral propagation of ErbB1 receptor phosphorylation in the plane of the plasma membrane. It was demonstrated that a focal stimulus with beads covalently coupled to EGF, or a saturating soluble dose of EGF, results in equivalent activation of ErbB1 receptors across the entire plasma membrane. Several interpretations as to the mechanism via which this might occur were proposed (see section 3.5 and Fig. 3.7). In Chapter 4 an investigation is presented into the mechanisms which underlie the lateral propagation of phosphorylation. Firstly, the involvement of ErbB1 downstream signalling to non-receptor PTKs is addressed. Secondly, to address the possible involvement of long-range ErbB1 receptor diffusion, fluorescence photobleaching studies on cells expressing ErbB1-GFP are presented. Thirdly, to examine the possibility that transphosphorylation in transient receptor dimers could be involved, the stability of ErbB1 receptor dimers is investigated. Finally, to begin to address the role of protein tyrosine phosphatase (PTP) inhibition, an EGF dose-response curve is presented in the presence and absence of a pharmacological PTP inhibitor.

The evidence obtained suggests that a mechanism based on activation of ErbB1 (or an independent cytosolic protein tyrosine kinase) at the bead contact point, followed by rapid diffusion into the periphery, cannot account for the widespread distribution of ErbB1 phosphorylation induced by EGF-beads. It is proposed instead that the beads present a local threshold dosage of EGF that is sufficient to initiate a wave front propagation of phosphorylation through ligand-free receptors. The relevance of two alternative models is discussed: 1. a transphosphorylation domino effect which relies on ErbB1 tyrosine kinase activity alone (Fig. 3.7 C), or 2. a positive feed-back loop between ErbB1 receptor tyrosine phosphorylation and PTP inhibition. It is argued that a transphosphorylation domino effect is unlikely to mediate the observed rapid spreading

and that the latter model, involving suppression of cellular PTP activity, is the mechanism via which the propagation of phosphorylation to ligand-unoccupied receptors proceeds.

4.2 The involvement of downstream signalling to PTKs in lateral propagation of ErbB1 phosphorylation

Cells possess many non-receptor PTKs (Hubbard & Till, 2000; Blume-Jensen & Hunter, 2001), some of which become activated as a downstream consequence of ErbB1 activation e.g. members of the Src family of PTKs (Thomas & Brugge, 1997). Activated Src is able to phosphorylate the EGF receptor at all known tyrosine autophosphorylation sites and at four unique sites (Fig. 1.1 D; Olayioye *et al.*, 2000). Src and other non-receptor PTKs are also implicated in the ErbB ligand-independent transactivation of ErbB1 after stimulation of GPCRs or non-ErbB RTKs (Thomas & Brugge, 1997; Luttrell *et al.*, 1999). Given these facts, a possible mechanism underlying the lateral propagation of ErbB1 phosphorylation is the activation of Src after direct phosphorylation by ErbB1 molecules underneath the bead. Activated Src could then diffuse throughout the plasma membrane surface and phosphorylate other ErbB1 receptors outside the bead contact area (see section 3.5; Fig. 3.7 A). To exclude the involvement of Src in the observed lateral propagation of ErbB1 phosphorylation, bead stimulation was performed in the presence of 50 nM PP2, a Src family PTK inhibitor. Under these conditions lateral signal propagation was still evident and the populations of phosphorylated receptors generated in these cells at 1 minute (45 ± 9%, n = 14 cells) was equivalent to that observed in cells stimulated with beads in the absence of the inhibitor (47 ± 7%, n = 15 cells; Fig. 4.1). The IC_{50} for Src kinase activity inhibition by PP2 is 50 nM, but it also inhibits ErbB1 kinase activity with an IC_{50} of 480 nM (Calbiochem). Accordingly, in cells stimulated with beads for 1 minute in the presence of 500 nM PP2, ErbB1 receptor phosphorylation was attenuated (populations = 26 ± 3%, n = 12 cells; Fig. 4.1). This confirms that the kinase activity of ErbB1 is required to mediate the spread of phosphorylation, but that Src kinase activity is not.

Cells stimulated for 20-30 minutes in the presence of 50 nM PP2 accumulated elevated amounts of phosphorylated receptor in comparison to stimulated cells not treated with PP2 (Fig. 4.1 A). A visual assessment of the amount of material present in

endosomes revealed that PP2 treated cells also appeared to contain less endocytosed ErbB1 receptor than non-treated cells. These data support the proposed role for Src tyrosine kinase activity in stimulating clathrin-mediated ErbB1 endocytosis and receptor down regulation (Wilde *et al.*, 1999).

Whilst Src family kinases are anchored to the plasma membrane via an N-terminal acylation, many other PTKs are cytosolic. To exclude the involvement of freely diffusing cytosolic kinases, EGF-coated bead stimulation experiments were performed on streptolysin-O permeabilised MCF-7 cells in the presence of ATP (Fig. 4.2). The average phosphorylated receptor populations observed in cells stimulated in the presence of the permeabilisation buffer was lower than that observed when stimulus was performed in normal medium. However, the spatial distribution and populations of phosphorylated receptors produced was comparable in permeabilised cells and cells incubated in the presence of buffer alone when stimulation was performed with EGF or EGF-beads (Fig. 4.2). MCF-7 cells expressing a cytosolic GFP (prepared by transfecting with pEGFP-C3, Clontech) lost cytosolic GFP fluorescence under these permeabilisation conditions, confirming the efficacy of the permeabilisation technique. This result makes it unlikely that a soluble freely diffusing PTK is involved in the lateral spreading of phosphorylation.

4.3 ErbB1-GFP diffusion characteristics in the plasma membrane

4.3.1 Calculation of the diffusion coefficient of ErbB1-GFP in living cells

It has been proposed that the phosphorylation spreading could occur via a mechanism based on rapid diffusion of receptors through the area where the EGF beads contact with the plasma membrane. In this model, receptors could become transphosphorylated by receptors that are already bound to the EGF-beads or by transiently binding to EGF presented by the beads (section 3.5; Fig. 3.7 B). In either case, following activation at the bead contact site, the phosphorylated receptors would then have to diffuse back out into the periphery of the cell in order to give rise to the extended pattern of phosphorylation observed. The diffusion coefficient, D, is a measure of the mean unit area covered by a molecule within a given time. It was reasoned that it should be possible to address the validity of the diffusion model by determining the diffusion

coefficient of ErbB1-GFP and then calculating whether this is fast enough to account for the extended pattern of ErbB1 phosphorylation observed after EGF-bead stimulus.

The diffusion coefficient of ErbB1-GFP in the plasma membrane of live MCF-7 cells was determined using the fluorescence recovery after photobleaching (FRAP) technique (see Fig. 4.3). The technique utilises time-lapse microscopy to measure the recovery of fluorescence within a region of a cell in which a population of fluorescent molecules has been photobleached. Recovery occurs due to the exchange of photodestroyed fluorescent molecules within the bleached region with native fluorescent molecules outside the bleached region by diffusion. The kinetics of recovery can be used to calculate an approximate *D* value for the fluorescent molecule (Axelrod 1976, Soumpasis, 1983; White & Stelzer, 1999).

ErbB1-GFP expressing MCF-7 cells were imaged on the stage of a confocal laser scanning microscope which was warmed to 37°C. Regions of interest within MCF-7 cells were chosen that exhibited a relatively homogeneous fluorescence signal. Flat areas near the cells' edge were chosen in order to maximise the chance that the imaged fluorescence was contributed mainly by plasma membrane-localised ErbB1-GFP and not by receptor molecules present within internal membranes (see section 3.3). Data from a typical experiment can be seen in Fig. 4.4. The circular bleached region is clearly visible in the first post-bleach image. Recovery of fluorescence within the bleach region, due to replenishment with fluorescent molecules, can be seen to occur in subsequently acquired images (Fig. 4.4 A). The kinetics of recovery were quantified by plotting the average intensity of the bleached region divided by the original pre-bleach intensity of the region (I/I_0) as a function of time (Fig. 4.4 B). The data is corrected for any bleaching due to repetitive illumination of the sample during recovery measurements. The plot shows that recovery in the bleached region was ~75% complete by 30 seconds and by 2 minutes had recovered to ~85% of the original level. Recovery to 100% of the original level is rarely observed in FRAP experiments. This phenomenon is due to the presence of immobile molecules within the bleached region. The fluorescence contribution of these immobile molecules cannot be replaced by exchange with molecules outside the bleach region (Axelrod *et al.*, 1976). The fraction of immobile ErbB1-GFP in a typical experiment was 15%.

The same FRAP experiment was performed on multiple ErbB1-GFP expressing MCF-7 cells, yielding a reproducibly similar result to that depicted in Fig. 4.4. The

diffusion coefficient of ErbB1-GFP was calculated by fitting a function to the recovery curves, as described by Soumpasis (see section 2.5.1). For ErbB1-GFP diffusion in the plasma membrane of MCF-7 cells a mean average D of 0.032 ± 0.010 μm^2/sec was calculated (n = 10 cells). This is comparable to D values calculated previously for native EGF receptors in the plasma membrane of living cells at 37°C by using both FRAP (0.085 μm^2/sec; Zidovetki et al 1981) and single particle tracking techniques (0.01-0.02 μm^2/sec; Kusumi *et al.*, 1993).

The area through which a molecule exhibiting Brownian motion could move in a given time can be related to the measured D for the molecule by the 2-dimensional diffusion equation originally formulated by Einstein:

$$< r^2 > = 4 \times D \times t$$

where, r (μm) is the radius of the circular area which could be covered by the diffusing molecule and t is time. Substitution of the measured D for ErbB1-GFP (0.032 μm^2/sec) into the equation shows that it will take approximately 10 minutes for a single receptor to diffuse within an area of 10 μm radius and approximately 1 hour to diffuse within an area of 20 μm radius. Given that the MCF-7 cells used in these studies were typically 30-50 μM in length it would be impossible for a substantial population of phosphorylated receptors, activated at the bead, to diffuse across the length of the entire cell within 1 minute. It is therefore deemed highly unlikely the appearance of phosphorylated receptors across the entire surface of the cell, after EGF-bead stimulation, is due to a mechanism based on phosphorylation of ErbB1-GFP receptors at the bead, followed by diffusion of the receptors into the periphery.

4.3.2 Residence time of ErbB1-GFP receptors bound to EGF-beads

Further evidence refuting a long-range ErbB1 diffusion-based model was gained from FRAP experiments performed on cells treated with EGF-beads. It has been proposed that phosphorylation of receptors at the bead might occur due to a transient interaction of receptors with EGF bound to the bead (see section 3.5; Fig 3.7 B). A rapid exchange of bead-bound receptors with the ligand-unoccupied receptor pool would be

necessary to elicit such an effect. It was deemed possible to evaluate this by photobleaching the ErbB1-GFP fluorescence beneath EGF-beads and thereby gain a measure of the ErbB1-GFP residence time beneath the beads.

FRAP experiments were performed exactly as described above, except that the cells were imaged shortly after the application of EGF-beads. Selected time points from a typical experiment are shown in Fig. 4.5. Microscopic observation of cells revealed that beads undergo Brownian motion whilst in free solution, but upon contact with cells they become stably bound and relatively immobile. Note that this eliminates the possibility that the observed extended pattern of phosphorylation could be due to rolling of the beads over the surface of the cell. It was apparent that underneath cell-bound beads a spot of GFP fluorescence accumulated. The intensity of the spot exceeded that in the surrounding area and was equivalent in size to the beads (beads 1-7, Fig. 4.5 A). This confirms that EGF-coated beads can bind and concentrate ErbB1 receptors. An area was bleached around a pair of beads (indicated as beads 4 and 5 in Fig. 4.5 A) in order to compare the recovery of fluorescence intensity under the bead and in the surrounding area (Fig. 4.5 B). It can be seen that fluorescence intensity in the area surrounding the bead recovered to ~85% of its original level by 1 minute (Fig. 4.5 C). However, even by two minutes the original high intensity underneath the bead did not recover (Fig. 4.5 D). If freely diffusing ErbB1-GFP molecules are in rapid exchange with bead-bound receptors then this fluorescence intensity would be expected to recover fully. The fact that it does not confirms that there is a tightly bound immobile pool of receptors attached to the bead that are not in free exchange with the external pool within the time scale of this experiment.

The presence of a stable bead-bound pool of receptors, which does not exchange with the external pool within a two minute period, has two important implications. Firstly, it is unlikely that receptors become activated by a transient interaction with EGF on the beads. The rate of exchange of bead-bound receptors with the external pool is too slow to allow for all cellular receptors to become activated by transiently binding bead-bound EGF. Therefore, this is not the mechanism via which receptors outside the bead contact point become phosphorylated. Secondly, the EGF-beads must act to bind and concentrate ErbB1 receptors, leading to a concentrated patch of ErbB1 kinase activity. A high local concentration of tyrosine kinase activity might therefore be implicated in the mechanism via which EGF-beads elicit lateral propagation of ErbB1 phosphorylation.

4.4 Transient interactions between ErbB receptors

The evidence thus far presented in this chapter diminishes the likelihood that the lateral propagation of ErbB1 phosphorylation is due to either of the diffusion-based models proposed in section 3.5 (see also Fig. 3.7 A and B). However, it was also proposed that the spreading of phosphorylation may occur via one of two wavefront propagation models (see Fig. 3.7 C and D). In the first model, ErbB1 receptors bound to the bead are proposed to phosphorylate adjacent ligand-unoccupied receptors. These phosphorylated, ligand-unoccupied receptors are subsequently implicated in spreading the signal to other ligand-unoccupied receptors by transphosphorylation: a transphosphorylation 'domino effect' amongst ligand-free receptors is invoked (Fig. 3.7 C). The mechanism would require ErbB receptors to be able to transiently interact with, and phosphorylate, multiple receptor partners. In the second model, ErbB1 receptors bound to the bead are proposed to initiate PTP inhibition. This PTP inhibition then allows collisions between ligand-free, kinase active, ErbB1 receptors to result in stable transphosphorylation. A positive feedback loop between receptor phosphorylation and PTP inhibition allows the phosphorylation to spread (Fig 3.7 D). This model also requires that ErbB1 transphosphorylation can occur during transient interactions between ErbB1 molecules. Independent evidence for the ability of a single ErbB molecule to phosphorylate multiple receptor partners, via transient inter-receptor interactions, is required to substantiate the plausibility of either wave front propagation mechanism.

ErbB3 is intrinsically kinase dead and it has been shown that another member of the ErbB family must be present in the same cell for ErbB3 to become phosphorylated in a ligand-dependent fashion (Soltoff *et al.*, 1994; Pinkas-Kramarski *et al.*, 1996). MCF-7 cells were transfected with an ErbB3-GFP construct, which was constructed identically to the ErbB1-GFP used in previous experiments described here. As expected, no phosphorylation of ErbB3 was observed when these cells were stimulated with EGF (Fig. 4.6 B). Cells were then co-transfected with two constructs by nuclear microinjection: a non GFP-tagged ErbB1 and ErbB3-GFP. Transfections were made such that cells were presented with a 10-fold molar excess of ErbB3-GFP DNA over ErbB1 DNA. Immunostaining with an ErbB1-specific antibody (monoclonal F4) showed that whilst the ErbB3-GFP fluorescence signal was strong in cells transfected with this 1:10 DNA mixture, ErbB1 expression levels were below the detection limit of immunofluorescence,

confirming that in individual cells ErbB3-GFP was present in a large excess with respect to ErbB1. Soluble EGF stimulation of these cells resulted in the phosphorylation of ErbB3 molecules across the entire plasma membrane (Fig. 4.6 A). On average, the population of ErbB3-GFP molecules which became phosphorylated in a single cell after 5 minutes EGF stimulation was 43 ± 8% (n = 13 cells). This is significantly more than the fraction of ErbB1 estimated to be present in a single cell (10%), which suggests that after activation by EGF, a phosphorylated ErbB1 molecule can interact with and phosphorylate multiple ligand-unoccupied ErbB3 molecules.

It should be noted that the exact stoichiometry of the ErbB1-ErbB3 complexes involved in these phosphorylation events cannot be directly inferred from the results of the experiment. It may be that the EGF-bound ErbB1 molecules form stable dimers that recruit ErbB3 molecules in a tetrameric configuration (see Fig 1.10 B) or in higher order oligomers. Alternatively, ErbB1 receptors may transphosphorylate in a preliminary, transient EGF-induced dimer and then disengage, allowing the ErbB1 molecules to phosphorylate multiple ErbB3 molecules (see Fig 1.10 C). In either case, in order to produce the large observed populations of phosphorylated ErbB3, the transphosphorylation of ligand-unoccupied ErbB3 by ErbB1 must be the product of multiple transient interactions between ErbB1 and ErbB3 species.

4.5 The effect of PTP inhibitors on the EGF dose-response

Evidence has been presented which suggests that PTP activity greatly exceeds kinase activity in resting cells and that the induction of maximal tyrosine phosphorylation, after ligand stimulus, is dependent on concomitant inhibition of PTP activity (Garcia-Morales *et al.*, 1990; Jallal *et al.*, 1992; Sundaresan *et al.*, 1995; Bae *et al.*, 1998; Lee *et al.*, 1998; Fischer, 1999). If this is the case, then PTP inhibition may also be required for the spreading of phosphorylation to ligand-unoccupied receptors.

In order to investigate the relationship between PTP activity and ErbB1 phosphorylation levels, an EGF dose-response curve was measured from cells stimulated with EGF in the presence or absence of phenylarsine oxide (PAO), a generic PTP inhibitor. In the absence of PAO, at EGF concentrations below 10 ng/ml phosphorylated receptor populations remained at a level comparable to resting cells. However, at EGF doses above this concentration there was a sharp increase in the amount of

phosphorylated receptors measured. Maximal phosphorylation was observed at an EGF dose of 100 ng/ml (Fig. 4.7).

In the presence of PAO, ErbB1 receptors became phosphorylated in an EGF dosage-independent manner (Fig. 4.7), which suggests that ErbB1-GFP molecules are kinase active in the absence of ligand, but are kept in a low net state of phosphorylation by PTP activity. Treatment with PTP inhibitors causes an equivalent level of ErbB1 receptor phosphorylation to saturating does of EGF or EGF-beads. This provides an indication that a mechanism which relies on PTP inhibition could plausibly underlie the lateral spreading of phosphorylation to ligand-unoccupied receptors that occurs after a focal stimulus with EGF-beads.

4.6 Discussion

Studies have been performed to further elucidate the mechanism of lateral propagation of ErbB1 receptor phosphorylation reported in Chapter 3. Receptor phosphorylation has been measured in cells stimulated with EGF-coated beads under conditions which inhibit the downstream action of PTKs. It has been established that the signal spreading is dependent on ErbB1 tyrosine kinase activity, but not dependent on downstream activation of Src or other soluble cytoplasmic PTKs (section 4.2; Fig 4.1 and 4.2). FRAP studies on ErbB1-GFP expressing cells have shown that bead-bound receptors undergo little or no exchange with the peripheral bead-unoccupied pool (section 4.3.2, Fig. 4.4) and that receptors diffuse too slowly for a long-range diffusion mechanism to account for the observed rapid spreading of phosphorylation (section 4.3.1). In Chapter 3 it was also proposed that the extended pattern of phosphorylation induced by EGF-beads may be due to one of two wavefront propagation models. Evidence supporting these final two models will now be further discussed.

4.6.1 EGF-beads represent a local threshold-exceeding dose that invokes the phosphorylation of ligand-free receptors

Stimulation with EGF-coated beads must initiate a cascade of phosphorylation that allows ligand-unoccupied receptors across the entire plasma membrane to become phosphorylated. Furthermore, the steep rise in the levels of receptor phosphorylation

observed at EGF doses above 10 ng/ml (Fig. 4.7) suggest that, once the EGF dosage exceeds a certain threshold level, a cascade of phosphorylation is initiated that results in the phosphorylation of receptors across the entire plasma membrane. It could be implied from these combined observations that: 1. the steep rise in receptor populations observed at threshold-exceeding soluble EGF doses is not due to saturation of all receptors with bound ligand, but is dependent on spreading of phosphorylation to ligand-unoccupied receptors, and 2. the EGF-coupled beads used in these studies represent a *localised* threshold-exceeding dosage of growth factor. To support this, it has been shown that EGF-beads can bind and concentrate receptors (see section 4.3) and therefore are liable to represent a highly concentrated local EGF dose. From these combined postulates it could be inferred that a sufficient rise in the level of ErbB1 kinase activity locally, allows phosphorylation of ligand-unoccupied receptors to occur. The precise mechanism via which this occurs is not yet clear, but it is predicted to be dependent on ErbB receptor transphosphorylation between ligand-unoccupied receptors.

4.6.2 Receptor transphosphorylation during transient receptor interactions

If the EGF-bead initiated spreading is assumed to be entirely dependent on ErbB1 tyrosine activity, and no other participating molecules, then ligand-bound receptors under the bead must be capable of phosphorylating adjacent ligand-unoccupied receptors *in trans* (Fig. 3.7 C). It has been demonstrated previously that, whilst EGF does not directly bind and activate ErbB2 or ErbB3, stimulation of cells with EGF can result in the phosphorylation of ligand-unoccupied ErbB2 or ErbB3 by heterodimerisation with ErbB1 (Beerli & Hynes, 1996; Tzahar *et al.*, 1996; Gamett *et al.*, 1997). A similar transphosphorylation step may be postulated to occur between EGF-bound receptors under the bead and ligand-unoccupied ErbB1 receptors outside the bead contact area. This might take place via one of two mechanisms: 1. the receptor disengages from its first dimerisation partner and forms a second dimer with a new ligand-unoccupied partner (Fig 1.10 C; Gamett *et al.*, 1997), or 2. ligand-unoccupied receptors become activated by recruitment onto a pre-existing phosphorylated dimer (Fig. 1.10 B; Huang *et al.*, 1998). The first mechanism would appear to be an unlikely candidate, because once bound to the beads receptors appear to be quite immobile (see section 4.3; Fig 4.5). In any case, once phosphorylated, the ligand-unoccupied ErbB1 receptors would be responsible for

phosphorylating other ligand-unoccupied receptors, and the phosphorylation cascade would be spread by transphosphorylation between these receptors, via a so-called 'domino effect' (Fig. 3.7 C). For a mechanism such as this to take place, it must be possible for ErbB receptors to form multiple, transient dimers.

An experiment presented in this chapter suggests that a single ErbB1 receptor can dimerise with, and phosphorylate, multiple ErbB3 molecules (section 4.4), presumably by sequentially interacting with different receptor partners. Each dimerisation event would involve a transient interaction that mediates transphosphorylation. Whilst it is generally assumed that ErbB1 dimers are stable structures, only small populations of ErbB1 homodimers can be demonstrated in the presence of covalent cross-linking agents (Cochet *et al.*, 1998; Kashles *et al.*, 1991; Sorokin *et al.*, 1994) or in radioactive ligand affinity assays (Pinkas-Kramarski *et al.*, 1996). In addition, previous efforts from this laboratory using FRET-based assays to demonstrate stable ErbB1 dimers in cells have failed (F.Wouters, personal communication). The difficulties associated with the convincing demonstration of large dimer populations in cells may be due to the fact that ErbB1 dimers are only transient intermediates in the spread of phosphorylation between receptors. These combined observations support a model whereby the transient interaction of ligand-unoccupied ErbB1 monomers may act to spread the phosphorylation signal across the surface of the cell, via a mechanism that is dependent on the tyrosine kinase activity of the receptors only.

In summary, there is considerable evidence to suggest that ligand-bound receptors could transphosphorylate adjacent ligand-unoccupied receptors. Furthermore, there is evidence to support a role for transient receptor interactions, between ligand-free receptors, that mediates the spreading of phosphorylation across the plasma membrane. This is the basis of wavefront propagation model 1 (see section 3.6; Fig 3.7 C). This model also assumes that tyrosine phosphorylation of ligand-unoccupied receptors stimulates the specific kinase activity of the receptors. However, it has been demonstrated that this is not the case for ErbB1 (Honegger *et al.*, 1988). This presents a problem for a model whereby the spread of stable tyrosine phosphorylation is dependent on ErbB1 tyrosine phosphorylation-induced tyrosine kinase activity alone. However, transient receptor interactions are still predicted to be involved, but must be coupled to PTP inhibition in order to explain the lateral propagation of receptor phosphorylation.

4.6.3 ErbB1 receptors possess basal kinase activity and tyrosine phosphorylation is regulated by PTPs

If ErbB1 tyrosine kinase activity is not stimulated by tyrosine phosphorylation of the receptor then it must be assumed that ErbB1 receptors have a basal kinase activity and can transphosphorylate during receptor collision events in the absence of ligand. Strong evidence for this comes from experiments with purified ErbB1 receptors. When purified receptors are reconstituted into large unilamellar lipid vesicles, the receptors become phosphorylated in the absence of ligand, but in detergent solubilised extracts EGF-dependence is restored (Ge *et al.*, 2001). Above the CMC, ErbB1 receptors must be able to collide and thereby transphosphorylate in the absence of EGF, because many receptors are present in the correct topology within large vesicles. In detergent solubilised extracts, receptors are diluted amongst many small micelles which are predicted to contain ≤ 1 receptor per micelle. Under these conditions the receptor collision frequency is low and the ligand is necessary to cross-link receptors between different micelles to induce transphosphorylation. Further to this, treatment of cells with PTP inhibitors results in the ligand-independent phosphorylation of RTKs (Heffetz *et al.*,1990; Jallal *et al.*, 1992; Knebel *et al.*, 1996). It was demonstrated in this chapter that PTP inhibitors also induce the ligand-independent phosphorylation of ErbB1 (see section 4.5; Fig 4.7). This confirms that RTKs possessing intrinsic kinase activity can become phosphorylated within cells in the absence of ligand. Presumably this occurs by transphosphorylation during collision events in the plasma membrane, but is normally counteracted by PTP activity. PTPs possess 10-1000 times greater specific activity towards substrates than RTKs, which presumably means that PTPs ensure a low level of phosphorylated receptors under steady-state conditions.

Therefore, in order for stable tyrosine phosphorylation to occur in response to ligand, a mechanism must exist which leads to the inhibition of receptor dephosphorylation by PTPs. It has been shown that maximal tyrosine phosphorylation of RTKs is dependent on the intracellular production of hydrogen peroxide, which is proposed to inhibit PTPs by oxidation of a critical active site residue (Fig. 4.8; Finkel, 2000; Rhee *et al.*, 2000). It is therefore deemed possible that EGF-beads elicit the phosphorylation of ligand-unoccupied receptors by a mechanism of PTP inhibition that relies on hydrogen peroxide generation. In this scenario, EGF-beads represent a local

threshold-exceeding dose of growth factor. This creates PTP inhibition by driving hydrogen peroxide production. This is presumed to allow not only ligand-bound receptors under the bead to become phosphorylated, but also to allow ligand-unoccupied receptors outside the bead contact point to become phosphorylated. These ligand-unoccupied receptors become stably phosphorylated because transphosphorylation during collision events is no longer downregulated by PTP activity. Once phosphorylated, ligand-unoccupied receptors are predicted to be capable of mediating further hydrogen peroxide generation, maintaining the PTP inhibition, and thereby allowing the phosphorylation of ligand-unoccupied receptors yet further from the bead. According to this model the spreading of phosphorylation therefore proceeds via a rapid positive feedback loop which relies on hydrogen peroxide-dependent PTP inhibition and tyrosine phosphorylation during transient receptor interactions (Fig. 3.7 D).

Further investigation is required to establish: 1. whether the EGF-beads used in this study represent a local threshold dosage of EGF, 2. whether the phosphorylation of ligand-free receptors is mediated by PTP inhibition, and 3. how PTP inhibition could be invoked, i.e. does it require the production of hydrogen peroxide. In Chapter 5 an investigation into these questions is presented.

Figure 4.1 ErbB1-GFP phosphorylation in the presence of the Src inhibitor PP2
MCF-7 cells grown on glass coverslips were transfected with ErbB1-GFP and serum starved. They were then stimulated with EGF-coated beads for various times in the presence of 50 nM or 500 nM PP2, or in the absence of inhibitor (cells stimulated in the presence of PP2 were additionally pre-incubated with the same concentration of inhibitor for 15 minutes prior to stimulation). After stimulation, cells were fixed, permeabilised and stained with Cy3-PY72. Phosphorylated receptor populations were quantified using global analysis of FLIM data, as previously described. **A.** Mean average populations of phosphorylated ErbB1-GFP generated after stimulation with EGF-coated beads under different conditions (10-15 cells per data point). Example images of cells incubated for 1 minute with EGF-coated beads in the absence of inhibitor (**B**), in the presence of 50 nM (**C**) or 500 nM (**D**) PP2. Left panel, ErbB1-GFP fluorescence; middle panel, Cy3-PY72 staining; right panel, populations of phosphorylated receptors. Phosphorylated receptor populations in given images are 0.48 (**B**), 0.50 (**C**) and 0.26 (**D**).

Fig. 4.1

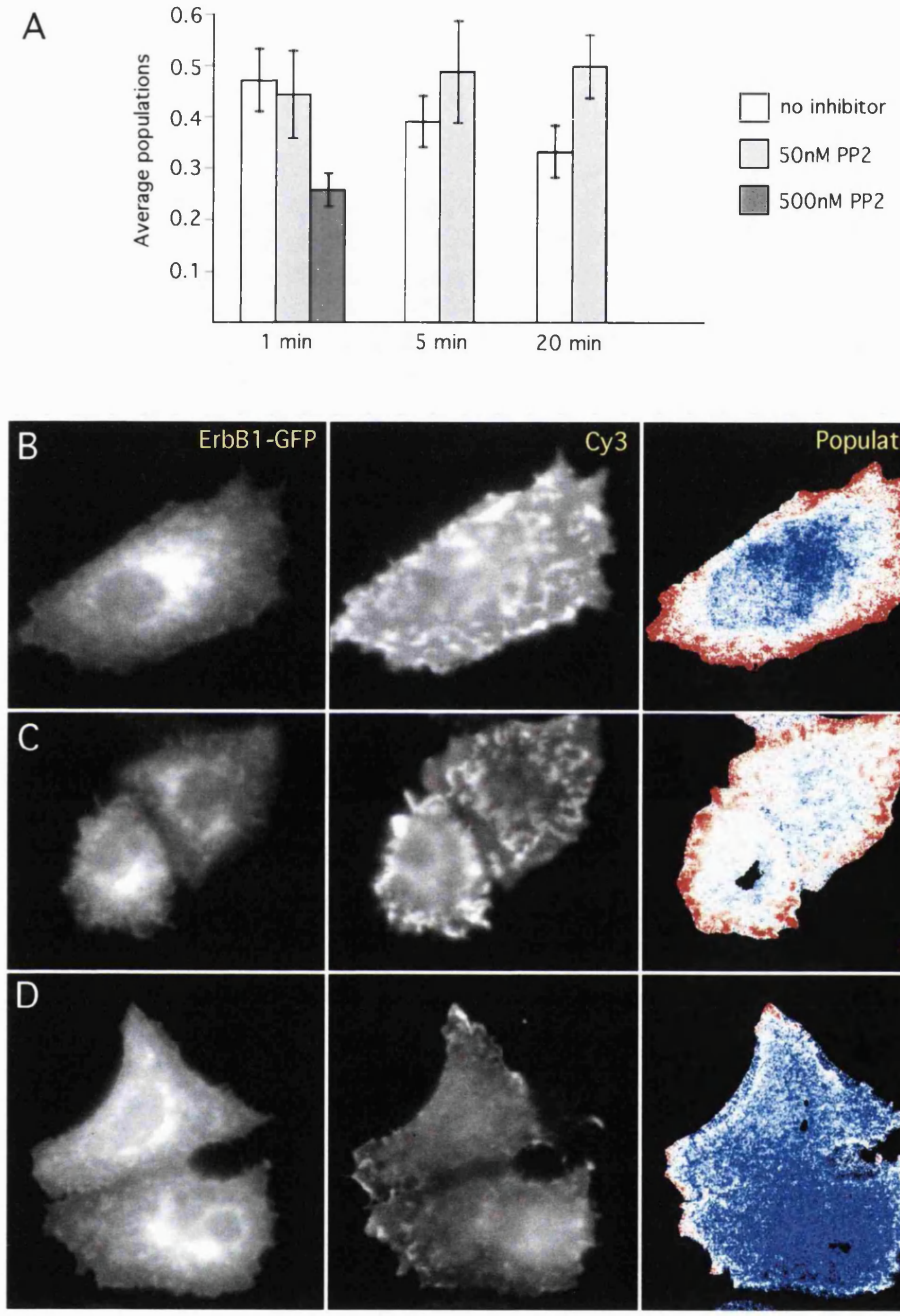
A
Average populations
0.6
0.5
0.4
0.3
0.2
0.1
1 min
5 min
20 min
no inhibitor
50nM PP2
500nM PP2
B
ErbB1-GFP
Cy3
Populations
C
1
0
D

Figure 4.2 ErbB1-GFP phosphorylation in streptolysin-O permeabilised cells
MCF-7 cells grown on glass coverslips were transfected with ErbB1-GFP and serum starved. 30 minutes prior to stimulation cells were treated with buffer in the presence or absence of added streptolysin-O (for buffer formulation see section 2.3.8). Cells were then stimulated with EGF or EGF-coated beads for 5 minutes in the presence of the same buffer. Samples were fixed, stained with Cy3-PY72 and phosphorylated receptor populations quantified using global analysis of FLIM data, as previously described. **A.** Mean average populations of phosphorylated ErbB1-GFP after stimulation under different conditions (10-15 cells per data point). Example images of cells incubated for 5 minutes with EGF-beads after prior incubation with buffer only (**B**) or buffer and streptolysin-O (**C**). Left panel, ErbB1-GFP fluorescence; middle panel, Cy3-PY72 staining; right panel, populations of phosphorylated receptors. Phosphorylated receptor populations in given examples are 0.36 (**B**) and 0.34 (**C**).

Fig. 4.2

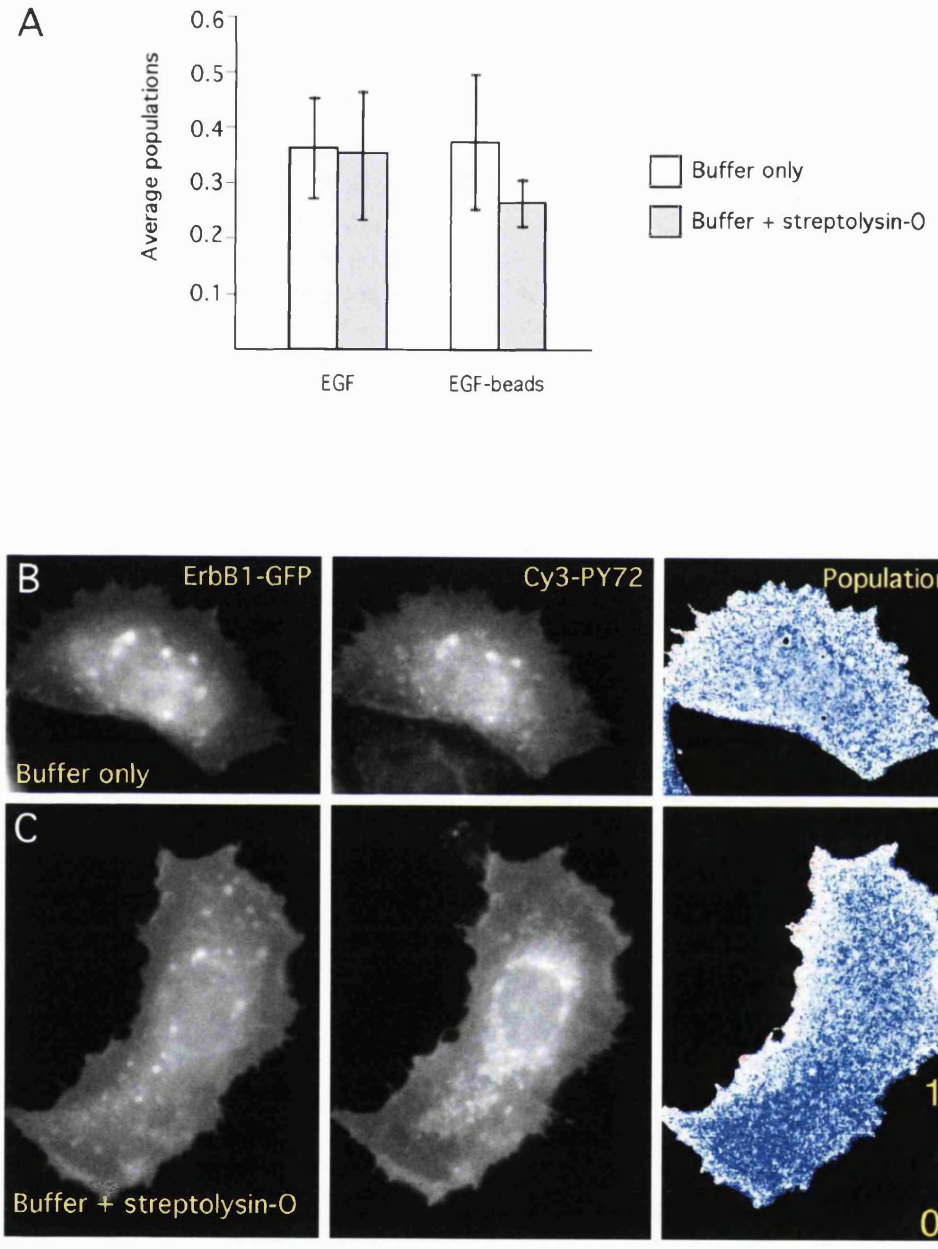
A
Average populations
0.6
0.5
0.4
0.3
0.2
0.1
EGF
EGF-beads
Buffer only
Buffer + streptolysin-O
B
ErbB1-GFP
Cy3-PY72
Populations
Buffer only
C
Buffer + streptolysin-O
1
0

Figure 4.3 FRAP experimental protocol

FRAP experiments are performed on living cells using a confocal scanning microscope. **A.** A region of interest (ROI) within a cell is selected (dashed-line box) and is imaged with a laser set to low power transmission (pre-bleach image). **B.** A second, smaller, circular ROI within the first ROI is then rapidly bleached with the laser set to high power transmission. **C.** Once the region in the smaller ROI is bleached to near background levels, time lapse images are acquired of the first ROI (with the same laser scanning and detector settings as for the pre-bleach image) to monitor recovery of fluorescence (post-bleach images).

Fig. 4.3

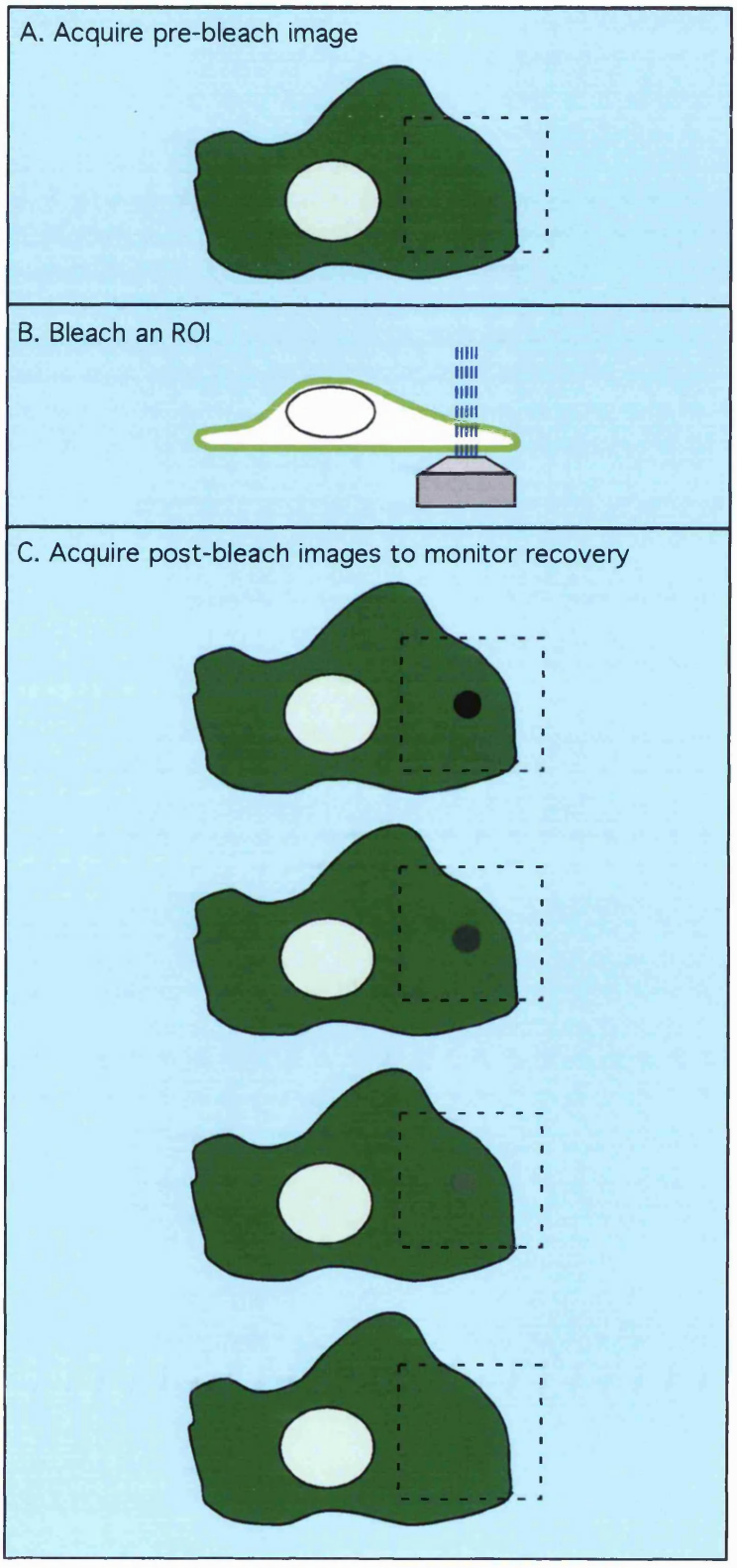
A. Acquire pre-bleach image
B. Bleach an ROI
C. Acquire post-bleach images to monitor recovery

Figure 4.4 Measurement of ErbB1-GFP diffusion coefficient

MCF-7 cells grown on glass-bottomed petri dishes were transfected with ErbB1-GFP, serum starved and then imaged at 37°C with a Zeiss LSM 510 confocal microscope (see section 2.3.7). A 30 x 30 μm ROI near the egde of an MCF-7 cell was selected. The fluorescence intensity of the region was recorded before and after bleaching a 4.6 μm diameter circular region within the confines of the first region. Post-bleach images were acquired every 2 seconds for 120 seconds. **A.** Selected time points from a typical FRAP experiment used to calculate the ErbB1 diffusion coefficient. **B.** Fluorescence recovery of bleached region as a function of time. I_0 = average pre-bleach intensity of bleached ROI; I = average intensity of bleached ROI at post-bleach time, t (seconds).

Fig. 4.4

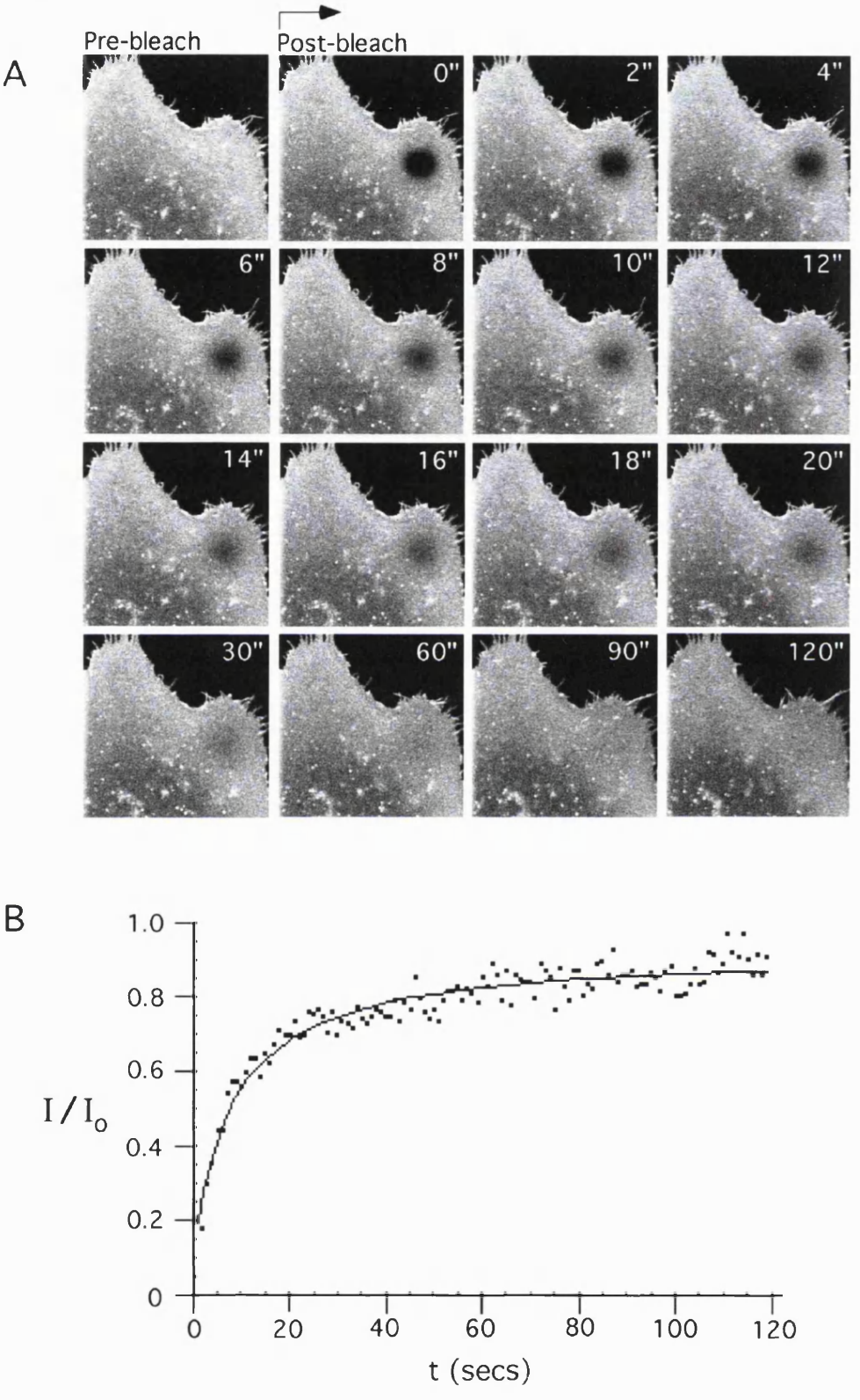
A
Pre-bleach
Post-bleach
0"
2"
4"
6"
8"
10"
12"
14"
16"
18"
20"
30"
60"
90"
120"
B
I / I$_o$
1.0
0.8
0.6
0.4
0.2
0
0
20
40
60
80
100
120
t (secs)

Figure 4.5 ErbB1-GFP forms a stable complex with EGF ligand presented by beads

MCF-7 cells grown on glass-bottomed petri dishes were transfected with ErbB1-GFP, serum starved, treated with Cy3 labelled EGF-coated beads and imaged at 37°C with a Zeiss LSM 510 confocal microscope. Left panels, ErbB1-GFP; middle panels, Cy3-labelled beads; right panels, RGB merge of ErbB1-GFP and Cy3 fluorescence with colocalisation in yellow. Four selected time points are shown. **A.** Pre-bleach image (points of colocalisation between concentrated ErbB1-GFP and Cy3-beads are numbered 1-7). **B.** Zero time point post-bleach image. **C.** 1 minute post-bleach image. **D.** 2 minutes post-bleach image.

Fig. 4.5

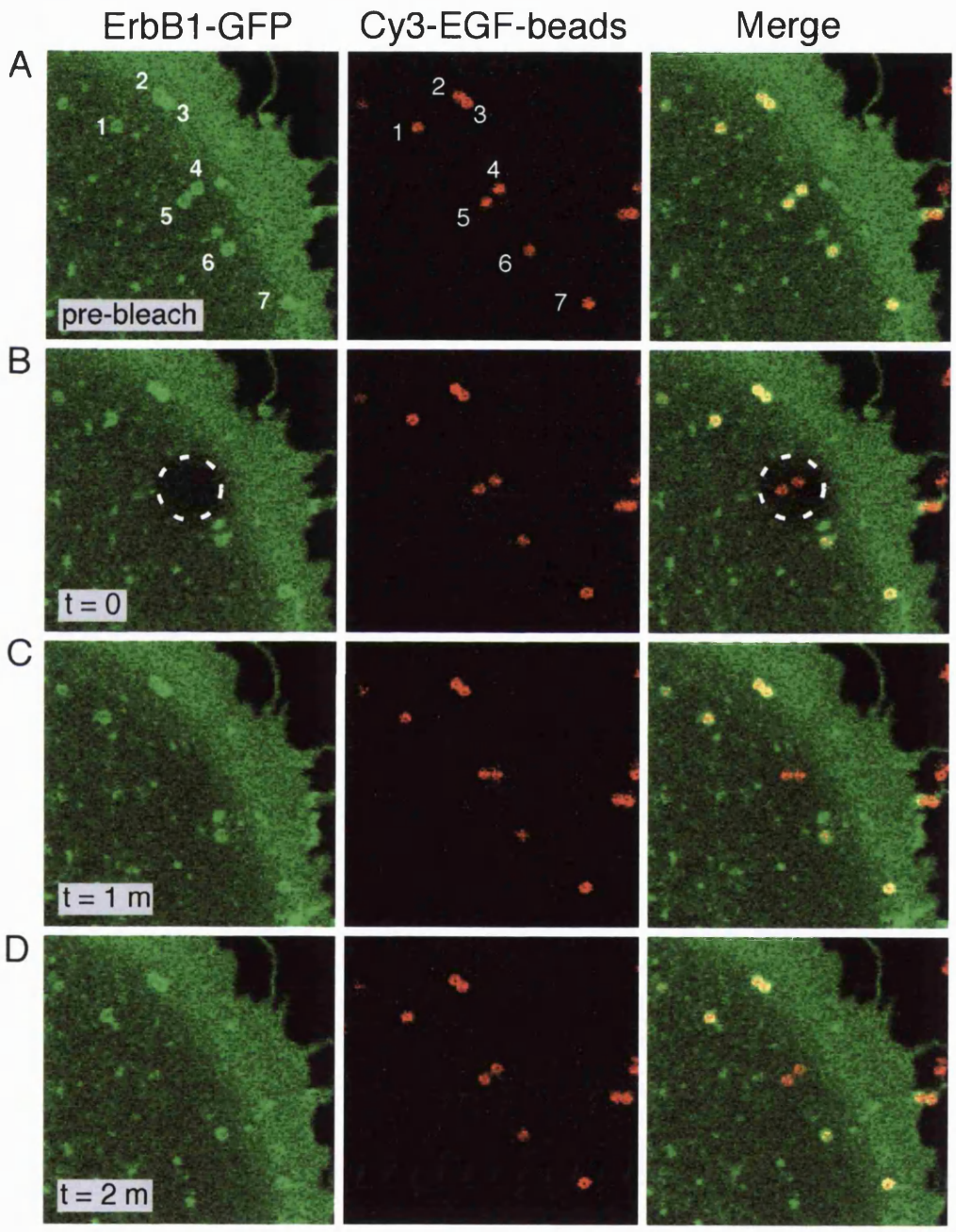
ErbB1-GFP
Cy3-EGF-beads
Merge
A
B
C
D
1
2
3
4
5
6
7
pre-bleach
t = 0
t = 1 m
t = 2 m

Figure 4.6 ErbB3-GFP phosphorylation in the presence of a minor population of ErbB1

MCF-7 cells grown on glass coverslips were transfected with a 1:10 molar ratio of ErbB1:ErbB3-GFP DNA (**A**) or ErbB3-GFP DNA only (**B**). After serum starvation, cells were stimulated with soluble EGF for 5 minutes, fixed, permeabilised and stained with Cy3-PY72. Phosphorylated receptor populations were quantified using global analysis of FLIM data as previously described. Left panels, ErbB1-GFP fluorescence; middle panels, Cy3-PY72 staining; right panels, populations of phosphorylated ErbB3-GFP.

Fig. 4.6 A. ErbB1:ErbB3-GFP (1:10 ratio) B. ErbB3-GFP only

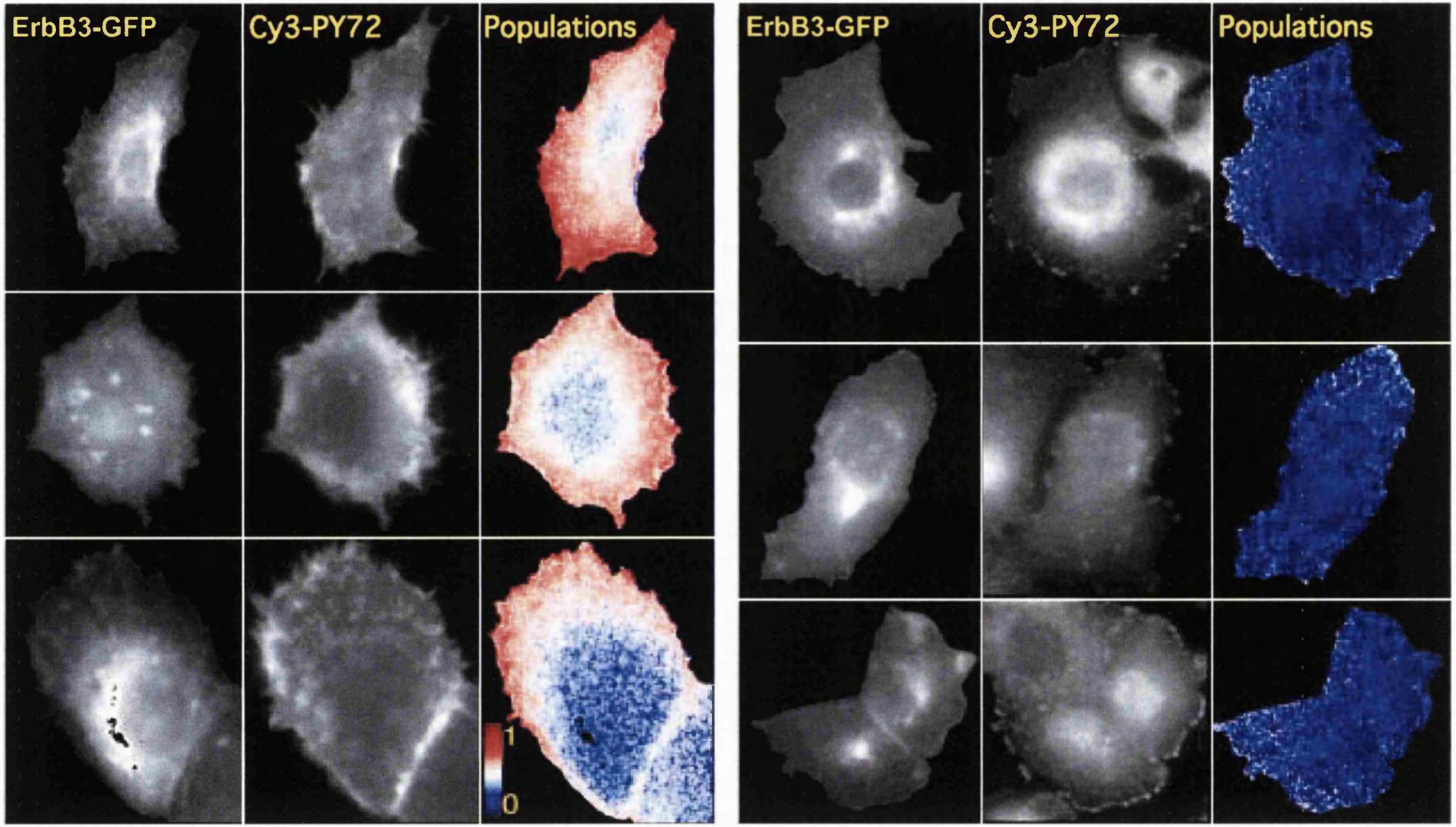

Figure 4.7 The effect of phosphatase inhibition on the EGF dose-response of ErbB1-GFP phosphorylation.

MCF-7 cells grown on glass coverslips were transfected with ErbB1-GFP and serum starved. Cells were stimulated for 5 minutes with EGF at a concentration of 0.1, 1, 10, 50, 100 or 200 ng/ml EGF in the presence (filled squares) or absence (filled circles) of 1 μM PAO (cells stimulated in the presence of PAO were additionally pre-incubated with the same concentration of inhibitor for 5 minutes prior to stimulation). Samples were fixed, permeabilised and stained with Cy3-PY72. Phosphorylated receptor populations were quantified using global analysis of FLIM data (15-20 cells per data point).

Fig. 4.7

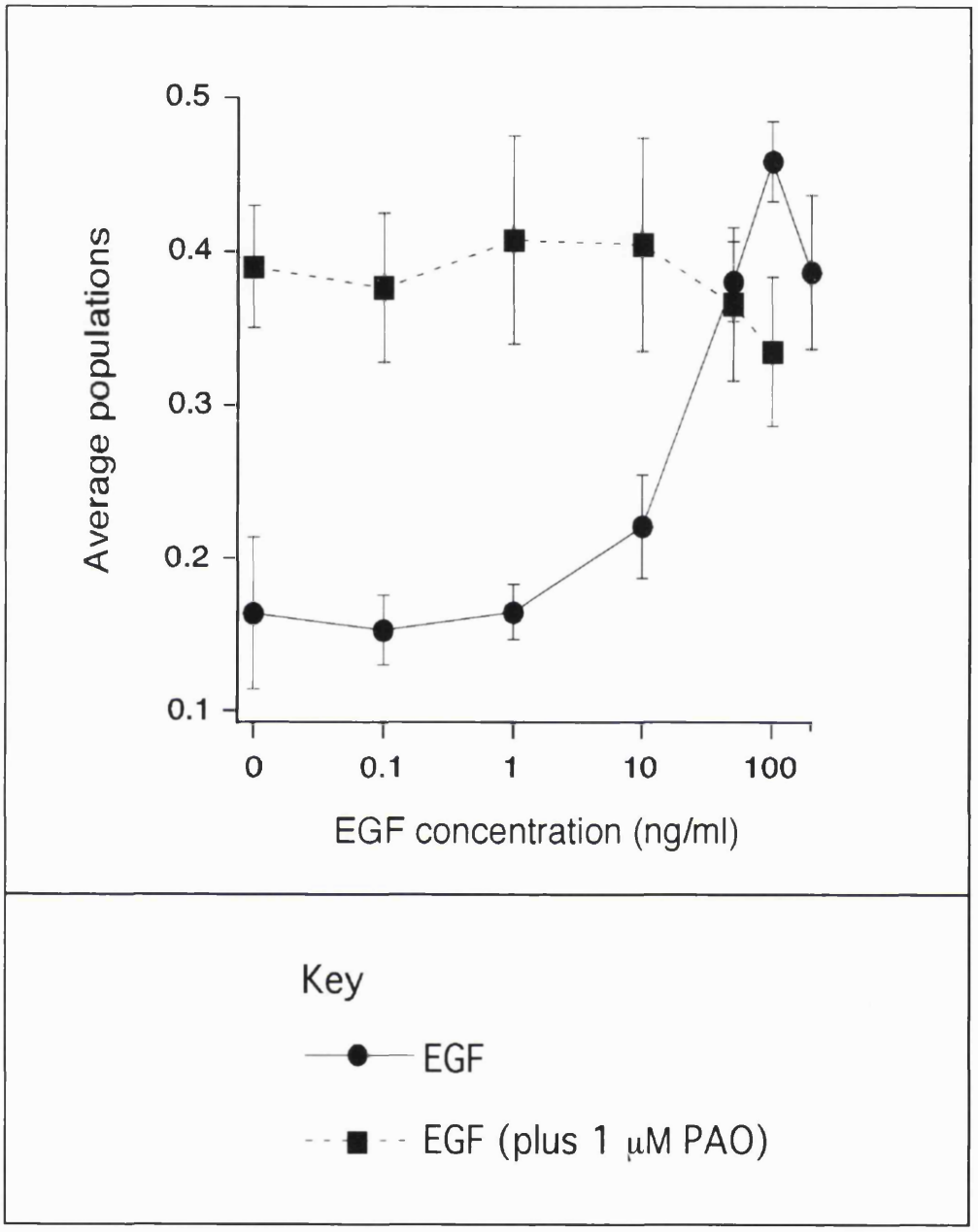
0.5
0.4
0.3
0.2
0.1
Average populations
0
0.1
1
10
100
EGF concentration (ng/ml)
Key
EGF
EGF (plus 1 μM PAO)

Figure 4.8 Proposed model for extracellular signal-coupled PTP inhibition via the generation of hydrogen peroxide

Diagram illustrates mechanism through which receptor tyrosine kinases may elicit PTP inhibition after ligand stimulus, based on the model proposed by various authors e.g. Finkel, 2000; Rhee *et al.*, 2000. After ligand binding, the phosphorylated receptor may signal to the plasma membrane enzyme NADPH oxidase resulting in up regulated activity of the enzyme. Oxidation of NADPH to NADP+ at the intracellular face of the enzyme is coupled to the generation of hydrogen peroxide at the extracellular face. Hydrogen peroxide is thought to diffuse rapidly back into the cell where it may oxidise susceptible amino acid side chains. A cysteine group present in the active site of most PTPs is highly susceptible to oxidation by hydrogen peroxide. The cysteine is oxidised to sulfenic acid, rendering the PTP catalytically inactive. The reaction is reversible, so active site oxidation may represent a mechanism via which PTP activity is modulated in cells in a manner which is dependent on the local cellular concentration of hydrogen peroxide.

Fig. 4.8

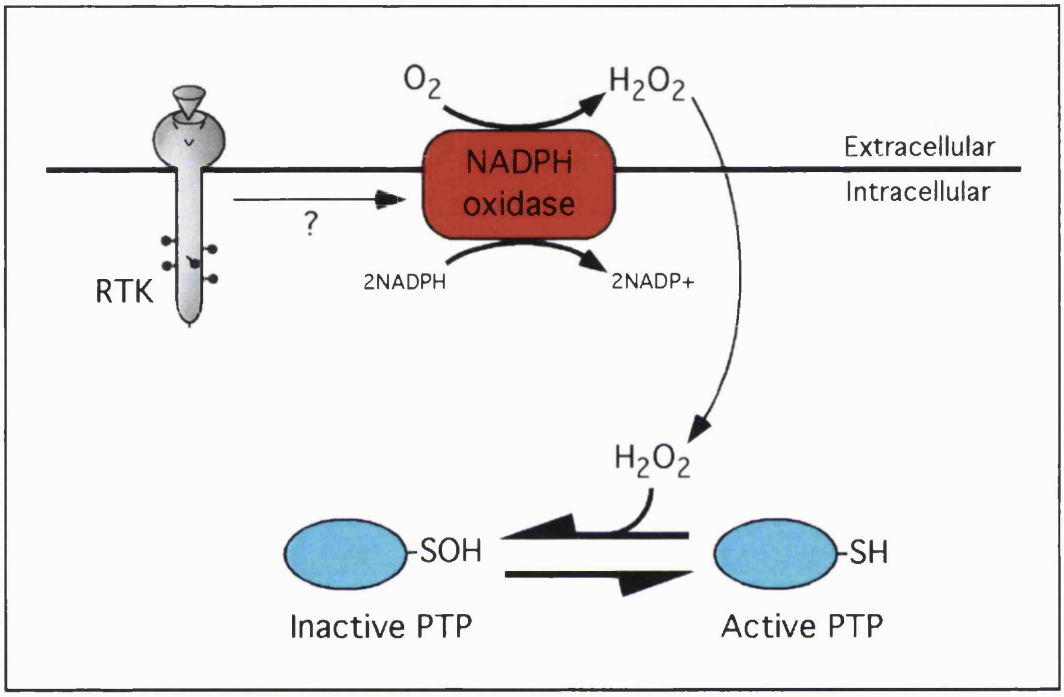
O_2
H_2O_2
NADPH oxidase
Extracellular
Intracellular
?
RTK
2NADPH
2NADP+
H_2O_2
-SOH
-SH
Inactive PTP
Active PTP

Chapter 5

Protein Tyrosine Phosphatase Inhibition Mediates Lateral Spreading of ErbB1 Receptor Phosphorylation

Protein tyrosine phosphatase inhibition mediates lateral spreading of ErbB1 receptor phosphorylation

5.1 Introduction

In Chapter 4 it was proposed that lateral spreading of phosphorylation to ligand-unoccupied ErbB1 receptors was due to a wavefront propagation of phosphorylation originating at the EGF-beads. ErbB1 transphosphorylation that occurs during transient receptor interactions was proposed to mediate the spreading of phosphorylation between ligand-unoccupied receptors outside the bead stimulation area. However, it was argued that a mechanism based on receptor transphosphorylation alone was not adequate to explain how the EGF-beads initiate spreading or how the spreading of phosphorylation proceeds across the cell. Instead, the initiation of spreading was proposed to be dependent on an EGF-bead induced local concentration of tyrosine kinase activity that gives rise to PTP inhibition. Lateral spreading of ErbB1 phosphorylation outside the bead stimulation point was then proposed to proceed via a positive feedback loop involving PTP inhibition and tyrosine phosphorylation. A critical factor in this model is understanding how the PTP inhibition could be invoked.

Insight comes from the observation that maximal ligand-induced phosphorylation of RTKs is dependent on the production of the reactive oxygen species, hydrogen peroxide, which inhibits PTPs by oxidising the thiol group of an active site cysteine residue to a non-reactive sulfenic acid group (Fig. 4.8; Sundaresan *et al.*, 1995; Bae *et al.*, 1997; Bae *et al.*, 2000; Finkel, 2000; Mahadev *et al.*, 2001). It was therefore considered plausible that hydrogen peroxide production could be the basis for a PTP inhibition mechanism that permits lateral propagation of receptor phosphorylation. The validity of this mechanism is addressed in this chapter. Furthermore, following the completion of the work described in the previous chapters, it was reported that EGF-coupled beads give rise to phosphorylated receptors only at the point of contact between the bead and the cell (Brock & Jovin, 2000). The disparity between this report and the results presented in this thesis are also addressed in this chapter.

It is shown that the lateral propagation of ErbB1 phosphorylation is dependent on the local delivery of threshold densities of EGF and that the density of EGF required to initiate spreading is reduced in the presence of PTP inhibitors. It is also demonstrated that PTP inhibitors, including hydrogen peroxide, can induce the ligand-independent phosphorylation of receptors across the entire plasma membrane on a similar time scale to that observed with EGF ligand. Finally, it is shown that hydrogen peroxide production is necessary for lateral spreading of ErbB1 tyrosine phosphorylation and is therefore the mechanism via which the PTP inhibition is invoked. These data indicate that lateral spreading of RTK phosphorylation is initiated only when RTK activity is raised sufficiently locally to surpass a PTP activity barrier. Lateral spreading of receptor phosphorylation is then predicted to proceed rapidly via a positive feedback loop which relies on kinase activity-dependent PTP inhibition and tyrosine phosphorylation.

5.2 Lateral spreading of ErbB1 phosphorylation requires local delivery of EGF above a certain threshold density

Carboxylate-modified, 0.8 μm diameter latex beads were covalently coupled with different amounts of EGF in order to determine whether the EGF density effected the lateral spreading of ErbB1 phosphorylation. EGF-coupling to the beads was achieved via a two-step procedure, as described in section 2.2.6. Firstly, the carboxylate groups on the surface of the beads were derivatised into amine-reactive succinimide ester groups. The batch of derivatised beads was then divided in half and reacted with the same molar excess of EGF, in the presence or absence of a buffer containing free amino groups (e.g. Tris), which will compete with EGF for covalent coupling to the derivatised beads. Any apparent differences in the biological activity of beads labelled in this fashion must be due to differences in the density of covalently coupled EGF and not due to differences in the levels of non-specifically absorbed EGF on the bead surface, because all bead preparations are incubated in the presence of the same concentration of EGF. Following EGF coupling, any non-reacted groups on the beads were quenched with excess free amine and the beads were extensively washed to remove free EGF. Washing resulted in the complete removal of free EGF, demonstrated by the fact that supernatant from the final wash of the beads did not induce ErbB1-GFP phosphorylation when applied to cells.

A relative determination of the EGF density coupled to the beads in both preparations was performed by immunofluorescence staining of the beads with anti-EGF antibodies. The beads that were coupled to EGF alone stained more intensely than those incubated in the presence of competing amino groups, indicating that they had a higher surface density of EGF and were designated HD (high density) beads. The beads labelled in the presence of competing free amino groups, that stained less intensely, were designated LD (low density) beads (Fig. 5.1 A).

Serum starved, ErbB1-GFP expressing MCF-7 cells were stimulated with the LD or HD EGF-beads for two minutes, fixed and then stained with Cy3-labelled antiphosphotyrosine antibodies. The extent of receptor phosphorylation was assayed by observing the pattern of anti-phosphotyrosine staining and by determining the populations of phosphorylated receptors by global analysis of the time-resolved GFP fluorescence that was obtained by FLIM. Stimulation of cells with HD EGF-beads resulted in elevated anti-phosphotyrosine staining, and elevated populations of phosphorylated ErbB1, across the entire plasma membrane (Fig. 5.1 C). This corresponded well with the spatial extent of phosphorylation observed with the EGF-beads used for experiments in Chapters 3 and 4. In contrast, cells stimulated with LD EGF beads exhibited raised anti-phosphotyrosine staining levels at the bead contact point only (Fig. 5.1 D).

Quantification of data from multiple cells stimulated for 5 minutes with beads from either batch showed that phosphorylated receptor populations produced in cells by HD beads were significantly higher than those produced by LD EGF-beads (Fig. 1B). Even after five minutes stimulation with LD EGF-beads, phosphorylation was still only present at the point of cell contact with the LD-EGF beads. Therefore, LD EGF-beads do not merely show delayed phosphorylation spreading kinetics. It was also noted that multiple LD EGF beads could land on a cell and yet still only elicit phosphorylation at the bead contact point, whereas one HD bead per cell was sufficient to activate receptors across the entire plasma membrane. These data show that beads coupled with a high density of EGF induce lateral spreading of ErbB1 receptor phosphorylation, whereas low densities of EGF do not.

By immunofluorescence staining of samples with anti-EGF antibodies the density of EGF presented on the beads could be compared to the extent of receptor phosphorylation induced *in situ*. As expected, HD EGF beads, which induced lateral

spreading of receptor phosphorylation, stained more intensely than LD EGF beads, which induce only local receptor phosphorylation. Furthermore, phosphorylated receptor populations directly beneath HD EGF-beads were generally higher than those present below the LD EGF-beads (compare Fig. 1 C and D). These observations confirm that a high density of EGF coupling to the beads is required to initiate lateral spreading of ErbB1 phosphorylation. Furthermore, it suggests that low densities of EGF induce insufficient local kinase activity to initiate lateral spreading of phosphorylation.

5.3 Kinetics of ErbB1 phosphorylation in the presence of a PTP inhibitor

If the lateral spreading of ErbB1 tyrosine phosphorylation is dependent on PTP inhibition, then the kinetics of ErbB1-GFP phosphorylation induced by PTP inhibitors should be similar to the kinetics of receptor phosphorylation observed after stimulation with the EGF ligand. Cells were incubated for different time periods with a saturating dose (50 μM) of the PTP inhibitor phenyl arsine oxide (PAO). Populations of phosphorylated receptors were quantified by global analysis of FLIM data (Fig. 5.2 A). Elevated populations of phosphorylated receptors were observed in some cells after only 10-30 seconds of PAO treatment and phosphorylation levels peaked by 1 minute. Receptor phosphorylation occurred across the entire surface of the cell (Fig. 5.2 B) and extensive membrane ruffling was also evident. These kinetics and morphological characteristics closely resemble those that were previously observed in cells stimulated with EGF-coupled beads or with soluble EGF (see Chapter 3). This indicates that a mechanism that relies on PTP inhibition could plausibly underlie the spreading of phosphorylation to ligand-unoccupied receptors that is induced by HD EGF-bead stimulation.

After prolonged incubation with PAO (20-30 minutes) an increased presence of ErbB1 receptors in large endocytosed vesicles was observed, which indicates that PTP inhibition alone can induce the internalisation of ErbB1 on a similar time scale to EGF stimulation. It can be concluded from this that PTP inhibition must permit phosphorylation of ErbB1 tyrosine residues that are required for recruitment of protein components of the endocytic machinery and subsequent internalisation.

5.4 The EGF density that induces lateral spreading of phosphorylation is reduced by attenuating cellular PTP activity

It is clear that PTP inhibition alone can result in phosphorylation of receptors across the entire plasma membrane and that this occurs on a similar time scale to the activation induced by HD EGF-beads or soluble EGF. It has been demonstrated by others that a ligand-induced increase in RTK phosphorylation levels is accompanied by concomitant inhibition of cellular PTP activity. This PTP inhibition is required to achieve maximal RTK phosphorylation levels (Sundaresan *et al.*, 1995, Bae *et al.*, 1997; Mahadev *et al.*, 2001; Rhee *et al.*, 2000). To test whether PTP inhibition is the key step required for lateral spreading of RTK phosphorylation, cells were incubated with subsaturating concentrations of PAO (up to 1 μm) for two minutes in the presence or absence of LD EGF-beads. The average populations of phosphorylated ErbB1 receptors generated under these conditions were calculated from measurements of many cells (Fig. 5.3 A). In the absence of PTP inhibitors LD EGF-beads induced phosphorylation of receptors at the bead contact point only, as previously observed (see Fig. 5.1 D). However, stimulation of cells with LD EGF-beads in the presence of 0.1 - 1 μM PAO resulted in raised populations of phosphorylated receptors across the entire membrane (Fig. 5.3 C) that were significantly higher than the populations measured when cells were treated at these PAO concentrations without LD beads (Fig. 2 A and B).

These data show that when cellular PTP activity is partially attenuated, a lower density of EGF presentation locally can induce lateral spreading of phosphorylation. This has an important implication for the mechanism of RTK activation. It shows that ErbB1 kinase activity-dependent PTP inhibition must rise sufficiently locally to overcome a PTP activity barrier, in order to trigger lateral spreading of phosphorylation.

5.5 Hydrogen peroxide production is implicated in the PTP inhibition mechanism

If PTP inhibition mediates the lateral spreading of ErbB1 tyrosine phosphorylation, the next logical step is to characterise the mechanism via which locally-increased ErbB1 tyrosine phosphorylation could inhibit PTPs, thereby leading to a rapid spreading of phosphorylation. Many groups have shown that growth factor stimulation of

cells elicits the production of the reactive oxygen species, hydrogen peroxide, which can inhibit PTPs by oxidising an active site cysteine to sulfenic acid (Finkel, 2000; Rhee *et al.,* 2000). Hydrogen peroxide is produced rapidly after EGF stimulus, is required for maximal tyrosine phosphorylation of the cellular pool of RTKs and it is predicted to diffuse quickly away from the site of production because it is a small molecular species. All of these features make hydrogen peroxide a good candidate for the mediator of PTP inhibition that permits lateral spreading of phosphorylation to occur.

5.5.1 Raised intracellular catalase activity inhibits lateral propagation of ErbB1 receptor phosphorylation

A role for hydrogen peroxide production in lateral spreading of phosphorylation was investigated. Overexpression of the hydrogen peroxide degrading enzyme, catalase, is an effective means to scavenge hydrogen peroxide in cells. For example, this has been used to inhibit superoxide radical-mediated oxidative injury (Bai *et al.,* 1999, Schriner *et al.,* 2000). Stable ErbB1-GFP expressing MCF-7 cells were microinjected in the nucleus with an expression plasmid encoding human fibroblast catalase. Immunofluorescence staining confirmed that the expressed catalase protein was present in excess within the cytoplasm and not restricted to the peroxisomal compartment. Lateral spreading of phosphorylation was prevented, or attenuated, in most catalase overexpressing cells stimulated with HD EGF beads. In Fig. 5.4 A a catalase expressing cell (top) is seen next to a cell that does not express catalase (bottom). Note that despite the presence of multiple HD beads on both cells, ErbB1 phosphorylation occurs only in the cell which is not expressing catalase. Significantly, there is no local tyrosine phosphorylation at the bead contact point either, as indicated by the lack of anti-phosphotyrosine staining at the sites of the beads (top right panel, Fig. 5.4 B). This indicates that hydrogen peroxide is also required to initiate local tyrosine phosphorylation of ErbB1 bound to the bead.

In some cells the overexpression of catalase did not inhibit lateral propagation of phosphorylation. Histograms showing the distribution of phosphorylated receptor populations revealed that two distinct groups of cells were evident amongst the catalase expressing group: a population of cells in which phosphorylation levels were equivalent to non-stimulated cells and a population of cells where the phosphorylation was equivalent to stimulated cells that did not express catalase (Fig. 5.4 B). Catalase requires

a heme group and NADP as cofactors for its catalytic activity. It is therefore possible that in some cells the presence of these factors is limiting and therefore not all the overexpressed catalase is active. This may explain why the overexpression of catalase was not equally effective in all cells. As a control for the effects of protein overexpression on receptor phosphorylation, cells were also microinjected with plasmid DNA encoding a soluble form of syntaxin 6, a protein predicted to have no effect on ErbB1 phosphorylation. Phosphorylation levels were normal in these cells when they were stimulated with HD EGF-beads.

5.5.2 ErbB1-GFP phosphorylation in the presence of hydrogen peroxide

To test directly for the effects of hydrogen peroxide on ErbB1 receptor phosphorylation, cells were treated for different time periods with a saturating dose (100 mM) of hydrogen peroxide. Phosphorylation of ErbB1 was detected after only 10-30 seconds of hydrogen peroxide treatment and peaked after 2 minutes of treatment (Fig. 5.5 A). Elevated phosphorylated receptor populations were observed across the entire plasma membrane (Fig. 5.5 B). The time scale of ErbB1 phosphorylation induced by hydrogen peroxide treatment was therefore similar to that of EGF, HD EGF-beads and PAO. In combination with the results presented for the effects of catalase overexpression, this data strongly supports a role for hydrogen peroxide-mediated PTP inhibition in the lateral propagation of phosphorylation to ligand-unoccupied receptors that occurs after stimulation of cells with HD EGF-beads.

5.6 Phosphatase inhibitors induce tyrosine phosphorylation of intracellular ErbB1

Higher populations of phosphorylated plasma membrane ErbB1 receptors are observed around the edge of cells than in the centre when cells are stimulated with EGF ligand (for example see Fig. 5.1 C, or for more extensive examples see Fig 3.5 A,B). This is mainly due to the fluorescence contribution from ErbB1-GFP within intracellular membranes, which is associated with a higher fluorescence lifetime because it is not phosphorylated as a direct consequence of EGF treatment (see section 3.3). In contrast, in cells stimulated with the PTP inhibitors, PAO or hydrogen peroxide, elevated populations

of phosphorylated receptors were often observed not just near the edge of cells, but deep into the centre of cells (Fig. 5.6 A). This suggested that phosphatase inhibition can induce the phosphorylation of ErbB1 receptors within intracellular membranes, since the fluorescence in the centre of the cell is contributed mainly by intracellular ErbB1-GFP.

The regulation of ErbB1-GFP phosphorylation within intracellular membranes was of particular interest, because it has relevance to other work presented by our laboratory (Haj *et al.,* 2002). It has been known for sometime that ErbB1 can be dephosphorylated by PTP-1B, a phosphatase that is exclusively localised to the cytoplasmic face of the endoplasmic reticulum (Flint *et al.,* 1997). This was a somewhat puzzling observation, because ErbB1-GFP is mainly localised to the plasma membrane of cells and is unlikely to be accessible to the ER-localised PTP-1B. In Haj *et al,* the interaction between ErbB1-GFP and a substrate-trapping mutant of PTP-1B was demonstrated in cells using a FRET-based approach. It was shown that whilst PTP-1B has no access to plasma membrane-localised receptors, EGF-induced internalisation of ErbB1-GFP allows ErbB1 that accumulates in endosomes to be dephosphorylated by PTP-1B. This is a plausible situation, because the ER pervades the entire cytoplasm, which presumably allows the membranes of the ER and endosome to come within close approach, and the catalytic domains of PTP-1B and ErbB1 both reside on the cytoplasmic side of the lumen. PTP-1B is therefore implicated in the termination of ErbB1 signalling that occurs during internalisation.

If endosomal ErbB1 is dephosphorylated by intracellular PTPs it was reasoned that PTP inhibitors should induce the phosphorylation of endosomal ErbB1. In order to investigate this, I took advantage of the fact that, within a given population of transfected MCF-7 cells, some cells retain ErbB1-GFP entirely within large endosomes or within the ER, with little or no plasma membrane expression visible (see left panels Figs 5.6 B and 5.6 C). This internal ErbB1 population does not become phosphorylated after EGF treatment, because it is not accessible to ligand. In contrast, ErbB1-GFP that was present in these intracellular compartments became highly phosphorylated after 1-5 minutes of PTP inhibitor treatment (Fig. 5.6 B and C). Longer stimulation times (20-30 minutes) with EGF or PTP inhibitors causes the appearance of phosphorylated ErbB1 in large endosomes, presumably by stimulating internalisation (see section 5.3). However, since phosphorylated ErbB1-GFP was observed in large endosomes after only 1 minute exposure to hydrogen peroxide, it appears unlikely that the endosome-localised receptors

shown in Fig. 5.6 B are the product of receptor activation at the membrane followed by subsequent internalisation. It can therefore be inferred that the appearance of phosphorylated ErbB1 in endosomes, after short incubation times with PTP inhibitors, is due to the inhibition of PTPs that act on endosomal ErbB1. The presence of phosphorylated receptors in the ER provides additional evidence that PTP inhibitor treatment can lead to the appearance of phosphorylated ErbB1 within intracellular membranes, such as endosomes, without the prior requirement for surface activation and internalisation of ErbB1. Furthermore, phosphorylation of ER-localised ErbB1 in response to PTP inhibitors suggests that during synthesis in the ER, ErbB1 receptors may be kept in a dephosphorylated state by local PTP action, as has been previously postulated (Flint *et al.*, 1997).

These results provide additional proof that endosomal ErbB1 is dephosphorylated by PTPs (Haj *et al.*, 2002), because this activity can be overcome by PTP inhibitor treatment. They also indicate that the hydrogen peroxide production that facilitates phosphorylation of plasma membrane receptors must be highly local to the plasma membrane cytoplasmic surface. If the hydrogen peroxide produced upon ligand stimulus extended deeper into the cell it would allow incidental phosphorylation of endosomal ErbB1 by preventing the down regulation of ErbB1 phosphorylation by PTP-1B. The observation that EGF stimulus only induces phosphorylation of plasma membrane receptors without causing phosphorylation of intracellular ErbB1, whilst exogenous application of high concentrations of hydrogen peroxide induces the indiscriminate phosphorylation of intracellular ErbB1, shows that ligand-induced hydrogen peroxide production must be local to the plasma membrane.

It has been reported that EGF treatment of cells results in a transient attenuation of PTP-1B activity that peaks at 10 minutes post-stimulation, followed by a gradual rise in PTP-1B activity, which returns to normal levels 40 minutes post-stimulation (Lee et al., 1998). If hydrogen peroxide production is the mechanism via which this transient inhibition of PTP-1B is invoked, it is possible that hydrogen peroxide produced at the plasma membrane may extend far enough into the cell to inhibit PTP–1B molecules on ER membranes that are close to the cell surface, but that the hydrogen peroxide formation is attenuated after 10 minutes. In support of this, measurements of cellular oxidant levels in cells stimulated with EGF have shown that ROS production peaks at 10 minutes post-stimulus and falls by 15 minutes. Hydrogen peroxide formation at the plasma membrane

is predicted to be due to the activity of the plasma-membrane localised enzyme, NADPH oxidase (see section 5.7.3). An intriguing possibility is that endocytosis of activated ErbB1 molecules from the cell surface removes their ability to signal to membrane localised NADPH oxidase. This could be a mechanism which attenuates hydrogen peroxide production shortly after ligand activation, allowing dephosphorylation of receptors to occur, both at the plasma membrane and in membrane-proximal endocytosed vesicles.

The attenuation of hydrogen peroxide signalling after stimulus is also predicted to be dependent on the activity of cytosolic enzymes which mediate hydrogen peroxide breakdown (peroxidase activity). A family of cytoplasmic peroxidases, the peroxiredoxins, has been characterised and at least one of these has been shown to be able to attenuate hydrogen peroxide-mediated signalling that occurs downstream of growth factor stimulus (Kang *et al.*, 1998). However, a direct role for a peroxiredoxin isoform in regulating hydrogen peroxide-mediated PTP inhibition has yet to confirmed.

5.7 Discussion

It has been demonstrated that beads coupled to low densities of EGF induce only local phosphorylation of ErbB1 and that lateral propagation of ErbB1 phosphorylation is dependent on the presentation of high densities of EGF coupled to beads (section 5.2 and Fig. 5.1). Furthermore, low density EGF-beads, that give rise to only local activation of ErbB1 receptors, can cause lateral spreading of receptor phosphorylation in the presence of sub-saturating doses of a protein tyrosine phosphatase (PTP) inhibitor (see section 5.4 and Fig. 5.3). It has been shown that the application of saturating doses of PTP inhibiting compounds, such as phenyl arsine oxide and hydrogen peroxide, results in phosphorylation of receptors across the entire plasma membrane on a similar time scale to EGF ligand (see sections 5.3, 5.5; Fig. 5.2, Fig. 5.5), whilst overexpression of the hydrogen peroxide scavenging enzyme, catalase, impairs lateral phosphorylation spreading (see section 5.5 and Fig. 5.4). Phosphatase inhibitors can also induce the phosphorylation of ErbB1-GFP present within intracellular membranes (see section 5.6 and Fig. 5.6).

The results presented here suggest that the local density of EGF presented to ErbB1 receptors is a critical factor in determining the spreading of phosphorylation to

ligand-unocuppied receptors in cells. The demonstration that beads coupled to low densities of EGF induce only local phosphorylation of receptors shows that, at low ligand densities, only ligand-bound receptors become phosphorylated in cells. The demonstration that beads coupled to higher densities of EGF initiate lateral spreading of phosphorylation shows that at high EGF densities a mechanism exists which allows the phosphorylation of ligand-unoccupied receptors to occur. This provides a fundamental insight into the way that RTK phosphorylation is controlled in cells. It also explains the apparent contradiction between the results presented here (some of which have subsequently been published, see Verveer *et al.,* 2000) and the observations published in another report (Brock & Jovin, 2001).

5.7.1 A mechanism which couples ligand density to PTP inhibition via the production of hydrogen peroxide

The direction of the follow-up work to Chapters 3 and 4 was influenced mainly by the considerable evidence for the role of PTP activity in controlling cellular tyrosine phosphorylation levels (Ostman & Bohmer, 2001). In the absence of stimulus, receptors are maintained in a low net state of phosphorylation by the superior catalytic activity of PTPs. Therefore, in order for maximum ligand-induced tyrosine phosphorylation to occur, PTP activity must be switched-off. Evidence has been presented by others that, in response to extracellular ligand, tyrosine phosphorylated RTKs can directly switch off PTP activity via the production of hydrogen peroxide (Rhee *et al.,* 2000). Therefore, during ligand stimulus, sufficient levels of hydrogen peroxide must accumulate in order for PTP deactivation to occur. The concentration of intracellular hydrogen peroxide accumulated is therefore predicted to directly determine the levels of receptor tyrosine phosphorylation. We can deduce the mechanism via which phosphorylation is spread to ligand-unoccupied receptors in cells by 1. its ligand-density dependence, 2. its requirement for hydrogen peroxide production, and 3. the reduction in ligand density required to initiate spreading in the presence of PTP inhibitors; all of which have been demonstrated in this chapter.

If the density of ligand required to initiate lateral spreading of phosphorylation is reduced in the presence of PTP inhibitors, then the EGF density must directly dictate whether lateral spreading of phosphorylation occurs, by a mechanism that relies on PTP

inhibition. It can be assumed that the number of receptors activated by ligand binding directly beneath a bead is proportional to the number of ligands presented by the bead. In turn, it may be inferred that the level of hydrogen peroxide production at the bead is increased with the number of receptors activated and will therefore determine the level of PTP inhibition that is invoked. Since hydrogen peroxide production is required for lateral spreading of phosphorylation, and the level of hydrogen peroxide produced at the bead is predicted to determine the level of PTP inhibition invoked, this must therefore determine whether or not lateral spreading of phosphorylation proceeds or whether receptors only become phosphorylated locally. It is assumed that, when PTP activity is attenuated with a pharmacological inhibitor, the amount of ligand-induced hydrogen peroxide production necessary to initiate lateral phosphorylation spreading must be reduced. This explains the reduction in ligand density required to initiate spreading in the presence of a PTP inhibitor.

5.7.2 The model

At the bead contact site hydrogen peroxide is predicted to exist in the form of a localised 'cloud' centred around the production site. The size of the cloud is predicted to be related to the amount of activated receptors at the bead. When the ligand density is low, the hydrogen peroxide cloud produced is assumed to be confined to the area below the bead. In this situation, only stable phosphorylation of receptors under the bead is permitted, because the activity of PTPs can only be significantly suppressed locally (Fig. 5.7 A). This explains the localised phosphorylation of receptors in response to LD beads. However, if the ligand density exceeds a critical threshold level, sufficient hydrogen peroxide is produced to make a cloud that is larger in radius than the area occupied by receptors directly bound to ligand on the bead (Fig. 5.7 B). Under these conditions PTPs outside the bead contact area also become inhibited. This removes the silencing activity that keeps ligand-unoccupied receptors in a low net state of phosphorylation and thereby allows collisions between receptors outside the bead contact area to result in stable transphosphorylation (also see Fig 3.7 D, Chapter 3). These phosphorylated receptors will induce the production of more hydrogen peroxide, thereby leading to the activation of receptors further from the bead (Fig. 5.6 C). ErbB1 phosphorylation therefore spreads rapidly from the bead in the form of a wavefront which is mediated by a positive

feedback loop between ErbB1-induced hydrogen peroxide production (that inhibits PTP activity) and ErbB1 tyrosine phosphorylation (Fig 5.6 D). This is the model which explains the spreading of phosphorylation induced by EGF-beads coupled with high densities of EGF. Hydrogen peroxide and the PTP inhibitor, PAO, were both shown to induce phosphorylation of ErbB1 to a similar magnitude, and within a similar time scale, to EGF or EGF-beads. It is therefore plausible that the mechanism described above could mediate the rapid spreading of phosphorylation to ligand-unoccupied receptors when cells are presented with high densities of EGF that exceed a critical threshold level. Furthermore, the results show that hydrogen peroxide is a critical mediator of ErbB1 signal amplification at the plasma membrane. The production of hydrogen peroxide at the plasma membrane is predicted to be highly local to the cytoplasmic face of the membrane and attentuated following internalisation of ErbB1, allowing intracellular dephosphorylation of ErbB1 to proceed (see section 5.6).

5.7.3 The generation of hydrogen peroxide

The mechanism described above relies critically on the existence of hydrogen peroxide generating machinery at the plasma membrane. In phagocytic cells, hydrogen peroxide is produced by a well-characterised enzyme, NADPH oxidase; a multi-subunit complex located at the plasma membrane that is assembled into the active enzyme upon receipt of the appropriate signal(s) (Sauer *et al.*, 2001). The existence of a plasma membrane NADPH oxidase has been demonstrated in various non-phagocytic cell types and the production of reactive oxygen species in response to growth factors is a well-documented phenomenon in many cell types. However, the molecular details of the signalling pathway that couples extracellular ligand stimulus to NADPH oxidase is poorly characterised (Rhee *et al.*, 2001, Sauer *et al.*, 2001). Various signalling molecules have been reported to be involved including Rac, PKC, PI3 kinase and Ras (Sundaresan *et al.*, 1996, Tanabe, 1997; Bae *et al.*, 2000, Thannickal *et al.*, 2000). During the course of the presented study, a role for both PI3 kinase and PKC was addressed by stimulating cells with HD EGF-beads in the presence of the appropriate pharmacological inhibitors. However, no attenuation of the extent, or amplitude, of lateral spreading of phosphorylation was observed. In fact, populations of phosphorylated ErbB1 were generally higher under these conditions. This suggests that neither of these signalling

factors is involved in signalling to hydrogen peroxide production downstream of ErbB1 receptor activation. One of the components of the activated NADPH oxidase in HepG2 and Cos-1 cells is Rac (Cool *et al.,* 1998, Joneson & Bar-Sagi 1998). In addition, expression of a dominant negative Rac in cells has been shown to attenuate the production of ROS in NIH 3T3 fibroblasts treated with EGF (Sundaresan *et al.,* 1996). A role for Rac activity in the hydrogen peroxide generation that mediates lateral spreading of ErbB1 phosphorylation could be tested by expressing dominant negative Rac in MCF-7 cells. Since Ras has also been implicated in signalling to NADPH oxidase, Ras is potently activated by the EGF receptor and has been shown to lie upstream of a Rac, a role for Ras is also an obvious choice for investigation. In any case, it is clear that further studies will be required to elucidate the mechanism via which ErbB1 stimulates hydrogen peroxide production.

During the course of the investigation it also became desirable to be able to measure hydrogen peroxide production in cells. Ideally, an approach was sought which allows the production of this species to be imaged in living cells over time immediately after stimulus. It was expected that hydrogen peroxide should be visualised to spread from the bead contact point. A fluorescence-based assay does exist to measure hydrogen peroxide levels in cells after growth factor stimulus (Sundaresan *et al.,* 1995; Sundaresan *et al.,* 1996; Bae *et al.,* 1997; Bae *et al.,* 2000; Mahadev *et al.,* 2001). In these reports, cells are stimulated with growth factor and then loaded with 2'7'-dichlorofluorescin diacetate (DCFH-DA) for 5-10 minutes, followed by fluorescence imaging. DCFH-DA is a non-polar compound which enters the cells by diffusion, where it is hydrolysed by cellular esterases to the non-fluorescent polar derivative 2'7'-dichlorofluorescin (DCFH), effectively trapping it inside cells. Upon oxidation, DCFH is converted by an irreversible reaction to the fluorescent derivative 2'7'-dichlorofluorescein (DCF). The irreversible nature of the reaction means that DCF integrates the total cellular oxidant level over time, allowing only bulk cellular oxidant levels to be determined at single time points. There is also a necessity to load cells for several minutes after growth factor stimulus, so that the contribution of basal cellular oxidant levels are not measured and that only those induced by growth factor are measured. Due to these problems it was not possible to use this method to visualise the spatio-temporal generation of hydrogen peroxide at early time points after stimulus. It would therefore be of considerable advantage to design better

fluorescent sensors for the detection of hydrogen peroxide in cells, which would allow the generation of hydrogen peroxide to be spatially resolved in real time.

Figure 5.1 Biological activity of beads coupled with high and low surface densities of EGF

A. Histogram showing intensity of anti-EGF staining quantified from EGF-beads coupled in the presence (low density beads) or absence (high density beads) of competing amino groups (intensity values bin width = 75 arbitrary units). EGF-coupled beads were immobilised on glass coverslips and then stained by immunofluorescence with anti-EGF primary antibodies, followed by detection with Cy3-labelled secondary antibodies. Random fields of beads were imaged by wide field epifluorescence microscopy and the fluorescence intensity of 100 beads from each labelling reaction was determined using IPlab software (Signal Analytics Corporation). **B, C, D, E.** Serum starved, ErbB1-GFP expressing MCF-7 cells were stimulated with beads that possessed low or high surface densities of coupled EGF. After stimulation, cells were fixed, permeabilised and stained with Cy3-labelled anti-phosphotyrosine antibodies. Samples were also co-stained with anti-EGF antibodies that were detected with Cy5-labelled secondary antibodies. Populations of phosphorylated receptors were quantified by global analysis of FLIM data. Average populations of phosphorylated ErbB1-GFP detected in non-stimulated cells (NS, n = 13 cells) or cells stimulated for 5 minutes with beads coupled to low (LD, n = 5 cells) or high (HD, n = 13 cells) densities of EGF (**B**). Examples of cells that were stimulated for 2 minutes with HD EGF-beads (**C**) or LD EGF-beads (**D**) or that were not stimulated (**E**). Left panel, ErbB1-GFP fluorescence (green) and EGF-beads (red); middle-left panel, Cy3-PY72 staining; middle-right panel, anti-EGF staining; far-right panel, populations of phosphorylated receptors. Bead contact point is indicated with arrowheads in order to assist the reader in comparing staining and populations at the bead contact point in **C** and **D**.

Fig. 5.1

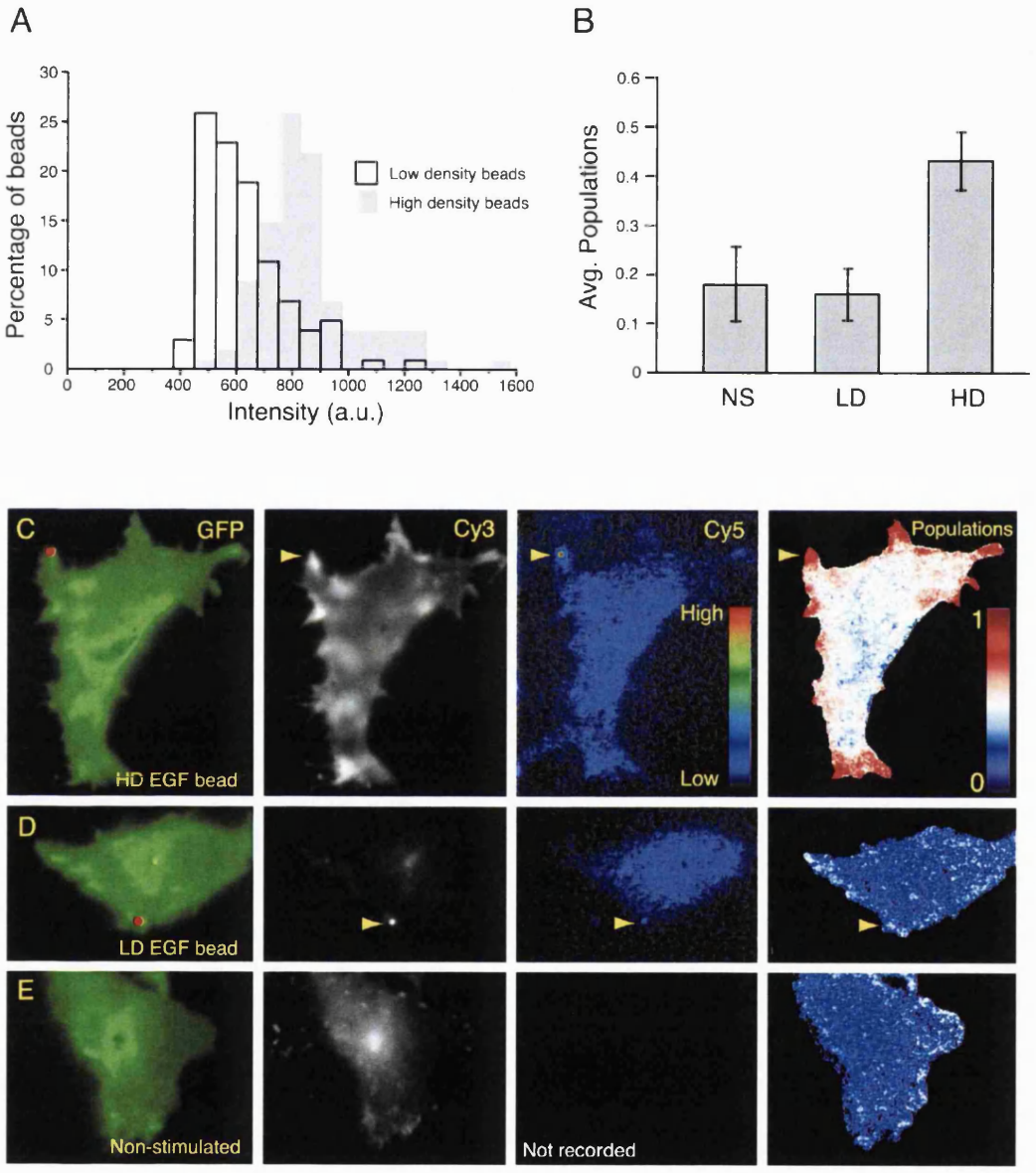
A
Percentage of beads
Intensity (a.u.)
Low density beads
High density beads
B
Avg. Populations
NS
LD
HD
C
GFP
HD EGF bead
Cy3
Cy5
High
Low
Populations
1
0
D
LD EGF bead
E
Non-stimulated
Not recorded

Figure 5.2 ErbB1-GFP phosphorylation in the presence of phenyl arsine oxide
A. Serum starved, ErbB1-GFP expressing MCF-7 cells were incubated for different time periods with 50 μM phenyl arsine oxide (PAO) and then fixed, permeabilised and stained with Cy3-labelled anti-phosphotyrosine antibodies. Phosphorylated receptor populations were quantified by global analysis of FLIM data (10-15 cells per data point). **B**. Example of a cell that has been incubated with 50 μM phenyl arsine oxide for 1 minute. Left panel, ErbB1-GFP fluorescence; middle panel, Cy3-PY72 staining; right panel, populations of phosphorylated receptors.

Fig. 5.2

A

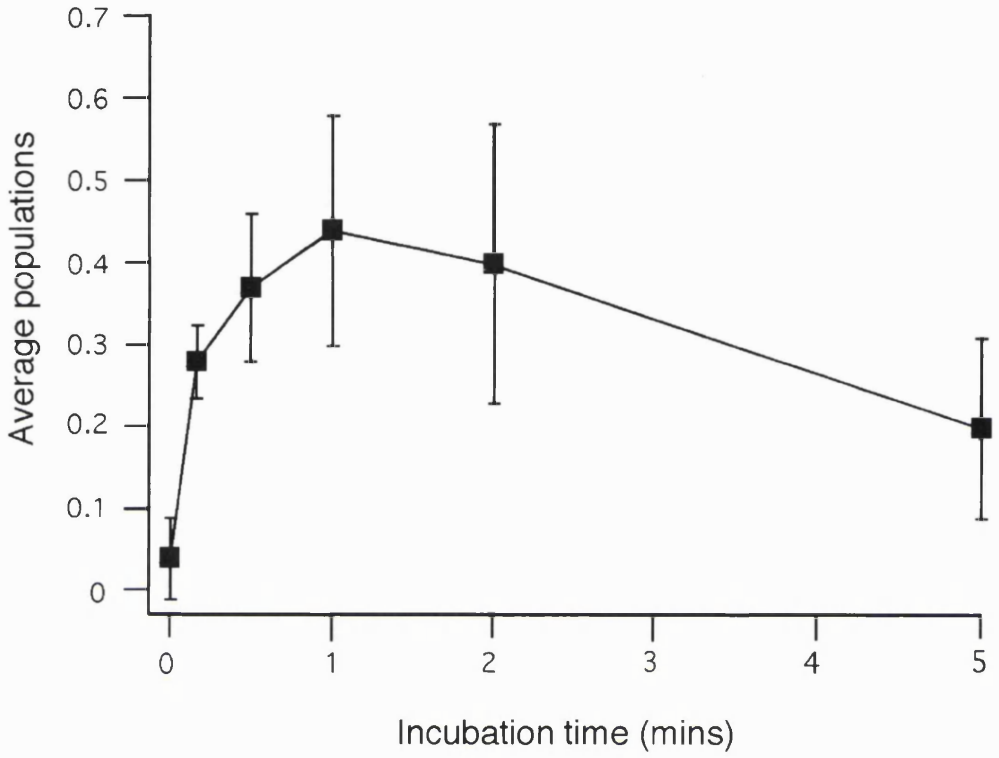
0.7
0.6
0.5
0.4
0.3
0.2
0.1
0
Average populations
0
1
2
3
4
5
Incubation time (mins)

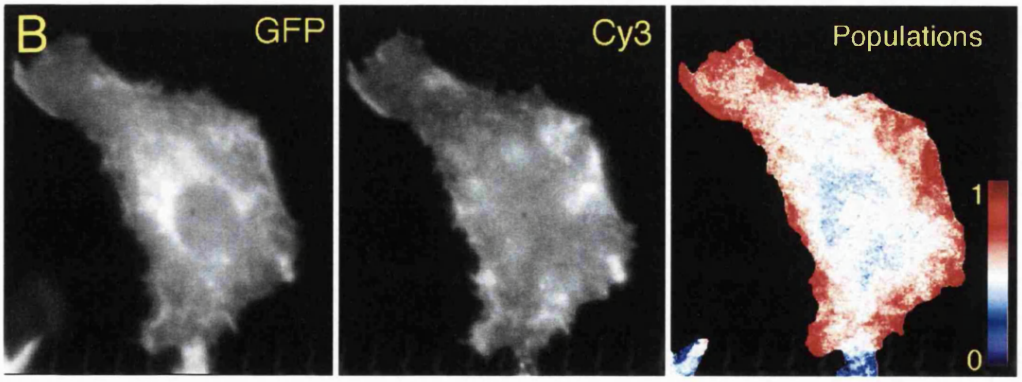
B
GFP
Cy3
Populations
1
0

Figure 5.3 Stimulation of cells with low surface density EGF-beads in the presence of a PTP inhibitor

A. Serum starved, ErbB1-GFP expressing MCF-7 cells were incubated in the presence of different concentrations of PAO for 2 minutes followed by a further 2 minutes incubation with the same concentration of PAO in the presence, or absence, of EGF-beads coupled to low surface densities of EGF (LD EGF-beads). Phosphorylated receptor populations were quantified by global analysis of FLIM data (~10 cells per data point). **B, C.** Example of a cell that was incubated with 0.1 μM PAO for 4 minutes (**B**), or incubated with 0.1 μM PAO for 2 minutes followed by stimulation with LD EGF-beads in the presence of 0.1 μM PAO for a further 2 minutes (**C**). Left panel, ErbB1-GFP fluorescence (green) and EGF-beads (red); middle panel, Cy3-PY72 staining; right panel, populations of phosphorylated receptors.

Fig. 5.3

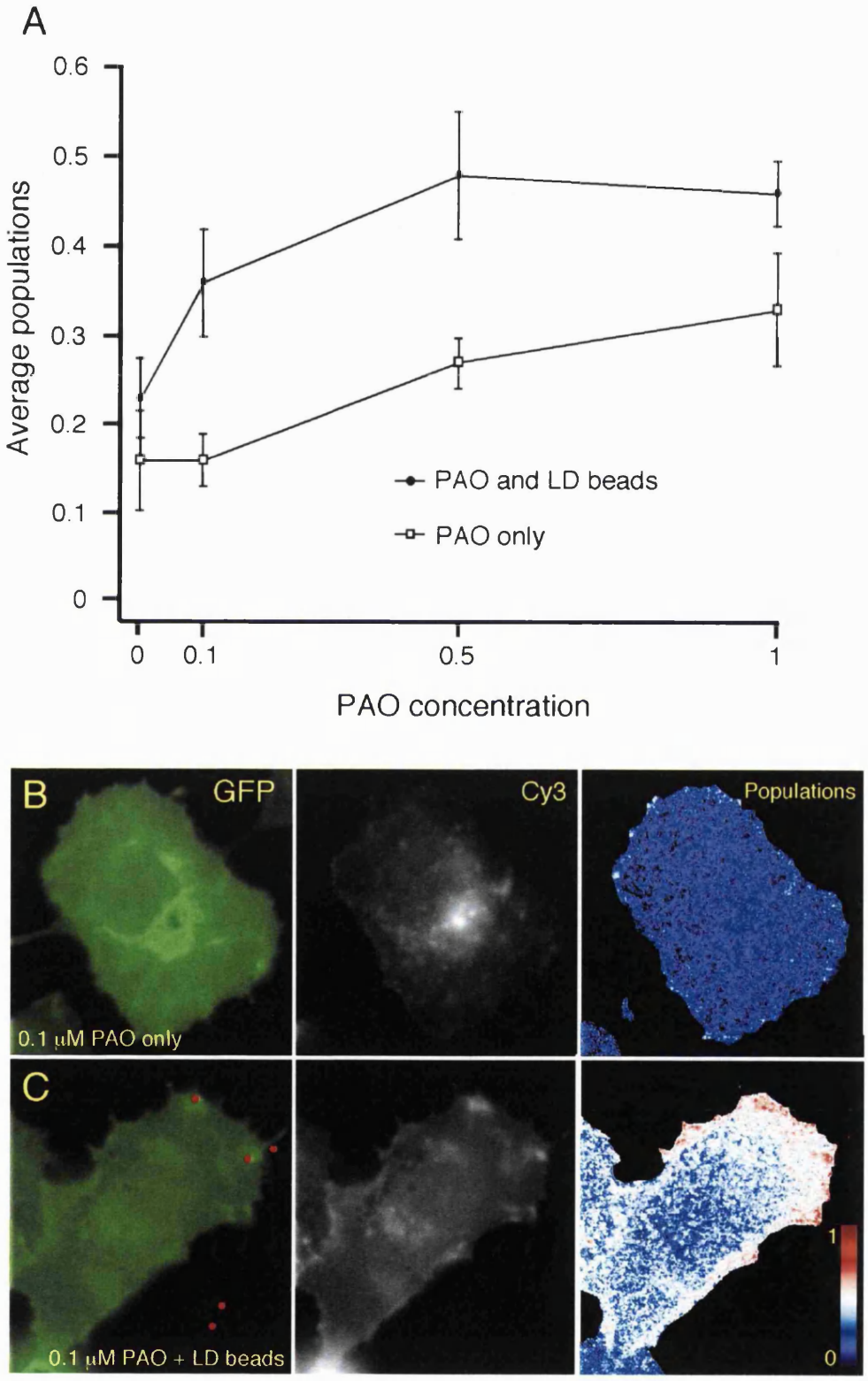
A
0.6
0.5
0.4
0.3
0.2
0.1
0
Average populations
PAO and LD beads
PAO only
0
0.1
0.5
1
PAO concentration
B
GFP
Cy3
Populations
0.1 μM PAO only
C
1
0
0.1 μM PAO + LD beads

Figure 5.4 ErbB1-GFP phosphorylation in cells that ectopically express catalase
Stable ErbB1-GFP expressing MCF-7 cells were microinjected with a 200 μg/ml solution of plasmid DNA encoding human fibroblast catalase. The cells were left to express the construct for 16 hours and 5 hours prior to stimulation the cells were transferred to starvation medium. After stimulation with HD EGF-beads for 2 minutes the cells were fixed, permeabilised and stained with Cy3-labelled anti-phosphotyrosine antibodies. Samples were also co-stained with anti-catalase antibodies that were detected with Cy5-labelled secondary antibodies. Phosphorylated receptor populations were quantified by global analysis of FLIM data. **A.** Example field of cells showing catalase expressing (top) and non expressing (bottom) cell. Top left panel, ErbB1-GFP fluorescence; top-right panel, Cy3-PY72 staining; bottom-left panel, Cy5-anti-catalase staining; bottom-right panel, populations of phosphorylated receptors. **B.** Histograms (see overleaf) showing number of pixels associated with a given population of phosphorylated receptors (pixel count is normalised to 1; population values bin width = 0.024 units). Data is shown for normal non-stimulated cells (top; n = 10 cells), cells ectopically expressing catalase stimulated with HD EGF-beads (middle, n = 10 cells) or normal cells stimulated with HD EGF-beads (bottom; n = 8 cells).

Fig. 5.4 A

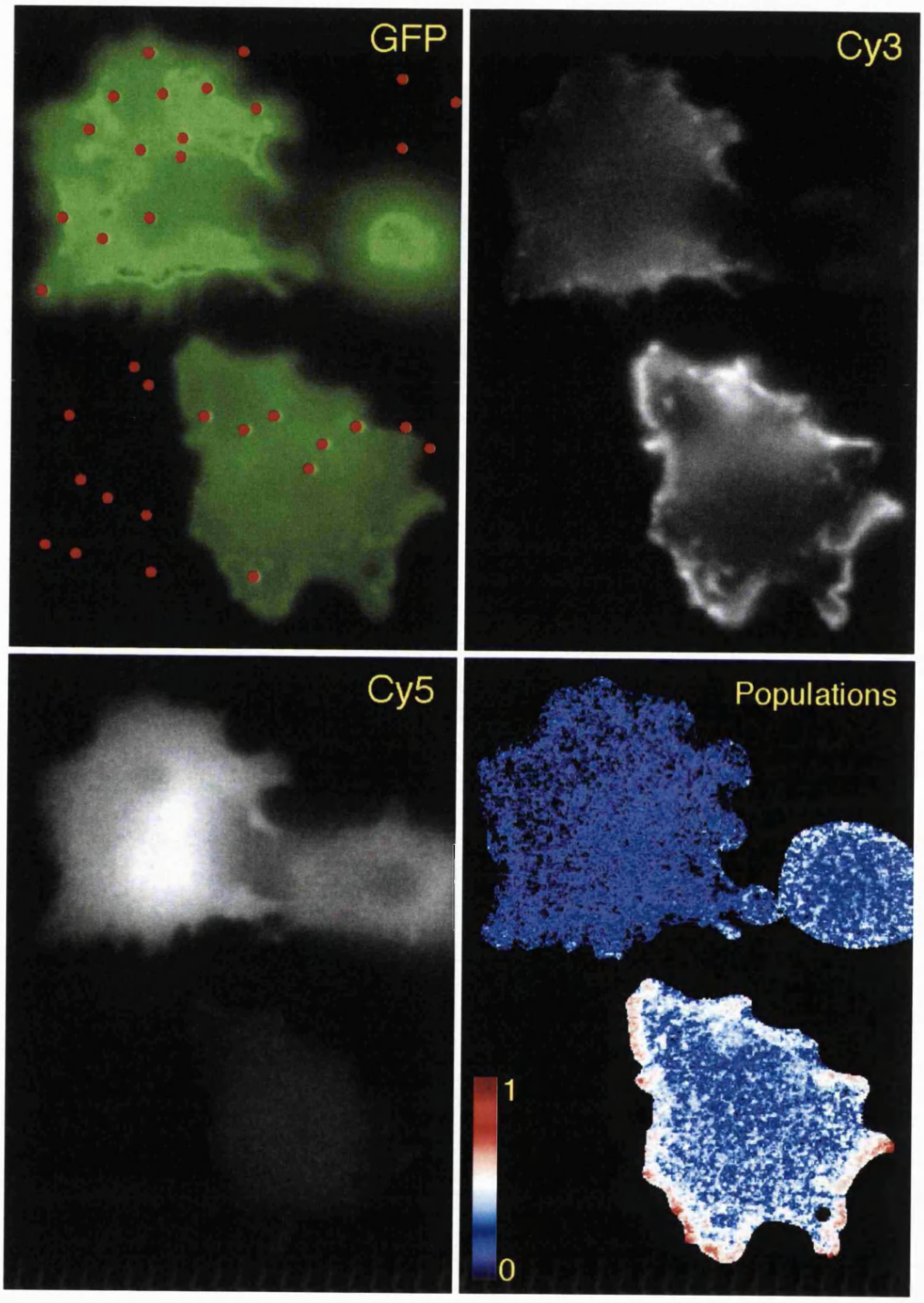

Fig. 5.4 B

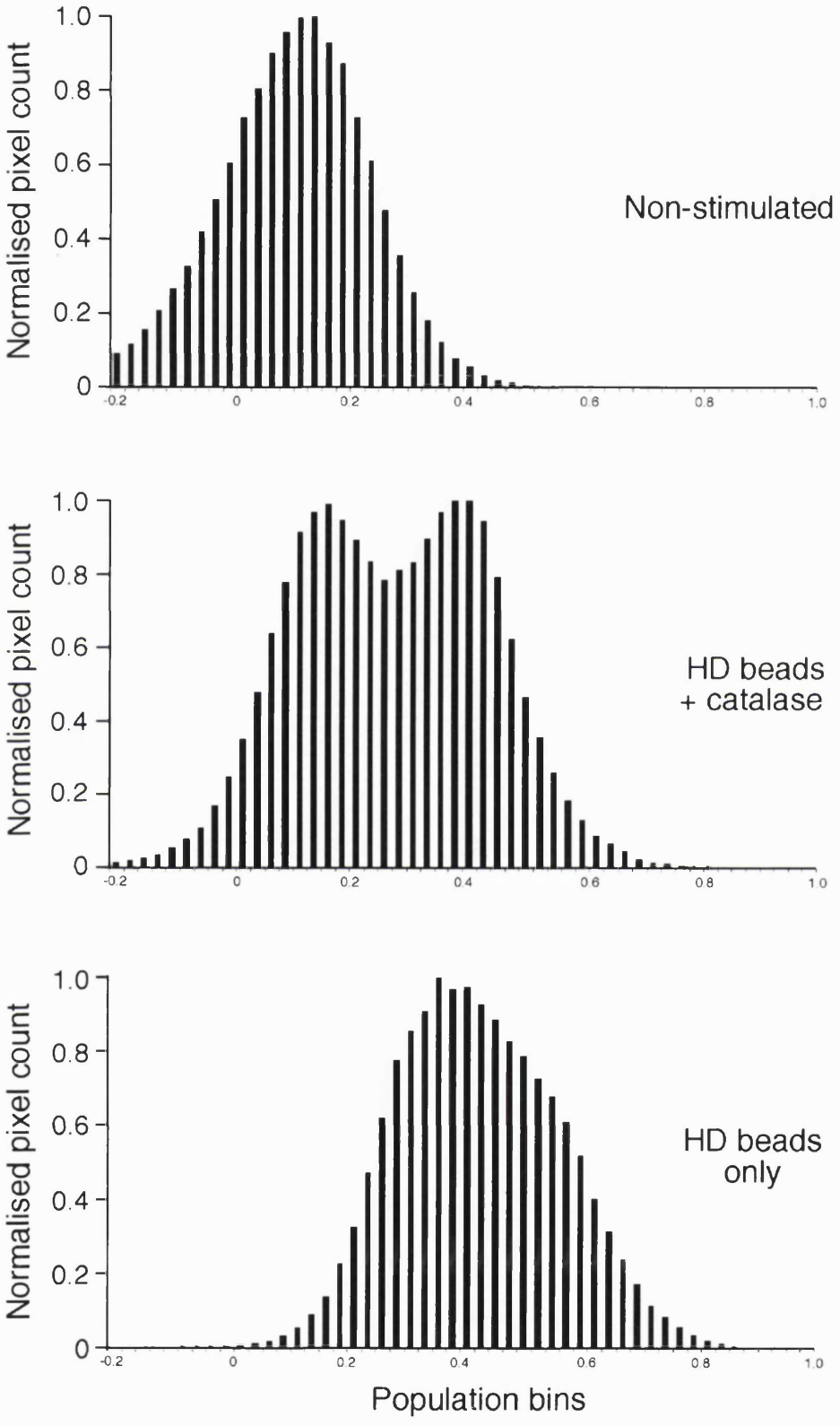
Normalised pixel count
1.0
0.8
0.6
0.4
0.2
0
-0.2
0
0.2
0.4
0.6
0.8
1.0
Non-stimulated
HD beads
+ catalase
HD beads
only
Population bins

Figure 5.5 ErbB1-GFP phosphorylation in the presence of hydrogen peroxide

A. Serum starved, ErbB1-GFP expressing MCF-7 cells were incubated for different time periods with 100 mM hydrogen peroxide and then fixed, permeabilised and stained with Cy3-labelled anti-phosphotyrosine antibodies. Phosphorylated receptor populations were quantified by global analysis of FLIM data (10-15 cells per data point). **B.** Example of a cell that has been incubated with 100 mM hydrogen peroxide for 2 minutes. Left panel, ErbB1-GFP fluorescence; middle panel, Cy3-PY72 staining; right panel, populations of phosphorylated receptors.

Fig. 5.5

A

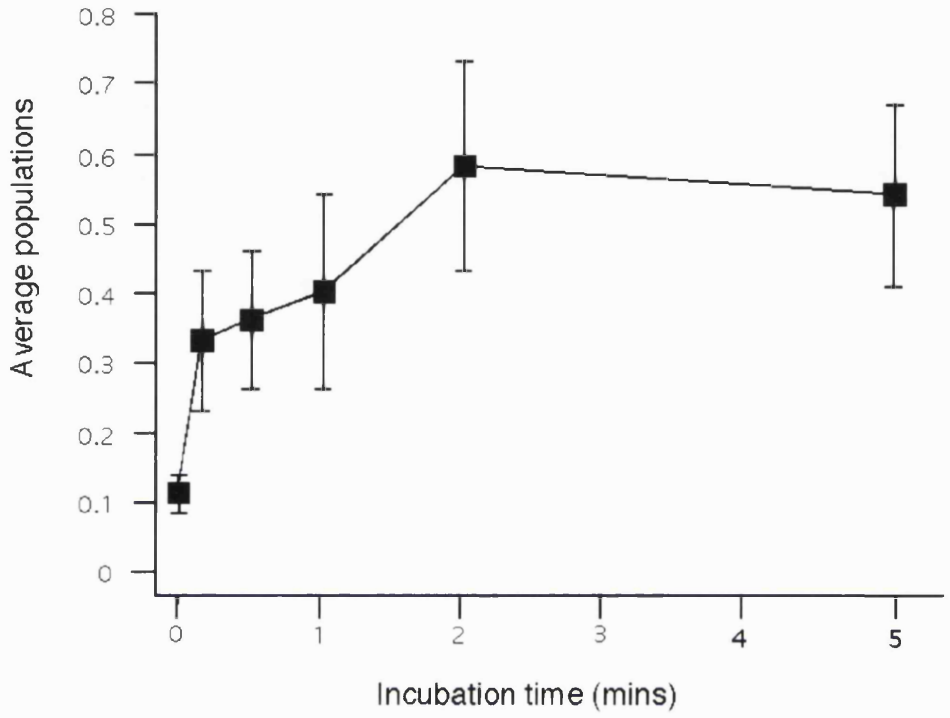
Average populations
0.8
0.7
0.6
0.5
0.4
0.3
0.2
0.1
0
0
1
2
3
4
5
Incubation time (mins)

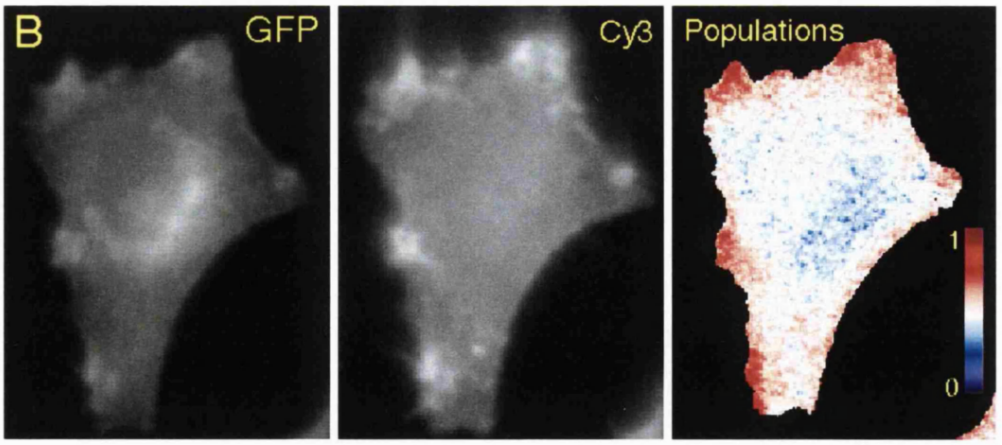
B
GFP
Cy3
Populations
1
0

Figure 5.6 Phosphorylation of intracellular ErbB1-GFP in the presence of PTP inhibitors

Serum starved, ErbB1-GFP expressing MCF-7 cells were incubated with PAO or hydrogen peroxide and then fixed, permeabilised and stained with Cy3-labelled anti-phosphotyrosine antibodies. Phosphorylated receptor populations were quantified by global analysis of FLIM data. **A.** A cell stimulated with 50 μM PAO for 2 minutes. **B.** A cell showing high levels of endosome-localised ErbB1-GFP that has been incubated with 100 mM hydrogen peroxide for 1 minute. **C.** A cell showing high levels of endoplasmic reticulum (ER) retained ErbB1-GFP that has been incubated with 5 mM hydrogen peroxide for 5 minutes. Left panel, ErbB1-GFP fluorescence; middle panel, Cy3-PY72 staining; right panel, populations of phosphorylated receptors.

Fig. 5.6

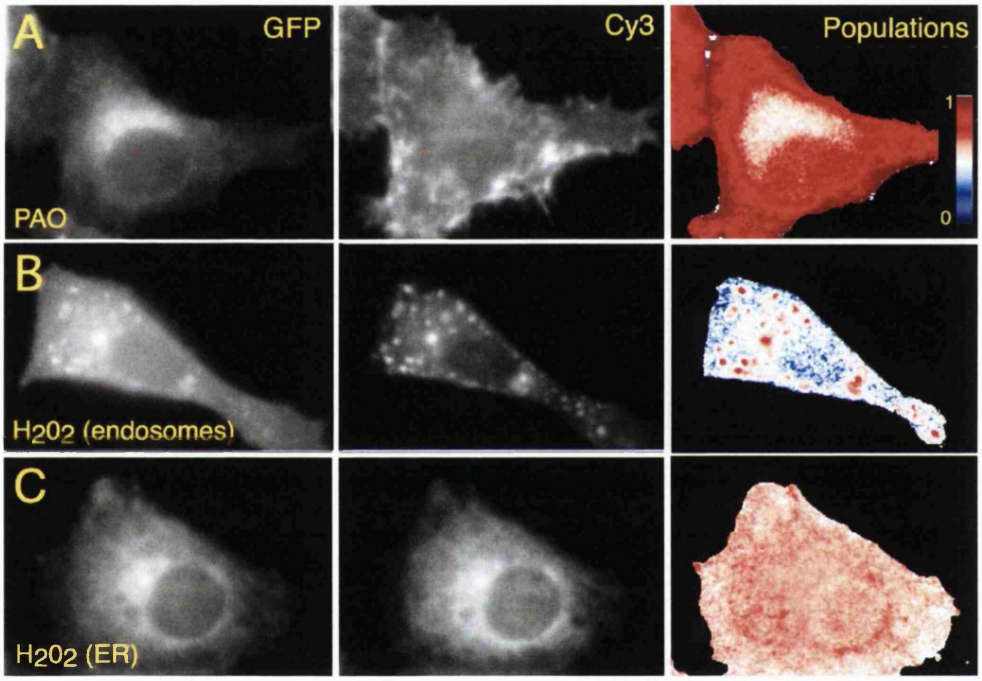

Figure 5.7 Model for EGF ligand-density dependent hydrogen peroxide production

See main text for details. Key: bead coupled to low surface densities of EGF (LD), bead coupled to high surface densities of EGF (HD), phosphorylated receptors (red), nonphosphorylated receptors (blue), hydrogen peroxide cloud (grey).

Fig. 5.7

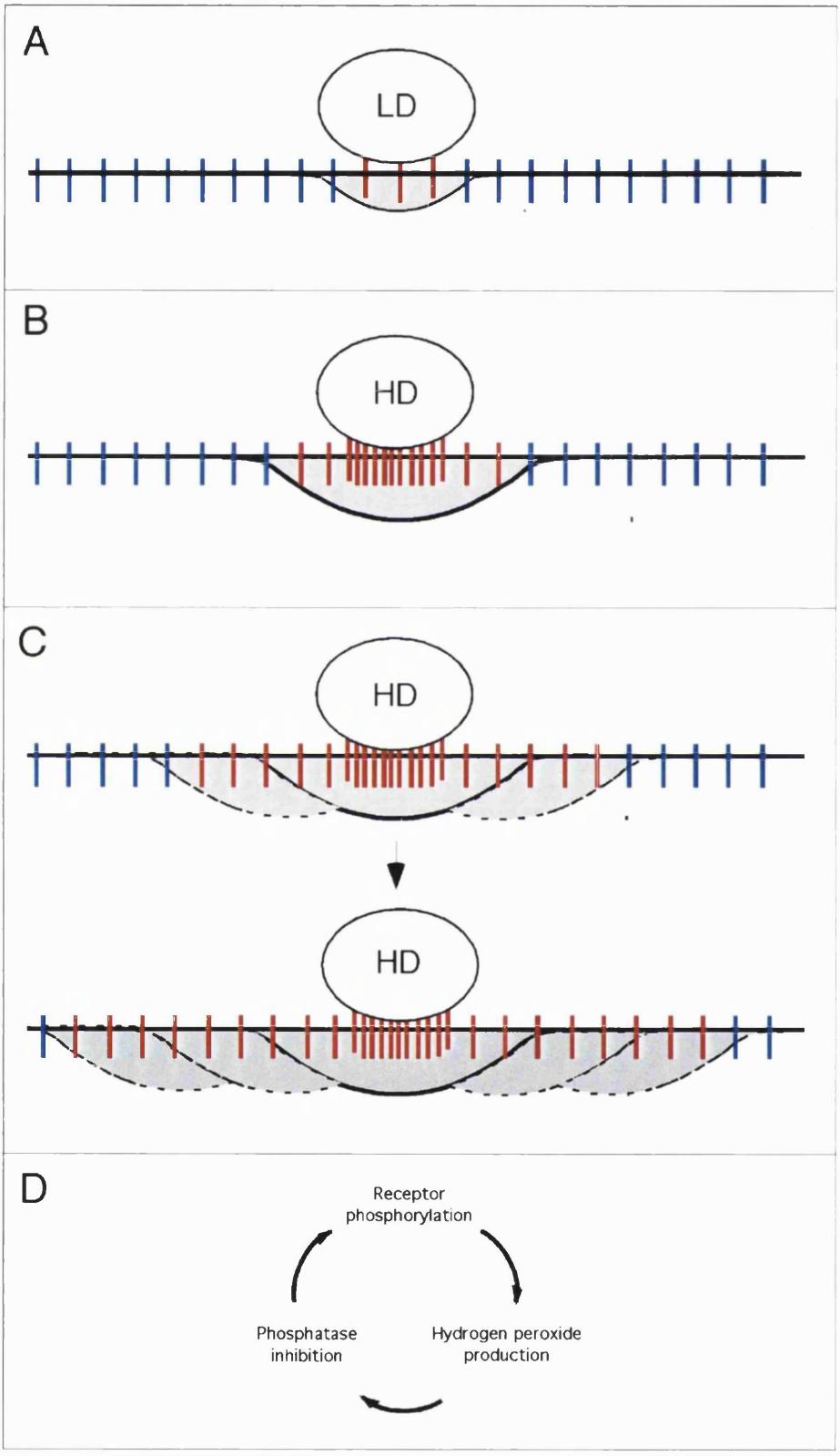
A
LD
B
HD
C
HD
HD
D
Receptor phosphorylation
Hydrogen peroxide production
Phosphatase inhibition

Chapter 6

Final Discussion

Final Discussion

6.1 Objectives of this thesis

Signalling that occurs via the ErbB family (ErbB1-4) of receptor tyrosine kinases (RTKs) has been extensively studied. This family of RTKs are involved in the differentiation and proliferation of human cells and aberrant signalling via these receptors is implicated in oncogenesis. Insight into the biochemical regulation of signalling by these receptors lets us understand how extracellular signals are decoded by cells and provides information on how these receptors contribute to disease.

It is well established that: 1. phosphorylation of receptors mediates downstream signalling by coupling to phosphotyrosine binding signalling factors (e.g. PI 3 kinase, PLCγ), and 2. the transmission of phosphorylation between receptors in the lateral plane of the membrane occurs (e.g. ErbB2 or ErbB3 phosphorylation after ErbB1-specific stimulus). Despite extensive research using standard biochemical techniques, the mechanisms which regulate the latter process are only poorly understood. We reasoned that insight would be provided by applying methods which allow the spatio-temporal aspect of receptor phosphorylation to be quantified directly in cells.

In this thesis a novel quantitative imaging approach was used to study the lateral propagation of phosphorylation between receptors. In contrast to existing biochemical techniques this allowed: 1. the relative populations of phosphorylated versus nonphosphorylated ErbB1 present within cells to be quantified, 2. inspection of the spatio-temporal regulation of phosphorylation, and 3. measurements of phosphorylation to be made under conditions which preserve the physiological context of the cell.

By implementing this approach evidence has been obtained which reveals a role for hydrogen peroxide in a novel ligand density-dependent mechanism, which allows the phosphorylation of ligand-unoccupied receptors to occur via protein tyrosine phosphatase (PTP) inhibition. The results have important implications for the control of receptor tyrosine phosphorylation by extracellular signals and the mechanisms via which amplification of tyrosine phosphorylation is achieved in cells.

6.2 Insight into the regulation of ErbB phosphorylation state

6.2.1 Existing evidence for a role of receptor oligomerisation

Phosphorylation of ErbB1 receptors occurs by a mechanism of intermolecular transphosphorylation (Honegger *et al.*, 1990). Ligand binding is presumed to invoke the formation of stable receptor dimers, in which transphosphorylation is highly favoured by virtue of the close molecular apposition afforded to receptors by dimer, or higher-order oligomer, formation (Ullrich & Schlessinger, 1992; Heldin, 1995). It has also been proposed that RTKs may exist in pre-formed dimeric complexes and that ligand binding induces a conformational change that is required for stable phosphorylation (Gadella & Jovin, 1995; Syed *et al.*, 1998; Moriki *et al.*, 2001; Bell *et al* ., 2001). It has therefore been suggested that a mechanism dependent on receptor oligomerisation alone is insufficient to mediate receptor transphosphorylation (Jiang & Hunter, 1999). However, a number of reports have shown that ligand stimulus induces the aggregation of plasma membrane ErbB receptors into clusters consisting of $10^2 - 10^3$ ErbB receptors (Schechter *et al.*,, 1979; Zidovetki *et al.*, 1981; van Belzen *et al.*, 1988, Nagy *et al.*, 1999). Clustering of receptors at high densities therefore appears to be a fundamental consequence of ligand stimulus, regardless of whether a conformational change is required to mediate transphosphorylation.

6.2.2 Existing evidence for a role of PTPs

The specific activities of PTPs for substrates are 10-1000 times higher than the specific activities of RTKs (Fischer *et al.*, 1991). Many RTKs appear to possess basal kinase activity, but are kept in a low net state of phosphorylation by the superior catalytic activity of PTPs, evidenced by the fact that treatment of cells with PTP inhibitors alone is sufficient to induce the phosphorylation of receptors and downstream substrates (Heffetz *et al.*, 1990, Jallal *et al.*, 1992, Gamou *et al.*, 1995; Knebel *et al.*, 1996). This has two important inferences: 1. even in the absence of ligand, receptor collision events in the plasma membrane are sufficient to allow receptors to transphosphorylate (N.B. this

refutes the relevance of a model in which a conformational change is required for ErbB1 transphosphorylation to occur, because collision events are not expected to emulate this conformational change), and 2. ligand stimulus can only give rise to tyrosine phosphorylation of receptors by inducing inhibition of cellular PTP activity. Evidence has been presented to suggest that this is mediated by the generation of hydrogen peroxide, which is a generic PTP inhibitor (Finkel, 1998; Finkel, 2000; Rhee *et al.,* 2000; Ostman & Bohmer, 2001)

6.2.3 Establishment of a link between the density of activated receptors and the level of PTP inhibition invoked

The work presented in this thesis provides evidence for a crucial link between the density of phosphorylated receptors aggregated locally in the plasma membrane and the extent of cellular RTK phosphorylation that is invoked, via a mechanism of PTP inhibition. It is proposed that RTKs possess basal kinase activity and can transphosphorylate during collision events, but are kept in a low net state of phosphorylation by the action of PTPs. It is suggested that ligand-induced aggregation of phosphorylated receptors overcomes the silencing activity of PTPs by stimulating the production of hydrogen peroxide. Furthermore, if the receptors are clustered beyond a threshold density, sufficient hydrogen peroxide-mediated PTP inhibition is invoked to allow ligand-unoccupied receptors to become phosphorylated also. This occurs because, in the absence of PTP activity, transphosphorylation which occurs during collision events between receptors cannot be silenced. In contrast, when phosphorylated receptors are present at low densities, insufficient hydrogen peroxide is produced to elicit this effect allowing only ligand-bound receptors to become phosphorylated.

6.3 Wider implications of the proposed model

6.3.1 Implications for heterotypic receptor activation

It has been shown here, that ligand binding to only a fraction of the ErbB1 receptors at the cell surface can induce phosphorylation of a large population of ligand-unoccupied ErbB1 receptors by a mechanism of hydrogen peroxide-induced PTP

inhibition (homotypic activation). Given that a redox-sensitive catalytic motif is shared by most PTP enzymes (Neel & Tonks, 1997; Finkel, 2000), this mechanism is predicted to also result in stable tyrosine phosphorylation of other RTK subtypes (heterotypic activation).

Heterotypic activation by PTP inhibition may explain the phosphorylation of ErbB3 that was observed in the presence of a minor population of ErbB1 in Chapter 4.4 and it may also explain some observations reported in the literature. There are numerous examples of RTKs becoming phosphorylated after stimulus of cells with ligands that are specific for other receptors (heterotypic receptor activation, otherwise known as receptor transactivation). For example, it has been shown that ErbB3 and ErbB4 can become phosphorylated after EGF stimulus of ErbB1 (Gamett *et al.,* 1997); phosphorylation of ErbB1 and ErbB2 can occur after NRG stimulus of ErbB3/ErbB4 (Riese *et al.,* 1995); stimulation of the PDGFR with PDGF results in phosphorylation of ErbB1 and downstream signalling from ErbB1 (Countaway *et al.,* 1989, Li *et al.,* 2000, He *et al.,* 2001, Saito *et al.,* 2000).

In most of these reports, the authors propose mechanisms based on transphosphorylation in stable receptor heterodimers to explain the observed transactivation. An alternative interpretation of these results is that the receptors constantly undergo a cycle of phosphorylation-dephosphorylation, mediated by collision events between kinase active receptors and PTP activity. Stable phosphorylation of receptors thereby occurs due to PTP inhibition which is initiated after stimulus of another receptor. For example, there is already clear evidence that transactivation of ErbB1 in response to PDGF could be dependent on hydrogen peroxide-mediated PTP inhibition, because PDGF stimulation initiates hydrogen peroxide-production (Sundaresan *et al.,* 1995, Bae *et al.,* 2000) and ROS scavengers inhibit the transactivation of ErbB1 by PDGF (Saito *et al.,* 2001).

Furthermore, stimulation of cells with a broad range of ligands that bind directly to G-protein coupled receptors (GPCRs) results in the phosphorylation of ErbB1 (Luttrel *et al.,* 1999). Although it is becoming increasingly clear that this is elicited by autocrine signalling due to metalloproteinase-mediated cleavage of surface-bound ErbB ligands (Geschwind *et al.,* 2001) an important role for hydrogen peroxide production in ErbB1 transphosphorylation has been proposed in the case of at least one GPCR ligand i.e. angiotensin II (Ushio-Fukai & Griendling, 2001). It is therefore possible that hydrogen

peroxide-mediated PTP inhibition may contribute, at least in part, to the transactivation of ErbB1 after stimulus of GPCRs.

6.3.2. Physiological implications

6.3.2.1 Generic RTK activation and signalling specificity

The implication that ligand-induced PTP inhibition can give rise to the generic phosphorylation of RTKs would appear to undermine any notion that signalling via specific receptors is linked to specific outcomes. Instead, it would imply that receipt of any stimulus of sufficient magnitude would activate all cellular receptors. This apparent redundancy is no more surprising than the knowledge that receptors can activate broadly overlapping downstream signalling effectors and induce the expression of broadly overlapping genes (Schlessinger, 2000; Fambrough *et al.*, 1999; Pawson & Saxton 1999). However, it would defy the purpose of organisms expressing so many different RTK receptors and ligands, yet considerable evidence from mouse knock-out studies suggest that receptor diversity is absolutely required for correct development (Madhani, 2000). It therefore suggests that this mechanism is present as a signal amplification mechanism within certain cell types only or only occurs when ligands are presented at a sufficiently high local density .

6.3.2.2 Dependence on PTP and RTK isoform specific properties and PTP / RTK expression patterns

It should be noted that not all PTPs are subject to regulation by hydrogen peroxide. For example, tyrosine dephosphorylation of ErbB2 can be mediated by prostatic acid phosphatase, which does not react with hydrogen peroxide due to the presence of a catalytic histidine instead of a cysteine in the active site (Meng & Lin 1998). Furthermore, it is expected that different PTPs will show different degrees of sensitivity to hydrogen peroxide and that other mechanisms which control PTP activity will influence the extent to which hydrogen peroxide inhibits their activity (e.g. interactions with other molecules or subcellular targeting). The PTP expression profile of a cell may thereby directly dictate the specific responses of a cell. The human genome

encodes for at least 40 PTPs, whose expression is controlled between tissues and as a function of development stages, as is the case with RTKs (Neel & Tonks, 1997). The expression profile of PTPs in different cells and tissue will therefore directly influence many signalling outcomes.

At least two RTKs characterised to date possess no kinase activity: ErbB3 and EphB6, a member of the Eph family of RTKs. Both receptors are thought to become phosphorylated *in trans* by associating with a kinase active receptor (Soltoff *et al.*, 1994; Kim *et al.*, 1994; Sliwkowski *et al.*, 1994; Carraway & Cantley, 1994; Freywald *et al.*, 2002). It is predicted that these receptors would not take part in a signal amplification mechanism which relies on PTP inhibition unless a suitable receptor was present, within the same cell, for which ErbB3 or EphB6 was a substrate i.e. ErbB1/ErbB2/ErbB4 or EphB1, respectively.

6.3.2.3 Relevance to cells which undergo a high rate of proliferation

Elevated expression of ErbB receptors and ligands results in elevated receptor tyrosine phosphorylation and is implicated in cellular transformation, both in culture and *in vivo* (Salomon, 1995; Mendelsohn & Baselga, 2000). It is considered possible that the model described in section 6.2.3 may be relevant to transformation in one of two ways, which have yet to be distinguished: 1. receptor overexpression may lead to increased receptor collisions in the membrane, which overcomes the PTP activity of the cell, resulting in heightened hydrogen peroxide production which further inhibits PTPs, or 2. receptor overexpressing cells may exhibit heightened sensitivity to the density of presented ligand, such that local high densities of ligand may give rise to signal amplification by PTP inhibition. In either situation, the resulting signal amplification gives rise to a high amplitude proliferative signal.

There may also exist non-pathological contexts where generic activation of many receptors, and the resultant signal amplification, may be desirable. For example, during development rapid proliferation is required to generate the tissues and organs of the developing organism. It is deemed possible that under these circumstances it might be advantageous for cells to be programmed to amplify mitogenic signals by PTP inhibition. Generic activation of many RTK subtypes in this situation would generate a high amplitude proliferative signal.

6.3.2.4 Relevance to physiological presentation of extracellular ligand

The model proposed in section 6.2.3 suggests that the local density of ligand that is presented to a cell will dictate the amplitude of the signalling response. It is predicted that at low local ligand densities only local activation of receptors will be induced, whereas at high local ligand densities the signal will be amplified by PTP inhibition. To the best of my knowledge, no independent study has approached the relationship between the density of growth factor presented locally to cells and the resultant signalling outcomes. However, a relevant study has been performed regarding the effects of integrin ligand density on PDGF-mediated motility (Maheshwari *et al.,* 2000). PDGF-mediated motility was vastly augmented in NR6 fibroblasts when ligand was presented in the form of clusters than when it was presented homogeneously at the substratum. This provides some independent evidence that the presentation of extracellular ligands to cells at high density, locally, elicits more potent effects than a signal presented at low density. The potential for ligands to be presented in clusters within tissue does exist, as many growth factor ligands are presented as cell-surface bound ligands or are immobilised in the extracellular matrix (ECM) in complex with ECM components, such as heparin (Massague & Pandiella, 1993; Taipale & Keski-Oja, 1997; Faham *et al.*, 1998). This means of presentation is predicted to prevent diffusion of growth factors and might mediate clustering. It is also known that signalling ligands may be shed from cells as vesicles, known as 'exosomes' (Denzer *et al.,* 2000). It has been shown that exosomes containing the drosophila ligand, Wingless, become dispersed throughout the imaginal disc epithelium and therefore are presented to cells as small, spatially-restricted clusters (Greco *et al.,* 2001). Furthermore, these clusters are removed from the tissue by heparinase treatment, suggesting that presentation is dependent on conjugation to the extracellular matrix.

6.3.3 PTPs regulate receptor tyrosine kinase phosphorylation in multiple compartments

6.3.3.1 Two 'PTP layers' define the boundaries of a 'signalling layer' for ErbB1

The results presented in this thesis, combined with those presented elsewhere (Haj *et al.,* 2002), suggest that the amplitude of ErbB1 signalling in cells is controlled by two spatially and temporally confined 'layers' of PTP activity. One layer, the PTP activity at the plasma membrane, controls signal amplification at the cell surface. The second layer, at the ER, controls the attenuation of signalling following receptor activation and internalisation. Therefore, the two PTP activity layers determine the boundaries of a third layer, which lies spatially and temporally in between the PTP layers, from which tyrosine phosphorylation-dependent signalling is elicited (the signalling layer). The balance between the level of PTP activity at the membrane and the level of PTP activity which acts upon internalised receptors is liable to dictate the duration and amplitude of the signalling response elicited within the 'signalling layer.'

6.3.3.2 PTPs dephosphorylate ER-localised receptors

In this thesis it was shown that PTP inhibitor treatment of cells results in phosphorylation of ER-localised receptors. This indicates that PTP activity may act to keep receptors in a dephosphorylated state during *de novo* synthesis. Significantly, studies on the intracellular location of ErbB1 dephosphorylation by ER-localised PTP-1B (Haj *et al.,* 2002) revealed no evidence for a role of PTP-1B in the dephosphorylation of ER-localised receptors (Philippe Bastiaens, unpublished observation). It may be that PTP-1B is unable to dephosphorylate receptors present within the same membrane due to steric constraints and it is proposed that an independent PTP is involved.

It has been demonstrated that expression of an ER-targeted single-chain antibody (scFv) against the extracellular domain of ErbB1 or ErbB2 results in the retention of *de novo* synthesised receptors in the ER, which inhibits the growth of several tumour cell lines (Jannot *et al.,* 1996). In another study, a mutant ErbB2, which lacked the transmembrane domain only, was found to still be able to transform NIH 3T3 cells when expressed at high levels, despite the fact that it was retained in the ER (Hudziak &

Ullrich, 1991). If PTPs regulate the phosphorylation state of ER-localised receptors, ER-retention of ErbB receptors may be an ineffective means to inhibit transformation of cells if ER-localised PTP activity is attenuated or saturated. Given that the ER is not considered to be the physiological location from which receptor signalling is elicited, the regulation and physiological relevance of signalling from this compartment is an open question.

6.3.4 The role of hydrogen peroxide in the spatio-temporal control of tyrosine phosphorylation

6.3.4.1 Hydrogen peroxide production is spatially and temporally regulated

Spatio-temporal co-ordination of intracellular hydrogen peroxide levels must contribute to the amplitude and specificity of tyrosine phosphorylation. For example, the work presented here suggests that the local ligand presentation density can result in local or widespread hydrogen peroxide production at the membrane, thus giving rise to different spatial extents of tyrosine phosphorylation. Furthermore, the hydrogen peroxide produced after growth factor stimulus is predicted to be limited to the membrane in order to prevent incidental phosphorylation of intracellular proteins. Restriction of hydrogen peroxide production to the membrane, and a reduction in hydrogen peroxide levels at a certain period after stimulus, is also proposed to be important for the intracellular attenuation of tyrosine phosphorylation-dependent signalling. Therefore, hydrogen peroxide production and breakdown must be spatially and temporally co-ordinated.

6.3.4.2 Inhibition of tyrosine phosphorylation at points of cell-to-cell contact

During the course of the work for this thesis it was evident that ErbB receptors at points of cell-to-cell contact exhibited lower levels of EGF-stimulated tyrosine phosphorylation than receptors in non-contacted membranes present within the same cell (for example, see population images of cells at 10 and 30 seconds of EGF stimulus, Fig. 3.5 A and Fig. 4.1 C). In contrast, it was observed that the tyrosine phosphorylation induced by saturating doses of PTP inhibitors appeared to be independent of cellular location, including sites of cell-to-cell contact.

It is known that cells grown at high densities possess greater intracellular PTP activity than cells present in lower density cultures. As a consequence RTKs within cells grown at higher densities undergo less tyrosine phosphorylation in response to growth factors than RTKs present in low density cultures (Mansbridge *et al.*, 1992, Sorby & Ostman 1996). Furthermore, it has been proposed that hydrogen peroxide production is attenuated in high density cultures, which results in raised intracellular PTP activity (Pani *et al.*, 2000). I propose that at points of cell-to-cell contact a mechanism is in place that attenuates the potential to produce high levels of hydrogen peroxide locally at the plasma membrane. An impaired potential for accumulating hydrogen peroxide locally at sites of cell-to-cell contact would explain the observed attenuation of ErbB phosphorylation that I observed at cell-to-cell contact sites. It is not clear whether this is mediated through regulation of hydrogen peroxide production or hydrogen peroxide breakdown. It is postulated that hydrogen peroxide regulation of PTP activity may contribute to contact inhibition. Since stimulation of RTKs can also be chemotactic, it is also predicted to be involved in regulating cell motility also.

6.3.4.3 Mechanisms regulating the local intracellular levels of hydrogen peroxide

The local intracellular concentration of hydrogen peroxide must be regulated by at least three mechanisms: 1. enzymatic generation, 2. enzymatic break-down, and 3. buffering effects due to reaction with proteins.

Enzymatic generation. Most studies implicate NADPH oxidase as the major enzymatic source of hydrogen peroxide production downstream of RTKs, although the signalling pathways involved are not well characterised. Hydrogen peroxide produced by this enzyme is predicted to be confined to the plasma membrane proximal area. Other intracellular enzymes may be eventually identified which generate hydrogen peroxide in a signal-regulated fashion at this, and other, intracellular sites.

Enzymatic break-down. A large family of cytosolic hydrogen peroxide degrading enzymes, the peroxiredoxins, have been characterised. There is evidence that at least one isoform can attenuate signalling by NF-κB through the sequestration of hydrogen peroxide (Kang *et al.*, 1998). A role for these enzymes in regulating the amplitude of RTK signalling has yet to be confirmed.

Buffering effects. The local hydrogen peroxide concentration is liable to be buffered by the presence of groups with which it can react. Apart from PTPs, various other proteins have been shown to be reactive with hydrogen peroxide (Kim *et al.*, 2000). This therefore suggests that the local levels of hydrogen peroxide are regulated by the local concentration of reactive proteins (buffering effects) as well as the local activity of molecules which mediate hydrogen peroxide production and breakdown.

6.3.4.4 Analogy between the second messengers hydrogen peroxide and calcium

It has not escaped my notice that signalling via hydrogen peroxide shares elements in common with calcium signalling. Firstly, both of these second messengers are small, rapidly diffusing molecules. Secondly, the intracellular levels are dependent on mechanisms which generate and remove the species from the cytosol. Thirdly, they both mediate their effects by directly reacting with target proteins and both are subject to buffering effects by reacting with proteins. In addition, it has been shown that local sub-threshold doses of stimulus give rise to only locally raised cytosolic calcium levels, whereas local stimuli of sufficient magnitude give rise to calcium release across the entire cell via a positive feedback mechanism. The work presented in this thesis suggests that a similar dose-dependent mechanism may operate for the spatial control of hydrogen peroxide levels. Many important insights have been made into calcium signalling by the use of fluorescent probes to visualise the spatio-temporal fluctuations of intracellular calcium levels, but an equivalent technique does not exist to permit the visualisation of hydrogen peroxide.

6.3.4.5 Reversible inhibition of PTP activity

The oxidation of the PTP active site cysteine to sulfenic acid is reversible, which makes hydrogen peroxide-mediated inhibition an elegant reversible mechanism via which PTP activity can be controlled spatially and temporally in cells. The mechanism via which the oxidation of PTPs is reversed in cells is unknown, but it is predicted to involve the reaction of the sulfenic acid with glutathione, followed by conversion of this species back to cysteine by the action of enzymes such as thioredoxin or glutaredoxin (Finkel, 2000).

6.4 Directions for future work

1. It should be investigated whether the model for signal amplification described in this thesis is a generic mechanism or whether it only occurs in certain cell types (e.g. cancer cells) or with certain ligand and receptor combinations only. A role for hydrogen peroxide-mediated PTP inhibition in receptor transactivation can be explored by testing for transactivation events with various ligands and receptors in the presence of ROS scavengers.

2. Independent means to deliver highly controlled densities of ligands locally to cells should be implemented to provide support for the work presented in this study. Also, the presentation of ligands to cells as dense clusters should be investigated within physiological contexts. The consequences of this means of stimulation could be assessed within living tissues in mice, or other animals, by introducing beads covalently coupled to ligand into the animal. Furthermore, the physiological distribution of growth factors within healthy human tissues and tumour tissues should be studied at the ultrastructural level to determine whether ligands are presented in the form of clusters. The density of these clusters has implications for cellular responses.

3. The regulation of PTP activity by hydrogen peroxide is critically implicated in controlling the amplitude of receptor phosphorylation. The means via which hydrogen peroxide levels are regulated in cells should be further investigated. The generation, breakdown and buffering of this species should all be explored. Furthermore, the role of hydrogen peroxide-mediated PTP inhibition in determining extracellular stimulus-coupled cell behaviour should be explored (e.g. proliferation, differentiation, motility, contact inhibition).

4. Appropriate means should be developed to image hydrogen peroxide levels in cells with high temporal and spatial resolution in order to provide further insight into the means via which this molecule regulates signalling.

5. There is a need for improved understanding of the synergy between RTKs and PTPs. This should proceed by: 1. high through-put screening to identify the physiological substrates of PTPs (e.g. via the use of substrate-trapping mutants), and 2. identifying the degree of spatio-temporal overlap between RTKs and PTPs both at the intracellular level and at the tissue level. Signalling activities are expected to be critically dependent on the colocalisation of RTKs and PTPs not just in the same cells, but at the same intracellular locations.

6. Both oxidative stress and PTP activity should be investigated as potential targets for cancer therapy. This might proceed by designing, and evaluating the efficacy of, pharmacological agents which are designed to: 1. attenuate intracellular hydrogen peroxide production, 2. prevent the inhibition of PTPs by hydrogen peroxide, or 3. augment the activity or expression of the appropriate PTPs in tumours.

6.5 Concluding remarks

In general, this thesis supports the concept that intracellular tyrosine phosphorylation levels are dependent on a balance between tyrosine kinase activity and protein tyrosine phosphatase activity. It is also suggested that hydrogen peroxide - mediated PTP inhibition is a key regulator of the spatial and temporal aspect of tyrosine phosphorylation events. Considerable effort is being devoted to developing pharmacological agents which inhibit signalling via ErbB1 and ErbB2 as a rational means to target cancers (Mendelsohn & Baselga, 2000). Given that this thesis points at a critical role for regulated PTP activity in determining the amplitude of ErbB signalling, it is considered vital that therapies based on the regulation of PTP activity in tumours should be developed. The deregulated production of ROS has already been implicated in the pathology of cardiovascular disease, pulmonary disease and neoplasias (Griendling & Ushio-Fukai, 2000; Thannickal & Fanburg 2000, Bicknell , 2001). The work presented here, and by others (reviewed by Rhee *et al.*, 2000), suggests that deregulated ROS production must contribute to deregulated tyrosine kinase signalling. Therefore,

antioxidant therapies are predicted to be important for the treatment of diseases in which deregulated tyrosine kinase signalling is a causative factor.

The presented work also highlights the potential of time-resolved fluorescence measurements to gain new insights into the spatio-temporal aspects of cell signalling. This approach is a versatile method that can be applied to study various biochemical processes. Apart from applications in tissue culture cells, this technique may also be applied to study biochemical activity in entire tissue sections and as a drug screening tool. It is hoped that the insights provided by this technique will have important implications for the understanding of physiology and disease.

Chapter 7

References

References

Alimandi, M., A. Romano, M. C. Curia, R. Muraro, P. Fedi, S. A. Aaronson, P. P. Di Fiore and M. H. Kraus (1995). "Cooperative signaling of ErbB3 and ErbB2 in neoplastic transformation and human mammary carcinomas." Oncogene **10**(9): 1813-21.

Alroy, I. and Y. Yarden (1997). "The ErbB signaling network in embryogenesis and oncogenesis: signal diversification through combinatorial ligand-receptor interactions." FEBS Lett **410**(1): 83-6.

Axelrod, D., D. E. Koppel, J. Schlessinger, E. Elson and W. W. Webb (1976). "Mobility measurement by analysis of fluorescence photobleaching recovery kinetics." Biophys J **16**(9): 1055-69.

Bae, Y. S., S. W. Kang, M. S. Seo, I. C. Baines, E. Tekle, P. B. Chock and S. G. Rhee (1997). "Epidermal growth factor (EGF)-induced generation of hydrogen peroxide. Role in EGF receptor-mediated tyrosine phosphorylation." J Biol Chem **272**(1): 217-21.

Bae, Y. S., J. Y. Sung, O. S. Kim, Y. J. Kim, K. C. Hur, A. Kazlauskas and S. G. Rhee (2000). "Platelet-derived growth factor-induced H_2O_2 production requires the activation of phosphatidylinositol 3-kinase." J Biol Chem **275**(14): 10527-31.

Bagowski, C. P., M. Stein-Gerlach, A. Choidas and A. Ullrich (1999). "Cell-type specific phosphorylation of threonines T654 and T669 by PKD defines the signal capacity of the EGF receptor." Embo J **18**(20): 5567-76.

Bai, J., A. M. Rodriguez, J. A. Melendez and A. I. Cederbaum (1999). "Overexpression of catalase in cytosolic or mitochondrial compartment protects HepG2 cells against oxidative injury." J Biol Chem **274**(37): 26217-24.

Bao, J., I. Alroy, H. Waterman, E. D. Schejter, C. Brodie, J. Gruenberg and Y. Yarden (2000). "Threonine phosphorylation diverts internalized epidermal growth factor receptors from a degradative pathway to the recycling endosome." J Biol Chem **275**(34): 26178-86.

Bar-Sagi, D. and A. Hall (2000). "Ras and Rho GTPases: a family reunion." Cell **103**(2): 227-38.

Bastiaens, P. I. H. and T. M. Jovin (1996). "Microspectroscopic imaging tracks the intracellular processing of a signal transduction protein: fluorescent-labeled protein kinase C beta I." Proc Natl Acad Sci U S A **93**(16): 8407-12.

Bastiaens, P. I. H, I. V. Majoul, P. J. Verveer, H. D. Soling and T. M. Jovin (1996). "Imaging the intracellular trafficking and state of the AB5 quaternary structure of cholera toxin." Embo J **15**(16): 4246-53.

Bastiaens P.I.H. and T.M Jovin. (1998). Fluorescence resonance energy transfer microscopy, in *Cell Biology A Laboratory Handbook*, Celis, J.E. (Ed.). Academic Press.

Bastiaens, P. I. H. and R. Pepperkok (2000). "Observing proteins in their natural habitat: the living cell." Trends Biochem Sci **25**(12): 631-7.

Bastiaens, P. I. H. and A. Squire (1999). "Fluorescence lifetime imaging microscopy: spatial resolution of biochemical processes in the cell." Trends Cell Biol **9**(2): 48-52.

Baulida, J., M. H. Kraus, M. Alimandi, P. P. Di Fiore and G. Carpenter (1996). "All ErbB receptors other than the epidermal growth factor receptor are endocytosis impaired." J Biol Chem **271**(9): 5251-7.

Beechem, J. M. (1992). "Global analysis of biochemical and biophysical data." Methods Enzymol **210**: 37-54.

Beerli, R. R. and N. E. Hynes (1996). "Epidermal growth factor-related peptides activate distinct subsets of ErbB receptors and differ in their biological activities." J Biol Chem **271**(11): 6071-6.

Bell, C. A., J. A. Tynan, K. C. Hart, A. N. Meyer, S. C. Robertson and D. J. Donoghue (2000). "Rotational coupling of the transmembrane and kinase domains of the Neu receptor tyrosine kinase." Mol Biol Cell **11**(10): 3589-99.

Berridge, M. J., P. Lipp and M. D. Bootman (2000). "The versatility and universality of calcium signalling." Nat Rev Mol Cell Biol **1**(1): 11-21.

Bhalla, U. S. and R. Iyengar (1999). "Emergent properties of networks of biological signaling pathways." Science **283**(5400): 381-7.

Blume-Jensen, P. and T. Hunter (2001). "Oncogenic kinase signalling." Nature **411**(6835): 355-65.

Bohmer, F. D., A. Bohmer, A. Obermeier and A. Ullrich (1995). "Use of selective tyrosine kinase blockers to monitor growth factor receptor dephosphorylation in intact cells." Anal Biochem **228**(2): 267-73.

Bootman, M. D., P. Lipp and M. J. Berridge (2001). "The organisation and functions of local Ca(2+) signals." J Cell Sci **114**(Pt 12): 2213-22.

Brock, R. and T. M. Jovin (2001). "Heterogeneity of signal transduction at the subcellular level: microsphere-based focal EGF receptor activation and stimulation of Shc translocation." J Cell Sci **114**(Pt 13): 2437-47.

Bromberg, J. and X. Chen (2001). "STAT proteins: signal tranducers and activators of transcription." Methods Enzymol **333**: 138-51.

Brown, N. S. and R. Bicknell (2001). "Hypoxia and oxidative stress in breast cancer. Oxidative stress: its effects on the growth, metastatic potential and response to therapy of breast cancer." Breast Cancer Res **3**(5): 323-7.

Buday, L. and J. Downward (1993). "Epidermal growth factor regulates the exchange rate of guanine nucleotides on p21ras in fibroblasts." Mol Cell Biol **13**(3): 1903-10.

Burden, S. and Y. Yarden (1997). "Neuregulins and their receptors: a versatile signaling module in organogenesis and oncogenesis." Neuron **18**(6): 847-55.

Canals, F. (1992). "Signal transmission by epidermal growth factor receptor: coincidence of activation and dimerization." Biochemistry **31**(18): 4493-501.

Cantrell, D. A. (2001). "Phosphoinositide 3-kinase signalling pathways." J Cell Sci **114**(Pt 8): 1439-45.

Carpenter, G. (1999). "Employment of the epidermal growth factor receptor in growth factor- independent signaling pathways." J Cell Biol **146**(4): 697-702.

Carpenter, G. (2000). "The EGF receptor: a nexus for trafficking and signaling." Bioessays **22**(8): 697-707.

Carraway, K. L., 3rd and L. C. Cantley (1994). "A neu acquaintance for erbB3 and erbB4: a role for receptor heterodimerization in growth signaling." Cell **78**(1): 5-8.

Carraway, K. L., 3rd, M. X. Sliwkowski, R. Akita, J. V. Platko, P. M. Guy, A. Nuijens, A. J. Diamonti, R. L. Vandlen, L. C. Cantley and R. A. Cerione (1994). "The erbB3 gene product is a receptor for heregulin." J Biol Chem **269**(19): 14303-6.

Carter, R. E. and A. Sorkin (1998). "Endocytosis of functional epidermal growth factor receptor-green fluorescent protein chimera." J Biol Chem **273**(52): 35000-7.

Cattaneo, E. and P. G. Pelicci (1998). "Emerging roles for SH2/PTB-containing Shc adaptor proteins in the developing mammalian brain." Trends Neurosci **21**(11): 476-81.

Chamberlain, C. and K. M. Hahn (2000). "Watching proteins in the wild: fluorescence methods to study protein dynamics in living cells." Traffic **1**(10): 755-62.

Clapham, D. E. (1995). "Calcium signaling." Cell **80**(2): 259-68.

Clegg .R. (1996). Fluorescence resonance energy transfer, in *Fluorescence Imaging Spectroscopy and Microscopy*, Wang. X.F. & Herman B. (Eds.). John Wiley & Sons, Inc.

Cochet, C., O. Kashles, E. M. Chambaz, I. Borrello, C. R. King and J. Schlessinger (1988). "Demonstration of epidermal growth factor-induced receptor dimerization in living cells using a chemical covalent cross-linking agent." J Biol Chem **263**(7): 3290-5.

Cohen, S., R. A. Fava and S. T. Sawyer (1982). "Purification and characterization of epidermal growth factor receptor/protein kinase from normal mouse liver." Proc Natl Acad Sci U S A **79**(20): 6237-41.

Cool, R. H., E. Merten, C. Theiss and H. Acker (1998). "Rac1, and not Rac2, is involved in the regulation of the intracellular hydrogen peroxide level in HepG2 cells." Biochem J **332**(Pt 1): 5-8.

Cornish, V. W., D. R. Benson, C. A. Altenbach, K. Hideg, W. L. Hubbell and P. G. Schultz (1994). "Site-specific incorporation of biophysical probes into proteins." Proc Natl Acad Sci U S A **91**(8): 2910.

Countaway, J. L., N. Girones and R. J. Davis (1989). "Reconstitution of epidermal growth factor receptor transmodulation by platelet-derived growth factor in Chinese hamster ovary cells." J Biol Chem **264**(23): 13642-7.

Deb, T. B., L. Su, L. Wong, E. Bonvini, A. Wells, M. David and G. R. Johnson (2001). "Epidermal growth factor (EGF) receptor kinase-independent signaling by EGF." J Biol Chem **276**(18): 15554-60.

Denu, J. M., J. A. Stuckey, M. A. Saper and J. E. Dixon (1996). "Form and function in protein dephosphorylation." Cell **87**(3): 361-4.

Denzer, K., M. J. Kleijmeer, H. F. Heijnen, W. Stoorvogel and H. J. Geuze (2000). "Exosome: from internal vesicle of the multivesicular body to intercellular signaling device." J Cell Sci **113 Pt 19**: 3365-74.

Domagala, T., N. Konstantopoulos, F. Smyth, R. N. Jorissen, L. Fabri, D. Geleick, I. Lax, J. Schlessinger, W. Sawyer, G. J. Howlett, A. W. Burgess and E. C. Nice (2000). "Stoichiometry, kinetic and binding analysis of the interaction between epidermal growth factor (EGF) and the extracellular domain of the EGF receptor." Growth Factors **18**(1): 11-29.

Downward, J., P. Parker and M. D. Waterfield (1984). "Autophosphorylation sites on the epidermal growth factor receptor." Nature **311**(5985): 483-5.

Downward, J., M. D. Waterfield and P. J. Parker (1985). "Autophosphorylation and protein kinase C phosphorylation of the epidermal growth factor receptor. Effect on tyrosine kinase activity and ligand binding affinity." J Biol Chem **260**(27): 14538-46.

Downward, J. (1996). "Control of ras activation." Cancer Surv **27**: 87-100.

Drebin, J. A., D. F. Stern, V. C. Link, R. A. Weinberg and M. I. Greene (1984). "Monoclonal antibodies identify a cell-surface antigen associated with an activated cellular oncogene." Nature **312**(5994): 545-8.

Dustin, M. L. and A. C. Chan (2000). "Signaling takes shape in the immune system." Cell **103**(2): 283-94.

Dykstra, M. L., A. Cherukuri and S. K. Pierce (2001). "Floating the raft hypothesis for immune receptors: access to rafts controls receptor signaling and trafficking." Traffic **2**(3): 160-6.

Edwards, A. S. and J. D. Scott (2000). "A-kinase anchoring proteins: protein kinase A and beyond." Curr Opin Cell Biol **12**(2): 217-21.

Faham, S., R. J. Linhardt and D. C. Rees (1998). "Diversity does make a difference: fibroblast growth factor-heparin interactions." Curr Opin Struct Biol **8**(5): 578-86.

Fambrough, D., K. McClure, A. Kazlauskas and E. S. Lander (1999). "Diverse signaling pathways activated by growth factor receptors induce broadly overlapping, rather than independent, sets of genes." Cell **97**(6): 727-41.

Ferguson, K.M., P.J. Darling, M.J. Mohan, T.L. Macatee and M.A. Lemmon. (2000). "Extracellular domains drive homo- but not hetero-dimerization of erbB receptors. Embo J **19**(17):4632-43.

Finkel, T. (1998). "Oxygen radicals and signaling." Curr Opin Cell Biol **10**(2): 248-53.

Finkel, T. (2000). "Redox-dependent signal transduction." FEBS Lett **476**(1-2): 52-4.

Fischer, E. H. (1999). "Cell signaling by protein tyrosine phosphorylation." Adv Enzyme Regul **39**: 359-69.

Fischer, E. H., H. Charbonneau and N. K. Tonks (1991). "Protein tyrosine phosphatases: a diverse family of intracellular and transmembrane enzymes." Science **253**(5018): 401-6.

Flint, A. J., T. Tiganis, D. Barford and N. K. Tonks (1997). "Development of "substrate-trapping" mutants to identify physiological substrates of protein tyrosine phosphatases." Proc Natl Acad Sci U S A **94**(5): 1680-5.

Forster, T. (1946). Energiewanderung und Floreszcenz. Naturwissenschaften **6**, 166-175.

Forster, T. (1951). *Fluorescenz Organischer Verbindungen.* Vandennoeck & Ruprecht, Goettingen.

Fretto, L. J., A. J. Snape, J. E. Tomlinson, J. J. Seroogy, D. L. Wolf, W. J. LaRochelle and N. A. Giese (1993). "Mechanism of platelet-derived growth factor (PDGF) AA, AB, and BB binding to alpha and beta PDGF receptor." J Biol Chem **268**(5): 3625-31.

Freywald, A., N. Sharfe and C.M. Roifman (2002). The kinase-null EphB6 receptor undergoes transphosphorylation in a complex with EphB1. J Biol Chem **277**(6): 3823-28.

Futter, C. E., A. Pearse, L. J. Hewlett and C. R. Hopkins (1996). "Multivesicular endosomes containing internalized EGF-EGF receptor complexes mature and then fuse directly with lysosomes." J Cell Biol **132**(6): 1011-23.

Gadella, T. W., Jr. and T. M. Jovin (1995). "Oligomerization of epidermal growth factor receptors on A431 cells studied by time-resolved fluorescence imaging microscopy. A stereochemical model for tyrosine kinase receptor activation." J Cell Biol **129**(6): 1543-58.

Gamett, D. C., G. Pearson, R. A. Cerione and I. Friedberg (1997). "Secondary dimerization between members of the epidermal growth factor receptor family." J Biol Chem **272**(18): 12052-6.

Gamou, S. and N. Shimizu (1995). "Hydrogen peroxide preferentially enhances the tyrosine phosphorylation of epidermal growth factor receptor." FEBS Lett **357**(2): 161-4.

Garcia-Morales, P., Y. Minami, E. Luong, R. D. Klausner and L. E. Samelson (1990). "Tyrosine phosphorylation in T cells is regulated by phosphatase activity: studies with phenylarsine oxide." Proc Natl Acad Sci U S A **87**(23): 9255-9.

Garrington, T. P. and G. L. Johnson (1999). "Organization and regulation of mitogen-activated protein kinase signaling pathways." Curr Opin Cell Biol **11**(2): 211-8.

Ge, G., J. Wu and Q. Lin (2001). "Effect of membrane fluidity on tyrosine kinase activity of reconstituted epidermal growth factor receptor." Biochem Biophys Res Commun **282**(2): 511-4.

Gillham, H., M. C. Golding, R. Pepperkok and W. J. Gullick (1999). "Intracellular movement of green fluorescent protein-tagged phosphatidylinositol 3-kinase in response to growth factor receptor signaling." J Cell Biol **146**(4): 869-80.

Goldman, R., R. B. Levy, E. Peles and Y. Yarden (1990). "Heterodimerization of the erbB-1 and erbB-2 receptors in human breast carcinoma cells: a mechanism for receptor transregulation." Biochemistry **29**(50): 11024-8.

Grabarek, Z. and J. Gergely (1990). "Zero-length crosslinking procedure with the use of active esters." Anal Biochem **185**(1): 131-5.

Graus-Porta, D., R. R. Beerli, J. M. Daly and N. E. Hynes (1997). "ErbB-2, the preferred heterodimerization partner of all ErbB receptors, is a mediator of lateral signaling." Embo J **16**(7): 1647-55.

Greco, V., M. Hannus and S. Eaton (2001). "Argosomes: a potential vehicle for the spread of morphogens through epithelia." Cell **106**(5): 633-45.

Griendling, K. K., D. Sorescu and M. Ushio-Fukai (2000). "NAD(P)H oxidase: role in cardiovascular biology and disease." Circ Res **86**(5): 494-501.

Griffin, B. A., S. R. Adams and R. Y. Tsien (1998). "Specific covalent labeling of recombinant protein molecules inside live cells." Science **281**(5374): 269-72.

Gschwind, A., E. Zwick, N. Prenzel, M. Leserer and A. Ullrich (2001). "Cell communication networks: epidermal growth factor receptor transactivation as the paradigm for interreceptor signal transmission." Oncogene **20**(13): 1594-600.

Gullick, W. J., J. J. Marsden, N. Whittle, B. Ward, L. Bobrow and M. D. Waterfield (1986). "Expression of epidermal growth factor receptors on human cervical, ovarian, and vulval carcinomas." Cancer Res **46**(1): 285-92.

Gullick, W. J. (1994). "A new model for the interaction of EGF-like ligands with their receptors: the new one-two." Eur J Cancer **14**(2186): 2186.

Gullick, W. J. (2001). "The Type 1 growth factor receptors and their ligands considered as a complex system." Endocr Relat Cancer **8**(2): 75-82.

Guy, P. M., J. V. Platko, L. C. Cantley, R. A. Cerione and K. L. Carraway, 3rd (1994). "Insect cell-expressed p180erbB3 possesses an impaired tyrosine kinase activity." Proc Natl Acad Sci U S A **91**(17): 8132-6.

Haj, F. G., P. J. Verveer,. A. Squire, B. G. Neel and P. I. H. Bastiaens. (2002). Imaging PTP1B/receptor interactions localizes RTK dephosphorylation on the surface of the endoplasmic reticulum. Science, *in press*.

Harpur A & P. I. H. Bastiaens. (2001). Probing protein interactions using GFP and fluorescence resonance energy transfer, in *Molecular Cloning A Laboratory Manual*, Sambrook and Russell (Eds.). Cold Spring Harbour Press, New York.

Harpur, A. G., F. S. Wouters and P. I. H. Bastiaens (2001). "Imaging FRET between spectrally similar GFP molecules in single cells." Nat Biotechnol **19**(2): 167-9.

Harris, B. Z. and W. A. Lim (2001). "Mechanism and role of PDZ domains in signaling complex assembly." J Cell Sci **114**(Pt 18): 3219-31.

Haugh, J. M., F. Codazzi, M. Teruel and T. Meyer (2000). "Spatial sensing in fibroblasts mediated by 3' phosphoinositides." J Cell Biol **151**(6): 1269-80.

He, H., A. Levitzki, H. J. Zhu, F. Walker, A. Burgess and H. Maruta (2001). "Platelet-derived growth factor requires epidermal growth factor receptor to activate p21-activated kinase family kinases." J Biol Chem **276**(29): 26741-4.

Heffetz, D., I. Bushkin, R. Dror and Y. Zick (1990). "The insulinomimetic agents H_2O_2 and vanadate stimulate protein tyrosine phosphorylation in intact cells." J Biol Chem **265**(5): 2896-902.

Heldin, C. H. (1995). "Dimerization of cell surface receptors in signal transduction." Cell **80**(2): 213-23.

Honegger, A., T. J. Dull, D. Szapary, A. Komoriya, R. Kris, A. Ullrich and J. Schlessinger (1988). "Kinetic parameters of the protein tyrosine kinase activity of EGF-receptor mutants with individually altered autophosphorylation sites." Embo J **7**(10): 3053-60.

Honegger, A. M., A. Schmidt, A. Ullrich and J. Schlessinger (1990a). "Evidence for epidermal growth factor (EGF)-induced intermolecular autophosphorylation of the EGF receptors in living cells." Mol Cell Biol **10**(8): 4035-44.

Honegger, A. M., A. Schmidt, A. Ullrich and J. Schlessinger (1990b). "Separate endocytic pathways of kinase-defective and -active EGF receptor mutants expressed in same cells." J Cell Biol **110**(5): 1541-8.

Huang, G. C., X. Ouyang and R. J. Epstein (1998). "Proxy activation of protein ErbB2 by heterologous ligands implies a heterotetrameric mode of receptor tyrosine kinase interaction." Biochem J **331**(Pt 1): 113-9.

Hubbard, S.R. and J.H. Till (2000). Protein tyrosine kinase structure and function. (2000). Annu. Rev. Biochem **69**:373-98.

Hudziak, R. M. and A. Ullrich (1991). "Cell transformation potential of a HER2 transmembrane domain deletion mutant retained in the endoplasmic reticulum." J Biol Chem **266**(35): 24109-15.

Hunter, T. and J. A. Cooper (1981). "Epidermal growth factor induces rapid tyrosine phosphorylation of proteins in A431 human tumor cells." Cell **24**(3): 741-52.

Hunter, T. and J. A. Cooper (1985). "Protein-tyrosine kinases." Annu Rev Biochem **54**: 897-930.

Hunter, T. (1995). "Protein kinases and phosphatases: the yin and yang of protein phosphorylation and signaling." Cell **80**(2): 225-36.

Hunter, T. (2000). "Signaling--2000 and beyond." Cell **100**(1): 113-27.

Hynes, N. E. and D. F. Stern (1994). "The biology of erbB-2/neu/HER-2 and its role in cancer." Biochim Biophys Acta **1198**(2-3): 165-84.

Ihle, J. N. and I. M. Kerr (1995). "Jaks and Stats in signaling by the cytokine receptor superfamily." Trends Genet **11**(2): 69-74.

Inagaki, N., M. Ito, T. Nakano and M. Inagaki (1994). "Spatiotemporal distribution of protein kinase and phosphatase activities." Trends Biochem Sci **19**(11): 448-52.

Jacobson, K. and C. Dietrich (1999). "Looking at lipid rafts?" Trends Cell Biol **9**(3): 87-91.

Jallal, B., J. Schlessinger and A. Ullrich (1992). "Tyrosine phosphatase inhibition permits analysis of signal transduction complexes in p185HER2/neu-overexpressing human tumor cells." J Biol Chem **267**(7): 4357-63.

Janetopoulos, C., T. Jin and P. Devreotes (2001). "Receptor-mediated activation of heterotrimeric G-proteins in living cells." Science **291**(5512): 2408-11.

Jannot, C. B., R. R. Beerli, S. Mason, W. J. Gullick and N. E. Hynes (1996). "Intracellular expression of a single-chain antibody directed to the EGFR leads to growth inhibition of tumor cells." Oncogene **13**(2): 275-82.

Jiang, G. and T. Hunter (1999). "Receptor signaling: when dimerization is not enough." Curr Biol **9**(15): R568-71.

Joneson, T. and D. Bar-Sagi (1998). "A Rac1 effector site controlling mitogenesis through superoxide production." J Biol Chem **273**(29): 17991-4.

Jordan, J. D., E. M. Landau and R. Iyengar (2000). "Signaling networks: the origins of cellular multitasking." Cell **103**(2): 193-200.

Kang, S. W., H. Z. Chae, M. S. Seo, K. Kim, I. C. Baines and S. G. Rhee (1998). "Mammalian peroxiredoxin isoforms can reduce hydrogen peroxide generated in response to growth factors and tumor necrosis factor-alpha." J Biol Chem **273**(11): 6297-302.

Karin, M. and T. Hunter (1995). "Transcriptional control by protein phosphorylation: signal transmission from the cell surface to the nucleus." Curr Biol **5**(7): 747-57.

Karunagaran, D., E. Tzahar, R. R. Beerli, X. Chen, D. Graus-Porta, B. J. Ratzkin, R. Seger, N. E. Hynes and Y. Yarden (1996). "ErbB-2 is a common auxiliary subunit of NDF and EGF receptors: implications for breast cancer." Embo J **15**(2): 254-64.

Kashles, O., Y. Yarden, R. Fischer, A. Ullrich and J. Schlessinger (1991). "A dominant negative mutation suppresses the function of normal epidermal growth factor receptors by heterodimerization." Mol Cell Biol **11**(3): 1454-63.

Keilhack, H., T. Tenev, E. Nyakatura, J. Godovac-Zimmermann, L. Nielsen, K. Seedorf and F. D. Bohmer (1998). "Phosphotyrosine 1173 mediates binding of the protein-tyrosine phosphatase SHP-1 to the epidermal growth factor receptor and attenuation of receptor signaling." J Biol Chem **273**(38): 24839-46.

Kim, H. H., S. L. Sierke and J. G. Koland (1994). "Epidermal growth factor-dependent association of phosphatidylinositol 3- kinase with the erbB3 gene product." J Biol Chem **269**(40): 24747-55.

Kim, J. R., H. W. Yoon, K. S. Kwon, S. R. Lee and S. G. Rhee (2000). "Identification of proteins containing cysteine residues that are sensitive to oxidation by hydrogen peroxide at neutral pH." Anal Biochem **283**(2): 214-21.

King, C. R., I. Borrello, F. Bellot, P. Comoglio and J. Schlessinger (1988). "Egf binding to its receptor triggers a rapid tyrosine phosphorylation of the erbB-2 protein in the mammary tumor cell line SK-BR-3." Embo J **7**(6): 1647-51.

Knebel, A., H. J. Rahmsdorf, A. Ullrich and P. Herrlich (1996). "Dephosphorylation of receptor tyrosine kinases as target of regulation by radiation, oxidants or alkylating agents." Embo J **15**(19): 5314-25.

Kokai, Y., J. N. Myers, T. Wada, V. I. Brown, C. M. LeVea, J. G. Davis, K. Dobashi and M. I. Greene (1989). "Synergistic interaction of p185c-neu and the EGF receptor leads to transformation of rodent fibroblasts." Cell **58**(2): 287-92.

Kraynov, V. S., C. Chamberlain, G. M. Bokoch, M. A. Schwartz, S. Slabaugh and K. M. Hahn (2000). "Localized Rac activation dynamics visualized in living cells." Science **290**(5490): 333-7.

Kuhl, P. R. and L. G. Griffith-Cima (1996). "Tethered epidermal growth factor as a paradigm for growth factor- induced stimulation from the solid phase." Nat Med **2**(9): 1022-7.

Kulas, D. T., B. J. Goldstein and R. A. Mooney (1996). "The transmembrane protein-tyrosine phosphatase LAR modulates signaling by multiple receptor tyrosine kinases." J Biol Chem **271**(2): 748-54.

Kusumi, A., Y. Sako and M. Yamamoto (1993). "Confined lateral diffusion of membrane receptors as studied by single particle tracking (nanovid microscopy). Effects of calcium-induced differentiation in cultured epithelial cells." Biophys J **65**(5): 2021-40.

Lakowicz J.R. (1999). *Principles of Fluorescence Spectroscopy.* Kluewer Academic/Plenum Publishers, New York.

Lander, H. M. (1997). "An essential role for free radicals and derived species in signal transduction." Faseb J **11**(2): 118-24.

Lee, S. R., K. S. Kwon, S. R. Kim and S. G. Rhee (1998). "Reversible inactivation of protein-tyrosine phosphatase 1B in A431 cells stimulated with epidermal growth factor." J Biol Chem **273**(25): 15366-72.

Lemmon, M. A. and J. Schlessinger (1994). "Regulation of signal transduction and signal diversity by receptor oligomerization." Trends Biochem Sci **19**(11): 459-63.

Lemmon, M. A., Z. Bu, J. E. Ladbury, M. Zhou, D. Pinchasi, I. Lax, D. M. Engelman and J. Schlessinger (1997). "Two EGF molecules contribute additively to stabilization of the EGFR dimer." Embo J **16**(2): 281-94.

Lenferink, A. E., R. Pinkas-Kramarski, M. L. van de Poll, M. J. van Vugt, L. N. Klapper, E. Tzahar, H. Waterman, M. Sela, E. J. van Zoelen and Y. Yarden (1998). "Differential endocytic routing of homo- and hetero-dimeric ErbB tyrosine kinases confers signaling superiority to receptor heterodimers." Embo J **17**(12): 3385-97.

Li, J., Y. N. Kim and P. J. Bertics (2000). "Platelet-derived growth factor-stimulated migration of murine fibroblasts is associated with epidermal growth factor receptor expression and tyrosine phosphorylation." J Biol Chem **275**(4): 2951-8.

Lillemeier, B. F., M. Koster and I. M. Kerr (2001). "STAT1 from the cell membrane to the DNA." Embo J **20**(10): 2508-17.

Lu, H. S., J. J. Chai, M. Li, B. R. Huang, C. H. He and R. C. Bi (2001). "Crystal structure of human epidermal growth factor and its dimerization." J Biol Chem **276**(37): 34913-7.

Lund, K. A., C. S. Lazar, W. S. Chen, B. J. Walsh, J. B. Welsh, J. J. Herbst, G. M. Walton, M. G. Rosenfeld, G. N. Gill and H. S. Wiley (1990). "Phosphorylation of the epidermal growth factor receptor at threonine 654 inhibits ligand-induced internalization and down-regulation." J Biol Chem **265**(33): 20517-23.

Luttrell, L. M., Y. Daaka and R. J. Lefkowitz (1999). "Regulation of tyrosine kinase cascades by G-protein-coupled receptors." Curr Opin Cell Biol **11**(2): 177-83.

Madhani, H. D. (2001). "Accounting for specificity in receptor tyrosine kinase signaling." Cell **106**(1): 9-11.

Mahadev, K., A. Zilbering, L. Zhu and B. J. Goldstein (2001). "Insulin-stimulated hydrogen peroxide reversibly inhibits protein- tyrosine phosphatase 1b in vivo and enhances the early insulin action cascade." J Biol Chem **276**(24): 21938-42.

Mahajan, N. P., K. Linder, G. Berry, G. W. Gordon, R. Heim and B. Herman (1998). "Bcl-2 and Bax interactions in mitochondria probed with green fluorescent protein and fluorescence resonance energy transfer." Nat Biotechnol **16**(6): 547-52.

Maheshwari, G., G. Brown, D. A. Lauffenburger, A. Wells and L. G. Griffith (2000). "Cell adhesion and motility depend on nanoscale RGD clustering." J Cell Sci **113**(Pt 10): 1677-86.

Majoul, I., M. Straub, S. W. Hell, R. Duden and H. D. Soling (2001). "KDEL-cargo regulates interactions between proteins involved in COPI vesicle traffic: measurements in living cells using FRET." Dev Cell **1**(1): 139-53.

Mangelsdorf, D. J., C. Thummel, M. Beato, P. Herrlich, G. Schutz, K. Umesono, B. Blumberg, P. Kastner, M. Mark, P. Chambon and et al. (1995). "The nuclear receptor superfamily: the second decade." Cell **83**(6): 835-9.

Mansbridge, J. N., R. Knuchel, A. M. Knapp and R. M. Sutherland (1992). "Importance of tyrosine phosphatases in the effects of cell-cell contact and microenvironments on EGF-stimulated tyrosine phosphorylation." J Cell Physiol **151**(3): 433-42.

Marais, R. and C. J. Marshall (1996). "Control of the ERK MAP kinase cascade by Ras and Raf." Cancer Surv **27**: 101-25.

Marshall, C. J. (1995). "Specificity of receptor tyrosine kinase signaling: transient versus sustained extracellular signal-regulated kinase activation." Cell **80**(2): 179-85.

Massague, J. and A. Pandiella (1993). "Membrane-anchored growth factors." Annu Rev Biochem **62**: 515-41.

Mendelsohn, J. and J. Baselga (2000). "The EGF receptor family as targets for cancer therapy." Oncogene **19**(56): 6550-65.

Meng, T. C. and M. F. Lin (1998). "Tyrosine phosphorylation of c-ErbB-2 is regulated by the cellular form of prostatic acid phosphatase in human prostate cancer cells." J Biol Chem **273**(34): 22096-104.

Miller, K., J. Beardmore, H. Kanety, J. Schlessinger and C. R. Hopkins (1986). "Localization of the epidermal growth factor (EGF) receptor within the endosome of EGF-stimulated epidermoid carcinoma (A431) cells." J Cell Biol **102**(2): 500-9.

Miller, W. E. and R. J. Lefkowitz (2001). "Expanding roles for beta-arrestins as scaffolds and adapters in GPCR signaling and trafficking." Curr Opin Cell Biol **13**(2): 139-45.

Miyawaki, A., J. Llopis, R. Heim, J. M. McCaffery, J. A. Adams, M. Ikura and R. Y. Tsien (1997). "Fluorescent indicators for Ca2+ based on green fluorescent proteins and calmodulin." Nature **388**(6645): 882-7.

Mochizuki, N., S. Yamashita, K. Kurokawa, Y. Ohba, T. Nagai, A. Miyawaki and M. Matsuda (2001). "Spatio-temporal images of growth-factor-induced activation of Ras and Rap1." Nature **411**(6841): 1065-8.

Mohammadi, M., A. Honegger, A. Sorokin, A. Ullrich, J. Schlessinger and D. R. Hurwitz (1993). "Aggregation-induced activation of the epidermal growth factor receptor protein tyrosine kinase." Biochemistry **32**(34): 8742-8.

Moriki, T., H. Maruyama and I. N. Maruyama (2001). "Activation of preformed EGF receptor dimers by ligand-induced rotation of the transmembrane domain." J Mol Biol **311**(5): 1011-26.

Myers, M. G., Jr., X. J. Sun, B. Cheatham, B. R. Jachna, E. M. Glasheen, J. M. Backer and M. F. White (1993). "IRS-1 is a common element in insulin and insulin-like growth factor-I signaling to the phosphatidylinositol 3'-kinase." Endocrinology **132**(4): 1421-30.

Nagai, Y., M. Miyazaki, R. Aoki, T. Zama, S. Inouye, K. Hirose, M. Iino and M. Hagiwara (2000). "A fluorescent indicator for visualizing cAMP-induced phosphorylation in vivo." Nat Biotechnol **18**(3): 313-6.

Nagy, P., A. Jenei, A. K. Kirsch, J. Szollosi, S. Damjanovich and T. M. Jovin (1999). "Activation-dependent clustering of the erbB2 receptor tyrosine kinase detected by scanning near-field optical microscopy." J Cell Sci **112**(Pt 11): 1733-41.

Neel, B. G. and N. K. Tonks (1997). "Protein tyrosine phosphatases in signal transduction." Curr Opin Cell Biol **9**(2): 193-204.

Ng, T., A. Squire, G. Hansra, F. Bornancin, C. Prevostel, A. Hanby, W. Harris, D. Barnes, S. Schmidt, H. Mellor, P. I. H. Bastiaens and P. J. Parker (1999a). "Imaging protein kinase Calpha activation in cells." Science **283**(5410): 2085-9.

Ng, T., D. Shima, A. Squire, P. I. H. Bastiaens, S. Gschmeissner, M. J. Humphries and P. J. Parker (1999b). "PKCalpha regulates beta1 integrin-dependent cell motility through association and control of integrin traffic." Embo J **18**(14): 3909-23.

Noh, D. Y., S. H. Shin and S. G. Rhee (1995). "Phosphoinositide-specific phospholipase C and mitogenic signaling." Biochim Biophys Acta **1242**(2): 99-113.

Olayioye, M. A., D. Graus-Porta, R. R. Beerli, J. Rohrer, B. Gay and N. E. Hynes (1998). "ErbB-1 and ErbB-2 acquire distinct signaling properties dependent upon their dimerization partner." Mol Cell Biol **18**(9): 5042-51.

Olayioye, M. A., R. M. Neve, H. A. Lane and N. E. Hynes (2000). "The ErbB signaling network: receptor heterodimerization in development and cancer." Embo J **19**(13): 3159-67.

Olson, M. F. and R. Marais (2000). "Ras protein signalling." Semin Immunol **12**(1): 63-73.

Ostman, A. and F. D. Bohmer (2001). "Regulation of receptor tyrosine kinase signaling by protein tyrosine phosphatases." Trends Cell Biol **11**(6): 258-66.

Pani, G., R. Colavitti, B. Bedogni, R. Anzevino, S. Borrello and T. Galeotti (2000). "A redox signaling mechanism for density-dependent inhibition of cell growth." J Biol Chem **275**(49): 38891-9.

Parekh, D. B., W. Ziegler and P. J. Parker (2000). "Multiple pathways control protein kinase C phosphorylation." Embo J **19**(4): 496-503.

Pawson, T. and J. D. Scott (1997). "Signaling through scaffold, anchoring, and adaptor proteins." Science **278**(5346): 2075-80.

Pawson, T. and T. M. Saxton (1999). "Signaling networks--do all roads lead to the same genes?" Cell **97**(6): 675-8.

Pearce, L. L., R. E. Gandley, W. Han, K. Wasserloos, M. Stitt, A. J. Kanai, M. K. McLaughlin, B. R. Pitt and E. S. Levitan (2000). "Role of metallothionein in nitric oxide signaling as revealed by a green fluorescent fusion protein." Proc Natl Acad Sci U S A **97**(1): 477-82.

Penninger, J. M., J. Irie-Sasaki, T. Sasaki and A. J. Oliveira-dos-Santos (2001). "CD45: new jobs for an old acquaintance." Nat Immunol **2**(5): 389-96.

Petrone, A. and J. Sap (2000). "Emerging issues in receptor protein tyrosine phosphatase function: lifting fog or simply shifting?" J Cell Sci **113**(Pt 13): 2345-54.

Phair, R. D. and T. Misteli (2000). "High mobility of proteins in the mammalian cell nucleus." Nature **404**(6778): 604-9.

Pinkas-Kramarski, R., L. Soussan, H. Waterman, G. Levkowitz, I. Alroy, L. Klapper, S. Lavi, R. Seger, B. J. Ratzkin, M. Sela and Y. Yarden (1996). "Diversification of Neu differentiation factor and epidermal growth factor signaling by combinatorial receptor interactions." Embo J **15**(10): 2452-67.

Plotnikov, A. N., J. Schlessinger, S. R. Hubbard and M. Mohammadi (1999). "Structural basis for FGF receptor dimerization and activation." Cell **98**(5): 641-50.

Plotnikov, A. N., S. R. Hubbard, J. Schlessinger and M. Mohammadi (2000). "Crystal structures of two FGF-FGFR complexes reveal the determinants of ligand-receptor specificity." Cell **101**(4): 413-24.

Plowman, G. D., G. S. Whitney, M. G. Neubauer, J. M. Green, V. L. McDonald, G. J. Todaro and M. Shoyab (1990). "Molecular cloning and expression of an additional epidermal growth factor receptor-related gene." Proc Natl Acad Sci U S A **87**(13): 4905-9.

Plowman, G. D., J. M. Culouscou, G. S. Whitney, J. M. Green, G. W. Carlton, L. Foy, M. G. Neubauer and M. Shoyab (1993). "Ligand-specific activation of HER4/p180erbB4, a fourth member of the epidermal growth factor receptor family." Proc Natl Acad Sci U S A **90**(5): 1746-50.

Pollok, B. A. and R. Heim (1999). "Using GFP in FRET-based applications." Trends Cell Biol **9**(2): 57-60.

Prigent, S. A. and W. J. Gullick (1994). "Identification of c-erbB-3 binding sites for phosphatidylinositol 3'- kinase and SHC using an EGF receptor/c-erbB-3 chimera." Embo J **13**(12): 2831-41.

Prior, I. A., A. Harding, J. Yan, J. Sluimer, R. G. Parton and J. F. Hancock (2001). "GTP-dependent segregation of H-ras from lipid rafts is required for biological activity." Nat Cell Biol **3**(4): 368-75.

Rhee, S. G., Y. S. Bae, S. R. Lee and J. Kwon (2000). "Hydrogen peroxide: a key messenger that modulates protein phosphorylation through cysteine oxidation." Sci STKE **2000**(53): E1.

Rickert, P., O. D. Weiner, F. Wang, H. R. Bourne and G. Servant (2000). "Leukocytes navigate by compass: roles of PI3Kgamma and its lipid products." Trends Cell Biol **10**(11): 466-73.

Riese, D. J., 2nd, T. M. van Raaij, G. D. Plowman, G. C. Andrews and D. F. Stern (1995). "The cellular response to neuregulins is governed by complex interactions of the erbB receptor family." Mol Cell Biol **15**(10): 5770-6.

Riese, D. J., 2nd and D. F. Stern (1998). "Specificity within the EGF family/ErbB receptor family signaling network." Bioessays **20**(1): 41-8.

Robertson, S. C., J. A. Tynan and D. J. Donoghue (2000). "RTK mutations and human syndromeswhen good receptors turn bad." Trends Genet **16**(6): 265-71.

Rodriguez-Viciana, P., P. H. Warne, R. Dhand, B. Vanhaesebroeck, I. Gout, M. J. Fry, M. D. Waterfield and J. Downward (1994). "Phosphatidylinositol-3-OH kinase as a direct target of Ras." Nature **370**(6490): 527-32.

Saito, Y., J. Haendeler, Y. Hojo, K. Yamamoto and B. C. Berk (2001). "Receptor heterodimerization: essential mechanism for platelet-derived growth factor-induced epidermal growth factor receptor transactivation." Mol Cell Biol **21**(19): 6387-94.

Sakai, N., K. Sasaki, N. Ikegaki, Y. Shirai, Y. Ono and N. Saito (1997). "Direct visualization of the translocation of the gamma-subspecies of protein kinase C in living cells using fusion proteins with green fluorescent protein." J Cell Biol **139**(6): 1465-76.

Sako, Y., S. Minoghchi and T. Yanagida (2000). "Single-molecule imaging of EGFR signalling on the surface of living cells." Nat Cell Biol **2**(3): 168-72.

Salomon, D. S., R. Brandt, F. Ciardiello and N. Normanno (1995). "Epidermal growth factor-related peptides and their receptors in human malignancies." Crit Rev Oncol Hematol **19**(3): 183-232.

Sambrook.J., E.F. Fritsch, T. Maniatis. (1989). *Molecular Cloning A Laboratory Manual*, Second Edition. Cold Spring Harbour Press, New York

Sauer, H., M. Wartenberg and J. Hescheler (2001). "Reactive oxygen species as intracellular messengers during cell growth and differentiation." Cell Physiol Biochem **11**(4): 173-86.

Schaeffer, H. J. and M. J. Weber (1999). "Mitogen-activated protein kinases: specific messages from ubiquitous messengers." Mol Cell Biol **19**(4): 2435-44.

Schechter, Y., L. Hernaez, J. Schlessinger and P. Cuatrecasas (1979). "Local aggregation of hormone-receptor complexes is required for activation by epidermal growth factor." Nature **278**(5707): 835-8.

Schechter, A. L., D. F. Stern, L. Vaidyanathan, S. J. Decker, J. A. Drebin, M. I. Greene and R. A. Weinberg (1984). "The neu oncogene: an erb-B-related gene encoding a 185,000-Mr tumour antigen." Nature **312**(5994): 513-6.

Schlessinger, J. (2000). "Cell signaling by receptor tyrosine kinases." Cell **103**(2): 211-25.

Schriner, S. E., A. C. Smith, N. H. Dang, K. Fukuchi and G. M. Martin (2000). "Overexpression of wild-type and nuclear-targeted catalase modulates resistance to oxidative stress but does not alter spontaneous mutant frequencies at APRT." Mutat Res **449**(1-2): 21-31.

Servant, G., O. D. Weiner, P. Herzmark, T. Balla, J. W. Sedat and H. R. Bourne (2000). "Polarization of chemoattractant receptor signaling during neutrophil chemotaxis." Science **287**(5455): 1037-40.

Shoelson, S. E. (1997). "SH2 and PTB domain interactions in tyrosine kinase signal transduction." Curr Opin Chem Biol **1**(2): 227-34.

Simons, K. and E. Ikonen (1997). "Functional rafts in cell membranes." Nature **387**(6633): 569-72.

Simons, K. and D. Toomre (2000). "Lipid rafts and signal transduction." Nat Rev Mol Cell Biol **1**(1): 31-9.

Sliwkowski, M. X., G. Schaefer, R. W. Akita, J. A. Lofgren, V. D. Fitzpatrick, A. Nuijens, B. M. Fendly, R. A. Cerione, R. L. Vandlen and K. L. Carraway, 3rd (1994). "Coexpression of erbB2 and erbB3 proteins reconstitutes a high affinity receptor for heregulin." J Biol Chem **269**(20): 14661-5.

Soltoff, S. P., K. L. Carraway, 3rd, S. A. Prigent, W. G. Gullick and L. C. Cantley (1994). "ErbB3 is involved in activation of phosphatidylinositol 3-kinase by epidermal growth factor." Mol Cell Biol **14**(6): 3550-8.

Sorby, M. and A. Ostman (1996). "Protein-tyrosine phosphatase-mediated decrease of epidermal growth factor and platelet-derived growth factor receptor tyrosine phosphorylation in high cell density cultures." J Biol Chem **271**(18): 10963-6.

Sorkin, A., K. Helin, C. M. Waters, G. Carpenter and L. Beguinot (1992). "Multiple autophosphorylation sites of the epidermal growth factor receptor are essential for receptor kinase activity and internalization. Contrasting significance of tyrosine 992 in the native and truncated receptors." J Biol Chem **267**(12): 8672-8.

Sorkin, A., M. McClure, F. Huang and R. Carter (2000). "Interaction of EGF receptor and grb2 in living cells visualized by fluorescence resonance energy transfer (FRET) microscopy." Curr Biol **10**(21): 1395-8.

Sorokin, A., M. A. Lemmon, A. Ullrich and J. Schlessinger (1994). "Stabilization of an active dimeric form of the epidermal growth factor receptor by introduction of an inter-receptor disulfide bond." J Biol Chem **269**(13): 9752-9.

Soumpasis, D. M. (1983). "Theoretical analysis of fluorescence photobleaching recovery experiments." Biophys J **41**(1): 95-7.

Spaargaren, M., L. H. Defize, J. Boonstra and S. W. de Laat (1991). "Antibody-induced dimerization activates the epidermal growth factor receptor tyrosine kinase." J Biol Chem **266**(3): 1733-9.

Spivak-Kroizman, T., M. A. Lemmon, I. Dikic, J. E. Ladbury, D. Pinchasi, J. Huang, M. Jaye, G. Crumley, J. Schlessinger and I. Lax (1994). "Heparin-induced oligomerization of FGF molecules is responsible for FGF receptor dimerization, activation, and cell proliferation." Cell **79**(6): 1015-24.

Spivak-Kroizman, T., D. Rotin, D. Pinchasi, A. Ullrich, J. Schlessinger and I. Lax (1992). "Heterodimerization of c-erbB2 with different epidermal growth factor receptor mutants elicits stimulatory or inhibitory responses." J Biol Chem **267**(12): 8056-63.

Squire, A. and P. I. H. Bastiaens (1999). "Three dimensional image restoration in fluorescence lifetime imaging microscopy." J Microsc **193**(Pt 1): 36-49.

Stephens, D. J. and R. Pepperkok (2001). "The many ways to cross the plasma membrane." Proc Natl Acad Sci U S A **98**(8): 4295-8.

Stern, D. F. and M. P. Kamps (1988). "EGF-stimulated tyrosine phosphorylation of p185neu: a potential model for receptor interactions." Embo J **7**(4): 995-1001.

Suarez Pestana, E., T. Tenev., Gross, S., Stoyanov, B., M. Ogata and F.D. Bohmer. (1999). "The transmembrane protein tyrosine phosphatase (RPTP) sigma modulates signalling of the epidermal growth factor in A431 cells." Oncogene **18**(28):4069-79.

Sundaresan, M., Z. X. Yu, V. J. Ferrans, K. Irani and T. Finkel (1995). "Requirement for generation of H_2O_2 for platelet-derived growth factor signal transduction." Science **270**(5234): 296-9.

Sundaresan, M., Z. X. Yu, V. J. Ferrans, D. J. Sulciner, J. S. Gutkind, K. Irani, P. J. Goldschmidt-Clermont and T. Finkel (1996). "Regulation of reactive-oxygen-species generation in fibroblasts by Rac1." Biochem J **318**(Pt 2): 379-82.

Sweeney, C., D. Fambrough, C. Huard, A. J. Diamonti, E. S. Lander, L. C. Cantley and K. L. Carraway, 3rd (2001). "Growth factor-specific signaling pathway stimulation and gene expression mediated by ErbB receptors." J Biol Chem **276**(25): 22685-98.

Syed, R. S., S. W. Reid, C. Li, J. C. Cheetham, K. H. Aoki, B. Liu, H. Zhan, T. D. Osslund, A. J. Chirino, J. Zhang, J. Finer-Moore, S. Elliott, K. Sitney, B. A. Katz, D. J. Matthews, J. J. Wendoloski, J. Egrie and R. M. Stroud (1998). "Efficiency of signalling through cytokine receptors depends critically on receptor orientation." Nature **395**(6701): 511-6.

Taipale, J. and J. Keski-Oja (1997). "Growth factors in the extracellular matrix." Faseb J **11**(1): 51-9.

Tamir, I., J. M. Dal Porto and J. C. Cambier (2000). "Cytoplasmic protein tyrosine phosphatases SHP-1 and SHP-2: regulators of B cell signal transduction." Curr Opin Immunol **12**(3): 307-15.

Tanabe, T., H. Otani, K. Mishima, R. Ogawa and C. Inagaki (1997). "Phorbol 12-myristate 13-acetate (PMA)-induced oxyradical production in rheumatoid synovial cells." Jpn J Pharmacol **73**(4): 347-51.

Teruel, M. N. and T. Meyer (2000). "Translocation and reversible localization of signaling proteins: a dynamic future for signal transduction." Cell **103**(2): 181-4.

Thannickal, V. J., R. M. Day, S. G. Klinz, M. C. Bastien, J. M. Larios and B. L. Fanburg (2000). "Ras-dependent and -independent regulation of reactive oxygen species by mitogenic growth factors and TGF-beta1." Faseb J **14**(12): 1741-8.

Thannickal, V. J. and B. L. Fanburg (2000). "Reactive oxygen species in cell signaling." Am J Physiol Lung Cell Mol Physiol **279**(6): L1005-28.

Thomas, S. M. and J. S. Brugge (1997). "Cellular functions regulated by Src family kinases." Annu Rev Cell Dev Biol **13**: 513-609.

Tiganis, T., A. M. Bennett, K. S. Ravichandran and N. K. Tonks (1998). "Epidermal growth factor receptor and the adaptor protein p52Shc are specific substrates of T-cell protein tyrosine phosphatase." Mol Cell Biol **18**(3): 1622-34.

Ting, A. Y., K. H. Kain, R. L. Klemke and R. Y. Tsien (2001). "Genetically encoded fluorescent reporters of protein tyrosine kinase activities in living cells." Proc Natl Acad Sci U S A **98**(26): 15003-8.

Tzahar, E., H. Waterman, X. Chen, G. Levkowitz, D. Karunagaran, S. Lavi, B. J. Ratzkin and Y. Yarden (1996). "A hierarchical network of interreceptor interactions determines signal transduction by Neu differentiation factor/neuregulin and epidermal growth factor." Mol Cell Biol **16**(10): 5276-87.

Tzahar, E., R. Pinkas-Kramarski, J. D. Moyer, L. N. Klapper, I. Alroy, G. Levkowitz, M. Shelly, S. Henis, M. Eisenstein, B. J. Ratzkin, M. Sela, G. C. Andrews and Y. Yarden (1997). "Bivalence of EGF-like ligands drives the ErbB signaling network." Embo J **16**(16): 4938-50.

Ullrich, A., L. Coussens, J. S. Hayflick, T. J. Dull, A. Gray, A. W. Tam, J. Lee, Y. Yarden, T. A. Libermann, J. Schlessinger and et al. (1984). "Human epidermal growth factor receptor cDNA sequence and aberrant expression of the amplified gene in A431 epidermoid carcinoma cells." Nature **309**(5967): 418-25.

Ullrich, A. and J. Schlessinger (1990). "Signal transduction by receptors with tyrosine kinase activity." Cell **61**(2): 203-12.

Ushio-Fukai, M., K. K. Griendling, P. L. Becker, L. Hilenski, S. Halleran and R. W. Alexander (2001). "Epidermal growth factor receptor transactivation by angiotensin II requires reactive oxygen species in vascular smooth muscle cells." Arterioscler Thromb Vasc Biol **21**(4): 489-95.

van Belzen, N., P. J. Rijken, W. J. Hage, S. W. de Laat, A. J. Verkleij and J. Boonstra (1988). "Direct visualization and quantitative analysis of epidermal growth factor-induced receptor clustering." J Cell Physiol **134**(3): 413-20.

Vanhaesebroeck, B. and M. D. Waterfield (1999). "Signaling by distinct classes of phosphoinositide 3-kinases." Exp Cell Res **253**(1): 239-54.

Varma, R. and S. Mayor (1998). "GPI-anchored proteins are organized in submicron domains at the cell surface." Nature **394**(6695): 798-801.

Venkateswarlu, K., P. B. Oatey, J. M. Tavare and P. J. Cullen (1998). "Insulin-dependent translocation of ARNO to the plasma membrane of adipocytes requires phosphatidylinositol 3-kinase." Curr Biol **8**(8): 463-6.

Verveer, P. J., A. Squire and P. I. H. Bastiaens (2000a). "Global analysis of fluorescence lifetime imaging microscopy data." Biophys J **78**(4): 2127-37.

Verveer, P. J., F. S. Wouters, A. R. Reynolds and P. I. H. Bastiaens (2000b). "Quantitative imaging of lateral ErbB1 receptor signal propagation in the plasma membrane." Science **290**(5496): 1567-70.

Verveer, P.J., A. Squire and P. I. H. Bastiaens,. (2001). Frequency Domain Fluorescence Lifetime Imaging Microscopy: A Window on the Biochemical Landscape of the Cell, in *Methods in Cellular Imaging*, Periasamy. A (Ed). Oxford University Press.

Vojtek, A. B. and C. J. Der (1998). "Increasing complexity of the Ras signaling pathway." J Biol Chem **273**(32): 19925-8.

Wada, T., X. L. Qian and M. I. Greene (1990). "Intermolecular association of the p185neu protein and EGF receptor modulates EGF receptor function." Cell **61**(7): 1339-47.

Waterman, H., I. Sabanai, B. Geiger and Y. Yarden (1998). "Alternative intracellular routing of ErbB receptors may determine signaling potency." J Biol Chem **273**(22): 13819-27.

Waterman, H. and Y. Yarden (2001). "Molecular mechanisms underlying endocytosis and sorting of ErbB receptor tyrosine kinases." FEBS Lett **490**(3): 142-52.

Weber, W., P. J. Bertics and G. N. Gill (1984). "Immunoaffinity purification of the epidermal growth factor receptor. Stoichiometry of binding and kinetics of self-phosphorylation." J Biol Chem **259**(23): 14631-6.

Weiss, A. and J. Schlessinger (1998). "Switching signals on or off by receptor dimerization." Cell **94**(3): 277-80.

Wells, J. A. (1996). "Binding in the growth hormone receptor complex." Proc Natl Acad Sci U S A **93**(1): 1-6.

White, J. and E. Stelzer (1999). "Photobleaching GFP reveals protein dynamics inside live cells." Trends Cell Biol **9**(2): 61-5.

Whitmarsh, A. J. and R. J. Davis (1998). "Structural organization of MAP-kinase signaling modules by scaffold proteins in yeast and mammals." Trends Biochem Sci **23**(12): 481-5.

Wilde, A., E. C. Beattie, L. Lem, D. A. Riethof, S. H. Liu, W. C. Mobley, P. Soriano and F. M. Brodsky (1999). "EGF receptor signaling stimulates Src kinase phosphorylation of clathrin, influencing clathrin redistribution and EGF uptake." Cell **96**(5): 677-87.

Wilson, B. S., J. R. Pfeiffer and J. M. Oliver (2000). "Observing FcepsilonRI signaling from the inside of the mast cell membrane." J Cell Biol **149**(5): 1131-42.

Wouters, F. S. and P. I. H. Bastiaens (1999). "Fluorescence lifetime imaging of receptor tyrosine kinase activity in cells." Curr Biol **9**(19): 1127-30.

Wouters, F. S., P. J. Verveer and P. I. H. Bastiaens (2001). "Imaging biochemistry inside cells." Trends Cell Biol **11**(5): 203-11.

Xu, Y., L. F. Seet, B. Hanson and W. Hong (2001). "The Phox homology (PX) domain, a new player in phosphoinositide signalling." Biochem J **360**(Pt 3): 513-30.

Yarden, Y. and J. Schlessinger (1987). "Epidermal growth factor induces rapid, reversible aggregation of the purified epidermal growth factor receptor." Biochemistry **26**(5): 1443-51.

Yarden, Y. and J. Schlessinger (1987). "Self-phosphorylation of epidermal growth factor receptor: evidence for a model of intermolecular allosteric activation." Biochemistry **26**(5): 1434-42.

Zhang, J., A. K. Somani and K. A. Siminovitch (2000). "Roles of the SHP-1 tyrosine phosphatase in the negative regulation of cell signalling." Semin Immunol **12**(4): 361-78.

Zhang, K., J. Sun, N. Liu, D. Wen, D. Chang, A. Thomason and S. K. Yoshinaga (1996). "Transformation of NIH 3T3 cells by HER3 or HER4 receptors requires the presence of HER1 or HER2." J Biol Chem **271**(7): 3884-90.

Zhou, M., S. Felder, M. Rubinstein, D. R. Hurwitz, A. Ullrich, I. Lax and J. Schlessinger (1993). "Real-time measurements of kinetics of EGF binding to soluble EGF receptor monomers and dimers support the dimerization model for receptor activation." Biochemistry **32**(32): 8193-8.

Zidovetzki, R., Y. Yarden, J. Schlessinger and T. M. Jovin (1981). "Rotational diffusion of epidermal growth factor complexed to cell surface receptors reflects rapid microaggregation and endocytosis of occupied receptors." Proc Natl Acad Sci U S A **78**(11): 6981-5.